TECHNISCHE UNIVERSITÄT MÜNCHEN
Ingenieurfakultät Bau Geo Umwelt
Lehrstuhl für Ingenieurgeologie

Determining abrasivity for hard rock TBM tunnelling

Peter Ellecosta

Vollständiger Abdruck der von der Ingenieurfakultät Bau Geo Umwelt der Technischen Universität München zur Erlangung des akademischen Grades eines

Doktor-Ingenieurs (Dr.-Ing.)

genehmigten Dissertation.

Vorsitzender:	Prof. Dr.-Ing. Roberto Cudmani
Prüfer der Dissertation:	1. Prof. Dr. rer. nat. Kurosch Thuro
	2. Prof. Dr.-Ing. Michael Alber

Die Dissertation wurde am 29.07.2020 bei der Technischen Universität München eingereicht und durch die Ingenieurfakultät Bau Geo Umwelt am 06.10.2020 angenommen.

Abstract

Over the last few decades, there has been a constant development and improvement of tunnel boring machines (TBMs) and the excavation tools used in both hard and soft rock. To the same extent, the prediction models for the advance rates and the wear of the excavation tools used have also been further developed. Nevertheless, there are still projects today where the predicted wear rate is significantly exceeded. In most cases, the decisive factor is not the price of the tools to be changed, but the downtimes resulting from the tool change. If the wear is higher than expected, this has a significant influence on the advance rate and thus on efficiency.

A further improvement of the existing prediction models regarding wear is only possible if the processes behind are understood. This means that the processes in the contact area between the excavation tool and the rock, which lead to tool wear, must be understood. The processes taking place can be summarized under the term tribology. In practice, however, it is difficult to investigate the contact area between e.g. cutter rings and the tunnel face during active advance. Due to the high contact pressures and the rotary motion of the cutter head and the cutter rings themselves, it is extremely difficult to install sensors or measuring devices in the contact surface or to transmit sensor signals backwards to a data logger. Therefore, often the only possibility left is the analysis of the occurring wear shapes on the excavation tools.

The TBM tunnel project of the Koralm Tunnel (KAT2), with a length of about 19 km, offered the opportunity to investigate the wear shapes of the cutter rings used, which were caused by a large number of different rock types with a very broad strength spectrum. In a first step, the worn cutter rings were classified according to their macroscopic wear shape and correlated with the geotechnical conditions during excavation. This allowed certain geotechnical parameters to be assigned to the respective macroscopic wear shapes.

In a second step, a microscopic analysis of the surface and microstructure of the cutter rings was carried out using metallographic sections. With effects that apparently only occurred near the surface, larger and deeper, base-failure-like shear zones could be detected within the steel structure. This results in hardening and embrittlement along the shear zones. The effect of a so-called grinding burn (thermal damage) could also be determined for a large number of cutter rings. In the worst case, tensile forces can develop in such a layer and hardening and embrittlement can also occur. Areas with material embrittlement presumably lead to the formation of cracks and ultimately to the detachment of larger steel chips as the excavation process progresses, in which such areas are repeatedly rolled over and subjected to stress.

In the third step, wear-induced effects or changes in the microstructure of the cutter rings were demonstrated with the aid of hardness tests. Hardness tests according to Knoop, Vickers and Rockwell were carried out for this purpose. It could be shown that virtually every wear type results in a hardening of the contact area with the rock in addition to a structural change.

Microscopic wear analysis has shown that hard minerals such as quartz, in particular, have penetrated the cutter ring steel. In addition, several authors have been able to show in recent years that in addition to compressive strength, hardness also has a very large influence on tool wear. For this reason, Vickers and Knoop hardness tests, which are in principle suitable for hardness testing, have been tested for their suitability on a wide range of minerals and rocks. Loads of 25 grams to a maximum of 72.5 kilograms were used. It turned out that both methods are suitable in principle. The effect of load-dependent hardness (indentation size effect) was also shown: the lower the test load, the higher the hardness. On rocks, the use of very small and large test loads showed that smaller loads were more likely to indicate mineral hardness, while the influence of rock strength was found to be more likely to be present with large loads. For large loads, there was usually also a good correlation with the determined wear characteristics of the respective rocks.

The investigations carried out were also able to show that the rock hardness also depends on the grain size and the crystallographic orientation of the minerals. Determining the "Vickers Hardness Number Rock" (VHNR), for example, only mineral hardness values from the literature are considered. This means, influences of the grain size or the crystallographic orientation are not taken into account. With the investigations carried out here, a significantly higher degree of accuracy can be achieved by directly testing the hardness of the respective rock.

To determine the wear potential of a rock by hardness testing, the representation of the cumulative frequency distribution of the hardness of a certain test load was chosen. Based on previous tests, the Vickers hardness test with a test load of 200 g (HV0.2) proved to be the most suitable. The advantage of displaying the cumulative frequency distribution of a rock is that it is quick and easy to determine whether a rock has the potential to cause wear. To do this, the same hardness test is carried out on an appropriate tool and the values are plotted in the diagram. This means that it is already possible to see visually whether parts of a rock are harder than parts of the tool steel. It is also possible to show the percentage of a rock that exceeds the hardness of the steel. This allows a quick and easy wear prediction.

Zusammenfassung

Im Bereich des maschinellen Tunnelbaus erfolgte im Laufe der letzten Jahrzehnte eine stetige Weiterentwicklung und Verbesserung der eingesetzten Tunnelbohrmaschinen (TBM) und der verwendeten Abbauwerkzeuge sowohl in Fest-, als auch in Lockergestein. In gleichem Maße haben sich auch die Prognosemodelle für die Vortriebsraten und den Verschleiß der verwendeten Abbauwerkzeuge weiter entwickelt. Dennoch gibt es heute immer noch Projekte, bei denen die prognostizierte Verschleißrate deutlich überschritten wird. Dabei ist meist nicht der Preis der zu wechselnden Werkzeuge der ausschlaggebende Faktor, sondern die durch den Werkzeugwechsel resultierenden Stillstandszeiten. Ist der Verschleiß höher als erwartet, so hat dies also einen nicht zu vernachlässigenden Einfluss auf die Vortriebsgeschwindigkeit und damit die Effizienz.

Um eine weitere Verbesserung der vorhandenen Prognosemodelle in Bezug auf Verschleiß zu ermöglichen, ist ein möglichst genaues Verständnis der Prozesse notwendig, die zu Verschleiß, das heißt zur Abnutzung der Abbauwerkzeuge durch den Kontakt zum umgebenden Gestein, führen. Die ablaufenden Prozesse können unter dem Begriff Tribologie zusammengefasst werden. In der Praxis ist es jedoch schwierig, die Kontaktfläche zwischen z.B. Schneidringen und der Ortsbrust während dem aktiven Vortrieb zu untersuchen. Aufgrund der hohen Anpressdrücke und der Drehbewegung des Schneidrades sowie der Schneidringe selbst ist es äußerst schwierig, Sensoren oder Messgeräte in der Kontaktfläche zu installieren oder Sensorsignale rückwärts zu einem Datenlogger zu leiten. Deswegen bleibt oft nur die Analyse der auftretenden Verschleißformen an den Abbauwerkzeugen als einzige Möglichkeit übrig.

Das Tunnelbauprojekt Koralmtunnel KAT2 bot mit seinen etwa 19 km Länge die Möglichkeit, die auftretenden Verschleißformen der eingesetzten Schneidringe, die durch eine Vielzahl an unterschiedlichen Gesteinen mit einem sehr breiten Festigkeitsspektrum verursacht wurden, zu untersuchen. Hierbei wurden die verschlissenen Schneidringe in einem ersten Schritt nach deren makroskopischer Verschleißform klassifiziert und mit den geotechnischen Bedingungen während des Vortriebs korreliert. Damit war es möglich, den jeweiligen makroskopischen Verschleißformen gewisse geotechnische Parameter zuzuordnen.

In einem zweiten Schritt erfolgte eine mikroskopische Analyse der Oberfläche und des Gefüges der Schneidringe anhand von metallographischen Schliffen. Dadurch konnten bei Effekten, die augenscheinlich nur oberflächennah auftraten, größere und tiefer gehende, grundbruchartige Scherzonen innerhalb des Stahlgefüges nachgewiesen werden. Entlang der Scherzonen kommt es dabei zu einer Verhärtung und Versprödung. Auch der Effekt eines sog. Schleifbrandes (thermische Schädigung) konnte bei einer Vielzahl an Schneidringen festgestellt werden. Im schlimmsten Fall bilden sich in einer solchen Schicht Zugkräfte aus und es kann ebenfalls zu einer Verhärtung und Versprödung kommen. Bereiche mit einer Materialversprödung führen mutmaßlich beim fortschreitenden Abbauprozess, bei dem solche

Stellen immer wieder überrollt und belastet werden, zur Bildung von Rissen und letztendlich zum Ablösen von größeren Stahlspänen.

Der dritte Schritt bestand darin, verschleißinduzierte Effekte oder Veränderungen des Gefüges der Schneidringe mit Hilfe von Härteversuchen auch nachzuweisen. Hierfür wurden Härteversuche nach Knoop, Vickers und Rockwell ausgeführt. Es konnte gezeigt werden, dass bei quasi jeder Verschleißform der Kontaktbereich eines Schneidringes zum Gestein neben einer Gefügeveränderung auch eine Verhärtung erfährt.

Die mikroskopische Verschleißanalyse hat gezeigt, dass v.a. harte Minerale wie Quarz in den Schneidringstahl eindringen. Zusätzlich konnten mehrere Autoren in den letzten Jahren zeigen, dass neben der Druckfestigkeit auch die Mineralhärte einen sehr großen Einfluss in Bezug auf Werkzeugverschleiß besitzt. Aus diesem Grund wurden die für eine Härteprüfung prinzipiell geeigneten Härteversuche nach Vickers und Knoop auf deren Eignung an einer Vielzahl an Mineralen und Gesteinen überprüft. Dabei wurden Lasten von 25 Gramm bis maximal 72,5 Kilogramm verwendet. Es stellte sich heraus, dass beide Methoden prinzipiell geeignet sind. Auch zeigte sich der Effekt der lastabhängigen Härte: je geringer die Prüflast, desto höher die Härte. An Gesteinen hat die Verwendung von sehr kleinen und großen Prüflasten gezeigt, dass kleinere Lasten eher eine Korrelation mit der Mineralhärte zeigen, während bei großen Lasten der Einfluss der Gesteinsfestigkeit festgestellt wurde. Im Bereich von großen Lasten gab es meist auch eine gute Korrelation mit den ermittelten Verschleißkennwerten der jeweiligen Gesteine.

Die durchgeführten Untersuchungen konnten zudem zeigen, dass die Gesteinshärte auch von der Korngröße, sowie der kristallographischen Orientierung der Minerale abhängig ist. Bei der Bestimmung der „Vickers Hardness Number Rock“ (VHNR) z.B. fließen ausschließlich Mineralhärten aus der Literatur ein, wodurch die genannten Einflüsse nicht berücksichtigt werden. Bei den hier durchgeführten Untersuchungen kann durch die direkte Prüfung der Härte des jeweiligen Gesteins eine deutlich höhere Genauigkeit und damit Aussagekraft erzielt werden.

Um das Verschleißpotential eines Gesteins anhand von Härteversuchen zu ermitteln, wurde die Darstellung der kumulativen Häufigkeitsverteilung der Härten einer bestimmten Prüflast gewählt. Anhand der vorgenommenen Versuche zeigte sich die Härteprüfung nach Vickers mit einer Prüflast von 200 g (HV0,2) als am besten geeignet. Die Darstellung der kumulativen Häufigkeitsverteilung der unterschiedlichen, in einem Gestein vorkommenden Härtewerte hat den großen Vorteil, dass aus ihr schnell und einfach zu entnehmen ist, ob ein Gestein das Potential besitzt, Verschleiß zu verursachen. Dafür wird die gleiche Härteprüfung an einem entsprechenden Werkzeug durchgeführt und die zugehörigen Werte in das Diagramm eingetragen. Damit ist bereits qualitativ zu erkennen, welche Anteile eines Gesteins härter sind als die des Werkzeugstahls und diese Anteile können quantitativ prozentual erfasst werden. Somit ist eine schnelle und einfache Verschleißprognose möglich.

Acknowledgement

I would like to thank Prof. Kurosch Thuro for the opportunity to write this thesis as well as for the great support and valuable discussions on the topic. Thank you for providing the position at the Chair of Engineering Geology and for the confidence you placed in me throughout the whole period, I really appreciate that.

Many thanks also go to Prof. Michael Alber, who has agreed to act as co-supervisor for the dissertation.

I would also like to thank my mentor Dr. Heiko Käsling for the numerous constructive discussions about laboratory results and especially for supporting all the ideas, I brought forward.

A special thanks goes to my former colleague and doctoral student Lisa Wilfing. Together we worked on the Koralm Tunnel project. In this context, I would also like to thank the staff of Strabag and ÖBB, who made the investigations on the Koralm Tunnel possible.

Carola Wieser should also be mentioned as a special former colleague and doctoral student. I would like to thank her for the many exciting discussions. She always had an open mind and could always help with technical questions.

My very special thanks also goes to Dr. Bernhard Lempe, the supervisor of my Bachelor's and Master's thesis. During my time at TUM he was not only an outstanding colleague but also a consultant and friend in all situations of life.

Vladimir Ruttner also played a special role. He took me to a workshop on materials testing. The lectures were also about hardness tests. This finally gave me the idea of combining hardness testing on steel with hardness testing on minerals and rocks.

I would also like to thank Dr. Gerhard Lehrberger, who arranged the contact to the "Zentrum für Werkstoffanalytik Lauf" (ZWL) and always supported me with his expertise. In this context, I would also like to thank the staff of the ZWL, and in particular Werner Kachler, on whose excellent professional knowledge I could always trust. The ZWL also made it possible for me to cut the cutter rings professionally. I would like to thank Susanne Winter for the excellent SEM images.

In the final phase of my thesis, I was always able to turn to my former colleague and doctoral student Martin Potten with questions, who always gave me helpful tips. In the same context, I would also like to mention Matthias Brugger, who supported me especially in organizing the submission.

I would also like to thank the Materials Testing Office of the TUM, represented by Mr. Greubel and Dr. Niedermayer, as well as the Institute for Machine Tools, for providing me access to their hardness testing equipment. In this context I would also like to thank the staff of the Department of Environment, Land and Infrastructure Engineering (DIATI) of the

Politecnico di Torino for allowing me to use their hardness tester for several weeks. Prof. Marilena Cardu and Prof. Paola Marini should be mentioned here by name.

I also extend my thanks to all my master and bachelor students as well as the student assistants for contributing to this work.

Furthermore, I would like to thank all my former colleagues at the Chair of Engineering Geology for their help, their support and discussions.

My greatest thanks goes to my family and friends. None of this would have been possible without them. Thank you dear parents for your unlimited trust and support during my whole education. Thank you also for encouraging me and for always being there, whenever I need your advice.

My special thanks goes to Lucia. Without your encouragement, I would probably not have finished my doctorate. Thank you for your infinite support and motivation.

Contents

List of figures

List of tables

1. Introduction

Over the last few decades, mechanized tunnelling in both hard rock and soil has become very popular and has been further developed. In contrast to other methods such as drill and blast or excavation using roadheaders or dredgers, tunnelling with TBMs allows simultaneous excavation and building of the tunnel lining by tubbing segments or shotcrete (MAIDL et al. 2012; KÜPFERLE et al. 2016a). Especially long tunnels with lengths over 1.5–2 km can be excavated relatively quickly and easily with the TBMs used today (HASSANPOUR et al. 2011). The reasons for this are the safe working conditions and the generally high efficiency. In addition to machine technology, excavation tools have also developed considerably.

But there is also a dark side to the coin. Despite all the progress made, the TBM type and tools must be adapted to the geological conditions. If this does not happen due to an inaccurate forecast or a misjudgment, even the most modern machines will run into trouble.

This thesis focuses on the tool wear of hard rock tunnel boring machines and the resulting efficiency.

1.1 Motivation and background

Due to the development of more efficient and powerful machines, TBMs are used in various ground conditions from extremely hard and massive to broken and blocky grounds (HASSANPOUR et al. 2011). For planning purposes and to check whether the use of a TBM in a tunnel project is worthwhile, it is necessary to estimate and forecast the penetration, advance rate and cutter cost/life.

Despite all developments, tool wear is still one of the most important cost factors. Cutter consumption has a major impact on performance and the costs of tunnelling projects (MACIAS et al. 2017a). The reasons are not mainly the costs of the tools, but the downtimes produced by tool changes (SCHIMAZEK & KNATZ 1976). Thus, tunnelling performance and costs may be strongly influenced by the level of consumption of cutters, especially in hard and abrasive rock conditions (MACIAS et al. 2017a). To achieve a high cutter life time, a high hardness, toughness and strength must be provided simultaneously (RÖTTGER et al. 2015).

The TBM performance and the wear usually depend on the following three factors: machine specifications (cutterhead shape, cutter layout, thrust, RPM, penetration, etc.), ground characteristics (intact rock parameters, rock mass properties, etc.) and operating parameters (thrust, RPM) (HASSANPOUR et al. 2010; GENG et al. 2017). However, cutter wear may also have a direct influence on machine performance: worn cutters lead to a lower penetration or higher cutter thrusts with the same penetration rate due to the wider cutter tip width (ROSTAMI et al. 2012; MAIDL et al. 2012; HASSANPOUR et al. 2014; RÖTTGER et al. 2015; KÜPFERLE et al. 2016a).

However, tool wear is a system property and does not only depend on the abrasivity of the ground or the hardness of the tool materials (Küpferle et al. 2016). Wear involves complex

interaction between several processes and depends on different physical parameters which cannot be isolated and studied individually (RAMALHO & MIRANDA 2006; PETRICA et al. 2013). From a materials technology perspective, wear is considered in a tribological system that includes all components (e.g., load spectrum, geology, tool material, ambient medium) and interactions between the tool and the ground (ZUM GAHR 1987; KÜPFERLE et al. 2016a; VILLENEUVE 2017). The wear process has often simply been described as "abrasion" (BESTE et al. 2008). However, it is actually much more complex.

To understand the interaction between rock and excavation tool, the contact conditions (normal and friction forces, temperature, etc.) should be known and understood. But under real construction work it is difficult to measure such parameters so that laboratory tests are usually used for this. An additional problem with systematic wear evaluation is that different machines and different rocks and also different TBM operators produce different results (BESTE et al. 2008). At best, the results within a project are comparable. As a result, no general approach to predicting wear is, as yet, available, although more than a hundred ''laws'' relating to wear can be found in the literature (LUDEMA 1991; ESPALLARGAS et al. 2015).

In order to properly understand the reasons for wear, even on a microscopic scale, many and complex investigations are necessary. An example of a wear analysis for drill bits is shown by OLSSON et al. (2017). The authors use the most modern material science analysis methods to find out changes in the microscopic structure. This enabled them to find out reasons for the wear of cemented carbides.

On the basis of different wear types that occur during excavation of hard rock, it is in principle possible to draw conclusions about intact rock parameters and rock mass parameters. In literature exists mainly information about macroscopic wear, such as THURO & PLINNINGER (2002), KÄSLING (2009) and FRENZEL (2010), etc. The authors have already developed a first classification scheme for macroscopic wear.

However, microscopic wear can be described and classified in the same way. Unfortunately there is very little literature on this subject. One of the first more detailed studies on this topic is MACIAS (2016). Only in the field of material sciences, there is a large amount of literature. However, this literature mostly does not deal with TBM disc cutters of hard rock tunnel boring machines. Nevertheless their findings and results can be transferred in principle. By means of a microscopic wear analysis, conclusions can also be drawn about the intact rock parameters and the rock mass parameters.

Additionally, conclusions can be drawn about the tribological processes and the interaction between tool (mostly steel) and rock mass. Metallographic sections can also be used to illustrate the microstructure of the tools and wear-induced changes therein. This leads to a better understanding of the wear process.

Today, laboratory tests, so-called index tests, are mainly used for TBM wear prediction. There are a large number of these tests, both for hard and soft rock. These are largely designed to determine the abrasive wear of a rock material. Depending on the project, however, partly only about 50 % of wear is caused by abrasive wear (ZUM GAHR 1987; STOLARSKI 2000; STACHOWIAK & BATCHELOR 2005; PETRICA et al. 2013).

Commonly used laboratory-scale test methods to determine the abrasivity of the ground, such as the CERCHAR abrasivity test and the LCPC abrasivity test, are used all over the world for the evaluation of wear prediction models (KÜPFERLE et al. 2017). The existing laboratory test methods do not reproduce the wear behavior encountered during tunnel boring (MACIAS et al. 2016). Due to inevitable simplifications and adjustments of such laboratory-scale experiments, there is a weak transferability to reality. Every system component (tool material, soil, ambient/intermediate medium, load spectrum) has to be considered (KÜPFERLE et al. 2017). The problems and weaknesses of the common test methods are well known in literature (ROSTAMI et al. 2014; KÜPFERLE et al. 2015). The use of crushed rock or sliding tool-rock contact, are the main weaknesses of the established methods (MACIAS et al. 2016).

A new approach, which is also covered in this thesis, is hardness testing on minerals and rocks. Well known in geology is the 10-step scratch hardness according to MOHS (1822), where the harder mineral scratches the softer one at the below grade. However, this form of hardness testing is not suitable for predicting wear, as it is far too inaccurate. Based on the Mohs hardness, the doctrine also developed that only minerals have a hardness, but not rocks. Rocks should only have abrasiveness, as they are often composed of different minerals (polymineral rocks).

In material sciences, there is a whole range of different hardness testing methods. Almost all methods are standardized. Depending on the material, the appropriate method must be applied. One of the most widespread methods is indentation hardness, e.g. according to Brinell, Rockwell or Vickers. It is mostly used on ductile materials such as metals and steels. Ceramics, which react much more brittle under load, can also be tested under special conditions.

Hardness testing on minerals and rocks, e.g. according to Vickers, has rarely been carried out to date. The problem is that minerals and rocks react very brittle under load and the tests are not designed for this. For this reason there is no standardization. Nevertheless, indentation hardness can be determined on minerals and rocks. For this reason, the statement that rocks do not have hardness is not correct in this case. In principle, a hardness can be determined as a material characteristic value on almost any material.

With the commonly used TBM disc cutters, standardized hardness tests can be performed on metallographic sections. These show their hardness and can be used to evaluate the quality of the cutter rings and their heat treatment.

With regard to the subject of tool wear, the sole consideration of the hardness of excavation tools or of minerals and rocks is not sufficient. Instead, a comparison of both hardness types is necessary. A first approach is given by CARDU & GIRAUDI (2012). The authors use the cumulative frequency distribution. A more detailed explanation can be found in the paper of CARDU & GIRAUDI (2012).

1.2 Objectives of the study

Today, the planning and calculation of a TBM drive in hard rock is usually based on index tests and empirical values. The mechanical design, the design of the cutter head and the selection of the tools are also based on this. During a TBM drive, usually only an adjustment of the tools is possible. Again, this is usually done on the basis of empirical values. A systematic analysis of wear phenomena and their background as well as the resulting recommendations is rarely found.

The aim of this thesis was a systematic wear analysis based on a case study of the Koralm Tunnel project KAT2. This should include a macroscopic and a microscopic wear analysis. This analysis is supposed to enable a better understanding of the tribological processes (i.e. the interaction between excavation tool and rock). This should lead to a better understanding of how wear occurs.

The macroscopic wear analysis was largely carried out according to known classifications as used by THURO & PLINNINGER (2002), KÄSLING (2009) and FRENZEL (2010). This is combined with a wear analysis on a microscopic basis. For this purpose the surface of worn cutter rings is analyzed. In addition, a large number of metallographic sections were prepared and etched to visualize the structure of the steel. From the combination of both methods it is possible to draw conclusions about the wear process and the tribological conditions.

The wear analysis was complemented by hardness tests. This enables not only the visual recording of wear-induced changes in the steel, but also the precise quantification of these changes. In addition to cutter rings from the Koralm Tunnel project, the hardness and microstructure of CERCHAR pins and LCPC impellers was also determined.

A new approach, also covered in this thesis, is the hardness testing of minerals and rocks. The idea behind this is to evaluate the wear potential of rocks by hardness tests. A rock with many soft minerals such as calcite is usually considered to be very low in wear, while quartz-rich rocks usually cause high wear. Several researchers have also found that the hardness of a rock material has a very large influence on the wear rate (HASSANPOUR et al. 2011, 2014; MACIAS et al. 2016, 2017a).

For this purpose, it was primarily necessary to determine a common and suitable method for hardness testing on minerals and rocks. To this end, Knoop and Vickers hardness tests were carried out on a large number of minerals and rock types with loads ranging from 25 g to a maximum of 72.5 kg. In the evaluation of the results, effects such as the indentation size

effect could be characterized very well. In addition, it could be shown that low test loads tend to indicate mineral hardness and high loads tend to indicate rock hardness. At high loads there was usually a good correlation between hardness and rock strength and wear characteristics.

In order to ultimately be able to compare the hardness of tools with the hardness of rocks, the Vickers hardness proved to be the most appropriate method. The most suitable test load is 200 g (HV0.2). The evaluation, which is based on the cumulative frequency distribution of CARDU & GIRAUDI 2012, should enable a quick and easy evaluation of the wear potential.

The advantage of the method is that changes in hardness of the excavation tool caused by wear can also be taken into account. A further advantage is that the hardness is measured directly on a rock sample. Previous methods like the Vickers Hardness Number Rock (VHNR, SALMINEN & VIITALA 1985) use literature values for the hardness of the minerals. Influences of grain size and cleavage are not considered. Thus, literature values can never be as accurate as the hardness test on a specific rock specimen.

2. State of the art

Every process with a mechanical relative movement in typical conditions on earth experiences friction. This friction causes heat and wear, depending on the material and possible lubrications. The science of friction is today universally known as tribology. In the field of engineering geology, this mainly concerns the wear of machine elements by all kind of rocks, rock detritus, rock dust and minerals. In particular, the excavation tools of the machines are affected here. The potential of a rock to cause wear is commonly referred to the term abrasivity which depends mainly on the properties of the mined rock. To determine and to predict wear, there exist a lot of tests. This chapter gives a short overview of the most common test principles and explains the reasons which lead to tool wear.

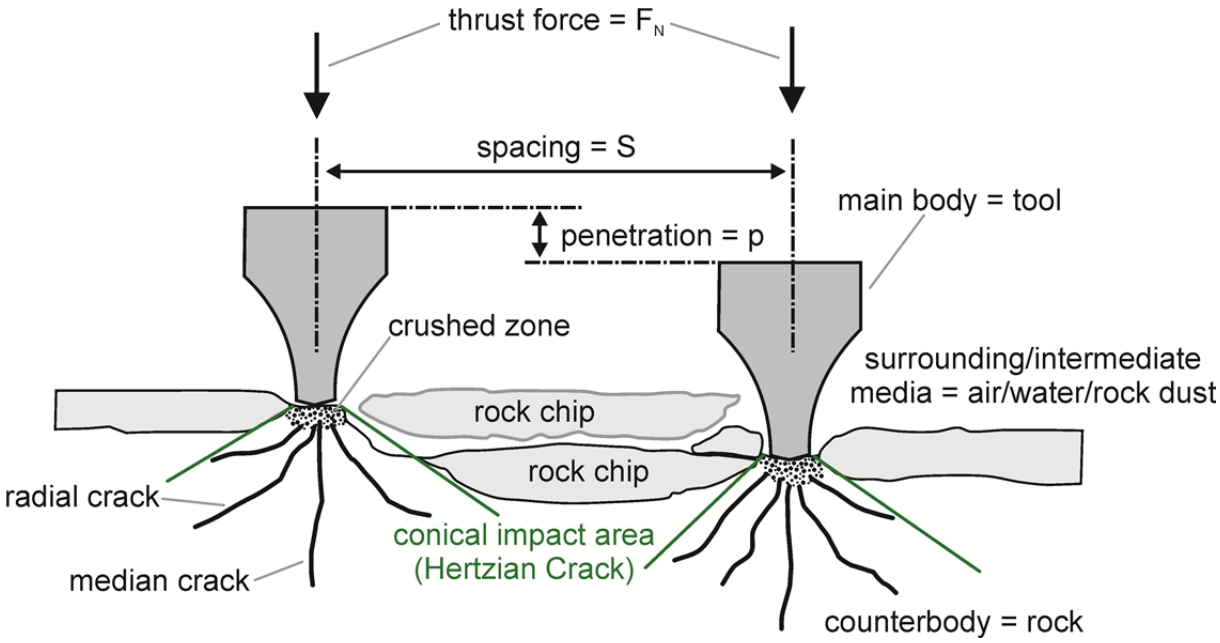

Fig. 1: Schematic figure of the cutting process during rock excavation with disc cutters in hard rock (mod. from ROSTAMI 1997: 23). In addition to ROSTAMI (1997), the tribological system with main body, counterbody and sorrounding / intermediate media is indicated.

In real construction works, there is often a relationship between TBM performance and wear. In this thesis, the performance is only briefly discussed. A close investigation of the influence of geological parameters on TBM performances was done by MACIAS et al. (2014). MACIAS et al. (2014) also provides a comprehensive literature overview: WANNER & AEBERLI (1979), HOWARTH (1981), LINDQVIST & HAI-HUI (1983), SANIO (1985), ZHAO et al. (2007), BRULAND (1998), BARTON (2000), RIBACCHI & FAZIO (2005), GONG et al. (2005, 2006), BIENIAWSKI et al. (2006), YAGIZ (2009b, 2009), HASSANPOUR et al. (2009, 2010, 2011, 2014), BEJARI & KHADEMI HAMIDI (2013), FARROKH et al. (2012). A further description of the individual papers is summarized in MACIAS et al. (2014). TBM performance is often put into context with the drillability, which is defined as the ability of the rock to be drilled or bored and has a great impact on

performance predictions, cost evaluations and selection of an excavation method (MACIAS et al. 2017b). It considers the influence that intact rock properties, breakability and abrasivity have during drilling and boring in hard rock.

To understand the mechanisms that cause wear, it is important to understand the excavation process of disc cutters in hard rock, which is shown in Fig. 1. There is a large number of researchers who investigated this fragmentation process over the last 40 years: BENJUMEA & SIKARSKIE (1969), ROXBOROUGH & PHILLIPS (1975), WANNER & AEBERLI (1979), SANIO (1983), LINDQVIST & HAI-HUI (1983), BÜCHI (1984), ROSTAMI (1997), GEHRING (1997) etc. All authors agree in the point that the fragmentation is divided into two parts (Fig. 1): a zone of crushed material below the cutter tip (crushed zone) and the formation of rock chips (chipping) (WILFING 2016). The force, applied by a disc cutter, causes an indentation into the rock surface and produces a zone of crushed material beneath the cutter. The stresses from the thrust of the cutter are transmitted through this crushed zone into the adjacent undamaged rock (SNOWDON et al. 1982; BRULAND 2000b; CIGLA et al. 2001; ZHANG 2001; ROSTAMI et al. 2002; VILLENEUVE 2017). Penetration can only be possible, when the applied forces exceed the uniaxial compressive strength of the rock (ROXBOROUGH & PHILLIPS 1975).

If too little force is transmitted to the disc cutters during TBM operation, a crushed zone is produced, but this is not sufficient for chipping and is called grinding. According to VILLENEUVE (2017), grinding is the generation of fines when fractures do not propagate through the rock and only comminution occurs at the cutter-rock interface (VILLENEUVE 2015). The crushed zone can be up to approx. 3 mm/rev. penetration (WILFING & THURO 2017). VILLENEUVE (2017) continues to conclude that the induced stresses and dilation within the crushed zone cause tensile fracturing of rock away from the crushed zone. Eventually, fractures generated by subsequent cutter passes extend either to the rock surface or to the fractures propagating from adjoining kerfs and coalesce to form chips. Depending on the rock, this happens at different cutter thrust magnitudes. If the cutter thrust necessary for tensile fracture propagation is not achieved, due to excessively high cutter thrust requirements or an underpowered TBM, then only grinding at the crushed zone occurs (VILLENEUVE 2017).

If the cutter thrust reaches a certain level called critical thrust point, effective rock excavation due to chipping occurs. The critical thrust point and also the slope of the penetration curve during chipping (discussed in SAMUEL & SEOW (1984); ZHANG et al. (2003); GEHRING (2009)), are related to rock strength, brittleness, mineralogy, fabric (VILLENEUVE et al. 2007; VILLENEUVE 2008; VILLENEUVE et al. 2012), and the stress at the tunnel face (YIN et al. 2014). According to VILLENEUVE (2017), chipping is defined as the process of the generation of chips when tensile fractures are induced into the rock, and then propagate parallel to the tunnel face (VILLENEUVE 2015). This is a more efficient excavation process because generating chips through tensile fracturing is much more efficient than the formation of fines in the crushed zone (TEALE 1964; SNOWDON et al. 1982; BRULAND 2000b;

GERTSCH et al. 2007; YIN et al. 2014; VILLENEUVE 2017). The formation of chips by the chipping process is therefore critical for achieving high penetration rates (VILLENEUVE 2017). It should be noted, however, that the critical stress required to achieve an effective excavation with chip formation does not depend on the uniaxial compressive strength of the rock (WILFING & THURO 2017). The compressive strength is only responsible for the formation of the crushed zone (ROXBOROUGH & PHILLIPS 1975).

The excavation process with disc cutters is not a continuous process because the rock surface is irregular leading to a high variation of cutter load during the mining process. The indentation into the rock mass takes place under sudden stress peaks (WILFING 2016). This causes very high contact stresses at the cutter tip resulting in the crushing of the rock material and the formation of a high pressure zone which shows plastic flow properties (BÜCHI 1984). Fine crushed rock material is displaced to the side. The literature of the past was the opinion, that if the pressure level is sufficient to exceed the shear or tensile strength of the rock, new cracks develop (LINDQVIST & HAI-HUI 1983: 200; GERTSCH 2000). The trend in the investigations of WILFING & THURO (2017) shows that the required critical stress for chipping also increases exponentially with increasing tensile strength of the rock. According to WILFING & THURO (2017), the tensile strength has thus a certain influence, but with a correlation coefficient of 0.37 it is only moderate. The LCPC breakability coefficient (LBK), which has a high correlation coefficient of 0.92, has proved to be a much more decisive parameter (WILFING 2016; WILFING & THURO 2017).

The formation of a conical crack (Hertzian crack) at the cutter edge is proven by GONG et al. 2005). This agrees with the theory of contact mechanics between a rigid indenter and brittle material. Radial cracks and a median crack are also developing. If these cracks grow and coincide with cracks from adjacent cuts reaching a free rock surface, rock chips are formed and chipping takes places (WILFING 2016). According to LISLERUD (1997: 129), cutters have to pass the same position at the tunnel face two or three times until a rock chip is being formed, depending on geotechnical parameters of the rock and applied thrust force.

The resulting penetration rate is limited not only on the rock properties but above all by TBM design parameters, which define performance limits (VILLENEUVE 2017). The penetration limit is a function of muck conveyance, bucket design, cutter wear and the maximum head revolution speed (FRENZEL et al. 2012). The torque limit provides the transition from the penetration limit to the maximum thrust (FRENZEL et al. 2008), which is a function of the rotational speed and is controlled by the maximum torque capacity (VILLENEUVE 2017). The thrust limit is controlled by the TBM head design, the cutter type and the maximum thrust capacity. Current hard rock TBM have typically a penetration limit of approximately 11 mm/rev and a torque limit of approximately 30 % of the maximum torque capacity (VILLENEUVE 2017). These values may vary depending on machine and manufacturer. The maximum net thrust on 432 mm cutters (17 inch) is typically around 250 kN

(FRENZEL et al. 2008; MAIDL et al. 2008) and therefore specifically lower than the maximum of 267 kN.

Another important topic is the aspect that concerns wear in general and especially in engineering geology. It describes which types of wear generally exist, where this type comes from, and how this affects the tool and the tool wear. In addition, the influence of hardness is shown, and the possibilities of hardness testing are considered. The last topic is the field of cutter life prediction models. It summarizes the most important and commonly used prediction models.

2.1 Tribology

The term tribology was used from about 1966 as a technical term in literature, especially in England. JOST (1966) defines tribology as the science and the technology of interacting, relatively moving surfaces and related practical processes. A standardized definition gives the withdrawn DIN 50323 (DIN 50323-1 1988; DIN 50323-2 1995; DIN 50323-31993): Tribology is the science and technique of interacting surfaces in relative motion. It covers the entire field of friction and wear, including luKnobrication, and includes appropriate interfacial interactions both between solids and liquids or gases. According to CZICHOS (1978) and CZICHOS & HABIG (1992), tribology is defined as an interdisciplinary field for the optimization of mechanical technologies by reducing friction and wear-related energy and material losses. According to these definitions, all kind of mining or excavation works and drilling processes are part of tribology.

The first chapter (2.1.1) in this section is about tribology in TBM tunnelling, the second chapter (2) about contact mechanics. Abrasion is amongst others one of the main mechanisms recognized in tribology literature (RABINOWICZ 1965; CZICHOS 1978; STACHOWIAK & BATCHELOR 2005) and a special wear type caused by material loaded against particles having equal or greater hardness (STACHOWIAK & BATCHELOR 2005). This is typically experienced in TBM applications. This is the reason for a special chapter for abrasivity in TBM tunnelling (chapter 2.1.2). The next chapter (2.1.3) covers wear which is caused by abrasivity of minerals and rocks. The last chapter of this section (2.1.5) discusses the basic laboratory tests for breakability and performance models.

2.1.1 Tribology in TBM tunnelling

As tribology is a multi-disciplinary subject combining many different scientific disciplines, including studies of lubrication, friction and wear of materials, it has to be considered in TBM tunnelling (ESPALLARGAS et al. 2015). Tribology wants to describe or summarize all influencing factors on the wear process in a specific system (CZICHOS et al. 1995) and it can be concluded that wear is a system-dependent and not a material dependent property (ZUM GAHR 1985). KÜPFERLE et al. (2017) shows the tribological system for a generalized

TBM tool with its four main components, based on DIN 50320 (1979) and DETERS et al. (2002):

- **Main body**: tool mounted on the cutter head
- **Counterbody**: tunnel face or quarried ground
- **Surrounding** or **intermediate media**: air, water, conditioning media, rock dust and rock flour
- **Load spectrum**: controlled by machine advance data (e.g. penetration rate, rotational speed), that define the contact forces and velocities impacting on the tools

The previous Fig. 1 on page 6 gives a schematic overview of the cutting process during rock excavation with disc cutters in hard rock. In addition to the original model from ROSTAMI (1997) our model indicates the tribological system with main body, counterbody and sorrounding / intermediate media. According to ZUM GAHR (1985), not only knowledge about each system component is important, also the interactions between the components during the wear process are necessary to analyze and represent the tribological system. This provides the basis for a successful and significant wear prediction.

TBM and cutter head design

Recent studies show that in addition to the tools used also the cutter head design may influence the tool wear (MACIAS 2016; GENG et al. 2017; CHEN et al. 2018). Fig. 2 illustrates different design cases of the disc cutter layout with different patterns which can be contemplated and are already in use today. Previous studies (HUO et al. 2009, 2010, 2011; SUN et al. 2011; ZHANG & QIAO 2011; GENG et al. 2013) mainly looked at the cutterhead force balance, but there is hardly any literature on the influence of cutter layout on cutter consumption. Some authors (HUO et al. 2009, 2010, 2011; SUN et al. 2011) tried an optimization based on different algorithms. They used a series of multi-objective optimization algorithms like the genetic algorithm, the ant colony algorithm and the cooperative evolutionary algorithm to optimize the layout of TBM disc cutter patterns. GENG et al. (2013) proposed a cutter layout optimization approach based on the Grey relational analysis (GRA) method. Here, the cutterhead force balance is improved by adjusting the cutter position angles. ZHANG & QIAO (2011) used a comparison between the cutterhead eccentric force and overturning moment of a multi-spiral layout pattern with different spirals. Simulations and empirical studies by CHEN et al. (2018) show an improvement by arranging the tools in a double helix after the Archimedes spiral theory.

GENG et al. (2017) investigated the ideal cutter position on the cutter head. They found out that the relatively lowest consumption rate is at the relative cutter position of about 0.4 times viewed from the center. This means the rock cutting conditions are the best around this position for the cutter consumption. Due to the small radii and the concomitant severe sliding in the inner positions, the consumption rate of the inner cutter positions in the face is higher. On top of that, the side sliding movement of a disc cutter on a small radius kerf is obviously

larger than a cutter on a larger radius kerf. GENG et al. (2017) indicates that the cutter sliding is proportional to the square of the cutter radius and inversely proportional to the position radius. Based on this relationship, the diameter of the center cutters is sometimes chosen smaller than the face cutters in order to reduce the side sliding. In the outer regions, the higher cutter consumption may be due to higher rolling speeds. This is associated with higher impact loads and higher temperatures. Moreover, the outer cutters, especially the gauge cutters, are moving in rock debris, which inevitably accumulates at the bottom of the gap between the rock face and the cutter head to a certain part. Both effects lead to a higher wear of the cutters in the outer regions. Despite these remarks, it is remarkable, that major TBM manufacturers like Herrenknecht seem to use completely different layout algorithms for their TBMs.

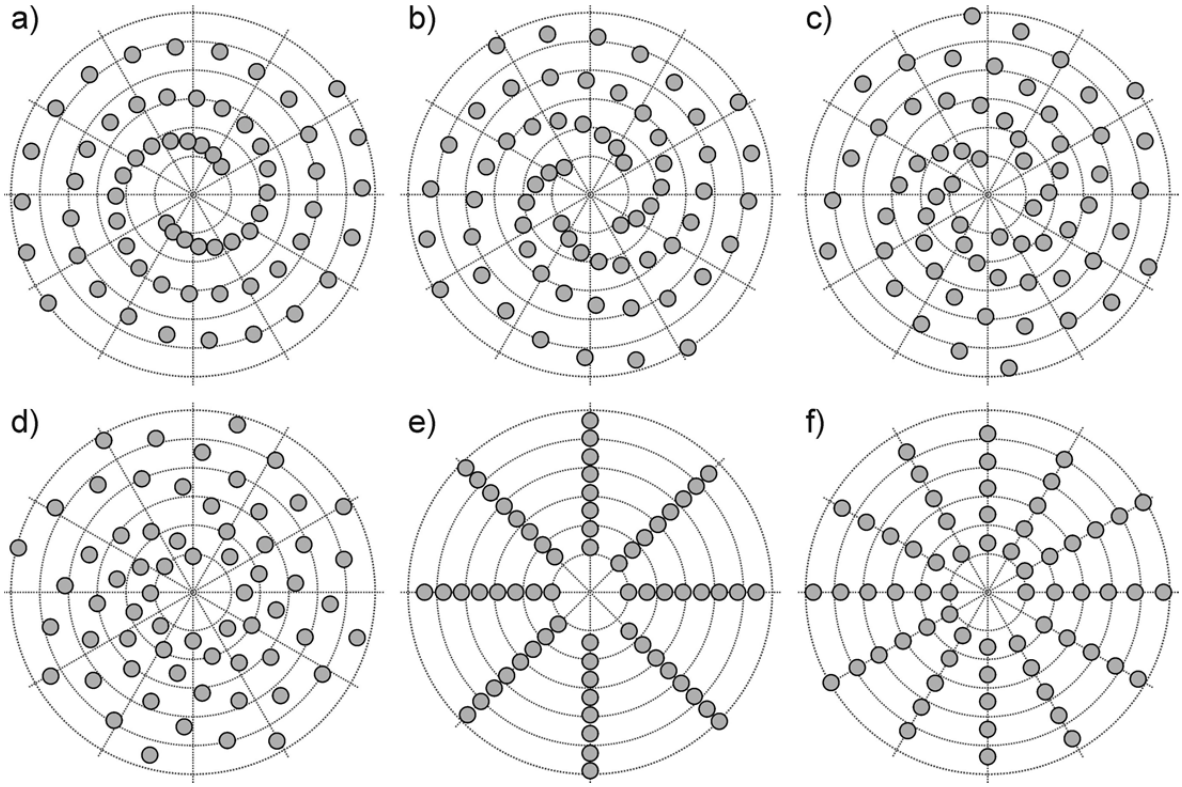

Fig. 2: Design cases of the disc cutter layout with different patterns:
a) 2-spiral; b) 4-spiral; c) 6-spiral; d) 8-spiral; e) 8-star; f) 12-star
(mod. after GENG et al. 2017).

Influence of the used material

The materials used for disc cutters in hard rock TBM tunnelling have a great impact on wear and the advance rate. The disc cutter steel has to counteract indentation and material removal by the abrasives as well as catastrophic failure due to a brittle material behavior in the case of an impact load (RÖTTGER et al. 2015). To fulfill these requirements, wear resistant materials should feature simultaneously a high hardness and a sufficient toughness including high fracture toughness and high fatigue resistance. A high hardness does not automatically provide a high wear resistance. KÜPFERLE et al. (2015) tested different types of steel with a

very similar hardness in the LCPC test. Despite the same material hardness, different abrasivity values were determined and the material with the highest hardness did not simultaneously have the lowest value. The explanation for this effect was the strong influence of the microstructure, which must also be considered in wear processes.

In hard rock TBM tunnelling, hot work tool steels like X40CrMoV5-1 (1.2344) and X50CrMoV5-1 (1.2345) are commonly used, regardless of the manufacturer (RÖTTGER et al. 2015; KÜPFERLE et al. 2016a; GENG et al. 2017). Typical compositions of both steels are given in Tab. 1. The hardness and the toughness of the two steel types are adjusted during heat treatment to provide high tool durability. The temperatures for quenching and tempering have to be chosen with respect to the respectively alloying concept and the expected ground conditions. The tempering temperature is customarily selected such that the region of secondary hardening is reached to provide high material hardness and toughness (KÜPFERLE et al. 2016a).

Tab. 1: Mean composition of important steel grades (according to www-01 and www-02).

Label	Number	Elements [wt.%]							
		Fe	C	Si	Mn	Cr	Mo	V	Other elements
X40CrMoV5-1	**1.2344**	90.5	0.4	1.0	0.4	5.2	1.3	1.0	0.2
X50CrMoV5-1	**1.2345**	90.6	0.5	1.0	0.3	5.0	1.4	1.0	0.2

Tab. 2: Average compostion of H13 tool steel used for hard rock cutter rings (according to ESPALLARGAS et al. 2015) which corresponds to X40CrMoV5-1 (1.2344) steel.

Label	Number	Elements [wt.%]								
		Fe	C	Si	Mn	Cr	Mo	V	Cu	Ni
X40CrMoV5-1	**1.2344 / H13**	90.8	0.6	0.9	0.3	4.8	1.3	0.9	0.1	0.1

In addition to own experience, ESPALLARGAS et al. (2015) and GENG et al. (2017) also came to the conclusion that there is a great reluctance from the cutter disc manufacturers to provide information about the composition of the cutter ring material. ESPALLARGAS et al. (2015) analyzed in their study with the help of XRF measurements a referenced AISI H13 tool steel used as a basis for hard rock cutter rings. The H13 steel corresponds to the X40CrMoV5-1 (1.2344). Their measurements indicate an average composition given in Tab. 2. Microstructural analyzes revealed that the steel is a typical tempered martensite with some lighter colored areas of retained austenite. By die-forging and heat treatment, a high hardness of approx. 639 VH (Vickers Hardness) was achieved (ESPALLARGAS et al. 2015). From these

values, the authors deduced that the steel was air-cooled from a temperature of about 1,000 °C and then tempered at about 500–550 °C.

Martensite is formed by a rapid quenching of steel. Tempering of the martensite is necessary to reduce its brittleness and reduce stresses. Tempering is therefore a heat treatment in which a material is heated in a targeted manner to influence its properties. Retained austenite is a phase that was not converted during quenching of steel. Due to its instability and other problems, retained austenite is undesirable.

The alloying elements have a decisive influence on the properties of the steel. The X40CrMoV5-1 steel and the X50CrMoV5-1 steel are closely related and behave similarly. The now following data and properties are taken from REINERT & SCHUBERT (n.d.) and ESPALLARGAS et al. (2015). The chromium (Cr) content improves mainly through hardening. Chromium also increases wear resistance, tensile strength, hardness and may provide some protection against corrosion. Molybdenum (Mo) increases hardenability, high-temperature strength, wear resistance and provides protection against chloride penetration (pitting). Vanadium (V) and also nickel (Ni) give the steel increased hardness, strength, resistance to impact loads and contributes to grain refinement. The carbon (C), silicon (Si) and manganese (Mn) will contribute to hardness and wear resistance on the one hand but will reduce ductility on the other hand. According to ESPALLARGAS et al. (2015), X40CrMoV5-1 and X50CrMoV5-1 steel represent a good balance between hardness and ductility/toughness concerning its heat treatment and the alloying elements. The two steel types also should exhibit some degree of protection against corrosion.

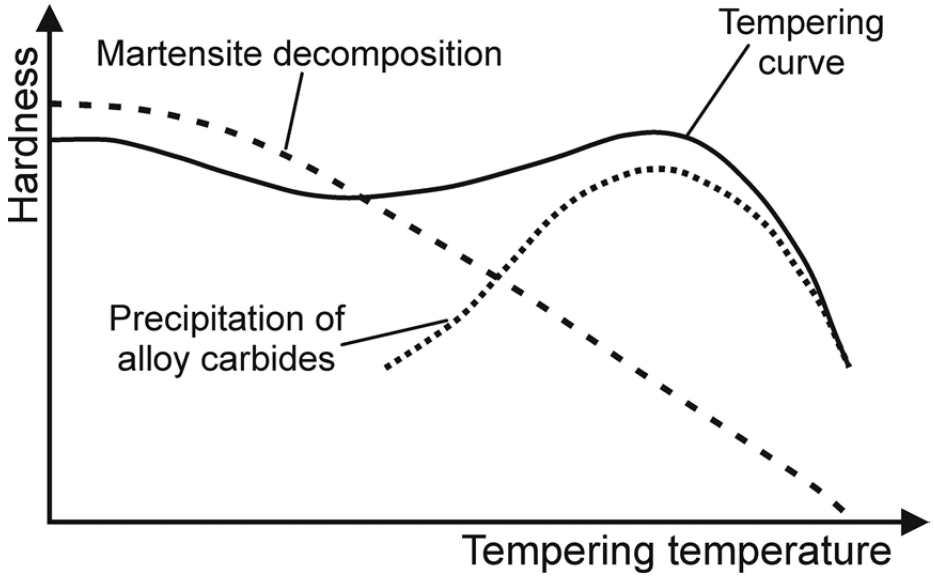

Fig. 3: Schematic tempering diagram of a typical hot work tool steel with additional martensite decomposition and precipitation of alloy carbides to illustrate secondary hardening (mod. after www-03).

Generally, it can be stated that the quench and temper process is based on the carbon content and the time temperature transition-characteristic (forming martensite, bainite, perlite, …). Thus, quenching is performed in water, oil or with gas. The subsequent tempering reduces hardness but increases toughness. For hot work tool steel, tempering is performed in the regime of secondary hardening with a temperature of about 500 to 550 °C (RÖTTGER et al. 2015; USTINOVSHCHIKOV 2013). Secondary hardening means an increase in hardness promoted by the precipitation of fine alloy carbides (see Fig. 3). For higher tempering resistance of hot work tool steel, a stronger secondary hardening (meaning more intense carbide precipitation) is necessary. The precipitation intensity depends on the amount of alloy elements. For hot work tool steel, it is common to temper twice (in the case of HSS steel three times) to transform the retained austenite into annealed martensite.

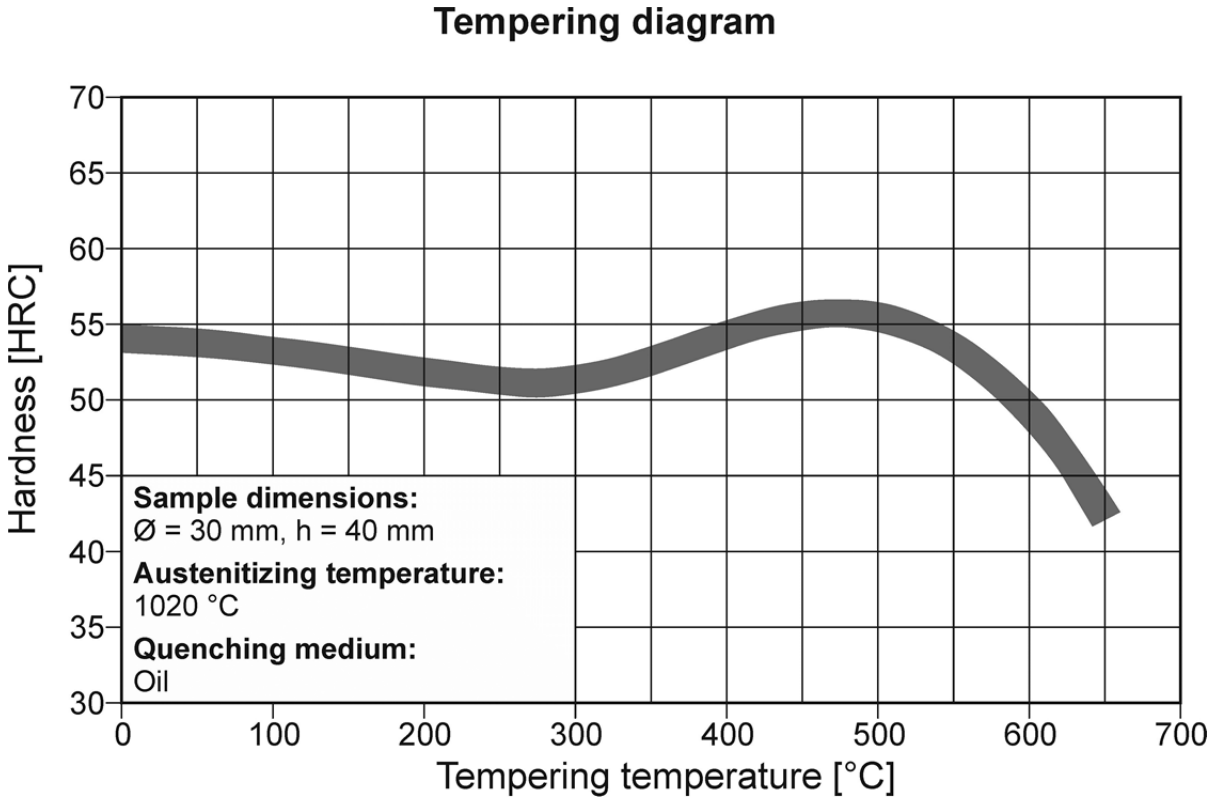

Fig. 4: Example of a tempering diagram based on a X40CrMoV5-1 / H13 steel. The martensite decomposition and precipitation of alloy carbides can be well distinguished (mod. after www-04).

The procedure of a typical quench and temper process explains RÖTTGER et al. (2015) exemplarily for the X40CrMoV5-1 / H13 steel (Fig. 4). For further details on the heat treatment of steels see BERNS & THEISEN (2008). Directly after quenching, this steel possesses high hardness due to a full martensitic microstructure. A first quenching (100 to 200 °C) increases toughness and decreases hardness. If the steel would be tempered at temperatures of about 300 and 500 °C, a strong decrease on toughness would result. The authors propose that the embrittlement effect at 300 °C can be traced back to the formation of cementite (blue

brittleness). An embrittlement at temperatures of about 500 °C (temper embrittlement) may occur due to the segregation of the elements phosphor (P), antimony (Sb), tin (Sn) and arsenic (As) at grain boundaries, thus promoting a brittle intergranular crack propagation (BERNS & THEISEN 2008). Knowing this, tempering has to be chosen with respect to these regions where blue brittleness or tempering embrittlement can be avoided. However, an increase in hardness (secondary hardening) is achieved by a tempering temperature of about 450 °C. The highest hardness with about 55 HRC is reached by a temperature of about 530 °C. At even higher temperatures, the hardness drops very quickly. This increase in hardness can be traced back to carbide formation. The microstructure consists here of an annealed martensite metal matrix with finely distributed secondary carbides. Based on the aforementioned relationships, highest hardness/strength and high toughness simultaneously can be achieved by quenching and tempering at temperatures of 500 to 550 °C. But it has to be mentioned that the heat treatment of steels is more complicated than represented. Secondary hardness and regions of embrittlement are strongly influenced by the alloying concept and the quenching temperature, for example.

As already mentioned, the microstructure of wear-resistant materials has to contain hard phases which represent the carriers of hardness (BERNS & THEISEN 2008). The hard phases must have a higher hardness compared to the abrasives and are mostly carbides, borides, carboborides and nitrides (RÖTTGER et al. 2015; KÜPFERLE et al. 2015). These are excreted primarily or eutectically by a modified alloy design, consisting of the metalloids (C, B and N) and additions of hard phase forming elements (e.g. Cr, Mo, W, Nb, V and Ti) during the solidification of metallic melts (ZUM GAHR 1987). In order to provide sufficient wear protection, these hard phases must be adapted to the attacking abrasives in terms of morphology, size, hardness and fracture toughness (KÜPFERLE et al. 2015). Cr-rich hard phases of type M_7C_3 are of high interest, characterizing the basic systems Fe-Cr-C. The M_7C_3 hard phases possesses a high hardness (M_7C_3~ 1500 to 2200 VH0.05) effecting a sufficient resistance against abrasion (RÖTTGER et al. 2015). In some special cases, hard composites or hard metals with a content of 75 to 96 % by volume are used to achieve a sufficient wear resistance (BERNS 1998).

2.1.2 Contact mechanics

In order to be able to describe the interaction between the disc cutters and rock, the mutually acting forces have to be investigated and described. This happens within the framework of contact mechanics. The stress under the disc cutters can be shown roughly simplified with the Rostami model (ROSTAMI 1997) on Fig. 5 which underlies the understanding of the general excavation process with disc cutters in hard rock (Fig. 1). This simplified model distinguishes between three forces: normal force (F_N), rolling force (F_R) and side force (F_S). However, this model is only an oversimplification of reality, as, for example, influences of the surface such as roughness are not taken into account.

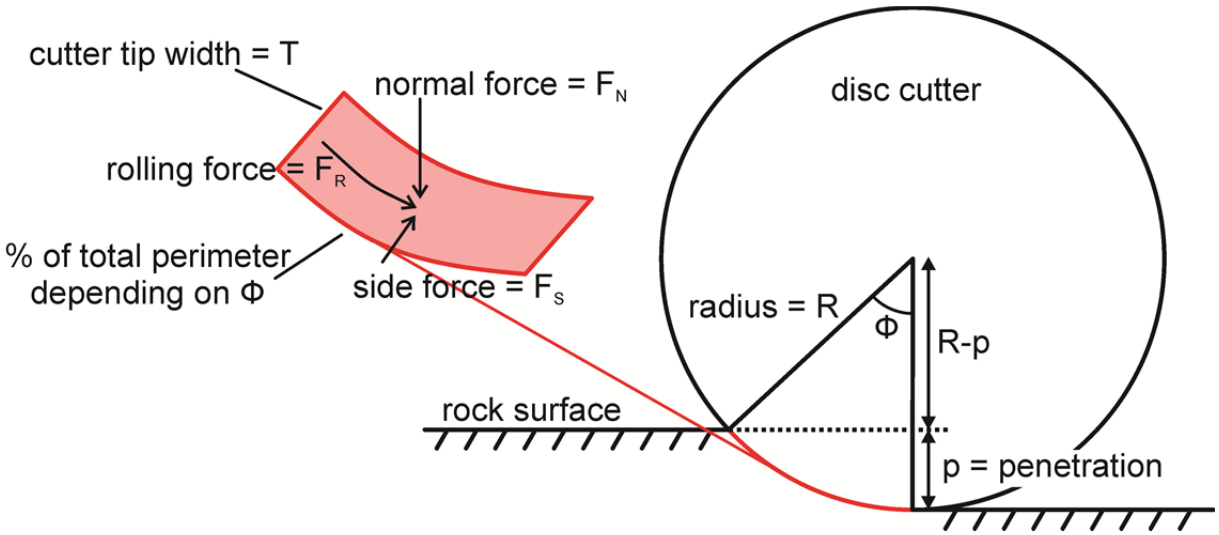

Fig. 5: Schematic figure of the contact area between the disc cutter and the rock face with the acting forces. The contact area is calculated with the cutter tip width T and a certain percentage of the total perimeter depending on the angle of contact Φ (based on ROSTAMI 1997: 38).

As even mentioned, the indentation into the rock mass with disc cutters takes place under sudden stress peaks (WILFING 2016). The reason is that this type of excavation process is not a continuous process because of an irregular rock surface leading to a high variation of cutter load during the excavation. In combination with high penetration rates and high rolling velocities of the cutter rings, especially in the outer regions of the cutter head, very high contact stresses arise at the cutter tip and high Hertzian stresses are introduced into the ground (RÖTTGER et al. 2015). Thereby, maximum stresses are formed below the mineral which interacts with the disc cutter. The high stresses lead to crack formation in the rock face. The formation of a conical crack (Hertzian crack) at the cutter edge is proven by GONG et al. (2005). This agrees with the theory of contact mechanics between a rigid indenter and brittle material. A detailed analysis of the stress distribution in discs cutters during tunnelling can be gathered from the work of ROSTAMI (2013).

MIRKOWSKA et al. (2016) and POPOV (2015) give a good overview of this topic in the following part of this chapter. Unless stated otherwise, the following information comes from one of the two sources.

Hertzian theory of non-adhesive elastic contact

Generally, non-adhesive contacts can be divided into two types: nonfrictional and frictional. In the case of non-frictional contact, the contact force is purely normal to the contact interface. In frictional contacts, a lateral shear and frictional forces also act in addition to the normal force. Apart from the non-frictional contact of two smooth surfaces, frictional contact is a highly non-equilibrium situation (URBAKH et al. 2004). The excavation with disc cutters can be assigned to frictional contacts. But that is only part of the truth; also, other distinctions for contacts can be made:

- Contacts without mechanical deformation
- Contacts with elastic/plastic deformation
- Contacts of smooth surfaces
- Multiple asperity contacts

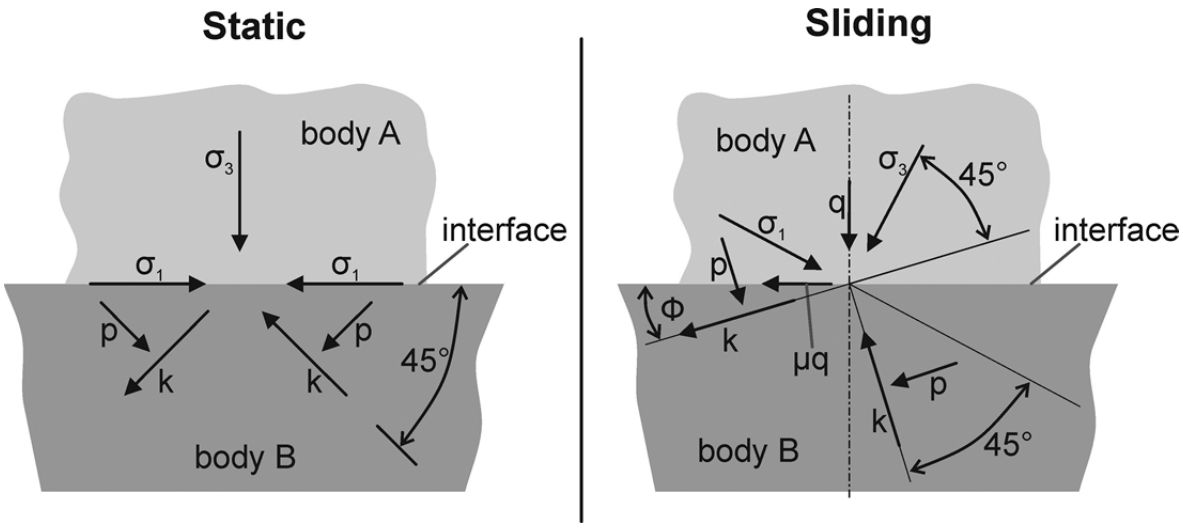

Fig. 6: Stresses during Hertzian contact: static and sliding; σ1 and σ3 are the main stresses, p is the hydrostatic pressure, k the shear yield stress of the material, μ the coefficient of friction, q the stress normal to the interface or compressive stress due to load, Φ the angle by which the principal planes are rotated from the corresponding zero friction positions to balance the frictional stress (mod. from STACHOWIAK & BATCHELOR 2005).

The model of Hertzian contacts (HERTZ 1881; STACHOWIAK & BATCHELOR 2005) is one of the most accepted and applied models to describe the contact of two solids. The Hertzian contact model defines a static (point or linear) and non-frictional contact between two homogenous, smooth bodies at rest and in equilibrium (STACHOWIAK & BATCHELOR 2005). In the classic case of a Hertzian contact, a rigid sphere penetrates into an elastic half-space. The

results of Hertz's theory can also be applied to the following cases with minor modifications: for two elastic bodies with a curved or straight surface, two opposite cylinders and a rigid conical indenter penetrating an elastic half space. It is possible (except for equilibrium) to consider rolling and sliding as a sequence of consecutive static point contacts except in the case of the penetrating indenter. Stresses appearing during a Hertzian contact of two bodies at a smooth interface are illustrated in Fig. 6 and Fig. 7.

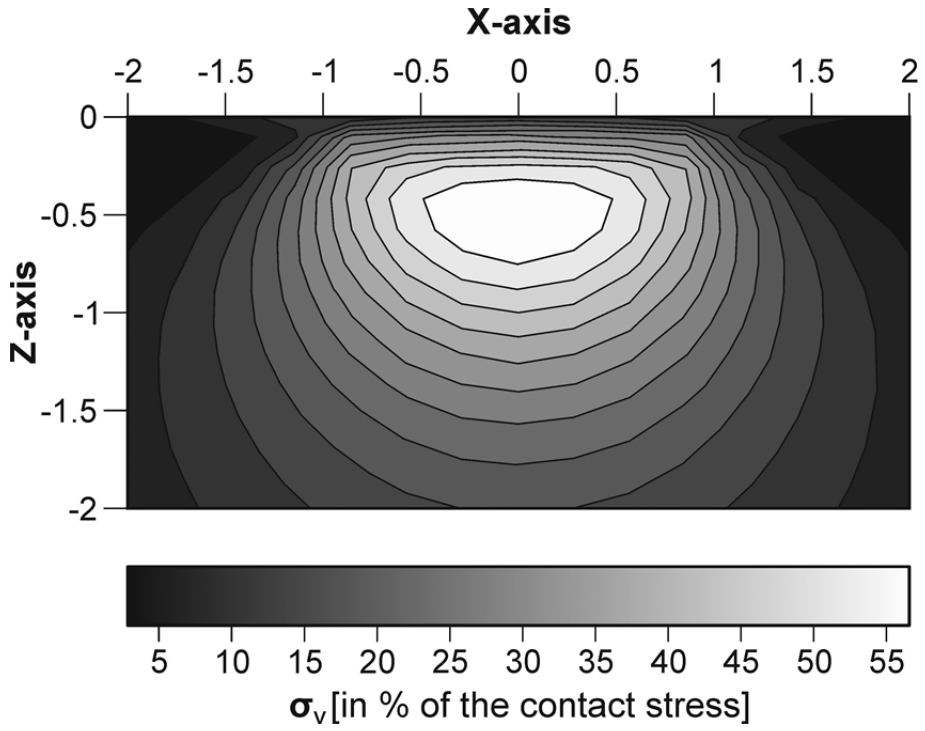

Fig. 7: Subsurface stress field for a static contact during Hertzian stress. The figure illustrates the stress distribution in the xz-plane (mod. after POPOV 2015: 7; MIRKOWSKA et al. 2016).

Without a relative movement between two bodies and only a static load, shearing does not occur. If the contact load is sufficiently high, i.e. in the elastic deformation regime, the material slips along the line of action of maximum shear stress, which is at 45° to the plane on which the shear stress is zero (the principal plane). An increase in the loads leads at a certain point to plastic deformation under the surface of the material (STACHOWIAK & BATCHELOR 2005). The largest shear stress occurs at the same depth as the maximum depth of the plastic deformation for a given load (Fig. 7). This value is in turn related to the contact area. In a circular static contact, for instance, the maximum shear stress occurs at a depth of approximately 0.6 times the radius of the contact area (STACHOWIAK & BATCHELOR 2005). For rolling and/or sliding, additional shear stress acts at the contact interface due to the frictional forces. In addition, the contact surface increases during friction contacts compared to static contacts. The additional shear thus changes the Hertzian stress field.

Contact loads lead to mechanical deformation of the materials used due to compressive stresses. This results in a deformation or even a rearrangement of the object atoms

(NAKAYAMA & MARTIN 2006). The interlayer spacing of the atoms are reduced along the direction of the contact load where compressive stress is acting while expansions take place in the other direction, e.g. where tensile stress dominates. Such a change of the lattice parameters of the crystal unit cell alters the electronic properties of the deformed area of the object. Examples of such a change are band gaps, different work functions and a different surface conductance. With an analysis of the changed parameters, the acting forces can be deduced.

A special significance has Hertzian stress when a high cycling contact load is present. This induces high shear stresses under the surface, whereby the maximum of these shear stresses depends on the particle size and the load. If these formed shear stresses under the tool surface are overlapping with microstructural defects like oxide inclusion, crack formation and propagation can occur, which is the well-known materials removal mechanism in component parts like bearings (WARREN et al. 1995).

Multi-asperity contacts

Surface roughness has a strong influence on all aspects concerning contacts between two or three bodies. Especially the contact through asperities (roughness peaks) is the most probable type of contact (BHUSHAN 2000), since all surfaces exhibit some roughness. The reason is that roughness limits the contact between bodies to small areas of true contact between the highest spots of the surfaces (Fig. 8). This is also called a “multi-asperity contact”.

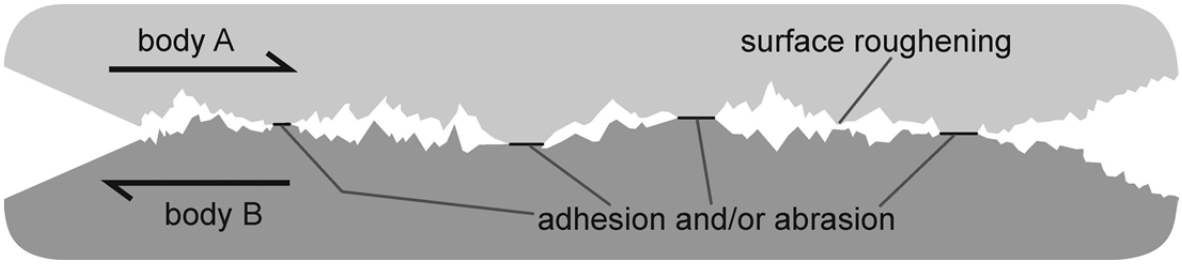

Fig. 8: Schematic illustration showing the influence of roughness. The relative motion between body A and B results in touching of asperities with a possibly occurring adhesion or abrasion (mod. after STACHOWIAK & BATCHELOR 2005).

Real surfaces are normally randomly rough. The simplest way to model such a non-regular area was suggested in 1966 by J.A. Greenwood and J.B.P. Williamson (GREENWOOD & WILLIAMSON 1966). The model of Greenwood and Williamson is based on the assumption that all asperities have the same radius of curvature, but the heights are stochastically distributed around a middle level. At a sufficient distance between two touching asperities, their deformation can be considered as independent of each other. Consequently, only the height distribution of the asperities is important, the respective position of the asperities (under the said assumption) has no influence.

Between contacts of flat surfaces and contacts through asperities, three important differences have to be mentioned: The first point is that the contact path of the asperity may be much shorter than the total path of rubbing (KNORR 2011) and thus the true contact area would be very different from the macroscopic contact area. Secondly, the contact pressure is much higher than that the pressure calculated by simple division of the contact load by the total contact area. This effect causes stronger deformation of the asperities (flattening) in softer material than expected (LABADZ & LOWELL 1991; STACHOWIAK & BATCHELOR 2005). The third point concerns the electric field which is enhanced at the asperities causing a stronger charging (ZHANG & SHAO 2013).

Equation 1: Calculation of the plasticity index ψ.

$$\psi = \frac{E \cdot \nabla z}{\sigma_0}$$

with:	ψ	*Plasticity index*	*[-]*
	E	*Young's modulus*	*[Pa]*
	∇z	*Roughness coefficient*	*[-]*
	σ_0	*Material hardness*	*[Pa]*

The model of Greenwood and Williamson (GREENWOOD & WILLIAMSON 1966) provides a formula that can be used to calculate if the asperities are in the elastic or plastic state (Equation 1). This is done using the plasticity index ψ [-] introduced by GREENWOOD & WILLIAMSON (1966). If ψ is bigger than 2, meaning the pressure is remarkable higher than the hardness σ_0, all asperities are in a plastic state. For ψ <2/3 the surface behaves elastically on contact. Thus, it could be shown that the applied normal force is not decisive whether the system behaves elastically or plastically. The roughness coefficient ∇z represents the root mean square gradient of the surface profile (for a precise calculation of ∇z, see POPOV 2015: 105). Experiments showed that almost all contact points on ground surfaces are in the plastic state, while highly polished surfaces almost result in almost pure elastic deformations. But it has to be mentioned that the slope ∇z generally depends on the resolution with which the surface is measured, since it is scale dependent.

However, it should be noted that the theory named by GREENWOOD & WILLIAMSON (1966) loses its validity as soon as the stress in the contact area becomes very large. In the highly plastic state, the material deforms in the contact areas until the compressive stress reaches the hardness of the material (Equation 2). It follows that the contact surface is also proportional to the normal force in the plastic range. STACHOWIAK & BATCHELOR (2005) found out that the contact between rock and tool occurs mostly in an elastic regime in mining processes. After an initial elastoplastic deformation, the asperities keep their shape and react afterwards mostly elastic.

Equation 2: Calculation of the contact surface A.

$$A \approx \frac{F_N}{\sigma_0}$$

with:	A	*Contact surface*	*[m²]*
	F_N	*Normal stress*	*[N]*
	σ_0	*Material hardness*	*[Pa]*

As the excavation process with disc cutters is not continuous in terms of the place and the forces (due to rolling, always another part of the tool has contact with the rock face), the local contact pressure between asperities which are constantly coming in and out of contact during shearing vary significantly. According to URBAKH et al. (2004) the pressure varies within microseconds between 1 Pa und 1 GPa, depending on the Young's modulus of the materials and the asperity geometry (STACHOWIAK & BATCHELOR 2005). This can possibly lead to an overload of the material, also due to fatigue. There are several models describing multi-asperity contacts based on both statistical methods and fractal geometry. An overview is given in (STACHOWIAK & BATCHELOR 2005).

Overall, it can be assumed that both static and sliding (dynamic) contacts, including all possible intermediate stages, occur during mining with disc cutters. But it is assumed that fundamental differences in structure and physical processes occur for static and sliding contacts (STACHOWIAK & BATCHELOR 2005). Static contacts between two rough surfaces can be seen as a random distribution of point contacts. For sliding contacts, the contact areas are normally larger and less numerous. This results in a larger distance between individual contact points when the surfaces are in motion. Moreover, only larger asperities survive mechanically during sliding and their contact areas increase due to the movement (STACHOWIAK & BATCHELOR 2005). According to this, the local contact pressure for a single asperity can differ between static and sliding contacts despite of the same total load and number of asperities

Friction, adhesion and wear

Friction, adhesion and wear are strongly correlated with each other. Local adhesion can result in a stick-and-slip motion of two bodies (URBAKH et al. 2004). In this context, friction is defined as the dissipation of energy between sliding bodies and obeys to empirical rules which are (STACHOWIAK & BATCHELOR 2005): There is a correlation between the maximum tangential force and the normal force and the frictional forces do not depend on the contact area and the sliding speed. Fig. 8 on page 19 illustrates schematically the rough surface of two bodies in relative motion. The contact area of two opposite lying and touching asperities in which local adhesion and/or abrasion can occur is marked. It has to be noted that adhesion is typical for two steel bodies (similar hardness) while abrasion is characteristic for the pair rock and steel (different material hardness). In the stick-and-slip motion, adhering areas are successively formed and broken (mainly in steel). This is the reason for the discontinuous

movement of two bodies in frictional contact. However, it should be noted that roughness can significantly reduce the adhesion. This result in a general rule: the rougher a surface, the lower the macroscopic adhesion. In return, the smoother a surface is, the larger the adhesion forces. However, it has to be taken into account that wear on disc cutters predominantly occurs due to abrasion and that adhesion is only of secondary importance.

Experiments have shown that during contact, adhesion of two dissimilar materials (rock and steel) in dry atmosphere is much higher than the adhesion of similar materials (two steel bodies). This can be due to different material hardness as well as physical properties such as lattice parameters and charges. Within a change of the humidity, the interaction of the surfaces also changes. This is due to the formation of a thin water layer which changes adhesion and friction. Experiments have even shown that the shear stress decreases dramatically with increasing humidity (MCGUIGGAN 2008). In a customized application, a reduction of wear is possible.

Regarding the wear processes of TBM disc cutters, it is recognized that friction leads to wear and that friction and wear have a narrow correlation. In addition to the macroscopically visible wear, however, the plastic deformation and abrasion of microcontacts also plays a decisive role. Concerning TBMs, wear is considered an undesirable phenomenon. But wear can also be the basis for various technological processes such as grinding, polishing or sandblasting. Though, this is not part of this thesis and therefore will not be considered further. If asperities come together, the stress in the microcontact regions reaches the dimension of the materials indentation hardness σ_0. Hardness therefore has a decisive influence on wear.

In the case of abrasive wear TBM tunnelling, asperities (roughness peaks) of the harder material penetrate into the softer material and cut it. The harder material is normally rock containing hard minerals like quartz and feldspar. The weaker material is usually the steel of the cutter ring. Grooves running in the sliding direction are a feature of abrasive wear. Experiments have shown that the worn volume is proportional to the normal force, the covered distance, and inversely proportional to the hardness of the material. Further considerations of wear can be found in chapter 2.1.3.

2.1.3 Abrasivity

Based on DIN 50320 (1979), abrasivity means the progressive loss of material from the surface of a solid (body) caused by mechanical processes, e.g. movement during contact and friction of a solid, liquid or gaseous counter body. Simplified, the term abrasiveness means the property of causing abrasive wear on the friction partner (KÄSLING 2009). Applied to the wear process of a TBM, abrasivity is the local material loss from the surface of the tool that is caused by mechanical contact and relative movements of the tool to the rock face (PLINNINGER 2002) – it is therefore a rock property. Abrasion can be provoked by grinding, rolling, beating or scratching processes and is explained in more detail in the next chapter (chapter 2.1.3). But rock abrasiveness is not an absolute material property; it has to be referred to the type and characteristics of the respective excavation tool.

Important abrasivity tests

In order to determine the abrasiveness and to be able to make predictions about the expected wear, a wide variety of laboratory tests are carried out today. Some researchers developed in the last decade studies for classifying rock abrasiveness (PLINNINGER & RESTNER 2008; THURO & KÄSLING 2009; DAHL et al. 2012). PLINNINGER & RESTNER (2008) present an overview of the most important and representative testing and classifications methods. A comparative study was performed by THURO & KÄSLING (2009), using three methods for abrasivity assessments, introduced a classification system for rock and soil based on the mineral content, the CERCHAR abrasivity index and the LCPC abrasivity coefficient.

One of the best-known and most widely used laboratory tests for hard rock abrasivity are the CERCHAR (CERCHAR 1986; ALBER et al. 2014) and LCPC abrasivity test (AFNOR 1990; BÜCHI et al. 1995; THURO & KÄSLING 2009). In addition, there are the well-known but also very complex and expensive wear tests of the NTNU/SINTEF in Trondheim (Norway) with the Abrasion Value (AV) and the Abrasion Value Cutter Steel (AVS) (Tab. 3). On this basis, DAHL et al.2012 developed drillability test methods with statistical analysis and evaluations of the existing test results in the NTNU/SINTEF database (MACIAS et al. 2016).

A different approach than model testing is the determination of mineralogical parameters like the quartz content, the Equivalent Quartz Content (SCHIMAZEK & KNATZ 1970; THURO 1996) or the Vickers Hardness Number Rock (VHNR) (SALMINEN & VIITALA 1985). They are both based on the mineral content since the content of quartz and other hard and abrasive minerals normally has a significant influence on the rock abrasiveness (MACIAS et al. 2016). In addition to the characterization of abrasiveness, these indices are also used in some cutter life estimation models.

Especially for soil or soil based ground conditions, a few researcher developed methods and/or devices to test their abrasivity, which are based on so called ‘‘mixing soil methods”: (SGAT at the NTNU in Trondheim (Norway) (JAKOBSEN et al. 2013), PSAI at the Penn State University in Pennsylvania (USA) (GHARAHBAGH et al. 2011), Wiener Abrasimeter at the TU

Wien in Vienna (Austria) (DRUCKER 2011) and SATC at University Tabriz in Tabriz (Iran) (BARZEGARI et al. 2015). BARZEGARI et al. (2015) and KÜPFERLE et al. (2016b) summarized most of the developed apparatuses.

Tab. 3: List of important laboratory tests for measuring hard rock abrasivity (mod. after MACIAS et al. 2017b).

Test method	Index	Principle	Rock sample	Testing tool
CERCHAR test (1986)	CERCHAR abrasivity index (CAI)	Indenter (hard steel) moves over a rock surface	Intact rock sample	Steel stylus
LCPC test (1990)	LCPC Abrasivity Coefficient (LAC, ABR)	Impeller (medium hard steel) rotating in a vessel containing crushed rock	Crushed rock (4 – 6.3 mm)	Steel impeller
NTNU/SINTEF abrasivity (1960)	Abrasion Value (AV)	Tungsten carbide piece sliding over crushed rock	Crushed rock (<1 mm)	Tungsten carbide piece
NTNU/SINTEF abrasivity (1983)	Abrasion Value Cutter Steel (AVS)	Cutter ring steel piece sliding over crushed rock	Crushed rock (<1 mm)	Cutter ring steel piece
SCHIMAZEK & KNATZ (1970)	Equivalent Quartz Content (EQC)	Mineral content multiplied with grinding hardness	Intact rock sample/ crushed rock	Microscope/ X-ray diffraction camera
SALMINEN & VIITALA (1985)	Vickers Hardness Number Rock (VHNR)	Mineral content multiplied with Vickers hardness	Intact rock sample/ crushed rock	Microscope/ X-ray diffraction camera

With the CERCHAR abrasivity test (Tab. 3), the CERCHAR Abrasivity Index (CAI) is determined. This test was originally developed and presented by the Centre d'Études et Recherches des Charbonnages de France in the 1970s (VALANTIN 1974; CERCHAR 1986). In the test, the wear of a steel stylus on the tip is measured. The steel must have a Rockwell Hardness of HRC 55 (ALBER et al. 2014) or HRC 40 (ASTM D7625 2010). During the test, a rock specimen is held tight in the test aparatus while a sharpened steel stylus with a normal force of 70 N is scratched over a distance of 10.0 mm across the rock surface. The wear of the stylus tip is measured in units of 0.01 mm and calculated by multiplying it with the factor 10. Accordingly, the CAI is dimensionless. For a description of the exact testing procedure, see also Chapter 5.2.1.

The LCPC abrasivity test (Tab. 3) is performed to determine the so called LCPC Abrasivity Coefficient (LAC after THURO & KÄSLING 2009, ABR after BÜCHI et al. 1995). The testing principle was originally developed and presented by the Laboratorie Central des Ponts et Chaussées in the 1980s (AFNOR 1990). In this test, a rectangular impeller with dimensions of 50 × 25 × 5 mm, made of a Rockwell Hardness of HRB 60–75, rotates for 5 minutes at a speed of 4,500 rpm inside a cylindrical container filled with 500 g air-dried rock sample material with a grain size of 4 – 6.3 mm. The weight loss of the impeller is measured and

provides the basis for calculating the abrasiveness. For a description of the exact testing procedure, see also Chapter 5.2.2.

Slightly older is the idea of Abrasion Value (AV) (Tab. 3). This index was originally developed and presented by NTNU at the beginning of the 1960s. The Abrasion Value Cutter Steel (AVS) (Tab. 3) is newer and was introduced by NTNU at the beginnings of the 1980s. The AV and the AVS became known as the "Norwegian abrasion test methods" and represent a measure of rock abrasion or the ability of a rock to induce wear on tungsten carbide and cutter ring steel respectively (MACIAS et al. 2017b). The indices are time-dependent and determined measuring the wear on tungsten carbide and cutter steel caused by crushed and sieved (< 1.0 mm) rock powder. The AV index is defined as the weight loss of the test piece after 5 min testing (100 revolutions) of testing while the AVS index is defined as the measured weight loss of the test piece in milligrams after 1 minute (20 revolutions) of testing (MACIAS et al. 2017b).

The Equivalent Quartz Content (EQC) was introduced from SCHIMAZEK & KNATZ (1970) as a wear index for rocks. Using this method, the mineral content has to be quantified with the aid of a thin section analysis or an X-ray-diffraction (XRD) analysis. On this basis, each mineral of the respective rock is multiplied with its grinding hardness after ROSIWAL (1896, 1916), normalized on quartz = 100. To get the EQC, the proportion of the grinding hardness of each mineral of the rock is added up (THURO 1996). If the EQCEQC multiplied by the uniaxial compressive strength (UCS), you get the Rock Abrasivity Index (RAI) (THURO & PLINNINGER 2002; PLINNINGER 2002). Recent work with a detailed description of the method is given by THURO (1996, 2002) and PLINNINGER (2002). For a description of the exact testing procedure, see also chapter 5.2.3.

Similar to the EQC, the Vicker's Hardness Number Rock (VHNR) can also be calculated, based on SALMINEN & VIITALA (1985). The only difference is that not the grinding hardness but the Vicker's hardness of each mineral of the respective rock is used. A detailed description of this method gives BRULAND (1998b). If the VHNR is multiplied with the uniaxial compressive strength (UCS), you get the Abrasiveness Index (ABI), developed by HASSANPOUR et al. (2011, 2014) (see also chapter 2.3.7). Accordingly, the ABI is the equivalent of the Rock Abrasivity Index (RAI) in relation to the test with Vickers hardness.

Weaknesses of the tests

The disadvantage of every laboratory-scale experiment is the weak transferability to the application case due to implemented simplifications or adjustments (KÜPFERLE et al. 2017). It is very difficult to consider all systemically relevant components like the tool material, the rock, the ambient/intermediate medium and the load spectrum. The problems and weaknesses of the commonly used test methods are well known and discussed in literature (e.g. PLINNINGER 2002; KÄSLING 2009; ROSTAMI et al. 2014; KÜPFERLE et al. 2015; MACIAS 2016).

Related to the cutter wear of a hard rock TBM, rock abrasiveness cannot simply be considered as an intrinsic rock property. A full description of the phenomenon requires consideration of the complete tribological system, as well as rock properties (MACIAS et al. 2017a). Since none of the current laboratory test methods were originally developed for cutter wear assessment, they do not reproduce the wear behavior encountered during tunnel boring in a realistic way (MACIAS et al. 2016). Real cutting tests, as they exist at the Colorado School of Mines (CSM) in Golden (USA) for example (linear cutting test, OZDEMIR et al. 1977), contribute little to an improvement in terms of abrasiveness and wear. The reason for this is that these appliances were constructed for the research of rock-cuttability or rock-penetration but not for abrasivity or wear prediction. The rolling distance of the cutter for a good measurable and reproducible wear would simply be too high.

Each index test has its own vulnerabilities. As an example, the CERCHAR test is selected to explain some problems. Besides the well-known problems of subjective wear reading on the steel stylus tip, especially the mineral quartz is problematic. MACIAS et al. (2016) describe in their study that the real rock-abrasivity would be much higher than the CERCHAR results indicate. This is, however, a commonly experienced problem associated with CAIs in connection with testing of very hard rock types (MACIAS et al. 2016). The reason for this problem is due to the fact that the tip of the stylus is not able to fully penetrate quartz-rich rock or the surface of a single quartz grain. This results in a so called ‘‘skating effect’’ on the surface and hence in an underestimation of wear (ALBER et al. 2014; MACIAS et al. 2015).

In addition to the index tests, there is also the possibility of directly using rock properties for abrasiveness. These include the Equivalent Quartz Content (EQC) and the Vicker’s Hardness Number Rock (VHNR). The weak point using the EQC for example, only the grinding hardness of the minerals contained is taken into account, but not the grain binding, or rather the cohesion of the structure. THURO (1997) concluded that some types of rock like hydrothermally decomposed crystalline rock or sandstones, especially those with higher porosity and a poor binding, show only a low or even no correlation with drill bits life and the EQC (MACIAS et al. 2016).

Newer developments

Newer developments try to consider all relevant components like the tool material, the rock, the ambient/intermediate medium and the load spectrum. It is aimed at a particularly realistic model of reality. However, the reduced scale cannot be changed in most cases because 1:1 models would be too large, complex and expensive.

The latest index test for cutter life assessments in hard rock tunnel boring, developed and presented by MACIAS et al. (2016, 2017a) and MACIAS (2016) at the NTNU is called: Rolling Indentation Abrasion Test (RIAT). This index test uses two miniature rolling discs, rolling over the the surface of an intact rock sample and penetrate it. The mini cutters have a constant tip width and are made of a commercial alloy used as the basis of actual TBM cutter rings

(hot work tool steel: AISI type H13/X40CrMoV5-1 (1.2344)) and Rockwell Hardness HRC 50±1 (MACIAS et al. 2016, 2017a). A suitable drive unit provides the rotation, torque and vertical thrust during the test. The RIAT Abrasivity Index (RIATa) is defined as the weight loss (in mg) incurred by a miniature cutter ring during a RIAT test (MACIAS et al. 2017b). The RIAT Indentation Index (RIATi) is defined as the average value of ten evenly distributed measurements of cutter penetration depth (measured in 1/100 mm) (MACIAS et al. 2017b). It reproduces wear behavior on hard rock tunnel boring in a more realistic way than the traditionally used methods by introducing wear by rolling contact on intact rock (MACIAS et al. 2017a).

In contrast to the test methods used so far, the RIAT has some significant advantages. This is because traditionally used test methods for determination of rock abrasiveness uses sliding or impact contact to cause wear (MACIAS et al. 2016). The main advantages of the RIAT are: the wear is caused by rolling contact, which is closer to reality. Intact rock samples are tested and only relatively small samples are required. The test is cost-effective because it is a straightforward procedure that allows several samples to be tested. The indentation resistance of the rock and the rock surface hardness are measured simultaneously and in addition it is possible to perform tests under wet conditions, with slurry or additives ... (MACIAS et al. 2016). This test is also closer to real TBM excavation works because the mini discs have been developed according to actual TBM cutter ring standards (MACIAS et al. 2016). It should be noted, however, that the hardness of 51 HRC is slightly lower than in real cutter rings. The obtained initial results by the RIAT indicate a good ability to assess abrasive cutter wear for a wide abrasivity range of rocks, capable to evaluate rock abrasivity on TBM cutters as well as indentation in hard rock by rolling discs simultaneously (MACIAS et al. 2016, 2017a).

A special test for TBMs in soil was developed by KÜPFERLE et al. (2016b) at the Ruhr-Universität Bochum (Germany). It has the same approach as RIAT to model the tribological influences in a downsized version as realistic as possible. More detailed information is given in KÜPFERLE et al. (2016b, 2017).

2.1.4 Wear

As already mentioned at the beginning, movement leads to wear under normal circumstances. According to BOWDEN & TABOR (1951) and ZUM GAHR (1987), wear is the damaging, gradual removal or deformation of material at solid surfaces. According to PETRICA et al. (2013), wear can also be defined as the volume loss. When looking at a TBM, this is due to the abrasiveness of the rock to be mined. The wear is mainly controlled by intact rock properties such as petrography, physical or mechanical properties (HASSANPOUR et al. 2014) and operational factors (FRENZEL et al. 2008). For this purpose, the wear on a TBM can be divided into primary and secondary wear (FRENZEL et al. 2008; FRENZEL 2010). According to FRENZEL (2010), primary wear in hard rock TBM tunnelling is defined as the loss of material at the edge of the cutter ring due to direct contact with the construction ground. Secondary wear, in turn, is the loss of material on all other surfaces of the disc cutter caused by passing rock dust and rock debris (FRENZEL 2010).

According to POPOV (2015 303ff.), the following basic types can generally be distinguished, based on their physical degradation mechanism:

- **Abrasive wear:** two bodies with substantially different hardness are in contact, or the intermediate layer contains hard particles
- **Adhesive wear:** occurs mainly in contact between bodies of the same or similar hardness
- **Corrosive wear:** chemical modification of the surface and final removal of the surface layer
- **Surface fatigue:** the surface is removed by repeated gliding/rolling stress with each individual stress attack apparently leaving no noticeable changes on the surface

From a material technology view on the wear of TBM disc cutters, RÖTTGER et al. (2015) distinguishes only between abrasion, wear due to a brittle material behavior and loses of tools functionality due to strong deformation of the cutter head (blunting of the cutter head).

Abrasive Wear

Considering the tool wear in hard rock TBM tunnelling, abrasive wear has normally the largest share. THURO & PLINNINGER (2002), KÄSLING (2009) and ELLECOSTA et al. (2018, 2019) provide an overview of the typical forms of wear. There are 5 different basic types and 3 special shapes that can be distinguished (Tab. 4).

Tab. 4: Overview of the basic wear types occurring in hard rock TBM tunnelling (mod. after THURO & PLINNINGER 2002; KÄSLING 2009; ELLECOSTA et al. 2018, 2019).

Wear type	Description	Symbolic image
Abrasive wear	**Abrasive wear / normal wear** symmetrical and uniform material removal of the edge of the cutter ring	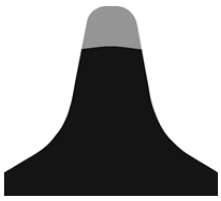
	Mushrooming plastic deformation of the cutter ring due to high contact forces – especially in the case of high-strength rocks	
	Chipping local overloads and inadequate heat treatment lead chipping	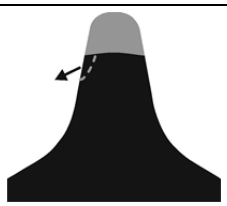
	Tapering abrasive wear and material flow to the side cause a sharpening – especially in the case of low strength rocks and loose rocks (also encountered in soils)	
	Asymmetric wear one-sided loads lead to asymmetric wear – especially on disc cutters in the caliber region	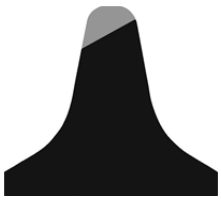
Special types	**Uniform wear** symmetrical material removal of the edge and shoulder of the cutter ring due to secondary wear (mainly encountered in soils)	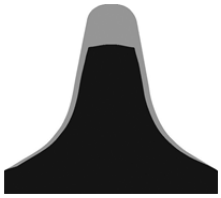
	Brittle fracture spontaneous and brittle fracture of the cutter ring or larger parts of it leads to a total failure of the disc cutter – mostly caused by incorrect heat treatment and high impact forces	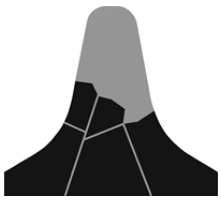
	Blockage asymmetrical and atypical wear due to the blocking of the roller bearing – caused by excessive mileage, high temperatures, incorrect lubricant or leakage of lubricant	

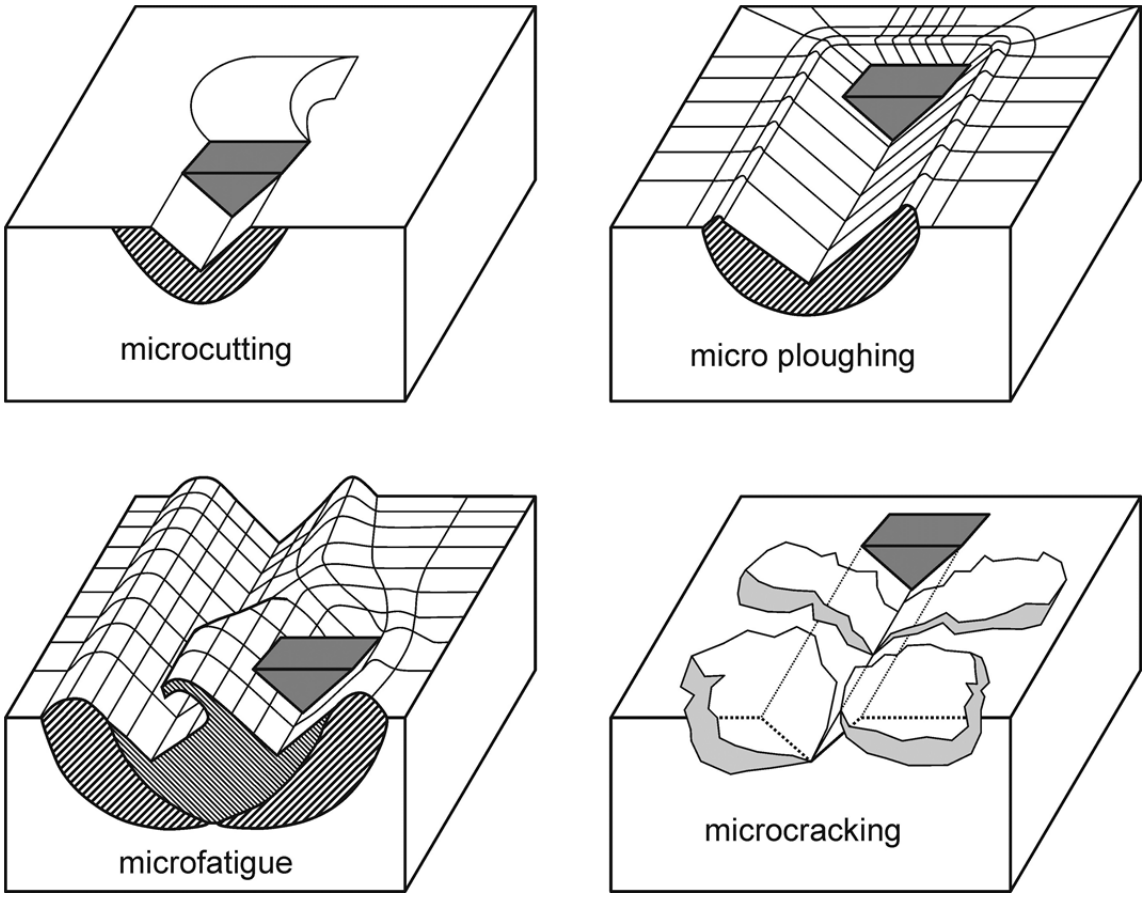

Fig. 9: Abrasive wear is typically divided into 4 basic microscopic mechanisms: microcutting, micro ploughing, microfatigue and microracking. The grey upside-down pyramid represents an abrasive particle (mod. after ZUM GAHR 1987).

In addition to macroscopic wear types, several different wear mechanisms can also be distinguished at the microscopic level. According to ZUM GAHR (1987), four different mechanisms can be distinguished (Fig. 9):

- **Microcutting:** the abrasive is significantly harder than the material of the tool, accordingly a groove is drawn in the tool surface and a chip is removed from it.
- **Micro ploughing:** the abrasive is harder than the material of the tool, but the material of the tool is so soft and deformable that when the groove is drawn with an abrasive particle, the material is displaced, and a wall is formed.
- **Micro cracking:** the abrasive is harder than the material of the tool, but the material of the tool is so hard and brittle that brittle fracturing occurs when pulling the trench with an abrasive particle.
- **Micro fatigue:** a constantly repeating, plastic deformation of the tool surface by a hard, abrasive material leads to a massive deformation and thus to embrittlement of the tool material over time, which promotes the removal of steel chips.

In general, abrasive wear must also be distinguished between two- and tree-body abrasion. According to ESPALLARGAS et al. (2015), two-body abrasion occurs when the harder particles or firmly held grits act like a cutting tool against a solid material while three-body abrasion occurs when the abrasive particles are free to roll and slide over the surfaces of two interacting solid materials. POPOV (2015) emphasizes that the abrasive particles are firmly embedded in the case of two-body abrasion, while in the three-body abrasion case they are part of the intermediate medium or even completely build it. An example of three-body abrasion in a TBM tunnelling context is the excavation of non-cohesive soils such as uniformly graded sands (ESPALLARGAS et al. 2015). In theory, hard rock excavation can be regarded as a two-body abrasion process, provided that the flushing and transport of rock chips and fines by the tunnelling system removes any loose particles prior to contact with the excavation tools (ESPALLARGAS et al. 2015).

PETRICA et al. (2013) concludes that some researchers developed models to describe two-body abrasion which arises due to the impact of abrasives to the surface concluding in sliding/scratching or embedment of the particles on the wearing surface (ZUM GAHR 1988; XIE & WILLIAMS 1996; MASEN et al. 2005; WHITTAKER & MATTHEWS 2004; TORRANCE 2005). However, these models are not sufficient as soon as there are freely moving particles between the two surfaces, as this is three-body wear. Two-body abrasive wear phenomena have been more extensively studied, although three-body abrasive wear is much more present in many industrial applications (PETRICA et al. 2013). PETRICA et al. (2013) further reports that there are wear rates for the three-body wear conditions that depend not only on the tested material but also on the test method itself (BADISCH et al. 2010; KATSICH & BADISCH 2011; ANTONOV et al. 2012). Accordingly, not only the respective materials but also the load and the mechanism are of decisive importance.

It is now recognized that the manner in which particles interact with the surface strongly influences the wear behavior because particles might roll and/or slide over the surface (PETRICA et al. 2013). According to this, the wear mechanism varies depending on the load and the type of loading. PETRICA et al. (2013) found out in experiments that under two-body conditions with granite, cutting and ploughing mechanisms are dominant due to particle impacts and a relative movement of the particles. RÖTTGER et al. (2015) confirm this wear mechanism and add that in reality hard abrasives are also indenting into the steel matrix and promote an elastic-plastic deformation of the disc cutter surface, accompanied by strain hardening.

Similar tests with meta-sandstones have shown that a mix of plastic deformation and particle embedment occurs. Using sandstones with a significantly lower strength, the tool showed an embedment of abrasives. PETRICA et al. (2013) were thus able to show that in the same experiment the strength of the rock has a clear influence on the wear mechanism. Experiments for three-body wear with the different abrasives have shown that the tool surface was heavily deformed (plastic deformation) due to scratching and grooving combined with multiple

indentations caused by rolling/sliding abrasive particles (PETRICA et al. 2013). Experiments with granite have even shown that the grooving on the tool surface is caused by hard quartz particles based on crushed granite (PETRICA et al. 2013). Moreover, it was possible to show that under three-body conditions the wear rate is lower than that under two-body conditions mainly due to this change of interaction between the particles and the surface (TREZONA et al. 1999; BADISCH et al. 2010; PETRICA et al. 2013).

Factors influencing wear

Since the development of full-face hard rock TBMs around 50 years ago, there have been numerous investigations into the causes of wear. GENG et al. (2017) provide a good overview of the most important works done so far: WIJK (1992), ROSTAMI (1997), BRULAND (1998a), WAN et al. (2002, 2003), MAIDL et al. (2008), YAGIZ (2008), FRENZEL (2011), HASSANPOUR et al. (2011), WANG et al. (2012), ALBER et al. (2014), WANG et al. (2015), MACIAS (2016) and MACIAS et al. (2016). These authors have all made great efforts in studying the influence of rock parameters and TBM boring parameters on the cutter consumption. The influence of the interaction of rock and the steel of the cutting tool (tribology) on abrasive wear was investigated by PETRICA et al. (2013), RATIA et al. (2014) and ESPALLARGAS et al. (2015). PETRICA et al. (2013) studied the wear behavior and the relation with physical and mechanical rock properties while RATIA et al. (2014) performed an analysis of the effect of abrasive properties on steels and hard metals (MACIAS et al. 2016, 2017a). ESPALLARGAS et al. (2015) evaluated the influence of corrosion on abrasive wear on TBM cutter steel during interaction with excavation fluids using several laboratory tests (MACIAS et al. 2016, 2017a).

According to ROSTAMI (1997), BRULAND (1998a) and FRENZEL (2011), the cutterhead velocity and the thrust (MACIAS 2016; GENG et al. 2017) were identified as important parameters with a severe influence on cutter consumption. The cutterhead velocity has a strong influence, since it determines the rolling speed of each individual cutter and thus also how much it is heated and stressed because of impacts because of the rough rock surface. For the investigation of the cutter thrust, MACIAS (2016) analyzed a hard rock TBM tunnel project in highly abrasive rock. He found out that the increment of the applied cutter thrust will reduce the cutter life considerably, while a reduction will result in a more limited increment (GENG et al. 2017).

The influence of geological parameters on the wear was studied by HASSANPOUR et al. (2014) in a recently finished hard rock TBM tunnel project excavated in pyroclastic and mafic igneous rocks. Their results indicate that the strongest relationship to cutter life was found with intact rock parameters like the Vickers Hardness Number Rock (VHNR) and the uniaxial compressive strength (UCS). It could therefore be shown that the content of hard and highly abrasive minerals like quartz can have a decisive influence. It is also assumed that the porosity or the quality of the cementation may influence the tool wear (MACIAS et al. 2017b). In addition, the ability of abrasives to form sharp edges must also be taken into account and

quartz is one of the best examples of this (POPOV 2015: 303ff.). WOLDMAN et al. (2012) confirm this and also point to the great importance of the shape and size of the particles, which describe the wear behavior of materials. A related issue here is the particle size effect on abrasion, which was reported by XIE & BHUSHAN (1996), GÅHLIN & JACOBSON (1999), STACHOWIAK & STACHOWIAK (2001) and PETRICA et al. (2013, 2014). This effect simply indicates that the smaller the grain size eg. of quartz, the lower the abrasion on the tool.

The experts all agree that normal TBM operation results mainly in abrasive wear of the cutter rings (MACIAS et al. 2016, 2017a), which has been verified to be proportional to cutter rolling distance by several researches (ROSTAMI 1997; BRULAND 1998a, 2000a; FRENZEL et al. 2008; FRENZEL 2010; POPOV 2015: 303ff.). Their analyses of various hard rock TBM tunnelling projects have shown that cutter ring wear of each cutter position increases linearly with the rolling distance. But a study of GENG et al. (2017) indicates that the cutters in the inner part of the cutterhead are worn faster than the cutters outside due to a slightly different tribological wear mechanism (lower rolling speed and smaller radius of the rolling circle).

PETRICA et al. (2013) and POPOV (2015: 303ff.) state that the wear volume is proportional to the normal load, the sliding distance and inverse of the hardness of the material. As long as the surface properties of the partners are not changed, the worn volume is proportional to the distance (POPOV 2015: 303ff.). The wear resistance of a material is therefore proportional to the hardness of the softer material and has been confirmed in many experiments (POPOV 2015: 303ff.). Popov's statement that the hardness of the abrasive, on the other hand, has only an insignificant influence on the wear rate is considered very critical. It should also be noted that the wear volume is proportional to the dissipated energy divided by the hardness of the material (POPOV 2015: 303ff.). The proportionality of the wear volume to the energy input also applies to the adhesive wear and erosive wear which is present in hard rock TBMs and is often applied as a general "wear law" also for other types of wear.

Generally concerning steel, corrosion is also a possible type of wear. In tribology this topic is taken up and called tribocorrosion. According to ESPALLARGAS et al. (2015), tribocorrosion is the interaction between mechanical damage and chemical degradation encountered in systems exposed to aqueous or aggressive, high-temperature environments (STACHOWIAK & BATCHELOR 2005; IGUAL MUÑOZ & ESPALLARGAS 2011). When analyzing such problems, it is not possible to investigate corrosion and abrasion separately and their contributions must be summed up, because the overall process is influenced by the mutual interaction and influence of abrasion/wear and corrosion, and corrosion will be influenced by abrasion/wear (ESPALLARGAS et al. 2015). According to ESPALLARGAS et al. (2015), the synergy of corrosion and abrasion may enhance the material removal rates and may be a source of additional defects that have the potential to influence the mechanical properties of the excavation tools (IGUAL MUÑOZ & ESPALLARGAS 2011). However, tribocorrosion is a rather minor issue for disc cutter wear, as the influence is usually not very pronounced.

As even mentioned, the critical cutter thrust point is where effective rock excavation due to chipping occurs. It depends on the rock strength, brittleness, mineralogy, fabric (VILLENEUVE et al. 2007, 2012; VILLENEUVE 2008), and the stress at the tunnel face (YIN et al. 2014). If all factors for the excavation process are unfavorable, this point may not be exceeded in some cases. A study of VILLENEUVE (2017) showed that granite with a moderate strength between 150 and 185 MPa has its critical thrust between 100 kN and 200 kN. Penetration tests showed the resulting curves above the critical thrust are torque limited and that chipping was occurring, but not very efficiently. In these rock masses, the high thrust caused deep indentations, but the mixed tensile-shear fracturing process in the kerf had led to high rolling forces and high torque (YIN et al. 2014) without generating chips effectively (VILLENEUVE 2017). This indicated a low cutter efficiency, which is controlled by the strength and ease of fracture propagation and coalescence once new fractures have been initiated (VILLENEUVE 2017). In similar granite, which mainly was excavated via the grinding process, only very little gain in penetration rate could be achieved by applying higher thrust on the cutters. In this case, wear and cutter damage could be minimized by lowering the thrust without substantially reducing the penetration rate (VILLENEUVE 2017). Chipping-dominated excavation may never be achieved in these rock types with very high strength, even if cutter thrust limits were increased, as the process will remain too energy intensive due to the high fracture initiation threshold and the poor fracture propagation in these rocks (VILLENEUVE 2017).

Knowing all these influencing factors, it becomes obvious that in many cases a reduction of the thrust and cutter head rotation on the TBM helps to optimize the mucking process, to prolong tool life, and avoid damage to the machine (MACIAS et al. 2014). MACIAS et al. (2014) points out, however, that to date and in the near future, not all TBMs have RPM control.

Efficiency of excavation

The efficiency of excavation in hard rock TBM tunnelling is strongly dependent on whether or not there is an effective rock chipping. As mentioned at the beginning, grinding dominated tunnelling cannot achieve the effectiveness of tunnelling with effective chipping (VILLENEUVE 2017). RISPOLI et al. (2016) were especially concerned with this topic and gave a good overview. Not only the material loss at the cutter rings can be associated with the energy used, but also the crack propagation and the particle size distribution of the overburden. Laboratory tests by PETRICA et al. (2013) showed that the calculated specific wear energy related to each type of rock could directly be correlated with the abrasive behavior of the investigated rocks. RISPOLI et al. (2016) looked at the size of the debris produced during excavation. According to ROXBOROUGH & RISPIN (1973) and TUNCDEMIR et al. (2008), such a determination is useful to evaluate the efficiency of the excavation. In order to obtain a complete picture of the excavation process, all relevant machine data were also considered. These include the cutter normal force [kN/cutter], the

cutter rolling force [kN/cutter], the field penetration index (FPI; after TARKOY & MARCONI 1991) [kN/cutter/mm/rev.], the spacing/penetration ratio of the cutters, the net power of the cutterhead [kW] and the field- specific energy [MJ/m³] spent during excavation (RISPOLI et al. 2016).

RISPOLI et al. (2016) compares the excavation of a TBM in hard rock within the same geological unit, mined on different days under comparable conditions. Only the fracture frequency and distribution were different. He showed that day A is more efficient than day B and brings this in line with the particle size distribution of the excavated rock debris. The debris of day B is thinner, and it is known as, for a given rock, a higher specific energy consumption results in a greater comminution of the debris (ROXBOROUGH & RISPIN 1973; TUNCDEMIR et al. 2008). Although the excavation takes place in the same lithological unit, this greater comminution observed on day B should be induced by a greater amount of fractures of the rock mass (joint spacing is 20-50 cm). Indeed, field observation by BRULAND (1998a) and numerical simulation by GONG et al. (2006) show as a decrease of the joint spacing involves an increase of the TBM penetration rate (RISPOLI et al. 2016). BALCI (2009), analyzing the performance of a TBM in a rock mass, observed that, contrary to the theory of the mechanism of rock breakage and to the test results obtained in the laboratory on intact rock, the thrust exerted on the cutterhead shows only minor relation with the rate of penetration recorded on site and that this is due to the great amount of rock cracks (RISPOLI et al. 2016).

Experience in the construction of the Lötschberg, Gotthard and Koralm Tunnel has shown that a reduction in joint spacing does not always mean an increase in penetration. At "normal" stress levels, the statement is correct that an increase in joint density also implies an increase in penetration. At very high horizontal or vertical stresses, the jointed rock bodies are literally clamped so that the penetration rate is reduced. Very low stresses also showed a reduction of the penetration rate. (personal information from THURO)

Material scientific background

Wear on metallic surfaces is typically caused by hard mineral particles (abrasives) which are indenting and moved relative to the softer tool surface, effecting material removal, deformation or/and strain hardening. Counteracting these negative interactions in soil TBM tunnelling, mining tools (teeth and shovel edges) are commonly protected by applying a wear resistant coating on a low alloyed steel substrate (RÖTTGER et al. 2015). Unfortunately, this is not possible with hard rock TBMs – another solution has to be found. This usually means using a high-alloy hot-work steel like X40CrMoV5-1 (1.2344) and X50CrMoV5-1 (1.2345) for the cutter rings (RÖTTGER et al. 2015; KÜPFERLE et al. 2016a; GENG et al. 2017). These steel types are quenched and tempered to provide high tool durability (tempered in the region of secondary hardness to provide high material hardness and toughness (KÜPFERLE et al. 2016a).

According to POPOV (2015: 303ff.), the basic property of metallic materials is that they deform plastically when a certain critical stress is exceeded. If the material is subjected to tensile stress, the fracture occurs only after a critical deformation. The stress in the microcontact regions reaches the magnitude of the penetration hardness of the material when the roughness asperities coincide. If the yield point of the material is not reached in microcontacts, only purely elastic deformations of the surfaces occur (provided that no chemical reactions take place between the surfaces).

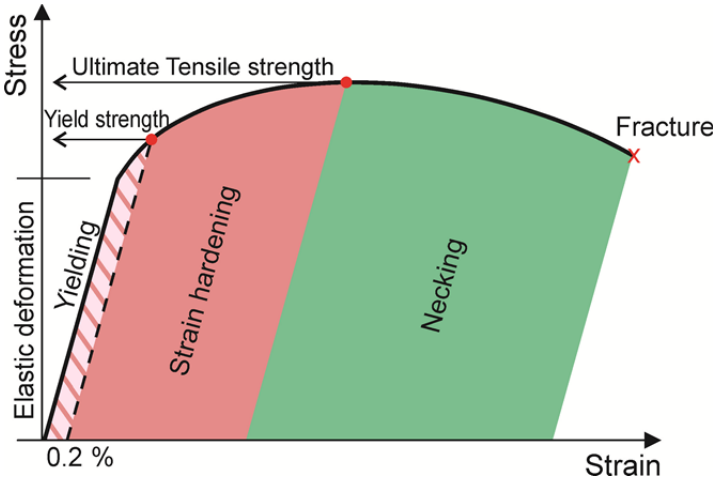

Fig. 10: Schematic stress-strain diagram of a tensile test of a quenched and tempered tool steel (mod. after WEIßBACH et al. 2015).

With the help of the tensile test, the behavior of the disc cutter steel under load can be shown. ELLECOSTA et al. 2018 give a good overview of this topic. Fig. 10 illustrates a schematic stress-strain diagram of a typical tensile test of quenched and tempered tool steel, as it is used for cutter rings. As soon as the steel is stretched, the stress increases uniformly. This is the range of elastic deformation. As soon as the curve bends (leaving the linear range), the elastic deformation ceases and the plastic deformation begins. In reality, the beginning of the plastic deformation often cannot be clearly identified by a bend in the curve. In such a case, the yield strength/elastic limit is used, indicating the plastic deformation used (often 0.2 for the yield strength at 0.2 % plastic deformation). The plastic and permanent deformation starts the zone of *strain hardening*, which is characterized by an arched curve. The plastic deformation can be shown microscopically in an alignment of the crystallites. In addition, the dislocation density, i.e. the number of defects in the atomic lattice increases. All of this leads to irreversible strain hardening while the residual formability decreases. As a result, the hardness, brittleness and strength increase as well, while the toughness decreases (ELLECOSTA et al. 2018). The peak of the stress-strain curve corresponds to the ultimate tensile strength of the material. This is also the onset of *necking* in the tensile test. When this happens, the curve slowly decreases until the final fracture occurs, and the material completely fails. The onset of *necking* corresponds to the point from which an overload

occurs. This leads to (uncontrolled) crack growth (ILSCHNER & SINGER 2016). Furthermore, pores and cavities can also form shortly before the final fracture.

The hard phases contained in the steel of the cutter rings have a decisive influence on their wear resistance and typically consist of carbides, borides, or nitrides (BERNS & THEISEN 2008). According to RÖTTGER et al. (2015) and KÜPFERLE et al. (2016a), small hard phases offer an insufficient protection against abrasion and will be worn out together with the soft metallic matrix (BERNS 1998) in the case of the presence of coarse abrasives and a high load. In laboratory tests with CERCHAR tests, KÜPFERLE et al. (2016a) was able to show exactly this fact. Although steel with a high hardness was used, the abrasion on this steel pin was not less than on softer steel pins. The reason for this was that the hardness was caused by many small carbides, which were simply scraped out in contact with coarse abrasive particles.

A high wear resistance is only obtainable, if the hard particles are adapted to the acting abrasives with respect to their volume fraction, size and hardness (RÖTTGER et al. 2015). Experiments by KÜPFERLE et al. (2016a) on a carbide-rich steel (X155CrMoV12-1) with a high content of Cr-carbides (M_7C_3) showed that the size of the hard phases should be as large as the groove width of the abrasives and the hard phase hardness should be equal or higher to those of the abrasives (KIEFFER & BENESOVSKY 1965). A solution for this could be an admixing of coarse ceramic particles (BERNS 1998). This type of material is well known under the designation of metal matrix composites (MMC) which, for example are used as build-up welds to the steel substrates (KÜPFERLE et al. 2016a). In this case, the high proportion of hard but brittle carbides or ceramic particles (low fracture toughness) has only the disadvantage that abrasion by micro cracking (delamination of bigger material constituents) becomes more evident (KÜPFERLE et al. 2016a). Against wear caused by sliding abrasion, MMCs are definitely the best choice (KÜPFERLE et al. 2016a).

This was the decisive factor for KÜPFERLE et al. (2016a) to further investigate the wear of MMC and to test its suitability for tunnel excavation. They found out that hard minerals like quartz can have a higher hardness than the cemented carbide. Thus, micro-scratching or micro ploughing can occur (CZICHOS et al. 1995). Normally, however, micro scratching and micro-ploughing are mainly observable in the case of softer steel substrate. Thereby, abrasives indent into the steel substrate and move relative to the steel surface as a result of the dynamic process (CZICHOS et al. 1995). In the case of MMC, both micro scratching, micro ploughing and micro cracking can occur (BERNS 1998). Thereby, the softer metal matrix interacts with the abrasives in a more ductile manner, thus leading to wear by micro scratching or micro ploughing. In contrast, hard particles have a high hardness and therefore a low fracture toughness (BERNS 1998), which is attributed with brittle material behavior (KÜPFERLE et al. 2016a). Depending on the rock, composition and hard phase size, it may make sense to use the MMC.

With this topic it is important to note that a high hardness does not offer a high wear protection at the same time. It is obvious that hard materials possess a high resistance against

being indented by abrasives which leads to less wear by micro scratching and micro ploughing, provided the indented abrasives are moved relative to the materials' surface (KÜPFERLE et al. 2016a). According to KÜPFERLE et al. (2016a), hard and less ductile materials have a low fracture toughness and respond with a mainly brittle material behavior, for which reason micro cracking is the dominant wear mechanism if impact loads are present. Especially in the case of high impact loads, this micro cracking can cause stronger wear to brittle materials than softer ones due to the low fracture toughness (KÜPFERLE et al. 2016a). Typical values for the fracture toughness of WC are in a range of 6-9 to 22-23 MPa $\cdot \sqrt{m}$ with a hardness of 500-800 to 1200-1300 HV0.05 and a grain size between 3-10 µm (BERNS 1998; RÖTTGER et al. 2015; KÜPFERLE et al. 2016a). In contrast, steel with 50 MPa $\cdot \sqrt{m}$ has at least twice the fracture toughness (BARGEL & SCHULZE 2005). This shows that steel is preferable for impact stresses.

2.1.5 Laboratory tests for breakability and performance models

In order to make TBMs economic in comparison with other classical methods, a reliable estimation of advance rates is needed for time planning, cost control and choice of excavation methods (RISPOLI et al. 2016). In this regard, several methods for predicting the performance of a TBM are available in literature. According to RISPOLI et al. (2016), these include empirical methods (BRULAND 1998a; BARTON 2000), deterministic-theoretical methods (eg. ROXBOROUGH & PHILLIPS 1975; ROSTAMI & OZDEMIR 1993), probabilistic methods (eg. NELSON et al. 1999; COPUR et al. 2014) or methods based on laboratory tests (eg. ROXBOROUGH & RISPIN 1973). Scientists have developed penetration formulas using net cutter thrust for intact rock (ROBBINS 1970; BRULAND 1999) and jointed rock masses (BARTON 2000). BIENIAWSKI et al. (2006) and SAPIGNI et al. (2002) demonstrate the value of analytical methods to predict penetration rate for design and performance assessment (VILLENEUVE 2017).

The most complex method would be on-site testing. In order to obtain reliable results, it is advisable to use at least two of the methods mentioned (BILGIN et al. 2014). As a consequence, great efforts have been made to correlate TBM performance with rock mass and machine parameters (SAPIGNI et al. 2002; ALBER 2008; GONG & ZHAO 2009; HASSANPOUR et al. 2011; FARROKH et al. 2012). In particular, in the last decades, models of performance prediction based on case histories which took into account as many geological conditions as possible (eg. BRULAND 1999; NELSON et al. 1999) were built (RISPOLI et al. 2016). MAIDL et al. (2008) showed that weaker rocks required lower thrust to achieve the same penetration rate as stronger rocks (VILLENEUVE 2017). A good and very detailed overview of current and partly outdated penetration models is given by WILFING (2016).

Methods determining breakability

It is known that rock breakability properties have a major influence on the drillability. The term breakability is very broad and its definition includes and covers a variety of more specific properties that could be classified as strength, brittleness and surface hardness properties (MACIAS et al. 2017b). There are currently several individual test methods which are used to determine breakability and some of the most well-known and commonly used are listed in Tab. 5 and based on an overview given by MACIAS et al. (2017b).

One of the most common tests is the Uniaxial Compressive Test. It is used to determine the uniaxial compressive strength UCS, Poisson's ratio and Young's modulus of the intact rock. According to MACIAS et al. (2017b), UCS is the primary test method and the most common used to characterize the mechanical behaviour of the intact rock, strength and deformability. This test uses circular cylinders of rock samples which are compressed along the longitudinal axes (ISRM 1979). Further information are avalable in section 5.1.1.

Tab. 5: Compilation of the most common laboratory tests measuring rock breakability in connection with hard rock drilling and boring (mod. after MACIAS et al. 2017b).

Testing method and index	Principle	Rock sample	Testing tool	Reference
Uniaxial Compressive Strength (UCS)	The specimen is loaded axially until failure occurs	Rock core; cut and grinded	Hydraulic press	ISRM (1979)
Brazilian Tensile Strength (BTS)	The specimen is loaded until failure occurs	Rock disc; cutted	Hydraulic press equipped with steel loading jaws	ISRM (1978b)
Point Load Strength (PLT)	The specimen is loaded until failure occurs	Rock core section or lumps	Hydraulic press equipped with spherically truncated, conical platens	ISRM (1985)
Indentation Hardness (IHI)	Indenter under applied load penetrates into the rock surface	Rock sample with tope end saw-cut	Loading frame and hard material conical indenter	ISRM (1998)
Punch Penetration/ Penetration Index (PI)	Indenter penetrating the surface of a confined rock core sample	Rock core section	Conical tungsten Carbice (WC) indenter	YAGIZ (2009a)
LCPC Breakability Coefficient (LBC)	Impeller (medium hard steel) rotating in a vessel containing crushed rock	Crushed rock (4 – 6.3 mm)	Steel impeller	KÄSLING & THURO (2010)
Surface hardness – resistance to penetration/Sievers' J-Value (SJ)	Penetration depth of drillings after 200 revolutions	Cut rock specimen with parallel sides	8.5 mm tungsten carbide (WC) drill bit	DAHL et al. (2012)
Brittleness Value (S_{20})	The prepared sample is exposed to 20 impacts	Crushed rock (11.2 – 16 mm)	Mortar with lid and a 20 kg weight	DAHL et al. (2012)

The second mentioned test, the Brazilian Tensile Test is an indirect tensile method to assess the tensile strength of the rock (ISRM 1978b; ASTM D3967 2008). The stress failure in the rock sample is a function of the applied load, the sample diameter and the thickness at the centre of the specimen resulting in the Brazilian Tensile Strength (BTS) (MACIAS et al. 2017b). Further information are available in section 5.1.2.

The Point Load Test (PLT) is intended as an index test for the strength classification of rock and it may also be used to predict other strength parameters as uniaxial tensile and compressive strength (ISRM 1985). Rock specimens (core, block or irregular lump) are broken by application of concentrated load through a pair of spherically truncated, conical platens (MACIAS et al. 2017b). Further information are available in section 5.1.3.

The Indentation Hardness Test (IHI) is an index test for classifying the resistance against penetration into the rock surface (ISRM 1998). According to KAHRAMAN et al. (2012), this test requires a loading system having a capacity of 30 kN and a conical platen having a 60º cone and 5 mm radius spherical tip, a point load apparatus is suitable for this purpose. After attaching a dial gauge to the point load apparatus for measuring penetration, indentation hardness tests can be carried out. The requirement for the rock surface is that it is smooth and even. This is achieved with a diamond saw.

The punch test was developed by HANDEWITH (1970) and has been used by many researchers to evaluate parameters such as rock drillability, cutting force estimates and TBM penetration rate (DOLLINGER et al. 1998; YAGIZ 2002; YAGIZ 2009a; MACIAS et al. 2017b). A good overview of this test is given by ERBEN (2013). In this test, a standard conical indenter is pressed into a rock sample that has been cast in a confining steel ring. The load and displacement of the indenter are recorded with a computer system. The slope of the force-penetration curve indicates the excavatibility of the rock, i.e., the energy needed for efficient chipping (MACIAS et al. 2017b). This is affected by the stiffness, brittleness, and porosity of the sample.

The LCPC test was originally developed for determination of rock abrasivity and presented by the Laboratorie Central des Ponts et Chaussées in the 1980s (AFNOR 1990). The LCPC is also used to determine an index called the “LCPC Breakability Coefficient” (LBC) to quantify the breakability or brittleness of the sample material (THURO et al. 2007; WILFING 2016). The LCPC Breakability Coefficient LBC is defined as the fraction below 1.6 mm in the grain size distribution curve after testing. Further information are available in section 5.2.2.

The Sievers J-miniature drill test was originally developed by H. Sievers in the 1950s. The Sievers J-Value (SJ) constitutes a measure of the rock surface hardness or resistance to indentation (MACIAS et al. 2017b). The SJ value is defined as the mean value of the measured drill hole depths in 1/10 mm, after 200 revolutions of the 8.5 mm miniature drill bit (DAHL et al. 2012).

The Brittleness Value (S_{20}) constitutes a measure of the rock brittleness or ability to be crushed by repeated impacts, and it is determined by use of an impact apparatus (MACIAS et al. 2017b). The Brittleness Value (S_{20}) is defined as the percentage of a pre-sieved fraction that passes through the finer sieve after 20 impacts.

In addition to the aforementioned test methods, rock properties like density and porosity should also be included and considered since they may have strong influence on the breakability of the rock (MACIAS et al. 2017b). The density is defined as the mass per volume of a substance (g/cm^3) and porosity is defined as the nonsolid or pore-volume fraction. Porosity is a volume ratio and thus dimensionless, and is usually reported as a fraction or percent (ISRM 1978a).

There are in addition some methods that adopt approaches that are different from model testing. According to (MACIAS et al. 2017b), the measurement of mineralogical parameters such as quartz content, the Equivalent Quartz Content (EQC) or the Vickers Hardness Number Rock (VHNR) are commonly also used to assess breakability of hard rock. The EQC parameter encompasses the influence of the entire mineral content of the rock on abrasiveness relative to quartz, while the VHNR is used as a measure of the hardness of each individual component mineral. Individual Vickers hardness values, combined with the percentage of each mineral found in a rock, can be used to calculate the VHNR (SALMINEN & VIITALA 1985).

Performance and tool life prediction models

Tab. 6: Compilation of the most important performance and tool life prediction models for drilling (mod. after MACIAS et al. 2017b).

Model	Basic input parameters		Output parameters	Reference
	Rock parameters	Machine parameters		
Tunnelling with drill-and-blast	UCS, destruction work W_z, porosity, joint spacing, EQC	Power of the percussive drill	Drilling velocity, tool life (m/bit)	THURO (1997)
Drilling	DRI	Drill bit diameter	Drilling velocity	HEINÖ (1999)
Rock Abrasivity Index (CAI) – Tunnelling with drill-and-blast	UCS, EQC	-	Drill bit lifetime (m/bit)	PLINNINGER et al. (2002); PLINNINGER (2010)
Tunnelling with drill-and-blast	DRI, VHNR	Power of the percussive drill, drill hole diameter	Drilling velocity, tool life	ZARE (2007)
Quarrying	DRI, VHNR	Drill bit / hole diameter, hole depth, percussive drill type and capacity	Drilling velocity, tool life	OLSEN (2009)

In drill-and-blast tunnelling and in rock quarrying, the drilling rate and the drill bit wear is dependent on several parameters. The net penetration rate of any drilling equipment (top hammer, coprod, DTH, rotary) is correlating well with the rock drillability (OLSEN 2009). According to THURO (1997), the principal parameters influencing drilling velocity may be jointing of rock mass, orientation of schistosity (rock anisotropy), degree of interlocking of microstructures, porosity and quality of cementation of clastic rock, degree of hydrothermal decomposition and weathering of a rock mass (MACIAS et al. 2017b). The content of abrasive minerals (e.g. EQC), porosity and the quality of the cementation/binding and interlocking of the minerals influence the drill bit wear.

According to MACIAS et al. (2017b), several models to predict the net penetration rate and tool consumption in drilling equipment have been developed and there is a wide variability of drilling applications. Tab. 6 summarizes some of the existing and most important performance and tool life prediction models for drilling equipment, based on MACIAS et al. (2017b).

2.2 Hardness testing

Generally, hardness tests can be divided into static and dynamic testing methods. Commonly known static test methods are indentation hardness tests like Brinell, Vickers and Rockwell or also scratch hardness tests (e.g. Mohs). The dynamic hardness tests are also known as rebound hardness and they measure the “bounce” of a tested material which is mainly related to its elasticity. In this work, the focus is on static hardness testing with penetration tests.

2.2.1 Indentation hardness

Indentation hardness tests are commonly used in mechanical engineering to determine the materials hardness, belonging on its deformation. There are a number of tests where the examined material is penetrated until an indentation is formed. These tests can be performed on a macroscopic or microscopic scale.

Hardness is therefore defined as the resistance of a body to the penetration of a harder test specimen (SCHUMANN 1991: 175). All methods calculate the hardness by forming a quotient from the applied test load and the corresponding size of the indentation or penetration depth. Depending on the structure and size of the indentation, this can lead to different hardness values from structural hardness to single crystal hardness (Fig. 11). Structural hardness is when the penetrator meets at least two different microstructural constituents and single crystal hardness is when only one crystal is hit by the penetrator. In between lies the multi-crystal hardness, where the penetrator meets several crystals belonging to the same structural component.

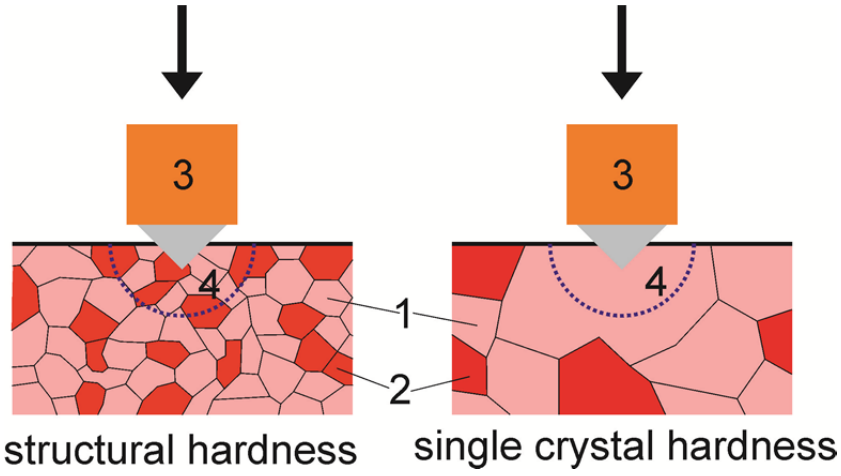

Fig. 11: Schematic illustration of the influence of microstructural constituents of hardness. 1 = soft grain, 2 = hard grain, 3 = indenter/test body, 4 = radius of the zone of influence (mod. after OETTEL & SCHUMANN 2011: 324).

Depending on whether the material reacts more elastic or plastic under indentation, there is a difference between the width of the indentation under full load and after the removal of the load (permanent indentation). This effect is shown in Fig. 12. For metals for example, the plastic part of the deformation is generally significantly higher than the elastic rebound, even for hard steel (700 HV) (POLZIN 2007: 50). By the plastic deformation, a small bulge occurs at the edges of the indentation because of the ductile displacement of the material (Fig. 12).

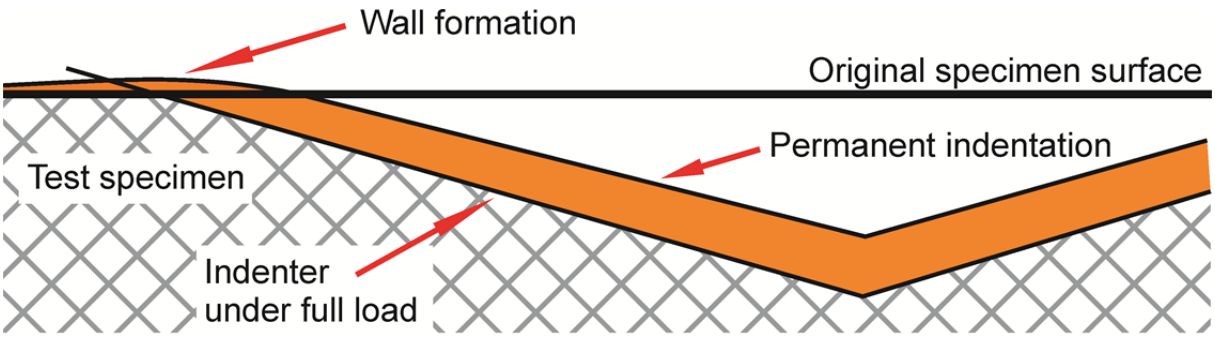

Fig. 12: Schematic effect of the elastic rebound and the accompanied wall formation at the rim of the indentation (mod. after POLZIN 2007: 50).

Vickers hardness

The method is suitable for testing all metals. The penetrator is a straight pyramid of diamond (square base) with a surface angle of 136°. According to POLZIN (2007: 46), this indenter shape has a particular advantage: the law of proportional resistances applies. This means that test load and indentation surface are proportional to each other. Therefore, the Vickers hardness value is basically independent of the selected test load. Despite the validity of this law, for small test indentations there is usually a test load dependency due to other causes, such as surface tension. The surface angle of the indenter pyramid was determined so that the

Vickers hardness values come close to the Brinell hardness values over a relatively wide range.

According to POLZIN (2007: 54), the advantages are:

- no limitation of application due to specimen hardness, specimen thickness or test surface size
- minimal damage to the specimen due to the test indentations
- comparability of the hardness values of different test laboratories for indentations greater than 70 µm diagonal length, if the same conditions apply
- applicable up to very small test loads under consideration of many boundary conditions

But there are also disadvantages which according to POLZIN (2007: 54) are the following:

- large expenditure of time for sample preparation and measurement of the test indentations
- high sensitivity to shocks and vibrations

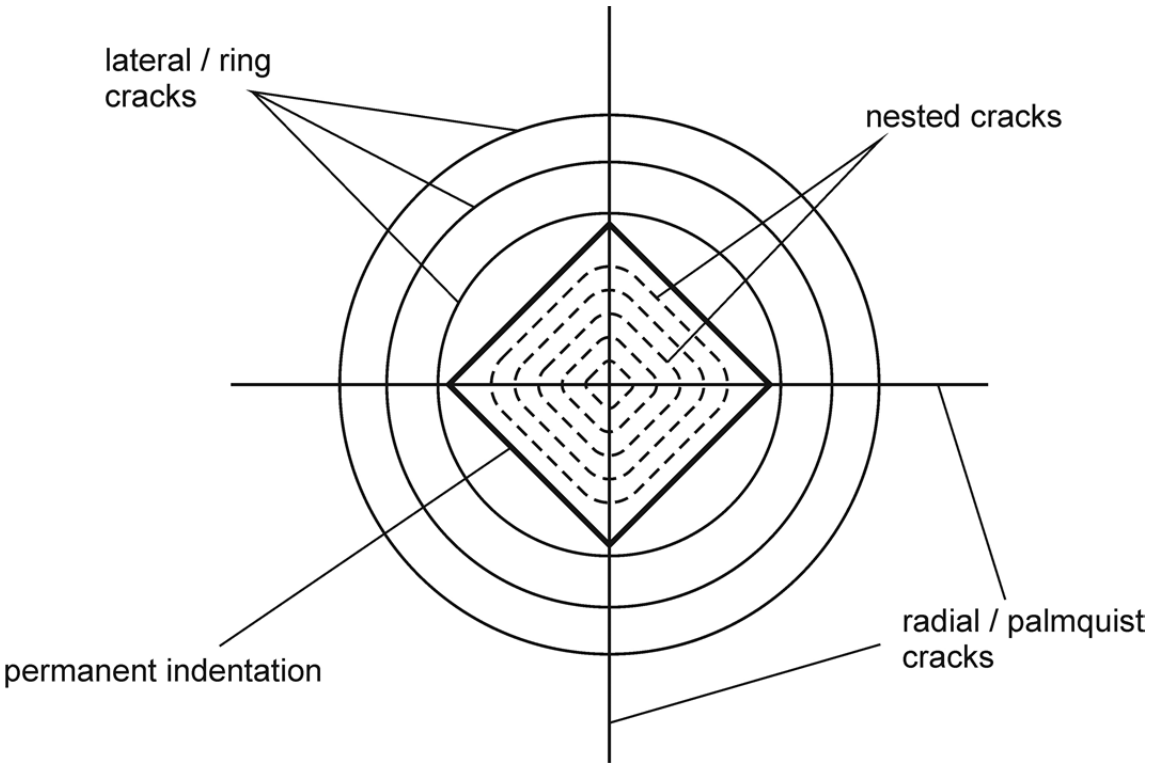

Fig. 13: Vickers indentation with schematic illustration of possible crack types (mod. after OETTEL & SCHUMANN 2011: 330; EICKHOFF BAUMANN 2008: 102).

A test in brittle materials may result in cracking. These are shown schematically in Fig. 13. When the Vickers Indenter penetrates, an elastic-plastic stress field develops in the phase after the critical stress level has been exceeded, which can lead to the formation of characteristic radial cracks (palmquist cracks) (EICKHOFF BAUMANN 2008: 102). The ring cracks are the result of bulge formation of the tested material (OETTEL & SCHUMANN 2011: 330). The nested

cracks, which occur directly under the indenter, are formed in particular by the high shear stresses coupled with bending stresses in the area (OETTEL & SCHUMANN 2011: 330).

Knoop hardness

The Knoop hardness test is very similar to that of Vickers. There are differences in the shape of the diamond penetrator and the calculation. The geometry of the indenter is an extended pyramid with the length to width ratio of 7:1 and respective face angles are 172.5° for the long edge and 130° for the short edge. According to POLZIN (2007: 70), the Knoop hardness testing method is particularly suitable for:

- for the testing of very hard and brittle materials, when the Vickers indentation would lead to cracks
- for ceramics and glass in international comparison
- for testing very thin or narrow specimens, when the Vickers indentation is too large for the test application
- for the detection of material anisotropies by hardness indentations in various directions

According to POLZIN (2007: 71), the advantages are:

- no limitation of the application by hardness or dimensions of the sample (also fulfilled by Vickers)
- only minor damage to the specimen surface (fulfilled to a lesser extent by Vickers, since Vickers indentations are deeper with the same test load; Knoop cracks at the end of indentations are less likely in glass and ceramics than in Vickers)
- possibility to detect material anisotropy
- longer measurement diagonal in relation to Vickers for the same penetration depth

But there are also disadvantages which according to POLZIN (2007: 71) are the following:

- dependence of the measured hardness value on the test load error due to unrecognized anisotropies
- large expenditure for the preparation of the test surface and the measurement of the indentation diagonals
- not widespread in Europe

Rockwell hardness

The Rockwell hardness tests differ slightly from the Vickers and Knoop tests. The Rockwell hardness unites different tests in which only the principle is similar, the load, the times and also the indenters differ. Because of the simplicity of their realization and the short time expenditure of a measurement, these methods are frequently used worldwide. Indenters are either a straight circular cone with a rounded diamond tip (cone angle 120°; radius 0.200 mm) or a carbide ball with different diameters (POLZIN 2007: 23ff.).

The indenter first penetrates the specimen under the test preload to a penetration depth defined as the reference plane for further measurement. The depth measuring device is set to zero and then the additional test force is applied. The maximum penetration depth is reached after the additional test force has been applied for a period defined in the standards. The test force is then withdrawn in such a way that only the test preload acts again. At the same time, the indenter moves back upwards by the elastic portion of the indentation depth at the total test force and remains at the remaining indentation depth, which is used to define the Rockwell hardness. The Rockwell hardness is basically defined arbitrarily and can therefore be understood as a mere material parameter without further explanation (POLZIN 2007: 23ff.).

According to POLZIN (2007: 42), the Rockwell hardness testing method is suitable for all types of metal and steel and has the following advantages:

- less time required for testing (no time-consuming sample preparation; direct display of hardness value)
- hardness testing machines are inexpensive (no expensive optics)
- processes can be automated

According to POLZIN (2007: 71), the disadvantages are:

- poor differentiation of materials with increasing hardness
- unknown effects of indenter on test result (effects may be reduced by indenters calibrated with functional test)

Instrumented indentation testing

The instrumented indentation test is based on a simple procedure principle. A penetrator of special geometry is pressed into the material to be tested while the force and displacement are measured simultaneously. As early as the end of the 19th century, Martens introduced a device that allows simultaneous measurement of indentation force and penetration depth ("hardness measurement under test force") (MARTENS 1912). However, it was not until the 70s of the 20th century that a level of development in displacement measurement was reached that triggered considerable activity for the introduction of a new hardness scale in Germany. In this respect, the works of Grau (FRÖHLICH et al. 1977; GRAU et al. 1996), Weiler (WEILER & BEHNCKE 1990) and Dengel (DENGEL 1989) have to be mentioned (ULLNER 2007: 267ff.).

The process principle not only provides the basis for a universal method, but also enables direct access to the results of contact mechanics (JOHNSON 1995). It deals with the models for the deformation of solid surfaces in contact with indenters of defined geometry. Depending on how pointed the penetrator is, plastic deformations occur as well as elastic deformations with increasing forces. Elastic parts of the indentation deformation always exist. Therefore, the contact mechanics are of great importance because of the separation of the elastic parts in instrumented indentation testing (ULLNER 2007: 267ff.).

2.2.2 Fracture Toughness

In materials science, fracture toughness is a characteristic material parameter which describes the ability of a material to resist against fracture. It can be used to characterize the materials resistance to brittle fracture when a crack is present. Ductile materials like metals have a high fracture toughness while this is low in brittle materials like minerals or ceramics. The basics of fracture mechanics are described in the literature (ROSSMANITH 1982; HECKEL 1991; BLUMENAUER & PUSCH 1993). The topic of crack formation, crack propagation and fracture toughness in rocks and minerals is covered by PASSCHIER & TROUW (2005) and PATERSON & WONG (2005), for example.

The fracture toughness of brittle materials can be determined with the aid of hardness indentations, the so-called indentation fracture mechanics (BLUMENAUER & PUSCH 1993: 100 f). For this purpose, a Vickers hardness test can be carried out in which the respective, material-dependent, elastic load limit must be exceeded. The penetration of the Vickers diamond pyramid causes an elastic-plastic stress field when the critical stress level is exceeded, leading to the formation of characteristic radial cracks (palmquist cracks, Fig. 13, page 44). The resulting fracture pattern can be analyzed according to the principles of fracture mechanics and the fracture toughness calculated. In simplistic terms, the crack length is a measure of the fracture toughness.

WIESER (2016) provides further information on the subject of stress, deformation, cracks in general, crack formation and crack propagation in rocks and minerals. The dissertation by Eickhoff-Baumann (EICKHOFF BAUMANN 2008) focuses more on the topic of fracture

toughness and uses the methods mentioned to determine the fracture toughness of brittle materials such as cement clinkers.

2.2.3 Correlations and conversions

For the most common static hardness tests, a hardness conversion according to DIN EN ISO 18265 is possible. In this table the hardness values after Brinell, Vickers and Rockwell can be compared and converted and correlated with the tensile strength. However, there are very great uncertainties and problems, which POLZIN (2007) points out in HERRMANN et al. (2007: 110-113). Roughly speaking, the main reasons for the limitations are in the revaluations of the different indenters (material and geometry) as well as the different test procedures and times. Further information and studies can be found in OTTO (2005), SCHMIDT (1990) and SCHMIDT (1995).

The correlation with the tensile strength is based on experiments which show that the mean contact pressure p_m is proportional to the yield stress Y of the material (HERRMANN 2007 in HERRMANN et al. 2007: 7). There are relationships between hardness and other mechanical properties, for example there are empirical relationships between hardness and tensile strength that depend on the material (HERRMANN 2007 in HERRMANN et al. 2007: 16). According to POPOV (2015), BOWDEN & TABOR (1951) have shown both theoretically and experimentally that in most cases the hardness is about three times the yield strength. Consequently, hardness measurement plays a central role in the tribological characterization of materials, since tribological processes are essentially determined by the interaction of microroughnesses and their geometry is very similar to a hardness test. The indentation hardness therefore hardly depends on the shape of the indenter. In a first approximation, this dependence can be neglected.

2.3 Cutter life prediction models

To predict tool wear of tunnel boring machines, a large number of different prediction models exist. In contrast to penetration prediction models, these only indicate the wear and not the advance rate. This chapter briefly introduces the most important and commonly used cutter life prediction models. Models are omitted which do not consider the abrasiveness, models which are already very old and partly only represent a modification of other known models, models which are practically not applied in practice and models which contain abrasiveness values but are mainly considered as penetration prediction models and which are mainly used for performance predictions.

Tab. 7 gives an overview of the cutter life models, which are also explained below (table based on HASSANPOUR et al. 2014; MACIAS et al. 2017b).

Tab. 7: Overview of the most common and used cutter life prediction models for mechanized hard rock tunnel boring (mod. after HASSANPOUR et al. 2014; MACIAS et al. 2017b).

Model	Input parameters (rock and machine)	Output parameter	Limitations	Reference
Gehring	CAI, UCS	Wear rate, cutter life	-	GEHRING (1995)
CSM	CAI, cutterhead rpm	Cutter life, delays, total cost	-	ROSTAMI (1997)
Maidl	CAI, UCS	Average cutter ring life	-	MAIDL et al. (2008)
RME	CAI, UCS	Cutter life	Limited to data from a single project	BIENIAWSKI et al. (2009)
Frenzel	CAI, cutterhead diameter[m]	Cutter life, delays, total cost		FRENZEL (2011)
NTNU	CLI, quart content [%], cutterhead diameter [m], cutter diameter [mm], number of cutters, cutterhead rpm	Cutter life, delays, total cost	Mainly based on data of igneous and metamorphic rocks from Norway	BRULAND (1998a); MACIAS (2016)
Hassanpour	UCS, Vickers Hardness Number of the Rock (VHNR)	Disc cutter wear	Based on data of blocky pyroclastic and mafic igneous rocks from Iran	HASSANPOUR et al. (2014)

One of the most common cutter life prediction models used for hard rock TBM tunnelling is the CSM-model (ROSTAMI 1997), developed at the Colorado School of Mines in Golden and the NTNU-model (BRULAND 1998a; MACIAS 2016), developed at Norwegian University of Science and Technology in Trondheim (MACIAS et al. 2016, 2017a; GENG et al. 2017). Especially in the Alpine region, the Gehring-model (GEHRING 1995) is used for estimating the wear rate (HASSANPOUR et al. 2014).

As good as these prediction models may be, they also have their weak points. They usually produce highly variable results as illustrated by SCHNEIDER et al. (2012). According to HASSANPOUR et al. (2014), the most important problem in most of these models is consideration of only one abrasiveness parameter in the model as the input parameter and ignoring the effect of other important parameters like rock strength and rock mass fracturing degree and structure. Another important point is that e.g. some models omit the relation between cutter load, penetration and rock parameters. This simply means that same levels of applied cutter load are not used in soft ground (as it applies to stronger rocks) and by default the use of lower applied load will ease off the extremely high rates of penetration (HASSANPOUR et al. 2011).

2.3.1 NTNU model

In 1979, BLINDHEIM (1979) introduced the NTNU model, which was extended, improved and adapted to the current conditions by BRULAND (1998a) and MACIAS (2016) in the course of time. Today, the NTNU model is very complex and based on time-dependent abrasion of the cutter rings. Accordingly, this model has a relatively high practical background and is based on a large amount field data from various case histories (HASSANPOUR et al. 2014). The model uses certain charts and simple equations for predicting cutter life and cost (HASSANPOUR et al. 2014).

According to MACIAS et al. (2016), the parameters influencing the cutter wear are the Cutter Life Index™ (CLI™; DAHL et al. 2012), abrasive mineral/quartz content (%), TBM diameter, cutter diameter, number of cutters and cutterhead RPM. The CLI™ is assessed on the basis of Sievers' J-value and the Abrasion Value Cutter Steel (AVS) (BRULAND 1998a). The cutter life, measured in hours, is combined with the net penetration rate (m/h) and the TBM diameter to calculate the cutter life in m/cutter and solid cubic meters per cutter sm^3/cutter (MACIAS et al. 2017a). Factors such as the total number of cutters, cutter costs, cutter change time, the influence of cutters on advance rate (m/week), and total excavation costs are also included (MACIAS et al. 2017a; GENG et al. 2017).

The advantages are that there are many influencing factors that can represent the complexity of a TBM drive as realistically as possible. However, this makes the model very complex, which is a disadvantage. In addition, the NTNU model requires special tests originated from drilling. These tests are not commonly available outside Norway (HASSANPOUR et al. 2011). Besides these facts, the model-data are mainly based on igneous and metamorphic rocks from Norway.

2.3.2 CSM model

ROSTAMI & OZDEMIR (1993) and ROSTAMI (1997) developed the CSM model for cutting force estimation of disc cutters based on the Brazilian tensile strength (BTS) and UCS of rock (HASSANPOUR et al. 2010). For wear prognosis, the CERCHAR Abrasivity Index (CAI), as defined by Cerchar (1986), AFNOR (1990), ASTM D7625 (2010) and/or ALBER et al. (2014) is used in combination with the cutterhead rpm (MACIAS et al. 2017a; GENG et al. 2017). According to MACIAS et al. (2017a), the CAI can be used to estimate the average rolling distance of a given cutter. Factors such as the total number of cutters, cutter costs and change times, as well as probable operational delays, can be predicted.

In 2002, YAGIZ (2002) modified the CSM model adding rock mass properties as input parameters into the model (HASSANPOUR et al. 2014). Three years later, RAMEZANZADEH (2005) has also followed up on this work and developed a database of TBM field performance for over 60 km of tunnels and offered adjustment factors for CSM models to account for joints and discontinuities (HASSANPOUR et al. 2011).

The advantages of this wear model are that it is designed to be transparent, uses globally accepted and accessible laboratory tests and has been updated over time. The main disadvantage is that it is mainly based on the CERCHAR test, which in case of doubt cannot adequately represent the complexity of the respective rock conditions.

2.3.3 Gehring model

The Gehring model is a relatively simple TBM wear model, developed by GEHRING 1995. He established a relationship between CAI and cutter ring weight loss (mg of steel) per meter rolling distance, based on TBM data from various projects (MACIAS et al. 2016; HASSANPOUR et al. 2014; SCHNEIDER et al. 2012). In addition to the CERCHAR method, which also uses the CSM model, the uniaxial compressive strength UCS is also included in the calculation. The parameters calculated from this are the wear rate and the cutter life.

Similar to the CSM model, the advantages are simplicity and ease of use. The age of the model, which no longer corresponds to the new conditions of current TBM machines, proves to be a disadvantage.

2.3.4 Maidl model

In 2008, MAIDL et al. (2008) proposed an empirical relationship between the mean rolling distance life (in kilometers) of 17-inch diameter cutter discs considering the uniaxial compressive strength (UCS) and the CERCHAR Abrasivity Index (CAI) for different intact rock types (HASSANPOUR et al. 2014; MACIAS et al. 2016, 2017a; GENG et al. 2017). The cutter wear is given in g/km of rolling distance. The representation in general indicates the rolling distance life of a disc decreases with increasing compressive strength of the intact rock and with the corresponding higher CAI values (HASSANPOUR et al. 2014).

Similar to the Gehring model, it is a simple model that takes into account the UCS and the CAI, which can be advantageous and disadvantageous at the same time. However, compared to the Gehring model, it is more up-to-date and can better represent the current TBM machines.

2.3.5 RME model

The third model based on the two input parameters of uniaxial compressive strength (UCS) and CERCHAR Abrasivity Index (CAI) is the Rock Mass Excavability Index (BIENIAWSKI et al. 2006, 2009). The so called RME model is also an empirical model which describes the correlation between the RME and the cutter consumption, based on the analysis of TBM and rock data from the Guadrama tunnel in Spain (HASSANPOUR et al. 2014; MACIAS et al. 2016, 2017a). The model uses three levels of variation for the CAI. The authors also established different correlations for values of Uniaxial Compressive Strength (UCS, expressed in MPa) of intact rock for values both above and below 45 MPa (MACIAS et al. 2016, 2017a).

Like the other CAI and UCS based models, it is a relatively simple model, which may be both advantageous and disadvantageous. A disadvantage is the fact that the model was only created on the data of only one tunnel project.

2.3.6 Frenzel model

In a more recent work, FRENZEL (2011) proposed an empirical prediction model for cutter consumption based on the analysis of a large range of tunnelling projects (127 km excavated length of 7 tunnelling projects), valid for 17 inch disc cutters (HASSANPOUR et al. 2014; MACIAS et al. 2016, 2017a; GENG et al. 2017). This model also uses the CERCHAR Abrasivity Index (CAI) to assess the rock drillability and direct empirical relations with cutter consumption or rather tool wear (wear coefficient) are carried out (MACIAS et al. 2016, 2017a). The cutterhead diameter serves as an additional input parameter. Relative costs for refurbishment are also discussed.

Like the previous models, this one is kept relatively simple, which brings advantages and disadvantages at the same time.

2.3.7 Hassanpour model

HASSANPOUR et al. (2011, 2014) have proposed a new empirical TBM cutter wear and life prediction model, based on data collected from a long tunnel project in Iran in pyroclastic and mafic igneous rocks. The rocks studied were blocky to very blocky or highly jointed pyroclastic rocks and massive to blocky mafic igneous rocks with a UCS range of 30 to more than 150 MPa. The authors found a relationship between cutter life and average mineral hardness (quantified using the Vickers Hardness Number of the Rock, VHNR) in combination with the uniaxial compressive strength (UCS). VHNR for a given rock can be calculated by weighted averaging of Vicker's hardness number (VHN) of individual minerals in mineralogical composition of the rock, as explained by BRULAND (1998b). Then the so-called abrasiveness index (ABI) is calculated as follow: ABI = VHNR x (UCS/100). (HASSANPOUR et al. 2014; MACIAS et al. 2016, 2017a; GENG et al. 2017)

HASSANPOUR et al. (2014) showed, that there is a strong correlation between the ABI and the real wear rates (cutter life) in the investigated project. Separately, the VHNR already achieves a very good correlation R of 63 % while the uniaxial compressive strength only achieves a correlation R of 55 %. The ABI which includes VHNR and UCS both, however, achieves a correlation R of 68 %. In addition, HASSANPOUR et al. (2014) was able to show that intact rock properties (VHNR, UCS, quartz content, ABI) show better correlations with cutter life than rock mass parameters (Jv, RQD, GSI and RMR). (HASSANPOUR et al. 2014; GENG et al. 2017)

The advantages of the Hassanpour model are that the ABI can be calculated by simply measuring or estimating two common and easily available intact rock properties including mineral content (VHNR) and uniaxial compressive strength (UCS, as an index of rock

strength) (HASSANPOUR et al. 2014). However, the weaknesses are that the used equations were developed based on data from blocky and highly jointed pyroclastic and mafic igneous rocks within a special UCS range. Impacts of the rock mass structure (or fracturing degree) have not been fully reflected in these equations and needs to be addressed in follow up studies. (HASSANPOUR et al. 2014)

2.3.8 Other models

Wijk model

WIJK (1992) proposed theoretical equations to predict the rolling distance life (km) of the flat and wedged tip cutters based on the simple rock strength parameters (UCS, BTS) and CAI (GENG et al. 2017).

Wang model

WANG et al. (2012, 2015) proposed an energy-based method to predict the disc cutter wear which was verified by data from engineering cases. WAN et al. (2002, 2003) analyzed the cutter wear and consumption of the Qinling Tunnel Project (tube 1) in detail and proposed some suggestions for TBM design and operation (GENG et al. 2017).

Ewendt model

EWENDT (1989) developed a prognosis model based on the wedge angle theory for the tool wear of disk cutters. The basis for this model is the cutting force estimation formula according to SANIO (1985). SANIO (1985) found strong correlations between uniaxial compressive strength (UCS) of rock and the specific energy defined as the amount of energy needed to excavate a unit volume of rock (HASSANPOUR et al. 2010). EWENDT (1989) related wear rate to some rock parameters like quartz content, grain size and rock strength. (HASSANPOUR et al. 2014)

Nelson model

NELSON et al. (1994) developed an empirical method for predicting cutter life. The model is based on comparing the input data with that in a TBM field performance database to estimate the probable rate of wear on the cutters. The input data for this method includes rock type, joint frequency and some other machine and operational parameters. (HASSANPOUR et al. 2014)

Farrokh model

FARROKH et al. (2012) has also developed a set of charts for estimation of the cutter wear in terms of volume excavated per cutter as a function of rock type, rock strength, rock mass properties, and abrasivity. He has also offered an estimated time for cutter change based on the analysis of data in an extensive database covering over 100 km of tunnels. (HASSANPOUR et al. 2014)

2.4 Research gap

The literature review could show that there are a large number of references that have dealt with the topics tribology, wear, abrasiveness and hardness. A disadvantage of the investigation of tribological topics is that the investigations are almost exclusively carried out by materials scientists. Often there is very little knowledge of the geological background. In the same way, investigations of abrasivity are mainly carried out by geologists or engineering geologists. These in turn usually have very little knowledge of materials science. One reason for this thesis is to combine the knowledge of both fields, geology and materials science.

Materials science is the basis for a wear analysis of excavation tools. Their strength is mainly in the microscopic analysis as well as the implementation of hardness tests. The strength of geology is the ability to record and evaluate the geotechnical properties of the rock to be excavated. All these investigations must be combined in order to better understand wear processes. This is the only way to ensure the continuous development of tunnel boring machines and their excavation tools. For this reason, methods of materials science and geotechnology are used in combination in this study.

The problem with today's prediction models is that they are mostly based on index tests or intact rock parameters, which are determined in the laboratory. Examples are the CERCHAR Abrasivity Index (CAI) or the Uniaxial Compressive Strength (UCS). Laboratory tests, however, are always a simplification of reality and can usually represent the wear processes occurring in reality only very unsatisfactorily. It is therefore important to find out which tribological processes lead to wear. This is done in this thesis with the help of a macroscopic and microscopic wear analysis. Only afterwards the appropriate test for a wear prognosis can be determined.

In the case of the present study it was found that mineral and rock hardness has a significant influence on wear. As there is very little literature on the subject of hardness testing on minerals and rocks, the testability was investigated. It was investigated which test and which test load is best suited for hardness testing on minerals and rocks.

The advantage of a direct hardness test on minerals and rocks is that influences of grain size and orientation of the minerals can be taken into account. Previous wear predictions based on the Vickers Hardness Number Rock (VHNR, SALMINEN & VIITALA 1985) and the resulting Abrasiveness value (ABI, HASSANPOUR et al. 2011, 2014) cannot take such influences into account, as they are based on literature values for hardness.

3. Study site: Koralm Tunnel

In the course of the dissertation by Lisa Wilfing (WILFING 2016), who has carried out penetration tests at the construction site of the Koralm Tunnel in the construction section KAT2, the task of this study was the analysis of tool wear. The central question concerned the cutter wear and how it is influenced by the rock parameters. In addition to a detailed geological mapping and laboratory program for the encountered rock types, also the used disc cutters had to be analyzed with a corresponding laboratory program.

3.1 General information

The 33 km long Koralm Tunnel is the centerpiece of the section Wettmannstätten – St. Andrä, which belongs to the new southbound railway line in Austria (Fig. 14). This is part of the Baltic-Adriatic axis, a trans-European railway from Tallinn (Estonia) to Venice (Italy). The new southbound railway is planned as a high-speed section of up to 250 km/h and connects the provinces Styria and Carinthia. The traveling time between both main cities (Graz and Klagenfurt) is reduced from three to only one hour. This is intended to sustainably strengthen and promote the southern Austrian economic area.

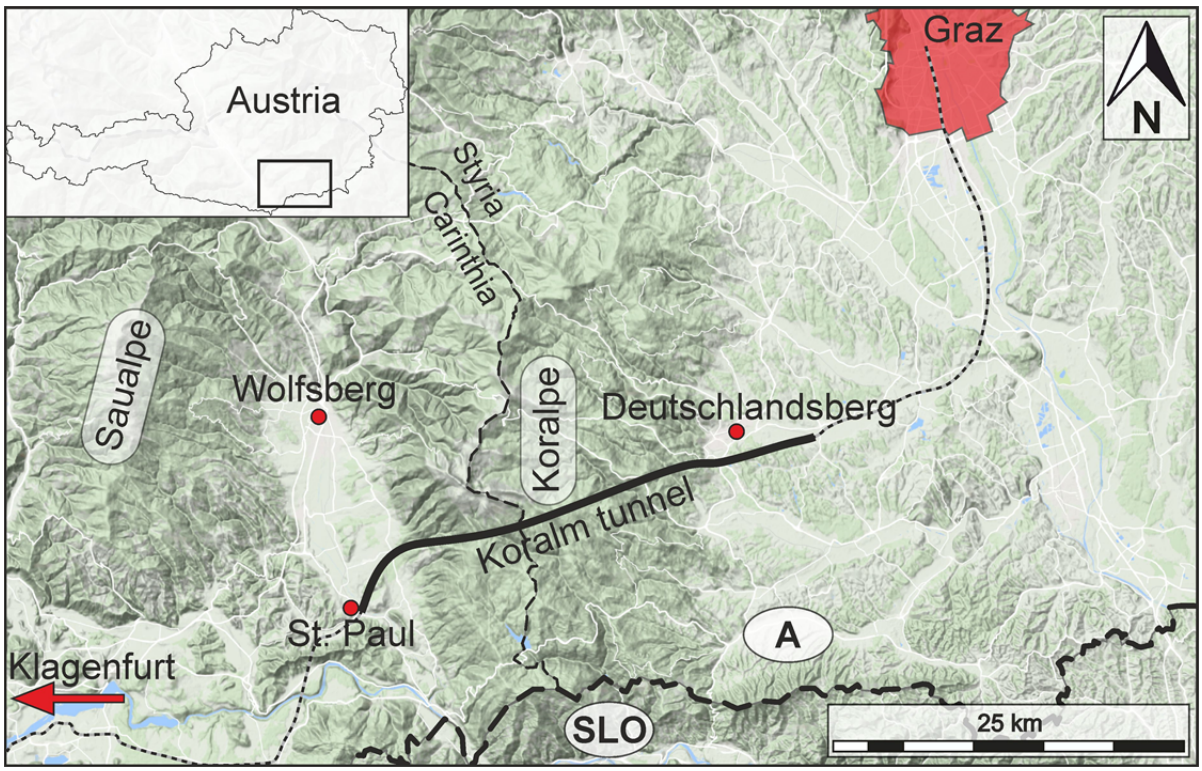

Fig. 14: Geographical overview of the Koralm railway line with the Koralm Tunnel as centerpiece (based on www-05 and www-06).

The double-tube tunnel (northern & southern tube) runs slightly curved east-west and passes through the mountain range of the Koralpe which is mainly north-south oriented (Fig. 15).

The highest peak is the “Große Speikkogel” with 2,140 m. The maximum overburden of the tunnel is about 1,200 meters. The eastern portal is located in the Laßnitz valley near Frauental and the western portal in the Lavanttal valley near Mitterpichling. The two tubes have an axle base of 40 to 50 m and are connected by cross headings every 500 m. The cross headings serve as emergency exits to the save second tube. In the central part of the Koralm tunnel, a 920 m long emergency room is located between the tubes. In its longitudinal direction, the tunnel has a straight crossfall and slopes of 5.44 ‰ on the Styrian side and 3.00 ‰ on the Corinthian side. The highest point is in the area of the provincial border between Styria and Carinthia (ÖBB-INFRASTRUKTUR AG 2012; JÄGER BAU GMBH n.d.).

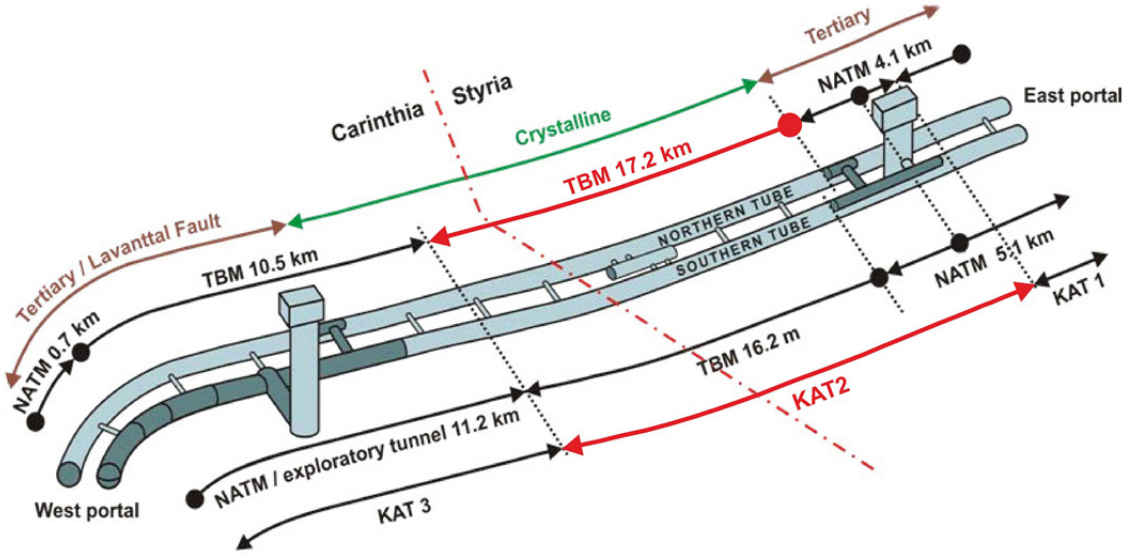

Fig. 15: Schematic sketch of the three construction sections at the Koralm tunnel. In the upper part in brown and green colors is given a rough geological classification. The bold red colors highlight KAT2 and the northern TBM section where research focuses on (mod. from www-07).

The total length of the 32.9 km long Koralm Tunnel is divided into three construction sections, called KAT1, KAT2 and KAT3. The focus of the thesis is on the northern tube of KAT2. This construction lot is mainly excavated with two double shield TBMs with a diameter of around 10 m. Over a length of about 10 km, TBM disc cutters and rock samples were taken and analyzed. Only the first 3 km at the transition from KAT1, the cross passages and the emergency room are excavated by drill and blast (NATM). The key information of KAT2 is given in Tab. 8.

Tab. 8: Key information for the construction section KAT2 at the Koralm Tunnel.

Construction section KAT2	
Length	18.8 km
Excavated diameter	9.9 m
Excavation profile	77 m^2
Max. overburden	1,200 m
Construction design	2 single tubes with axial distance ~ 40-50 m
Number of cross passages	39
Construction time	2011 –2019
Client	Österreichische Bundesbahnen Infrastruktur AG - ÖBB Infra
Contractor	Strabag SE & Jäger Bau GmbH

The construction work for the 18.8 km long section KAT2 was started 2011. In 2013, the mechanical tunnel drive started with the southern tube on the Styrian side. The entire tunnel will be opened 2023.

3.2 TBM-design KAT2

The construction section KAT2 is excavated by two Aker Wirth double shield TBMs of the type TB 993E/TS with a diameter of 9.93 m. The design and the equipment of the two machines are identical. For logistical reasons, the arrangement of the components was mirror-inverted.

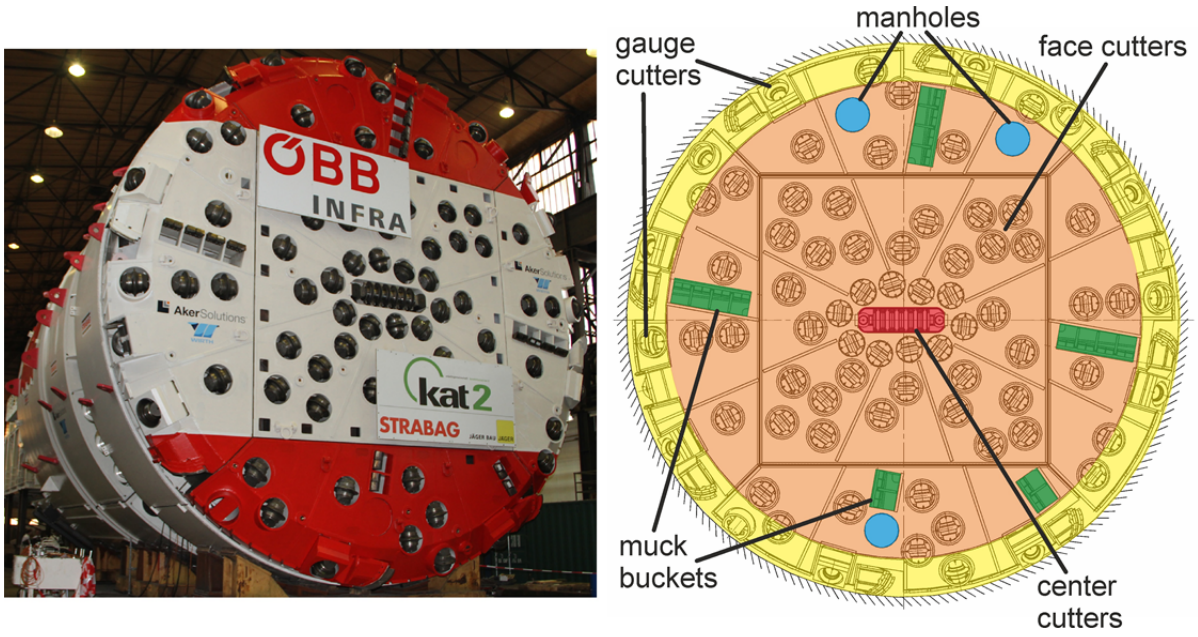

Fig. 16: Cutterhead design of the Aker Wirth TBMs used at KAT2 (www-08 and mod. from ÖBB-INFRASTRUKTUR AG 2009).

The cutterhead is equipped with two manholes, muck baskets and 80 cutters from which 67 are face cutters, 8 gauge cutters and 5 center cutters (Fig. 16). The cutters are constant cross section cutters with a diameter of 17 inch (432 mm) and a mean cutter tip width of 7/8 inch (22 mm). The average spacing is 65 mm. Some key information of the machine design used in KAT2 is summarized in Tab. 9 (WILFING 2016: 59; ÖBB-INFRASTRUKTUR AG 2009).

Tab. 9: Key information of the TBM-design of the Aker Wirth double shield TBM used at KAT2 (according to WILFING 2016; ÖBB-INFRASTRUKTUR AG 2009).

TBM-design KAT2	
Cutterhead diameter	9.93 m
Max. thrust force	23,000 kN
Max. torque	30,000 kN
Max. revolution per minute	5.5 rpm
Stroke length	1.9 m
Number of cutters	80 (red. 78)
Cutter diameter	17 inch (432 mm)
Cutter spacing	65 mm
Cutter tip width (mean)	7/8 inch (22 mm)
Max. force per cutter	267 kN

To get the force per disc cutter, the total thrust force must be reduced by friction of the shield and then divided by the number of the cutters. It is important to note that in this case the total number of cutters has to be reduced from 80 to 78 since gauge cutters only contribute to a small percentage of the penetration of the tunnel face (WILFING 2016: 58). Therefore, the number is considered by factor ¼ since their main goal is to ensure the tunnel's profile. Gauge cutters show less force transmission than face and center cutters as well. For 17 inch cutter rings, the maximum force is set at 267 kN (GIRMSCHEID 2013: 452).

3.3 Geology of project area KAT2

The Koralm Tunnel project is situated in the European Alps. In the past, the mountain range of the Koralpe was assigned after TOLLMANN (1977) to the Middle Austroalpine (Mittelostalpin). Since 2004 it is geologically put to the Upper Austroalpine (Oberostalpin) as major unit (SCHMID et al. 2004).

In this unit, it forms the basis of the Upper Austroalpine napes. This basement Koralpe-Wölz nape can be divided into the subunits called Murids, including the Glein- and Stubalpe, and the Korids including Sau- and Koralpe. The Murids are the lower unit (i.e. Wölz, Radenthein, Rappold, and Stallegg crystalline), which surprisingly shows lower metamorphosis than the Korids which are the upper unit (WILFING 2016: 59f.; TOLLMANN 1977: 20ff. and 211ff.).

This indicates an inverted metamorphic field gradient (SCHMID et al. 2004: 107ff.). The Korids, which are also called the Koralm crystalline complex, are overlain by the Plankogel crystalline complex (Upper Austroalpine) which is situated north of the Koralpe or rather even in the Packalpe region. It is overthrusted by the Ötztal-Bundschuh nappe system which is situated north of the city Graz or significantly further west. This in turn is overlain by the Drauzug-Gurktal nappe system which is well south of the project area. All these units belong to the Upper Austroalpine and show a normal metamorphic field gradient (SCHMID et al. 2004: 107ff.; SCHUSTER 2003).

The Koralm crystalline is limited by neogenic sediments in the east and the west. The Styrian basin in the east is an inneralpine molasse basin formed in the Tertiary with depths up to 3,000 m in the eastern part (TOLLMANN 1977: 234ff.). The basin is mainly filled with limnic fluviatile sediments and in Miocene and Pliocene volcanic activity also took place leading to spots with volcanic rocks such as tuff or trachyte (WILFING 2016: 59f.; FLÜGEL et al. 1984).

In the west, the Lavant basin delimits the Koralpe. This basin reaches a depth of around 800 m and is filled with debris from surrounding mountain ranges (BECK-MANNAGETTA 1952). The valley seen today has its origin in the Tertiary when there were great tectonic shifts and resulting fault tectonics with extreme high movement rates due to the formation of the Alps. The Lavanttal system can be associated with the main transversal fault zone of the eastern Alps, striking NNW-SSE and connecting with the Periadriatic fault in the south. The main activity occurred during the alpine orogeny and later in the Miocene age (23-5 Ma). The fault tectonics resulted in an offset of up to 5,000 m and led to an uplift of the Koralpe massif (BECK-MANNAGETTA 1952: 4). Subsequently, a subsidence of the southern and eastern part of the Koralpe caused a tilting of the rock layers in SE direction.

The longest part of the tunnel crosses the polymetamorphic basement of the Upper Austroalpine Koralpe-Wölz nape (WILFING 2016: 60). Fig. 17 shows a simplified geological map of the Styrian part of the Koralm Tunnel. The Carinthian part is missing because the directly adjacent geological map does not exist until now and the project area is mainly on the Styrian side. The metamorphosis in the Koralm crystalline took place during the Variscan (Hercynic) and Alpine orogeny. In the Variscan orogeny, two different metamorphic events can be distinguished. The first one was temperature controlled leading to fluids perfusing the rock and forming pegmatites. The second event was temperature and pressure controlled reaching the amphibolite and eclogite facies (TOLLMANN 1977: 240ff.). Due to the Alpine orogeny, the rock mass was overprinted in two stages (SCHMID et al. 2004: 107). During the Cretaceous period (100 Ma) the rocks got a significant, pressure dominated, Eoalpine overprint. Due to decompression after the orogenic peak period, a Barrow-type metamorphism followed afterwards. Nevertheless, the alpine metamorphosis was relatively weak (greenschist facies) and mainly characterized by high tectonic movement rates (FLÜGEL et al. 1984: 60ff.). The predominant folding direction during this deformation phase produced fold axis striking W-E / WNW-ESE.

According to TOLLMANN (1977: 236ff.), the Koralm crystalline can be divided into several geological series where the "Koralpenserie" and the "Schwanberger Serie" are affecting the tunnel excavation most. However, the classification of TOLLMANN (1977) is no longer recommended, but geological characteristics of encountered rock types are still useful. The "Koralpenserie" has a gradient from east to west: in the west, there are various types of gneiss while in the east the "Stainzer Plattengneis" is dominating. The "Schwanberger Serie" consists of gneiss with layers of amphibolite and eclogite as well as pegmatite dykes. Nevertheless, nearly all rock units of the project are pervaded by layers of amphibolite, eclogite, and marble and also pegmatite dykes. The "Stainzer Plattengneis" is particularly noteworthy because it has the highest metamorphic overprint (amphibolite – eclogite facies), builds up the core of the Koralpe and also appears at tunnel level. It is also worth mentioning that in the east of the Koralpe the rock layers are predominantly flat dipping to south while in the west they are steeper because of a stronger tectonic compression (TOLLMANN 1977: 246ff.). According to SCHMID et al. (2004: 107), the eclogitic parts are variscan MORB-type gabbros with Permian protolith ages and form the core of a recumbent fold with lower grade rocks in its limbs. These eclogites exist at the tunnel level as well as on the surface. The reason is that they are exhumed within an extrusion wedge.

As mentioned before, the division of the Alpine nappes is still subject to investigations. SCHMID et al. (2004) gives the current state of the art for the classification of the Alpine mountain range and differs from the previous classification according to TOLLMANN (1977). The Koralpe-Wölz nappe system is of major importance for understanding the Alpine orogeny, since the occurrence of high-pressure rocks like eclogite mark the suture of the subduction zone between the Adriatic and the European plate. However, the tectonic context is not emphasized in this thesis.

From the preliminary investigations for the tunnel project, a geological model was developed. This one is presented as a schematic longitudinal profile in Fig. 18 and sums up the geology in five major geological members: neogenic sediments in the east and the west, schistose gneiss and mica schist, fine to coarse grained gneiss and platy gneiss in the core of the Koralpe (ÖBB-INFRASTRUKTUR AG 2009). The study site is situated in the members of the schistose gneiss with also mica schist, the platy gneiss and the fine to coarse grained gneiss. As described above, lenses of marble, amphibolite, gabbro and eclogite, as well as pegmatite-dykes are perfused into these large units. According to this, these rock types were also partially found and tested. The main striking orientation of the schistosity is documented at an acute angle to the axis dipping flat to moderate against tunnel advance (WILFING 2016: 60). Due to small scale internal folding, the orientation may vary to a certain degree.

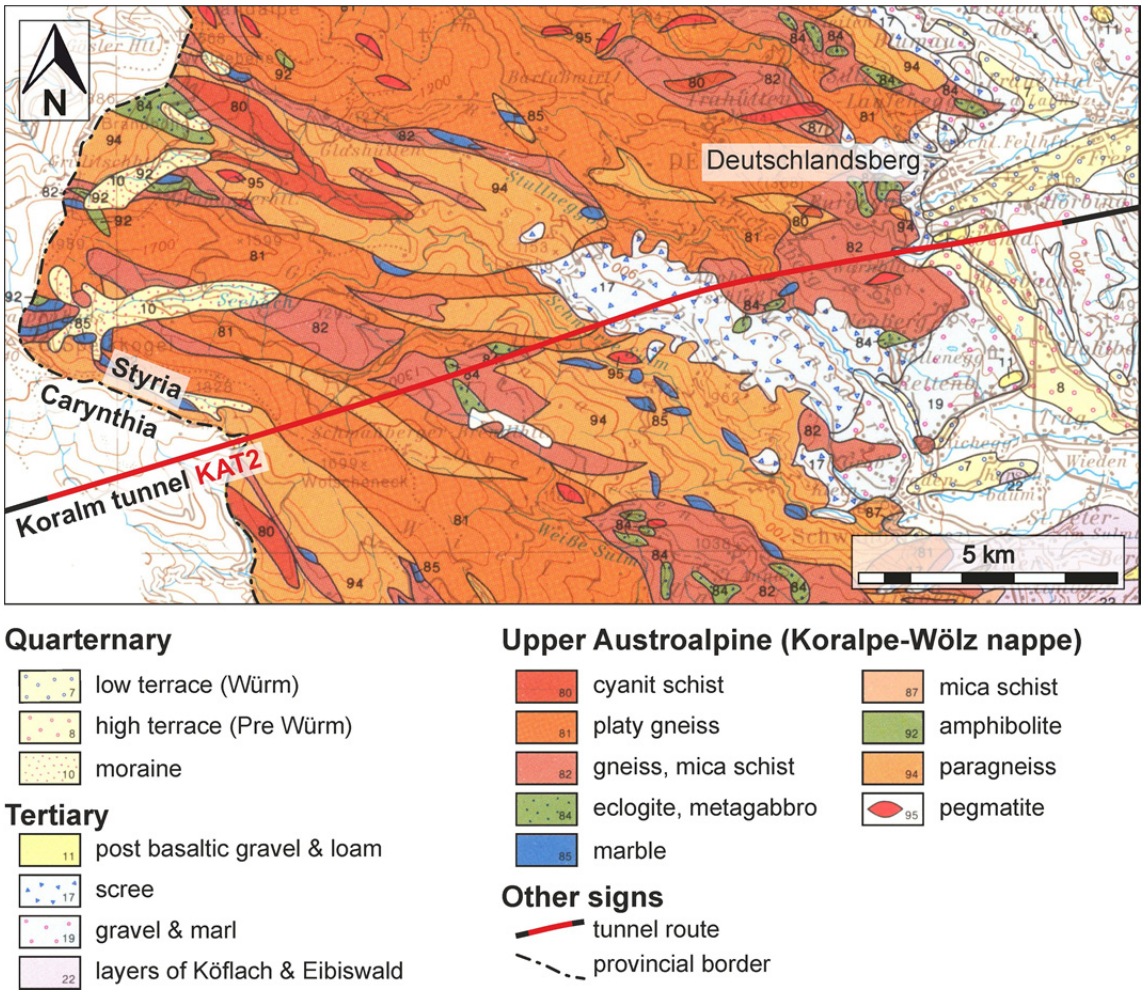

Fig. 17: Simplified geological map of the Styrian part of the project area with the tunnel route in black and red (mod. from FLÜGEL & NEUBAUER 1984; BECK-MANNAGETTA et al.1991; WILFING 2016: 61).

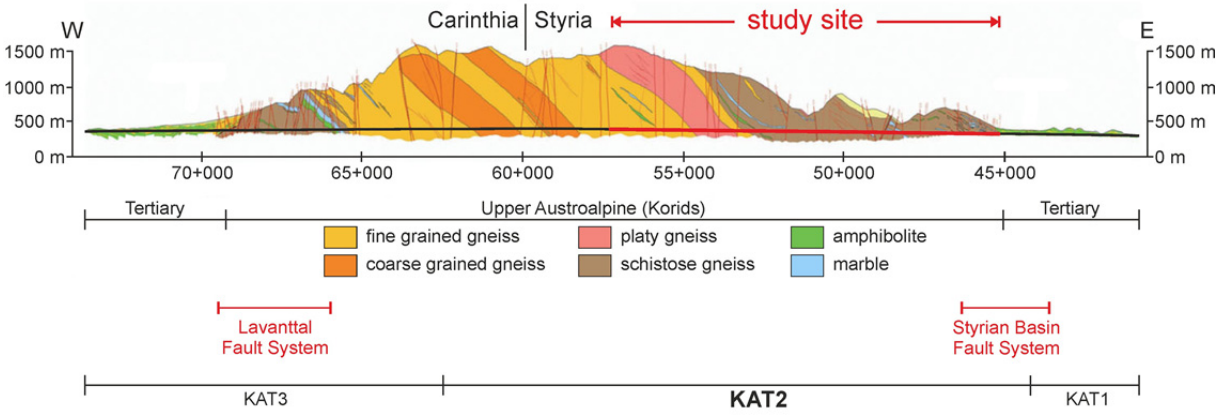

Fig. 18: Simplified geological longitudinal profile through the Koralm Tunnel showing the main contract sections KAT1-3, the major geological elements and the study site (mod. from MORITZ et al. 2011: 306; WILFING 2016: 61).

4. Sampling and sample description

In this part of the thesis, the samples are described and analyzed as well as the sampling strategy. The samples studied include different minerals, rock types, TBM disc cutters, CERCHAR pins and LCPC impellers.

4.1 Sampling strategy

4.1.1 Minerals

The selected minerals are frequently occurring and rock-forming minerals, which build up the majority of the rock types on the earth's surface. This also includes the minerals of the Mohs hardness scale. Since the Mohs hardness scale is the basis for the investigation of hardness in material science, geology and mineralogy, these minerals also serve as reference values. Other important minerals were extreme soft and hard ones, where a very low or high abrasiveness is assumed.

The selected minerals are typical forms, as they occur in nature. For this reason, the minerals do not have a particularly high degree of purity or even gem quality. They contain foreign ions, fluid inclusions and sometimes pores and cavities. This is in part also desired, since no database of maximum or minimum hardness is to be created. The minerals are only used to provide proper tests loads for the hardness tests and to check the test capability at all. Moreover, the minerals occurring in nature usually do not have any gem quality either.

4.1.2 Rock types

The selection of the rock types was very similar to the minerals. Hence, it was important to test mainly rock types that occur in the upper crust which form the earth's surface. These are the layers in which engineering structures are being built. These include excavations, tunnels, caverns, galleries, shafts and mines and wells in general.

For the selected rock types, all three rock units are represented: igneous rocks with plutonites and vulcanites, metamorphic rocks and sediments. In addition, it was paid attention that very low abrasive, as well as extremely abrasive rock types were present. Other criteria were e.g. rock types with a different grain size and type of binding or cementation.

4.1.3 Drilling tools and testing equipment

The focus in this part was on TBM disc cutters because their use is state of the art in mechanized tunnelling. These cutters are taken from the Koralm Tunnel project, which was presented in chapter 0. The advantage of this project is that it has a large range of soft, medium hard and very hard and solid metamorphic rocks in the excavated section of KAT2. These can be compared amongst each other with regard to the cutter wear. For this, cutters from the center, face cutters and also the caliber area were sampled in order to study the

differences in the direction of loading, rolling speed and cutter shape. Therefore, metallographic sections have been produced to analyze the microstructure and the hardness. In addition, the loading conditions (cutter thrust) and the wear on the surface were studied and evaluated using a light microscope and scanning election microscope (SEM).

Furthermore, the respective steel type (new and already worn) used for two wear tests, the CERCHAR Abrasivity Test (chapter 5.2.1) and the LCPC abrasivity test (chapter 5.2.2) were also analyzed by preparing metallographic sections. The surface again was studied and evaluated using a transmitted light microscope and scanning electron microscope (SEM).

4.2 Minerals

The used minerals were either collected in the field or taken from the mineral trade. Accordingly, it is usually not possible to provide information on the sample location, but this is not really necessary. Fig. 19 illustrates two example images of the used minerals before their preparation. Tab. 10 lists the minerals and their characteristic data.

Fig. 19: Left: pyrite with marking of the separation cuts; right: quartz as rock crystal.

A thin section of nearly each sample was prepared and analyzed for mineral analysis. In Tab. 10, this is indicated by the designation TSA (thin section analysis). Only pyrite was examined by reflected light microscopy (RLM) because it is an opaque ore mineral. Since the selected samples are mostly very pure minerals with only minor impurities and inclusions, the presentation and discussion of the thin sections was omitted.

Tab. 10: Compilation of the minerals used for investigations and conducted investigations.

Mineral	Numbering and abbreviation	Shape	Crystallographic orientation of the section	Conducted investigations
Talcum	TUM-MH1-1	finely dispersed	-	TSA, Knoop-, Vickers-hardness
Gypsum	TUM-MH2-1	finely dispersed	-	TSA, Knoop-, Vickers-hardness
Calcite	TUM-MH3-1	monocrystal	-	TSA, Knoop-, Vickers-hardness
	TUM-MH3-3	monocrystal	section 90° and 45° to the cleavage	TSA, Knoop-, Vickers-hardness
Fluorite	TUM-MH4-1	monocrystal	-	TSA, Knoop-, Vickers-hardness
Apatite	TUM-MH5-1	monocrystal	-	TSA, Knoop-, Vickers-hardness
Orthoclase	TUM-MH6-1	monocrystal	-	TSA, Knoop-, Vickers-hardness
Quartz	TUM-MH7-1	monocrystal	-	TSA, Knoop-, Vickers-hardness
	TUM-MH7-4	monocrystal	section 90° and 0° to the c-axis	TSA, Knoop-, Vickers-hardness
Topaz	TUM-MH8-1	monocrystal	-	TSA, Knoop-, Vickers-hardness
Corundum	TUM-MH9-1	monocrystal	-	TSA, Knoop-, Vickers-hardness
Almandine	TUM-GRT-1	monocrystal	-	TSA, Knoop-, Vickers-hardness
Pyrite	TUM-PYR-2	monocrystal	-	RLM, Vickers-hardness

4.3 Rock types

As already explained at the outset, the rock types are grouped into igneous rocks (magmatic and volcanic rocks), metamorphic rocks and sediments. Similar to the minerals, the name, the numbering and abbreviation and the origin is mentioned. In addition, a short petrographic description is made on the basis of a macroscopic analysis in combination with a thin section analysis. The description is thereby following DIN EN 12407 (2019), DIN EN 12440 (2018) and DIN EN 12670 (2019).

At the beginning, Fig. 20 gives an overview of the localities of the tested rock types. Please note that the Dala sandstone is a glacier transported boulder which was found in the Lausitz in the lignite opencast mine Jänschwalde (Point 13 a). The origin of this rock type is in the region Dalarna in middle-Sweden (Point 13).

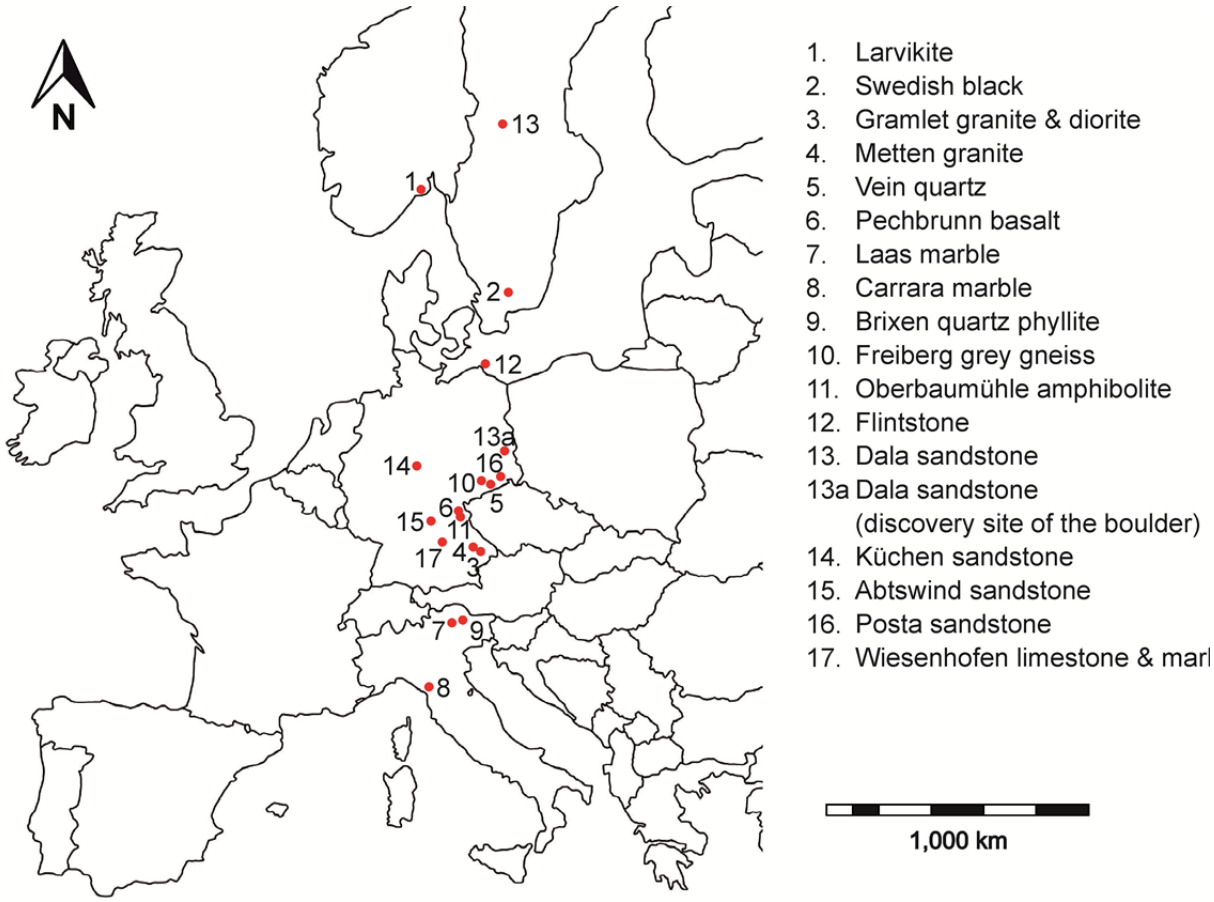

Fig. 20: European map with the localities of the tested rock types.

4.3.1 Igneous rocks: Magmatites

In this rock category, six different magmatic rock types are described. There are two different granitic rocks, one syenite (larvikite), one granodiorite, one micrograbbro (Swedish black/Ebony Black) and one quartzite.

Larvikite (TUM-LAR)

The larvikite is mined in several open pit quarries in the region around the eponymous city of Larvik, south-east Norway. The larvikite is a magmatic rock which consists of several smaller intrusions which form a big intrusion complex, called Larvik Plutonic Complex (LPC) (ANDERSEN et al. 2013: 63ff.). The intrusion took place in late Carboniferous to Permian due to the opening of the Oslo Rift. Today, the LPC is built up by 10 arc-shaped or circular intrusions of hypersolvus monzonite (larvikite) and nepheline syenite (ANDERSEN et al. 2013: 64). This is also the reason for the different rock types who are all called larvikite. However, it is not known from which quarry und which intrusion the tested rock originates. The larvikite is typically used in the natural stone industry or as a building stone.

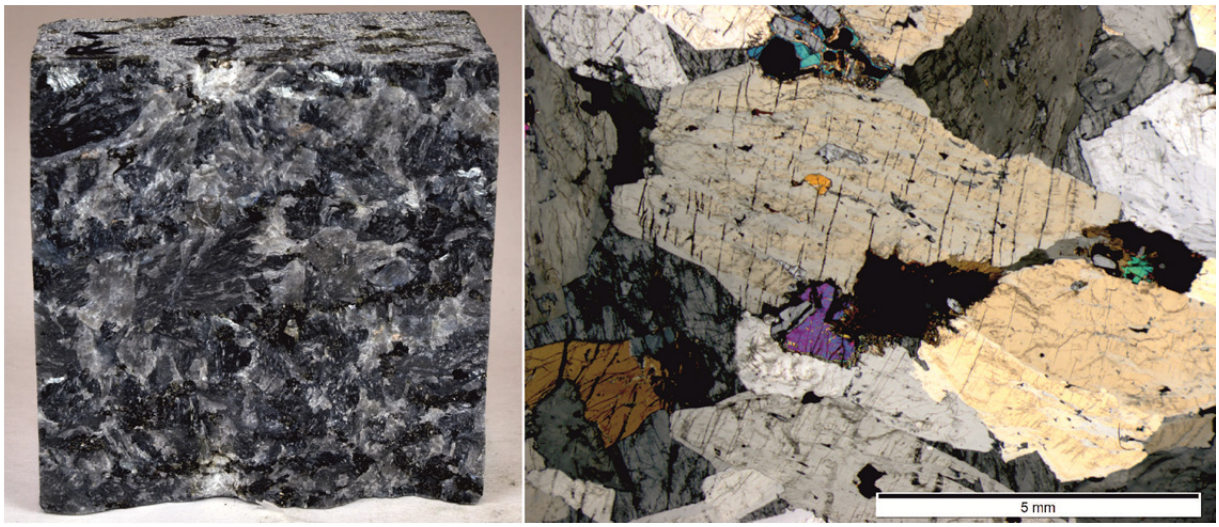

Fig. 21: Left: coarse-grained, blue-grey larvikite (cube width = 5 cm); right: microscopic photo with mainly anorthoclase and biotite as well as pyroxene and an opaque phase (X-pol).

The larvikite is a dense, coarse grained, holocrystalline, leucocratic, blue to dark-grey, homogeneous and isotropic rock. The macroscopically visible minerals are blue-grey alkali feldspar with a typical size between 1 and 3 cm and dark, up to 5 mm wide biotite (Fig. 21). Thus, the structure is porphyritic. The special characteristic of this rock type is the iridescence of the alkali feldspar. The microscopic analysis showed that quartz, pyroxene and amphiboles, apatite and an opaque phase (magnetite) are medium constituents. Epidote is an accessional mineral. The alkali feldspar was identified as anorthoclase, which is also typical for this rock (MÜLLER & KÖGLER n.d.c). It is remarkable that especially the pyroxenes are such strong corroded and altered that biotite is built out of them. It is also particularly evident that the

opaque phase often has a ring of biotite. According to STRECKEISEN (1980: 22), the larvikite is classified as alkali feldspar syenite. The latest classification is based on LE MAITRE (2005), who classifies the rock as monzonite. As there is no sign of weathering, the rock is classified as fresh. Further information of the rock is given in MÜLLER & KÖGLER (n.d.c).

Swedish Black/Ebony Black (TUM-SSW)

The tested rock is called Swedish Black or Ebony Black because of its origin in Sweden and its black color. It is mined in several open pit quarries in southern Sweden between Växjö and Kristianstad. The rock intruded into north-south oriented joints of the Baltic Shield due to volcanic activity and formed big, 10 to 55 m wide dykes around 900 Ma ago during early Neoproterozoic/Precambrian (FUCHS 1997). Thus, the quarries have an elongated shape. The Swedish Black is typically used in the natural stone industry.

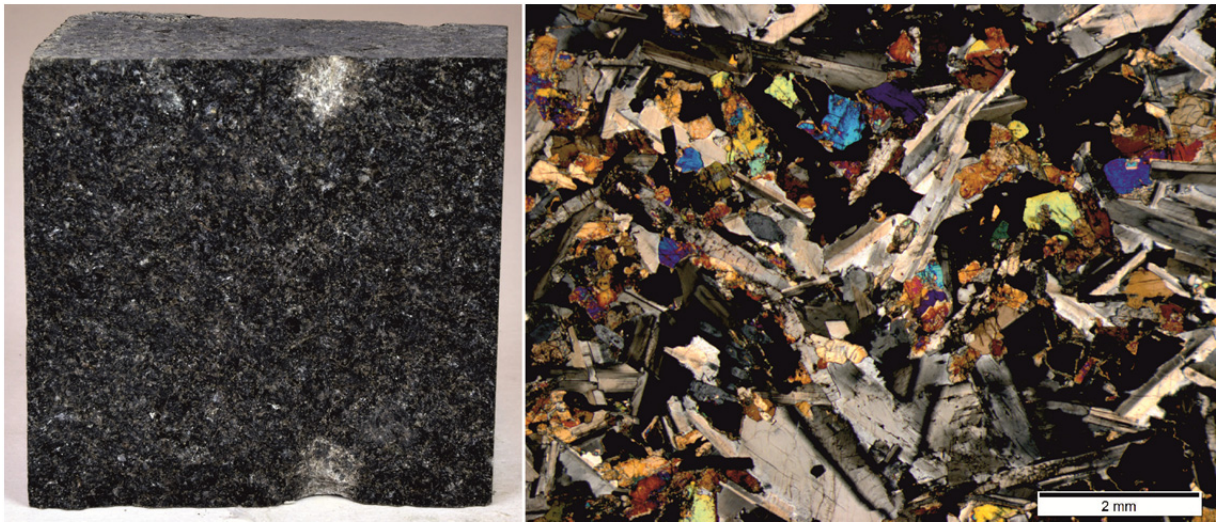

Fig. 22: Left: fine- to medium-grained Swedish Black (cube width = 5 cm); right: microscopic photo with elongated plagioclase-bars, pyroxene, biotite and an opaque phase (X-pol).

The rock is dense, fine- to medium grained, holocrystalline, melanocratic, dark-grey to black, homogenous and isotropic (Fig. 22). Macroscopically, dark and grey phases can be seen but not really distinguished. With the help of the microscopic analysis, plagioclase, amphiboles and pyroxenes are distinguished as main minerals. Medium constituents are apatite and an opaque phase (according to MÜLLER & KÖGLER (n.d.c) magnetite and ilmenite). Accessional minerals are biotite and chlorite. The structure is both porphyritic and ophitic. The macroscopic visible grey phase consists of plagioclase-bars with a maximum length of around 2.5 mm. According to MÜLLER & KÖGLER (n.d.c), the rock is classified as dolerite/coarse basalt while LE BAS & STRECKEISEN (1991) classifies it as micro gabbro. As there is no sign of weathering, the rock is classified as fresh. Further information of the rock is given in MÜLLER & KÖGLER (n.d.c).

Diorite (TUM-GRF)

The tested diorite is mined in the Bavarian Forest between Deggendorf and Passau northwest of Nammering, a little town east of Eging in a bigger open pit quarry called “Gramlet”. The operator is Kusser Granitwerke GmbH and the largest part of the quarried rocks are used as dimension stone, paving stone and aggregates. The diorite is nowadays interpreted as old intermediate rock which was carried upwards by younger, granitic magma (TROLL 1964: 124ff.). Thus, it is a rootless rock block. The diorite is part of a bigger intrusive body, the Fürstenstein intrusive complex which belongs to the western Bohemian Massif. The intrusion took place in Upper Carboniferous about 320 Ma ago (LEHRBERGER 2007).

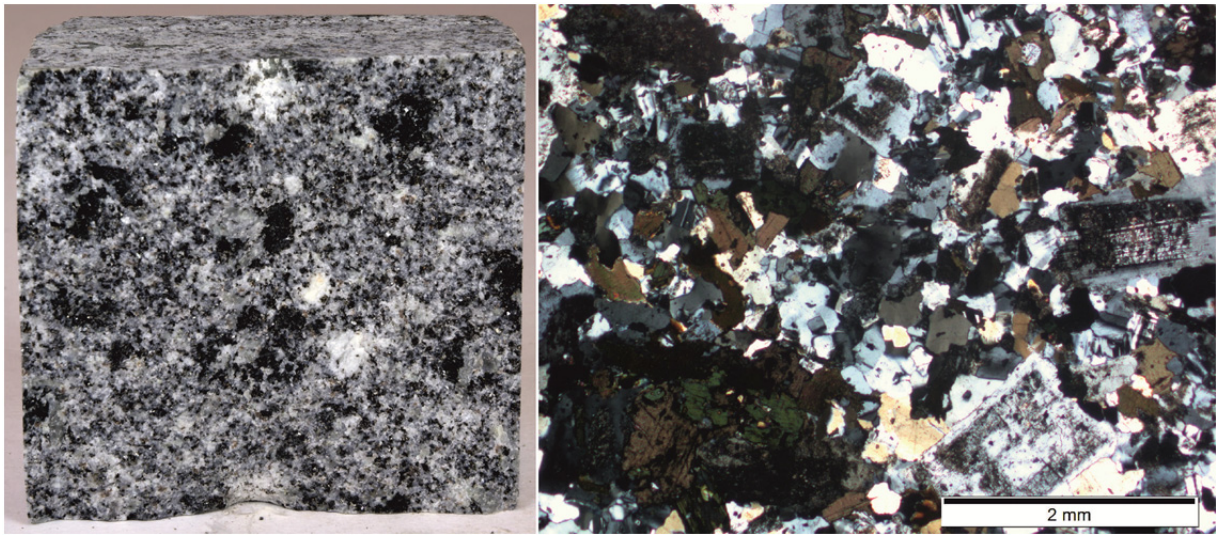

Fig. 23: Left: fine- to medium-grained granodiorite with the typical dark hornblende-biotite-chlorite spots (cube width = 5 cm); right: microscopic photo with plagioclase, quartz, biotite hornblende and chlorite (X-pol).

This rock is a holocrystalline, leucocratic to mesocratic, dense, fine to medium and equally grained, grey and isotropic rock (Fig. 23). Macroscopically, the minerals quartz, feldspar and biotite can be distinguished. A special characteristic are dark biotite-rich spots up to 10 mm in diameter. Microscopically, the feldspar can be divided in mainly plagioclase and less alkali feldspar. Medium constituents are biotite, chlorite, amphiboles and epidote. Accessional minerals are apatite and zircon. The dark spots consist of strong corroded amphiboles in the center, surrounded by chlorite, biotite and less epidote. Furthermore, much biotites show a chloritization. According to STRECKEISEN (1980: 22), the rock is classified as granodiorite. As the feldspar shows medium-strong sericitization and a chloritization of biotite, the rock is classified as slightly weathered.

Granite (TUM-GRZ)

The tested granite is also mined in the previously described open pit quarry Gramlet/Nammering of Kusser Granitwerke GmbH. The formation of the granite is different to the prior diorite. The granite is a former acidic magma which intruded around 320 Ma ago (LEHRBERGER 2007). Today, it is part of the bigger Fürstenstein intrusive complex which belongs to the western Bohemian Massif (TROLL 1964: 68ff). The granite is used as dimension stone, paving stone and aggregates.

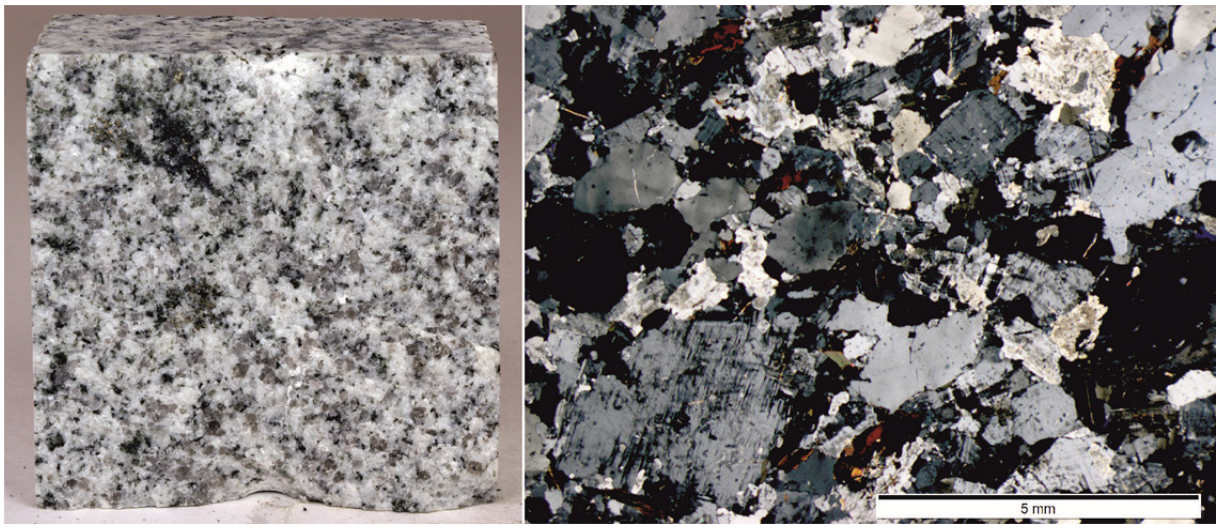

Fig. 24: Left: fine- to medium-grained granite (cube width = 5 cm); right: microscopic photo with alkali feldspar, quartz, plagioclase and biotite (X-pol).

Macroscopically, the granite is a holocrystalline, hololeucocratic to leucocratic, dense, fine to medium and equally grained, light-grey and isotropic rock (Fig. 24). The minerals quartz, two types of feldspar, much biotite, less muscovite, pyrite and chlorite can be seen with the pure eye and magnifier. With the help of the microscope, the feldspar can be divided into mainly alkali feldspar and less plagioclase. Accessional minerals are apatite and zircon. According to STRECKEISEN (1980: 22), the rock is classified as granite. As the feldspar shows slightly sericitization, the rock can be classified as slightly weathered.

Granite (TUM-MET)

The Metten granite is also mined in the Bavarian Forest north of Deggendorf near the village of Metten, which gives the name. It is part of a bigger intrusive body and belongs to the western Bohemian Massif (ROHRMÜLLER et al. 1996: 48). The intrusion took place in Upper Carboniferous about 320 Ma ago (LEHRBERGER 2007). The rock is typically used in the natural stone industry as dimension stone, paving stone and aggregates.

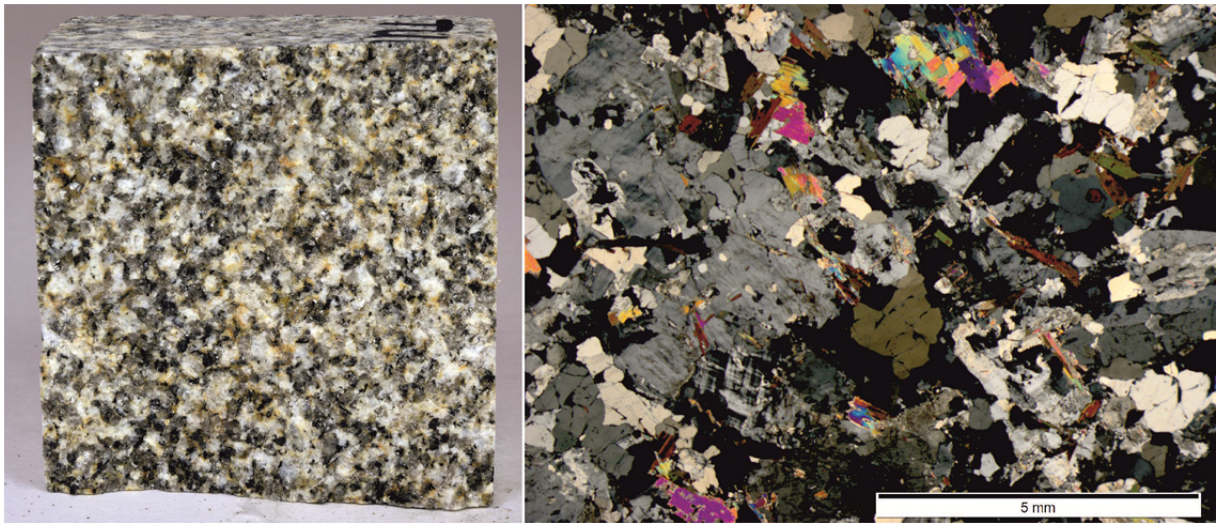

Fig. 25: Left: fine- to medium-grained granite (cube width = 5 cm); right: microscopic photo with alkali feldspar, quartz, plagioclase, biotite and muscovite (X-pol).

The Metten granite is a dense, fine to medium and equal grained, holocrystalline, leucocratic, beige-brown to gray, homogeneous and isotropic rock (Fig. 25). The main minerals are feldspar and quartz. Medium constituents are biotite and muscovite. On the microscopic scale, alkali feldspar and plagioclase can be distinguished, whereby alkali feldspar dominates. Apatite and zircon can be seen as accessory minerals. According to STRECKEISEN (1980: 22), the rock is classified as granite. Generally, this granite is described as slightly weathered because of a beginning sericitization of the two feldspar minerals and the brownish color around the biotite which is presumably limonite. Further information about the rock is given in MÜLLER & KÖGLER (n.d.a).

Quartzite (TUM-GQZ)

The tested quartzite is from a geotope called “Buttertöpfchen” south of the federal road S 184, 600 m west of the village Frauenstein in Saxonia, East Germany. Like the Freiberg Grey Gneiss, this rock type is also part of the Ore Mountains (Erzgebirge) which belong to the Saxo-Thuringian Variscian belt. The origin is either sedimentary or magmatic, but until yet, it has not been enlightened (SEBASTIAN 2013: 188ff.). However, it is part of a bigger, NW-SE oriented quartzite dyke. In the past, the rock was mined for and used as road gravel and building material (REINISCH 1920: 11f.). Today, the material is no longer used in practice.

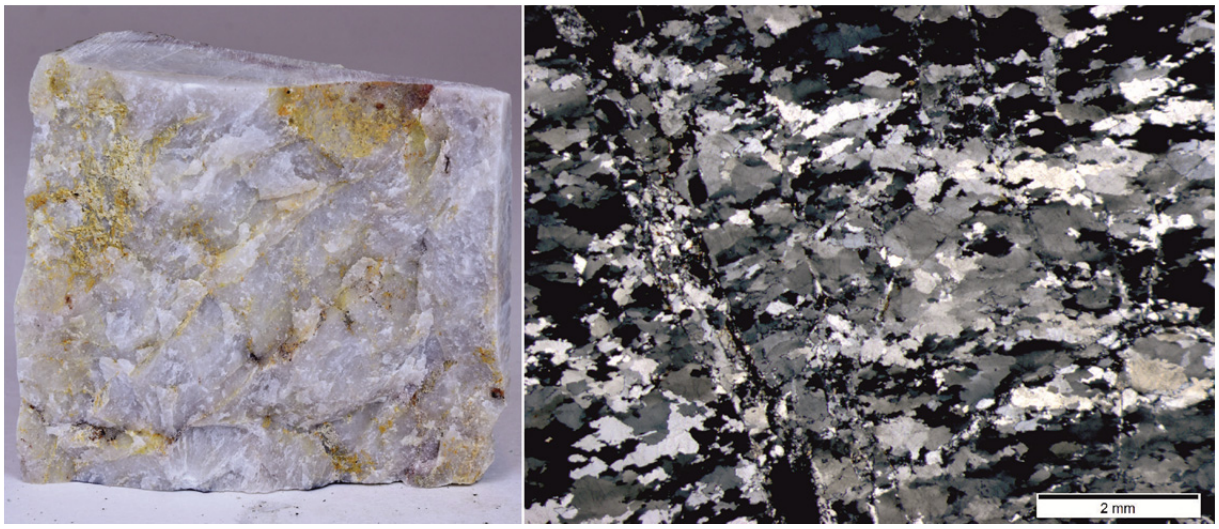

Fig. 26: Left: fine-grained quartzite with beige joints (cube width = 5 cm); right: microscopic photo of only quartz with big grains mainly on the right and small grains on the left side (X-pol).

The quartzite is a dense, extreme fine grained, hololeucocratic, holocrystalline, homogeneous, white to light grey rock with brownish joints (Fig. 26). With the help of the microscopic analysis, quartz can be identified as the major mineral. Accessional minerals are an opaque phase (presumably iron oxide) and less muscovite. The purity of the quartzite is estimated to be > 98 %. It is noticeable that the grain size of the quartz is variable. On the one hand side, there are big grains and on the other hand there are zones of very small grains. These zones with the small grain size are interpreted as areas with a relative motion. Due to the brittle behavior of the rock, it broke during uplift. Thus, with iron oxide filled joints pervade the quartzite. According to this, the rock can be classified as slightly weathered.

4.3.2 Igneous rocks: Vulcanites

In this category, only one rock was used in this thesis and is described below.

Basalt (TUM-PB)

The tested basalt is quarried in an open cast mine at the "Großer Teichelberg" by the Basalt AG in the northeast of Bavaria in the Upper Palatinate. Although it belongs to the Saxo-Thuringian Variscian belt, this volcanic rock is much younger. It was formed by the volcanism of the Miocene (21.4 Ma after STRUNZ et al. 1966) in the Fichtel Mountains, forming a sequence of basalt sheets. It emerged from fissures and volcanic vents in the center of the quarried hill. Today, the basalt is mainly used for the production of railway ballast.

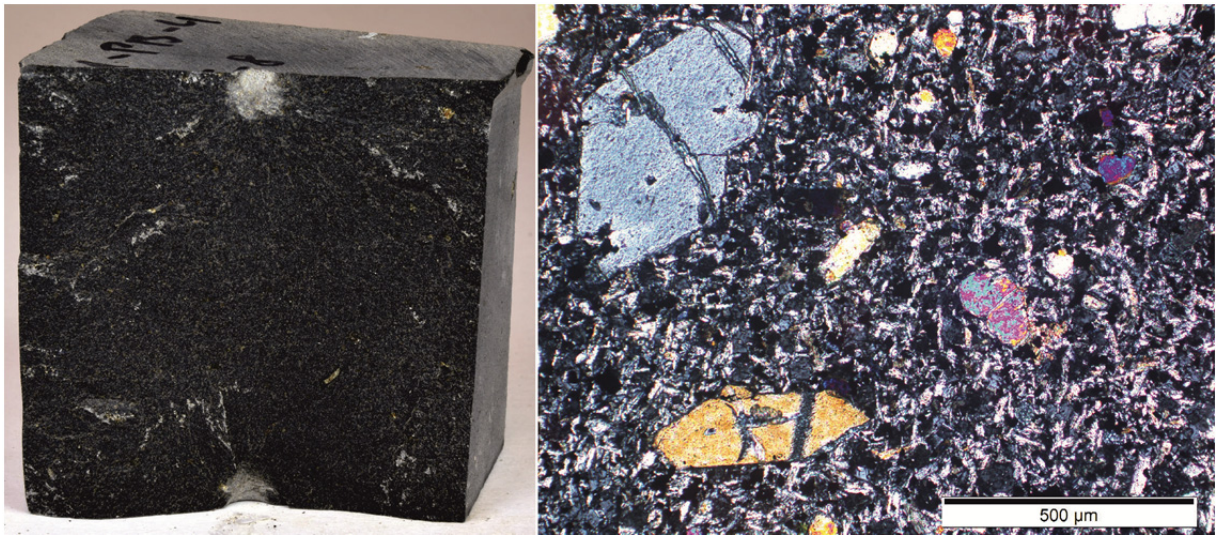

Fig. 27: Left: fine-grained basalt with some inclusions of olivine (cube width = 5 cm); right: microscopic photo with bigger olivine crystals in a matrix of nepheline and pyroxene (X-pol).

The basalt is a dense, dark grey to black, dense rock which shows conchoidal fractures when cracked. It has an aphanitic texture and contains macroscopically visible minerals of yellow-green olivine (Fig. 27). On the microscopic scale, the porphyritic texture is visible with idiomorphic and partly corroded phenocrysts of olivine and fewer pyroxene minerals. The dense and fine-grained matrix consists of Nepheline and Pyroxene (according to KAIM 1990 titanaugite). Accessory constituents are opaque magnetite, plagioclase, chlorite/serpentine, biotite and muscovite. The rock shows partly slight weathering/alteration because of chloritized/serpentinized pyroxene and olivine phenocrysts. A chemical analysis by NÄHER (1989) classified the Pechbrunn basalt as a plagioclase-bearing olivine nephelinite.

4.3.3 Metamorphic rocks

The tested metamorphic rock types contain two types of marble, one quartz phyllite, one gneiss and one amphibolite.

Marble (TUM-LAM)

This first marble is called Laas marble because of its natural stone quarries near Laas in South Tyrol, Northern Italy. In addition to Carrara, it is one of the most famous mining areas for a high quality of white marble in Central Europe. The marble belongs to the Ortler-Campo-Crystalline and got its metamorphic overprint during the Variscan and the Alpine orogeny (UNTERWURZACHER & OBOJES 2012). The usage is almost entirely restricted to building and dimension stone of all kinds.

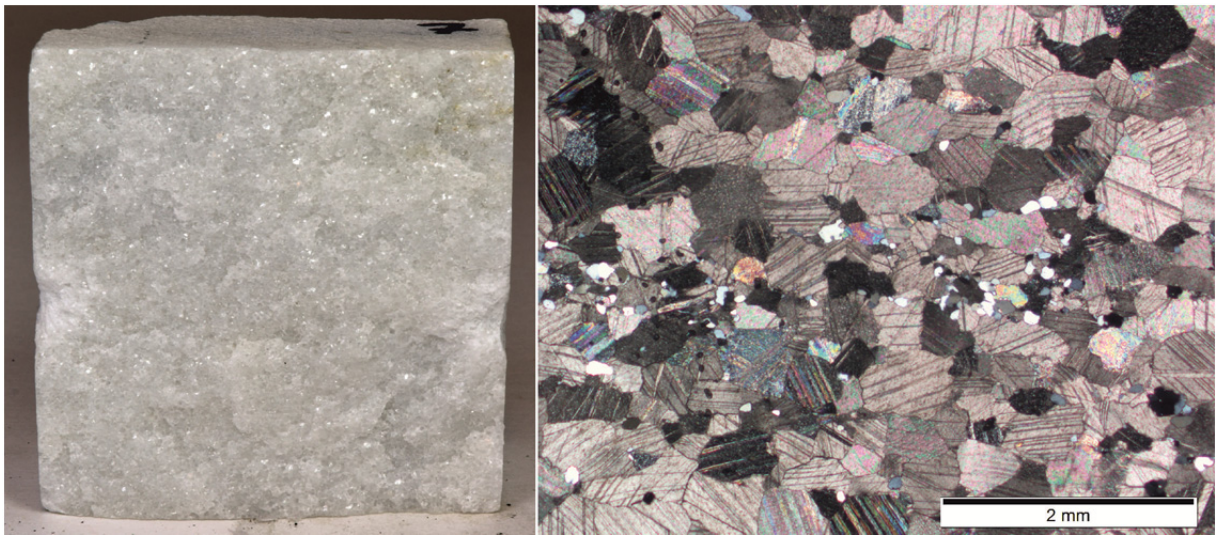

Fig. 28: Left: fine to coarse-grained Laas marble (cube width = 5 cm); right: microscopic photo with mainly calcite and a horizontal, quartz-rich zone with smaller quartz grains which indicate the ancient stratification (X-pol).

The Laas marble is a dense and almost pure white marble which consists of more than 95 % white calcite. The foliation can macroscopically be seen by the occurrence of dark inclusions (presumable graphite and pyrite) and occasional bands of muscovite which indicate the foliation. Accessory minerals can be quartz, dolomite, mica, feldspar, pyrite and graphite (UNTERWURZACHER & OBOJES 2012). The microscopic analysis revealed that the structure is granoblastic with a homogeneous equigranular texture. The calcite grains are hypidiomorphic to xenomorphic shaped and show typical high interference colours as well as calcite twins. The grain size is very uniform and in a range of 0.3 to max. 1.5 mm (Fig. 28). The grain size of the quartz is significantly smaller with up to 25 µm. The angle of 120° between the grains indicates equilibrium conditions during metamorphosis. Signs of weathering or an alteration cannot be seen. Thus, the Laas marble is classified as fresh. Further information of the rock gives MÜLLER & KÖGLER (n.d.b).

Marble (TUM-CAR)

The Carrara marble is as well as to the Laas marble one of the most famous high quality white marbles in Central Europe. It is mined near the eponymous City Carrara, which is south of La Spezia in Tuscany, Middle Italy. The marbles were once pure calcareous marine deposits from Lower Jurassic (Hettangian) which belong to the Tuscany-facies (DESSAU 1974: 69). They got a metamorphic overprint during Alpine orogeny in course of the orogeny of the Tuscan Apennine. It was a regional metamorphosis running at low temperature range (SHEREMETI-KABASHI 2002: 12ff.). The usage of the rock is almost entirely restricted to building and dimension stone of all kinds.

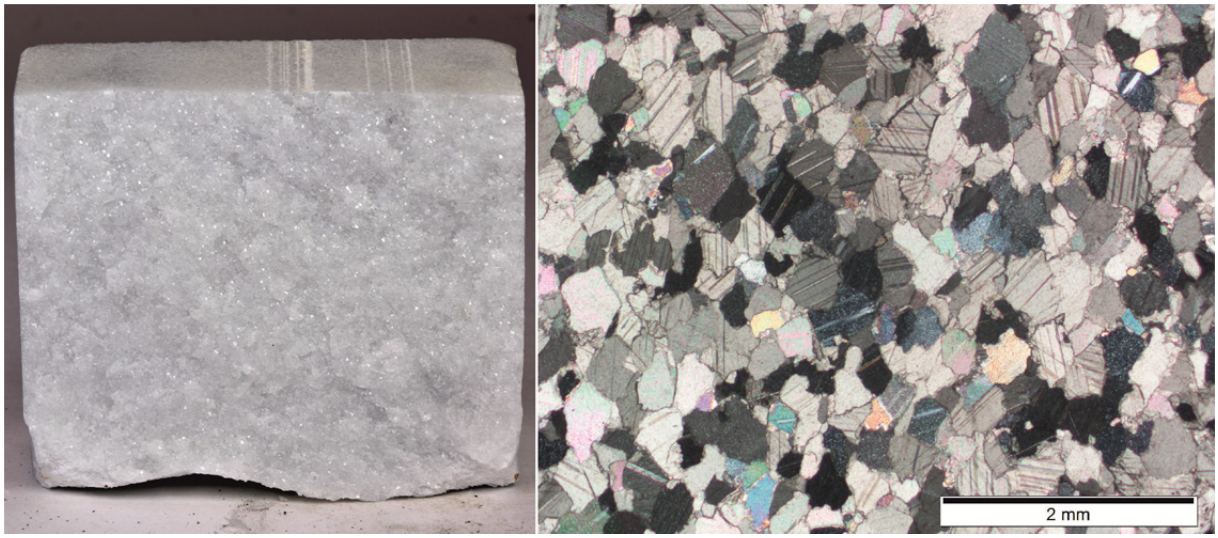

Fig. 29: Left: fine-grained Carrara marble (cube width = 6 cm); right: microscopic photo with mainly calcite and a single quartz grain in the right upper corner (X-pol).

The Carrara marble is a nearly pure white, dense, granoblastic, fine-grained, homogeneous and isotropic calcareous marble with nearly 100 % white calcite. In the present rock, the foliation is not visible since dark streaks or suchlike doesn't exist. The microscopic analysis confirms the high purity of nearly 100 % pure calcite (Fig. 29). Accessional minerals are only few quartz grains. The calcite grains are hypidiomorphic to xenomorphic shaped and show typical high interference colours as well as calcite twins. The grain size is very uniform and normally between 0.3 and 0.4 mm but a maximum of 0.8 mm was also observed. The angle of 120° between the grains indicates equilibrium conditions during metamorphosis. As no signs of weathering or alteration exist, the Carrara marble is classified as fresh. Further information of the rock can be seen in MÜLLER & KÖGLER (n.d.b).

Brixen Quartzphyllite (TUM-BQP)

The quartz phyllite was sampled at a road cut from the connection road between Lüsen and Flitt, two small villages near Brixen (South Tyrol/North Italy). The rock unit, to which the rock belongs, is called Brixen Quartzphyllite. As the name suggests, this rock is metamorphic. The educt are relatively carbonate-poor pelites and psammites with a Cambrian age (DULCE 1989: 19). The rock got its metamorphic overprint during the Variscan orogeny (400-300 Ma, STINGL & MAIR 2005: 40).

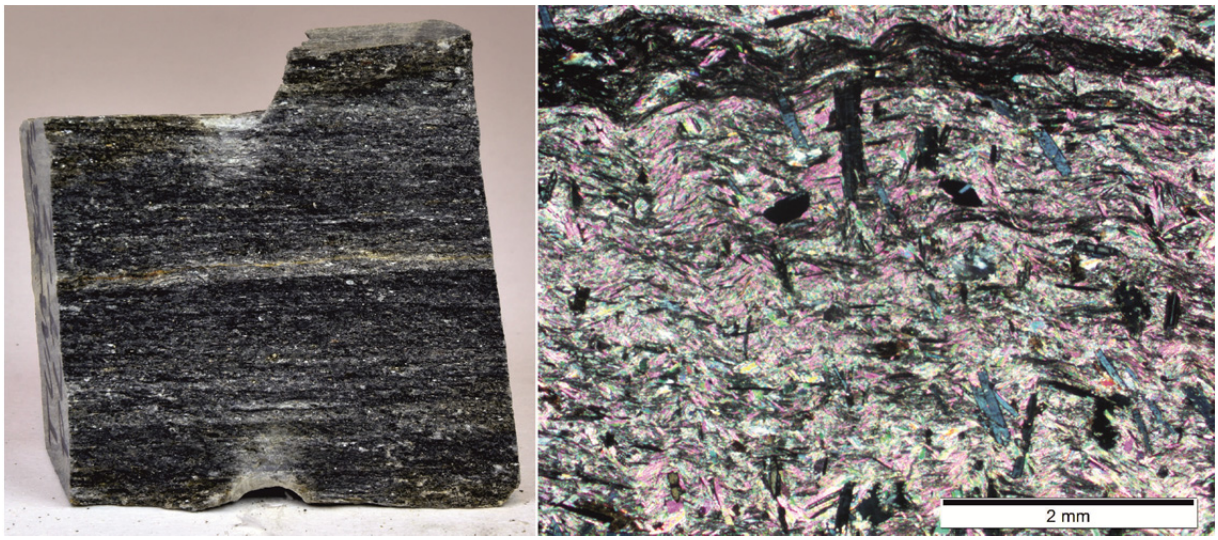

Fig. 30: Left: fine-grained Brixen Quartzphyllite (cube width = 5 cm); right: microscopic photo with a wavy foliation of muscovite and quartz, the upper dark zone is made up of graphite, the bigger blue chlorites and dark-brown biotites perpendicular to the foliation indicate a retrograde metamorphosis (X-pol).

The Brixen Quartzphyllite has a dark-brown to dark-grey color, is dense, fine grained and strongly planar foliated. A fine striping of grey and dark layers is visible macroscopically. Microscopically, quartz and muscovite are the main minerals (Fig. 30). Medium constituents are chlorite, opaque graphite and biotite. The foliation is wavy and mainly formed by muscovite and graphite. The grain size is mostly uniform and between 0.1 and 0.7 mm. But there are also larger chlorites, muscovites and biotites with a size up to 2 mm which lie perpendicular to the foliation. This is interpreted as a product of retrograde metamorphosis. The macroscopic visible striping is caused by an alternation of graphite and quartz-rich layers. However, the high graphite content shows, that the protolith was a carboniferous-rich sediment. With the macroscopic visible muscovite, the Brixen Quartzphyllite has to be classified as a graphite-mica slate. Signs of a slight weathering are brownish joints.

Gneiss (TUM-FGG)

The gneiss was sampled at the spoil dump of the ancient silver mine “Reiche Zeche” in Freiberg, Saxonia (Germany). The rock belongs to the formation of the Freiberg Grey Gneiss which is part of the Ore Mountains (Erzgebirge) which belong to the Saxo-Thuringian Variscian belt. The granodioritic educt of the Freiberg Grey Gneiss intruded during the Cadomian (650-550 Ma) orogeny and got his metamorphic overprint during the Variscan orogeny (400-300 Ma) (BAYER 1997: 28; SEBASTIAN 2013: 101ff.). Since the ore mineralization has no influence on the tested rock, this topic is not addressed here.

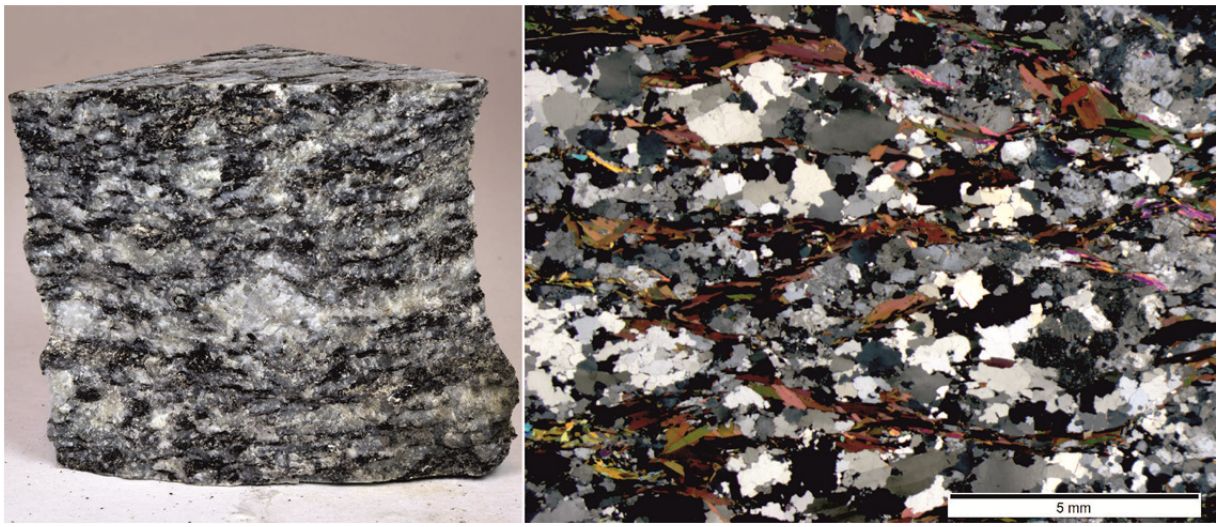

Fig. 31: Left: medium- to coarse-grained Freiberg Grey Gneiss with a clearly visible foliation and a alkali-feldspar eye in the middle (cube width = 5 cm); right: microscopic photo with quartz, feldspar, and biotite which traces the foliation (X-pol).

The Freiberg Grey Gneiss has a grey color, is leucocratic, dense, medium- to coarse grained and strongly foliated with bigger light grey feldspar eyes of up to 2 cm in size. Thus, the structure is partially porphyritic and strongly anisotropic because of mica and feldspar, which generate the foliation (Fig. 31). The change between dark biotites and bright, quartz- and feldspar-rich layers gives the rock its striped appearance. The microscopic analysis showed that quartz and alkali feldspar are the main minerals. Medium constituents are plagioclase, biotite and muscovite. Accessional minerals are apatite, an opaque phase and zircon. The bright layers are often either almost pure quartz or feldspar. The feldspar-eyes are alkali-feldspar porphyroblasts and presumably magmatic relicts. Some biotites are oriented perpendicular to the foliation which is interpreted as a result of a retrograde metamorphosis. The analyzed rock sample is slightly weathered because of a beginning sericitization of the feldspar.

Amphibolite (TUM-OBM)

The Oberbaumühle amphibolite is mined by the Basalt AG in an open pit quarry near Windischeschenbach in Upper Palatinate in the north of Bavaria. The amphibolite deposit belongs to the Bohemian Massif of the Moldanubian Variscian belt and is ancient basalt which erupted 485 Ma ago (STRUNZ et al. 1966). Today, the amphibolite is used as ballast rock.

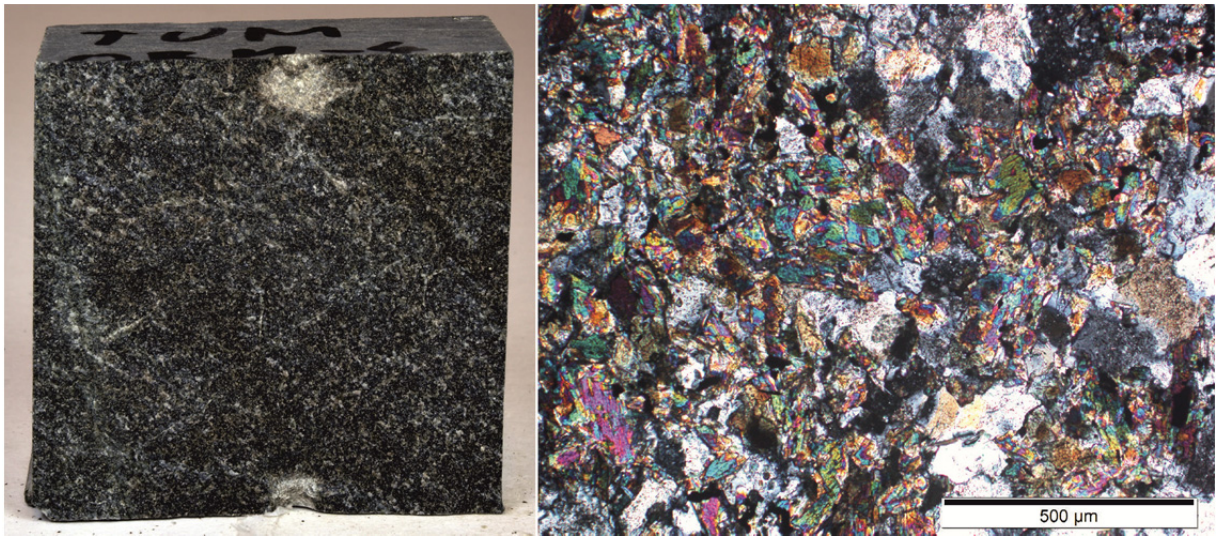

Fig. 32: Left: fine-grained amphibolite with no visible foliation (cube width = 5 cm); right: microscopic photo of the isotropic structure with a felt of amphiboles and plagioclase (X-pol).

The Oberbaumühle amphibolite is a dense, fine grained, meso- to melanocratic, greenish rock. Visible minerals are green to brown amphiboles and a white-grey phase of feldspar (Fig. 32). A straight foliation with an alignment of minerals is macroscopically not visible. Thus, the rock is mostly isotropic. In addition, some feldspar/quartz veinlets are irregularly dispersed throughout the rock. On the microscopic scale, green amphibole (presumably actinolite) and plagioclase can be identified as main constituents. Accessory minerals are an opaque phase, quartz, epidote, biotite and chlorite. The amphiboles are not particularly well shaped, rather it is a felt made of amphiboles. However, the amphiboles show a slight alignment in the felt, which is interpreted as a slight foliation. The typical grain size is between 0.1 and 0.5 mm. The analyzed rock types are slightly weathered because of a beginning saussuritization of the plagioclase and a chloritization of some amphiboles.

4.3.4 Sediments

This category houses eight different sedimentary rock types. These include five different clastic sediments (sandstones in the wider term), one flintstone, one limestone and one marl sample.

Flintstone (TUM-FLI)

The flintstone is a rock sample which comes from the national park Jasmund on Rügen, in the northeast of Germany. There, the sea cliff exposed the White Chalk, in which the flintstones are inside as concretions. Thus, it was possible to collect good samples. The White Chalk of Rügen belongs to the Hemmoor-formation of the White Chalk group and is named as Rügen member within this formation (www-09). Chronostratigraphically, the Rügen member is of an Upper Cretaceous age and belongs to Masstrichtian (72.1 till 66 Ma) (COHEN et al. 2020).

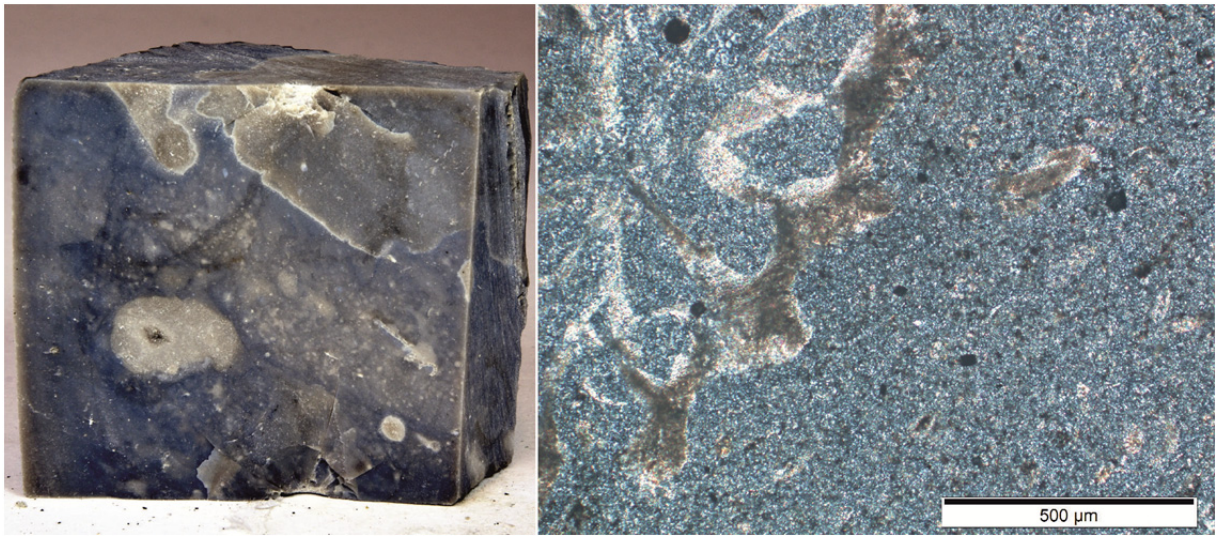

Fig. 33: Left: extreme fine-grained flintstone with biogenic residues (cube width = 6 cm); right: microscopic photo with the typical extreme fine grained matrix and a bigger biogenic residue on the left side and (X-pol).

The used flintstone is a dense, mostly grey concretion of very fine grained (microcrystalline) quartz with a roundish to amoeba-like shape and surrounded by a white layer. Partially, residues of biogenic components can be seen macroscopically. Under the microscope, several other residues of bioclasts become visible (Fig. 33). However, the flintstone consists of nearly 100 % pure microcrystalline quartz with a grain size under 6 µm. Signs of weathering are not present – so it is classified as fresh.

Sandstone (TUM-DST)

The Dala sandstone is typically found in the eponymous Region of Dalarna in Middle Sweden. It was sedimented as clastic rock (SALOP 1983: 213) in Middle Mesoproterozoic

(Proterozoic/Precambrian), 1.3 Ga ago (RUDOLPH 2016: 92f.). In the course of the Quaternary glaciation, the sandstone was transported to Central Europe as Nordic bed-load (THOME 1998: 70). The rock was found in the quaternary sands of the lignite opencast mine Jänschwalde in the Lausitz (Brandenburg, Northern Germany).

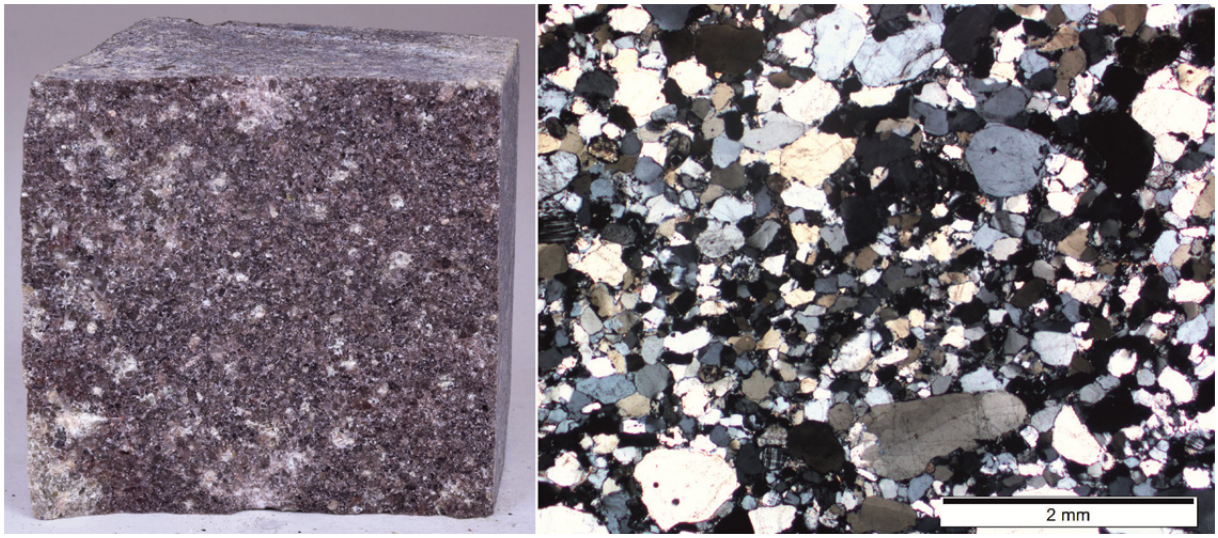

Fig. 34: Left: fine- to medium-grained Dala sandstone with the typical white spots (cube width = 5 cm); right: microscopic photo with mainly quartz, minor feldspar and lithoclasts, please note the graded stratification which leads to a difference in grain size (X-pol).

The clastic rock has a brownish-red color, is fine to medium grained, is dense with no visible pores and has a very good solidification. The layering is good to see and indicated by graded bedding. Though, there are also zones of a massive clastic rock with no stratification (Fig. 34). The structure is mostly grain supported, but also matrix-supported areas exist. The white spots on Fig. 34 are caused on the one hand by reduced areas and on the other hand from rock breaking. The microscopic analysis showed that quartz is the main mineral with over 90 %. Medium constituents are feldspar and lithoclasts with estimated 7.5 %. Accessional minerals are biotite, muscovite and an opaque phase (presumably hematite). This hematite also surrounds many grains with a thin layer. The grain size is from 0.01 until 2 mm. But there are two types of grains: the first one is very small and between 0.1 and 0.3 mm, the second one very big and between 1.0 and 1.5 mm. Thus, the rock is very poorly to poorly sorted and also mostly grain-supported. The grain shape is between sub-rounded to rounded. The few matrix is red colored by hematite and consists of quartz and hematite. The cement is also a combination of mainly quartz and less hematite. The pore space is very low and estimated to be under 5 %. After the sandstone consists of over 90 % quartz and only 7.5 % feldspar and lithoclasts, it has to be classified as a “subarcose” (FOLK 1959). As the feldspar and some lithoclasts show sericitization, the rock is classified as slightly weathered.

Sandstone (TUM-KUC)

The Küchen sandstone is excavation material from a German Motorway tunnel project (A44) under the village Küchen near Hessisch Lichtenau in the north of Hesse in Central Germany. The tested sandstone belongs to the Volpriehausen formation and was sedimented 249-247.5 Ma ago as the lower part of the Middle Bunter Sandstone (RICHTER-BERNBURG 1974: 142ff.). The Volpriehausen-alternation is characterized by a change from thin-banked to bladed, mostly fine grained, hard sandstones and solid mudstones (PRINZ & TIEDEMANN 1983: 142f.).

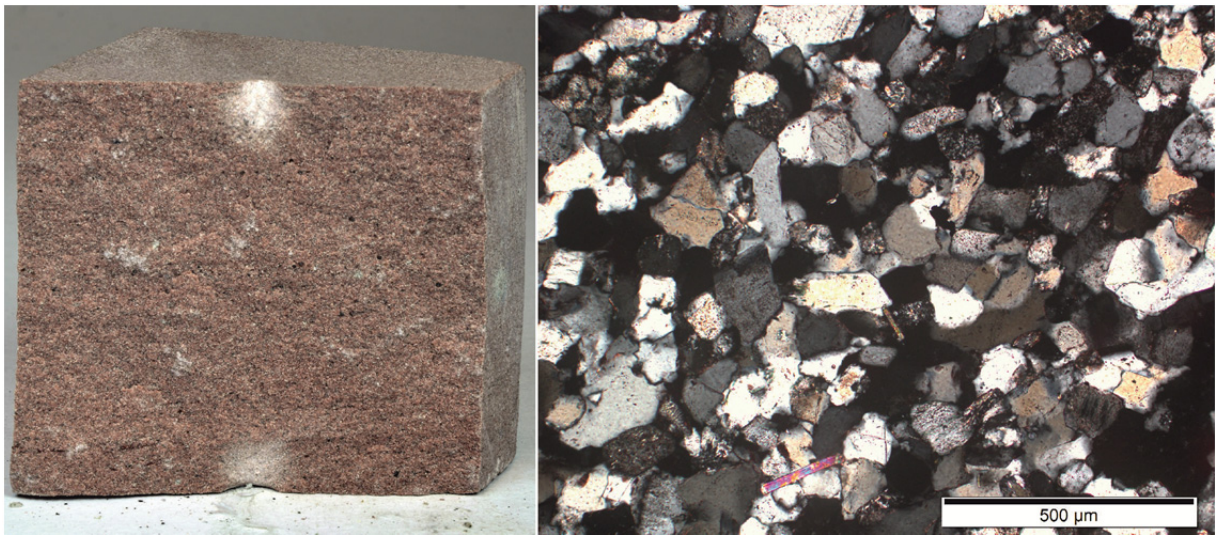

Fig. 35: Left: fine-grained Küchen sandstone (cube width = 5 cm); right: microscopic photo with mainly quartz, minor feldspar and lithoclasts as well as muscovite (X-pol).

This clastic rock has a pink to light red color, is medium to mostly equally fine grained and moderately sorted with very small visible and equally distributed porosity (Fig. 35). The solidification is good, the cement presumably siliceous. The layering is indicated by a slight grain size change and small light mica plates are located on the bedding plane. The microscopic analysis shows that the main mineral is quartz. Clearly slightly weathered feldspar and lithoclasts are medium constituents. Accessional minerals are muscovite and an opaque phase (probably hematite). The pore space is estimated with 25 % of volume. The roundness is not very good, the rock is classified as sub-angular to sub-rounded. The grain size is usually between 0.1 to 0.2 mm and the grain contact is partially grain to grain. But the range in grain size is between 0.1 and 0.65 mm. Partially, a red-brown, hematitic matrix exists. Some quartz grains are also surrounded by an iron oxide layer. After the sandstone is of around 70 % quartz and over 25 % feldspar and lithoclasts, it has to be classified as a "lithic arcose" (FOLK 1959). Signs of weathering are the already mentioned weathered feldspar and lithoclasts. Hence, it is classified as slightly weathered.

Sandstone (TUM-ABO & TUM-ABC)

This type of clastic rock is called Abtswind sandstone and belongs to the Stuttgart-Formation, known as "Schilfsandstein". It was sedimented during the Triassic, in the Middle Keuper as a channel sediment of a river delta which consists of finely clastic mud with clayey interlayers (EMMERT 1965; FREUDENBERGER 1996: 85). The mining sites are located in the western margins of the Steigerwald in Lower Franconia, on the western mountain slopes of the Friedrichsberg, east of the village Abtswind. The rock is mined in two open pit quarries, approximately 300 m apart from each other: the "Ortels"-quarry (ABO) in the north and the "Castell"-quarry (ABC) in the south. After the rock is slightly different in both quarries, they must be differentiated. Today, the rock is used as a popular building stone. The rock types from the Ortels-quarry are known as "Abtswind Sandstone Ortels" or "Abtswinder Grün" (www-10). Other spellings for the Ortels-quarry are "Ortler" (www-11) and "Ottels" (EMMERT 1965: 32f.). The rock types from the Castel-quarry are known as "Abtswind Sandstone Castell" or "Abtswinder Grün-Gelb" (www-12).

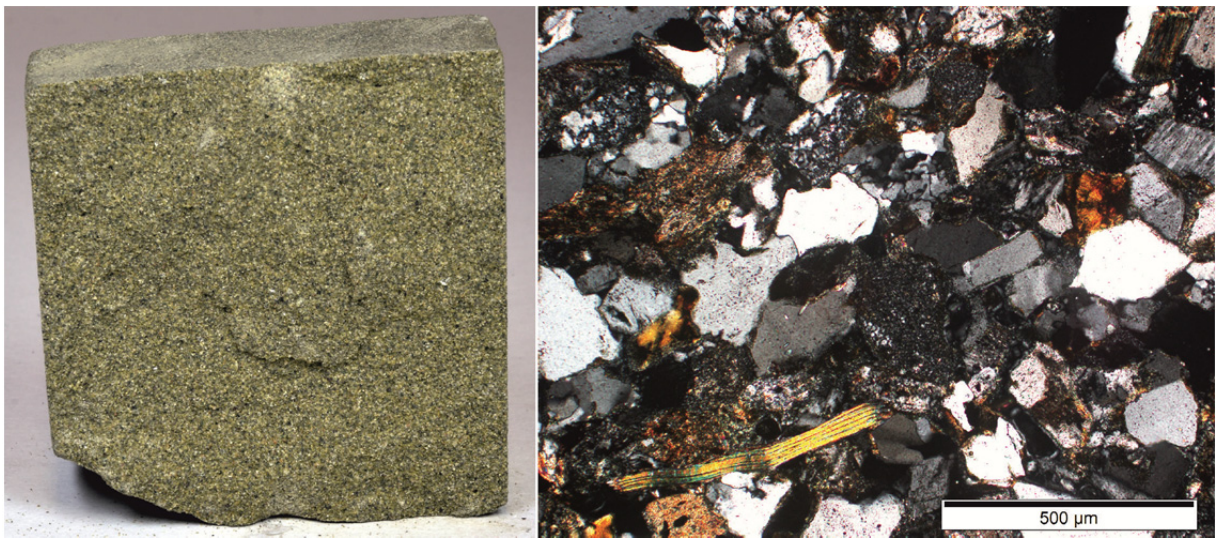

Fig. 36: Left: fine-grained Abtswind Sandstone Ortels (cube width = 5 cm); right: microscopic photo with mainly quartz, minor clay minerals, feldspar and lithoclasts, the mica left on the bottom indicates the stratification (X-pol).

The Abtswind Sandstone Ortels (ABO) is a homogeneous, greenish-yellow, fine grained, clastic rock with very small pores and a relatively poor grain binding (Fig. 36). A stratification is not visible, but elongated clay concretions with a diameter of 5 mm and a length of 30 mm are laid parallel to the stratification and indicate it. The microscopic analysis proves that the structure is mainly grain-supported and the texture is equigranular with a grain size mainly between 0.1 and 0.25 mm. The maximum observed grain size is 0.5 mm. Six different mineral-phases can be distinguished: mainly quartz and clay minerals, but also feldspar, lithoclasts, mica (muscovite and biotite in equal shares and less chlorite) and accessional an opaque phase. The degree of roundness is between sub-angular and well-

rounded, but the most clasts are sub-rounded to rounded. The cement consists of clay minerals which are also colored by chlorite and limonite. According to MÜLLER & KÖGLER (n.d.b) and ERMRICH (2017), the quartz content is 53 and 58 %, mostly feldspar and less rock fragments are between 20 and 35 %. In account of this, the rock has to be classified as a "lithic arcose" (FOLK 1959).

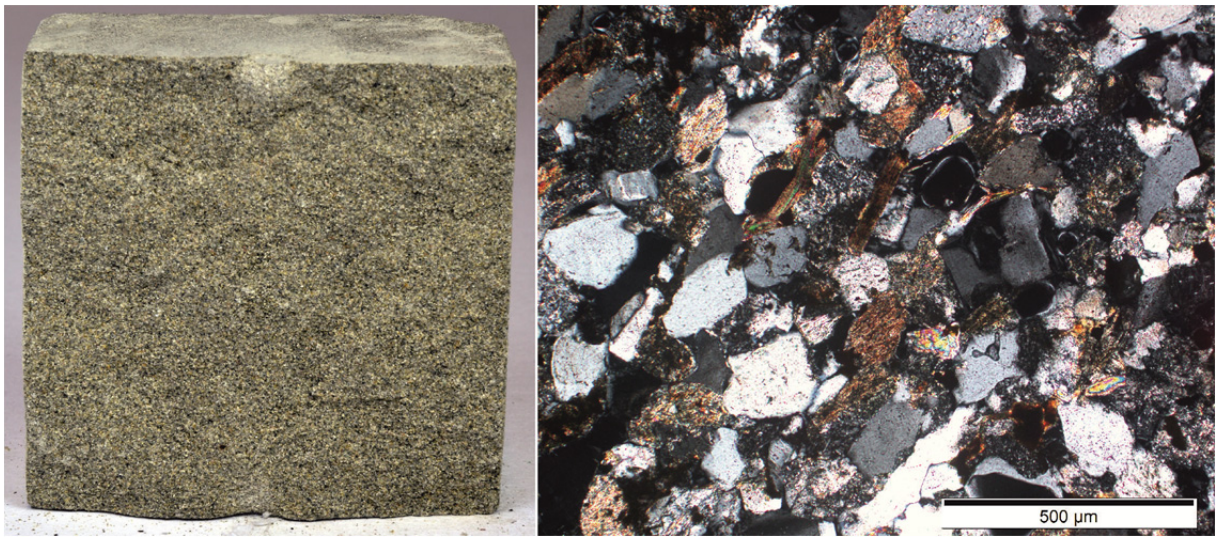

Fig. 37: Left: fine-grained Abtswind Sandstone Castell (cube width = 5 cm); right: microscopic photo with mainly quartz, minor clay minerals, feldspar and lithoclasts (X-pol).

The Abtswind Sandstone Castell (ABC) is also a homogeneous, beige, fine grained, clastic rock with very small pores and a relatively poor grain binding (Fig. 37). A stratification is not visible, but elongated clay concretions are laid parallel to the stratification and indicate it. The microscopic analysis shows, that the structure is mainly grain-supported and the texture is equigranular with a grain size mainly between 0.1 and 0.2 mm. The observed maximum grain size is 0.4 mm. This means, ABC is finer grained as ABO. But ABC has also six different mineral-phases: mainly quartz and clay minerals, but also feldspar, lithoclasts, mica (muscovite and less biotite and chlorite) and accessional an opaque phase. The degree of roundness is similar to ABO as well as the clayey cement. Also, the mineral contents are very similar. For this reason, this rock is also classified as a "lithic arcose" (FOLK 1959).

Sandstone (TUM-POS)

The Posta sandstone, or also called Wehlen sandstone is mined in several open pit quarries on the right bank of the Elbe River next to the town of Pirna in Saxonia, Germany. It is also known as "Over Ashlar" (German: Überquader) and belongs to the Elbe sandstones which were sedimented during the Late Cretaceous and today popular dimension and building stones in Germany (WIESER 2016). The formation of this sandstone took place in a marine environment in a shallow shelf sea in the Bohemian Basin (SKOČEK & VALEČKA 1983).

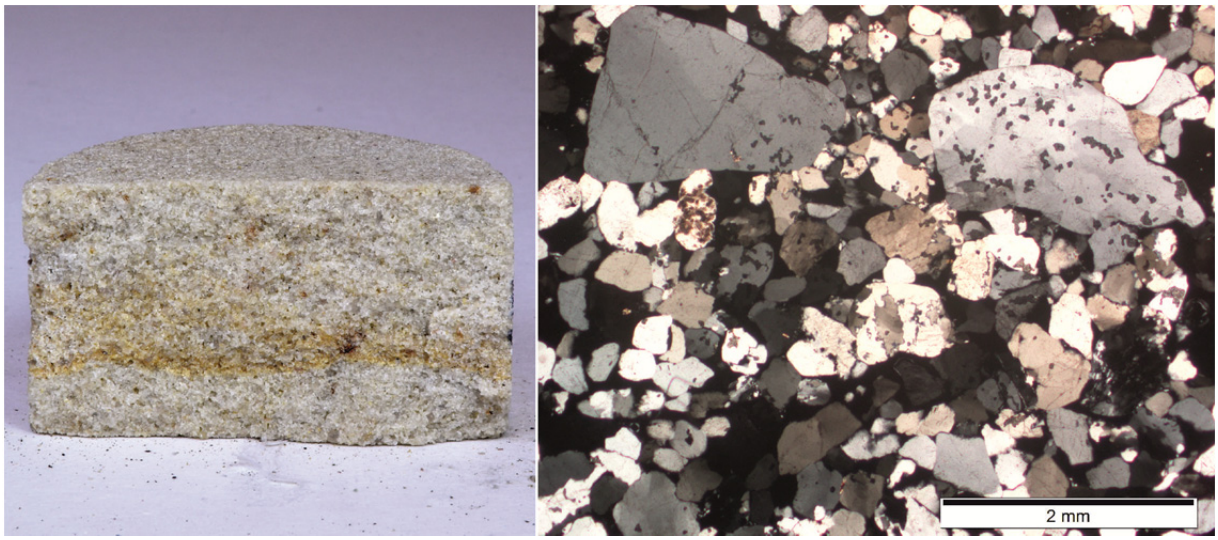

Fig. 38: Left: fine-grained Posta sandstone with a horizontal periodic precipitation (width = 5 cm); right: microscopic photo with nearly pure quartz in different grain-sizes (X-pol).

This clastic rock has a yellow-beige color, is mostly medium and equally grained with an equal porosity and the solidification is good. The layering is indicated by a slight grain size change. Noticeable is the periodic precipitation, which forms brown streaks (Fig. 38). The microscopic analysis showed that it is a quartz sandstone which is very pure (> 95 %). In addition to the main mineral quartz, also feldspar, lithoclasts, light and dark mica and an opaque phase occur accessional. The opaque phase is presumably a combination of iron and manganese hydroxides and can mostly be found in grain gussets. It is a mature siliceous sandstone with grain sizes mainly between 0.2 and 0.5 mm. The maximum observed grain size was 2.5 mm. The grains are subangular until well rounded; the most grains are sub-rounded to rounded. The grain contact is usually planar, the cement siliceous. The rock is grain-supported, a matrix is not present. The pore spaces are largely open, and the porosity reaches a value of 22 % (GRUNERT 2007), which was confirmed in the laboratory by SCHALLHAMMER (2014). Further information about the rock can be found in MÜLLER & KÖGLER (n.d.b).

Limestone (TUM-WIE)

The Wiesenhofen limestone is quarried by the company Max Bögl in an open cast quarry near Wiesenhofen, a municipality in Upper Bavaria. Besides the limestone, the adjacent marl (WME) is also quarried there. Both rock types were deposited there in a lime-marl alternation in the Franconian shelf sea in the Upper Jurassic (formerly called "Malm") (MEYER & SCHMIDT-KALER 1996: 103). Today, the limestone is used as concrete aggregate, various aggregates, fertilizer and armourstone.

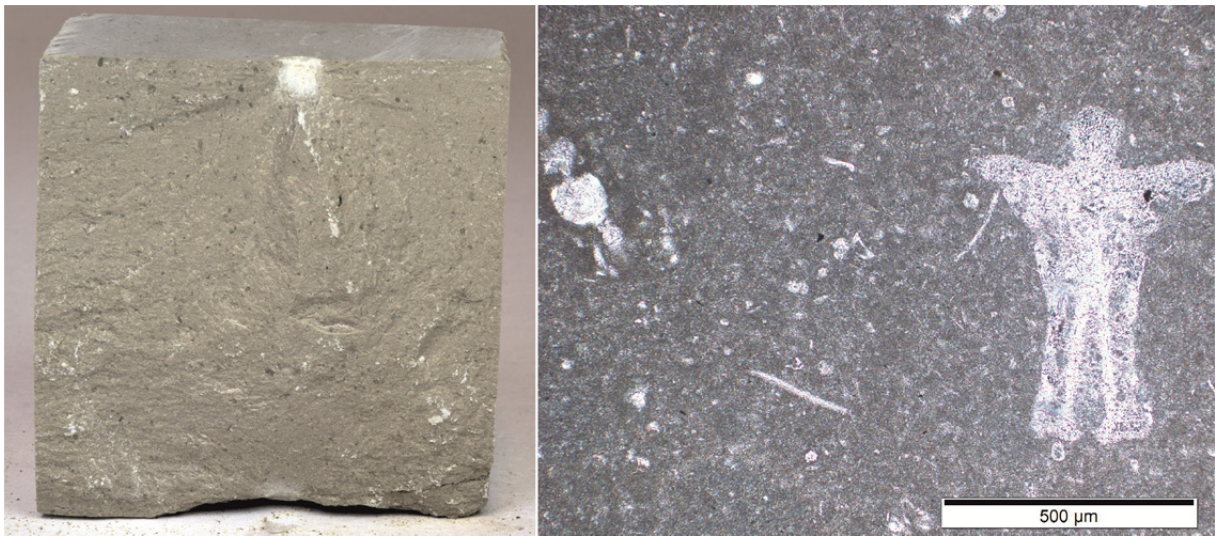

Fig. 39: Left: fine-grained, lutitic Wiesenhofen limestone (cube width = 5 cm); right: microscopic photo with nearly pure calcite, the matrix is micritic calcite and contains various calcareous bioclasts.

The Wiesenhofen limestone is a dense and massive homogeneous, isotropic, lutitic (extreme fine grained), beige rock which shows conchoidal fractures when cracked. A layering is not visible. Macroscopically, the rock shows little fossil content, but ammonites and belemnites are occurring occasionally. The microscopic analysis confirms the extreme fine grain size. The main mineral is calcite. Accessional minerals are pyrite, quartz and clay minerals. The matrix is micritic and was formed by a lutitic lime mud. The matrix contains bioclasts up to 1 mm in size and their share is estimated to be between 15 and 20 % (Fig. 39). According to RANZINGER (2013: 15), the clay content is between 0 and 3.2 %. Since the content of bioclasts is estimated > 15 %, the Wiesenhofen limestone is classified as a „sparse, biomicritic wackestone" (DUNHAM 1962). As no evidence of weathering could be observed, it is classified as fresh.

Marlstone (TUM-WME)

The Wiesenhofen Marl is quarried by Max Bögl near Wiesenhofen, just like the previous limestone (WIE). It was deposited in the Upper Jurassic as an alternating sequence with the Wiesenhofen limestone. Since in the south a connection with the Tethys existed, lime-rich deep waters could reach the shallow Franconian shelf sea. There they were precipitated and formed, together with the clayey and silty first cycle sediments of the Middle German barrier, a chalky-marly series (MEYER & SCHMIDT-KALER 1996: 103). For industry, the marl cannot be used and must be separated from the limestone.

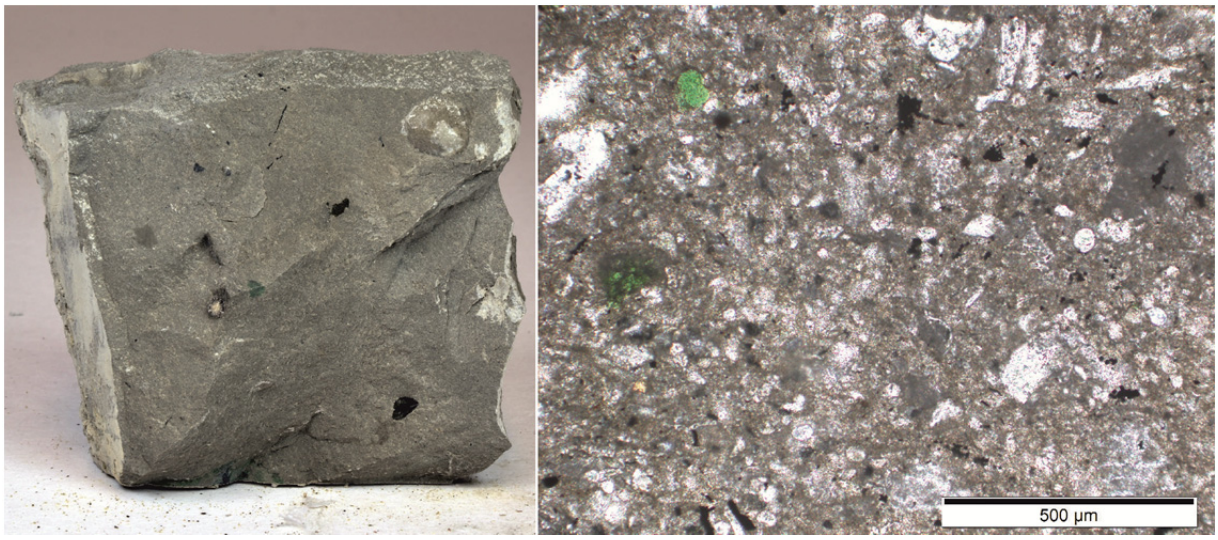

Fig. 40: Left: fine-grained, lutitic Wiesenhofen marl (cube width = 5 cm); right: microscopic photo with nearly pure calcite, the matrix is micritic and consists of calcite and clay minerals, it contains a high content of various calcareous bioclasts and two green glauconite grains on the left side.

The Wiesenhofen marl is a clayey and calcareous rock with grey color. Up to 0.5 cm in size, green spots are visible, which are either bound to fine crack structures or are spot-shaped. Macroscopically no components can be seen in the fine-grained matrix (Fig. 40). With the help of the microscopic analysis, many bioclasts can be identified with a size between 0.05 and 0.5 mm. They are in a matrix of micritic calcite and clay minerals and often oriented parallel to the stratification. The main mineral is calcite. The medium constituents are clay minerals with a share of about 15.7 % (RANZINGER 2013: 15). Accessional minerals are glauconite. According to the classification of DUNHAM (1962) and the revised version according to WRIGHT (1992), the Wiesenhofen marl has to be called "fossiliferous calci-mudstone". Darker colored joints are an evidence of weathering. On that account, it is classified as slightly weathered.

4.4 Drilling tools and testing equipment

In this chapter, the chosen TBM disc cutters as well as the used steels for CERCHAR pins and LCPC impellers are presented in tabular form. For this purpose, all three steel types were treated in different chapters.

In order to visualize the structure and especial the microstructure of the used steel under the microscope, the samples were prepared metallographically. They were cut and embedded in a mixture of resin, quartz and SiC. In the images shown in chapter 6.3, this is marked with "embedding agent". After grinding with SiC-powder (220 → 400 → 800 → 1,000 → 1,200 mesh), the polishing starts with diamond-plates (1,200 → 2,000→ 4,000 mesh) and is finished by a 1 µm diamond-suspension. To image the microstructure with a reflected light microscope (RLM, Leica DM LM) or a scanning election microscope (SEM, Zeiss LEO 1525 Gemini), the samples were contrasted by etching with Nital (3 cm³ HNO_3, 97 cm³ C_2H_5OH) if necessary. During the SEM imaging, energy dispersive X-ray spectroscopy (EDX-analysis) was used to examine the steel and the buildup on the surface.

In order to find out which material the steels used are, representative samples were examined in the laboratory of H-O-T Härte- und Oberflächentechnik GmbH & Co.KG in Nuremberg with the aid of a spark spectrometer (OES – Optical Emission Spectrometer). The exact results can be found in the appendix.

4.4.1 TBM disc cutter

As already mentioned, the TBM disc cutters come from the Koralm Tunnel project. Accordingly, the numbering applied in this project is considered. With date and cutter number, the individual disc cutters can be allocated on the tool replacement records. Furthermore, the position of the cutters in the cutterhead, the location of use and the distance of use in meters of advance, the replacement reason, the macroscopic wear type, special characteristics and the conducted investigations are named.

Tab. 11: Compilation of the TBM disc cutters used for the investigations in this study.

TBM disc cutter	Position on TBM	Location of use in meters of advance [m]	Distance of use in meters of advance [m]	Reason for replacement according to the records	Wear type	Manufacturer	Material type, other data	Conducted investigations
520	54	2,602.1	260.9	Wear	Tapering + Grooving	Bartz	-	Knoop-, Vickers-hardness
1786	58	6,526.80	179.0	Oil leakage	Abrasive wear + Tapering	-	-	Knoop-, Vickers-hardness
5837	61	6,821.50	405.5	Wear	Blockage	-	-	RLM
2408	61	7,136.30	336.6	Wear	Abrasive wear	Aker Wirth	-	RLM, SEM, EDX

TBM disc cutter	Position on TBM	Location of use in meters of advance [m]	Distance of use in meters of advance [m]	Reason for replacement according to the records	Wear type	Manufacturer	Material type, other data	Conducted investigations
1811	64	7,136.30	336.6	Wear	Abrasive wear + Brittle Fracture	Aker Wirth	-	RLM, SEM, EDX
5840	62	8,402.50	28.2	Wear	Mushrooming	Aker Wirth	-	RLM, SEM
5669	64	8,402.50	28.2	Wear	Mushrooming	-	-	RLM, SEM
ZN1.2	Center cutter	9,135.80	384.2	Blockage	Abrasive wear + Tapering	Aker Wirth	1.2345 (hot-working steel)	OES, SEM, EDX
1319	36	9,169.00	402.3	Blockage	Abrasive wear + Tapering	Aker Wirth	-	RLM, SEM, EDX
586	70	9,169.00	33.2	Blockage	Blockage	Palmieri	-	RLM
901	72	9,169.00	33.2	Ring Breakage	Mushrooming + Chipping	Aker Wirth	-	RLM
QS25-N7	-	approx. 9,170	-	-	Blockage + Brittle Fracture	Palmieri	-	RLM
QS25-N8	-	approx. 9,170	-	-	Tapering + Grooving	Aker Wirth	-	RLM, SEM, EDX
QS25-N9	-	approx. 9,170	-	-	Brittle Fracture + Chipping + Blockage	Aker Wirth	-	RLM
U2	-	approx. 10,000	-	Wear	Mushrooming + Chipping	Aker Wirth	1.2345 (hot-working steel) on eclogite layer	OES, RLM
U3	-	approx. 10,000	-	Wear	Mushrooming + Chipping	Aker Wirth	on eclogite layer	SEM, EDR
1555	35	10,605.51	0.2	Ring Breakage	hardly used, no wear	Aker Wirth	1.2345 (hot-working steel)	OES, RLM
1472	65	11,439.24	30.5	Wear	Mushrooming + Chipping	Aker Wirth	-	RLM, Vickers-, Rockwell-hardness
1688	54	11,642.05	88.5	Wear	Abrasive Wear + Mushrooming	Aker Wirth	-	RLM
5678	62	11,745.95	2.2	Blockage	Mushrooming + Chipping + Brittle Fracture + Blockage	Aker Wirth	-	RLM, SEM, EDX
1650	8	12,103.48	119,9	Wear	Brittle Fracture	Palmieri	-	Vickers-, Rockwell-hardness
6483	52	12,116.80	133.3	Oil leakage	Mushrooming	Aker Wirth	-	RLM
573	76	12,118.65	180.8	Wear	Abrasive wear + Tapering + Grooving	Aker Wirth	1.2345 (hot-working steel)	OES, RLM, Rockwell-hardness

Structural analysis

A large number of TBM disc cutters were analyzed for the study. It is estimated that approximately 110 cutter rings with a weight of about 2.75 tons were involved. The spark spectroscopy of several cutters showed that presumably all are made of easily hardening high-alloy hot-work tool steel which is quenched and tempered and has the material number 1.2345 or is also referred to as X50CrMoV5-1. This material is typical for heavy duty (hd) cutter rings, which are common for hard rock TBMs today. Hardness, strength and toughness of the hot work tool steel can be adapted by heat treatment with quenching and tempering. In the case of this steel, tempering is performed twice for secondary hardening and to transform the retained austenite into annealed martensite.

All examined cutters showed a mostly very fine-grained and isotropic structure of tempered martensite. Fig. 41 illustrates exemplary two different cutters: The left image is taken from cutter 573 and the right image of cutter 5837. Both images show the structure of tempered martensite mentioned above, but in direct comparison small differences in grain size can be seen. The structure of tempered martensite shown here gives the material a high hardness and at the same time a high toughness, which is largely retained even at higher temperatures.

In addition, comparing different cutters from different manufacturers, it could also be seen that sometimes the steel structure ranges from highly martensitic to pure bainitic. This results in a clearly recognizable diversity of hardness, toughness, and thus wear resistance. Thus, differences in the production process (forging and heat treatment) and consequently a difference in quality can be identified (ELLECOSTA et al. 2018).

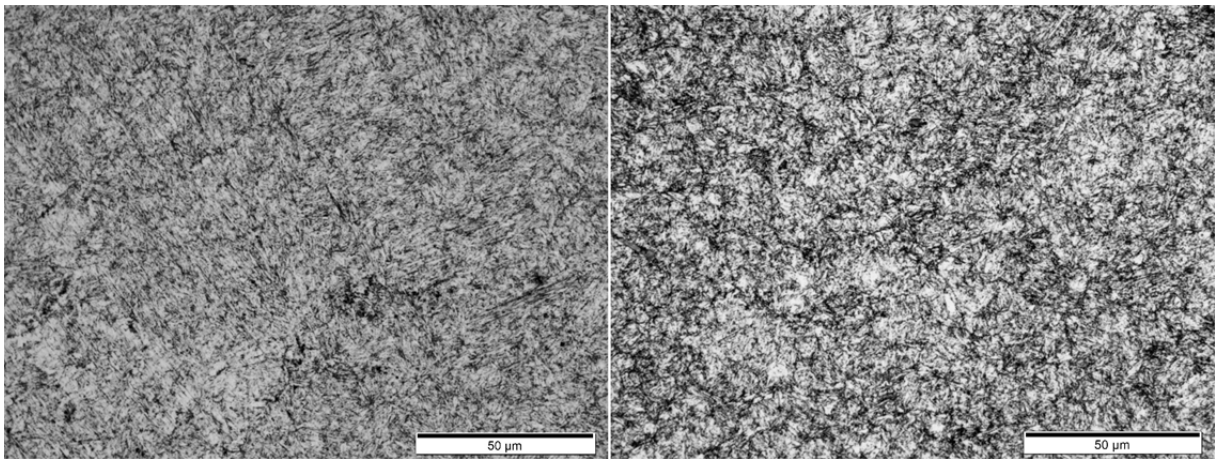

Fig. 41: Microscopic photos of polished and etched metallographic cross sections from TBM disc cutters from the Koralm project. Both images show a fine-grained and isotropic structure of tempered martensite. Left: cutter 573; right: cutter 5837.

4.4.2 CERCHAR pins

The CERCHAR (CAI) pins were purchased from the store Geotechnik Dunkel. The manufacturer of the pins and with it the steel type and its tempering are unknown. According to Geotechnik Dunkel, the pins correspond to the specifications, as explained in chapter 5.2.1. The overview Tab. 12 provides information on the numbering, the material type and the conducted investigations.

Tab. 12: Compilation of the CERCHAR pins used for investigations in this study.

CAI pin	Material type	Conducted investigations
CAI-A1-62	1.2210 (cold-working steel)	OES, RLM, Knoop-, Vickers-hardness
CAI-A2-45	1.2210 (cold-working steel)	OES, RLM, Knoop-, Vickers-hardness

Structural analysis

For the investigations, two new an unused exemplary CERCHAR (CAI) pins were selected and designated as follows: CAI-A1-62 and CAI-A2-45. The spark spectroscopy showed that both steels are made of the material 1.2210. The microscopic structure analysis with the reflected light microscope on metallographic cross sections showed that the exemplary samples CAI-A1-62 and CAI-A2-45 are both of bainitic structure with parts of ferrite Fig. 42.

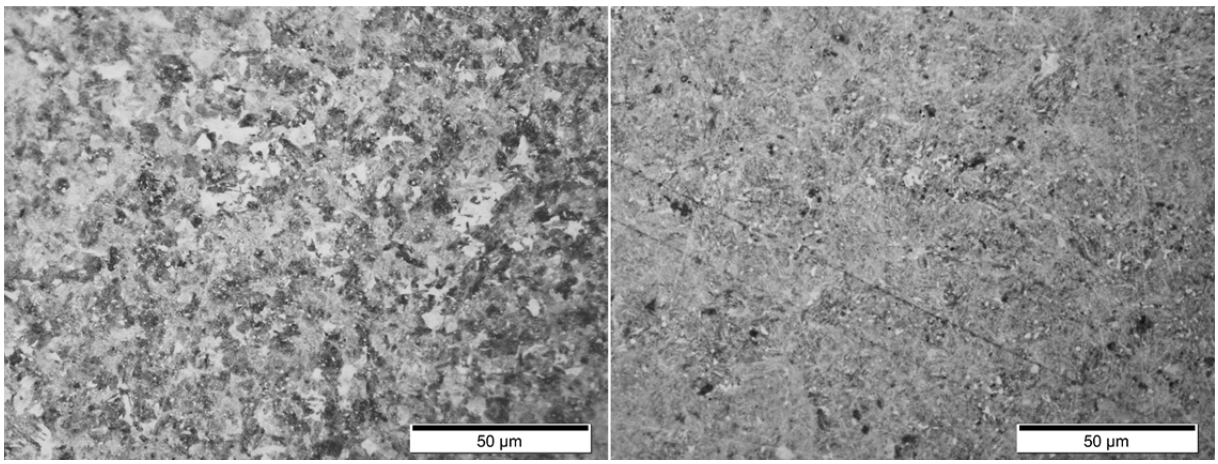

Fig. 42: Microscopic photos of polished and etched metallographic cross sections.
Left: CAI-A1-62, fine grained, isotropic, bainitic structure with estimated 15 % ferrite;
right: CAI-A2-45, extremely fine grained, isotropic, bainitic structure with an estimated ferrite content ≤ 5 %.

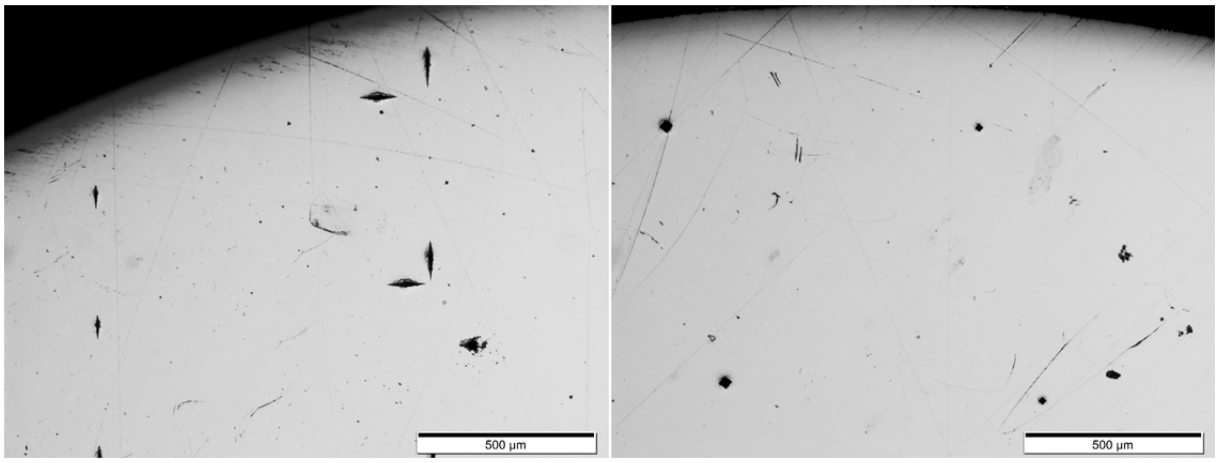

Fig. 43: Microscopic photos of polished metallographic cross sections (images taken after hardness testing). The bright color shows the structureless surface with some preparation relicts and Vickers and Knoop indentations. Some small grey dots indicate carbides. Left: CAI-A1-62; right: CAI-A2-45.

However, it could also be shown that the microstructure of both samples is different. Fig. 42 illustrates that the sample CAI-A1-62 (left image) is much coarser than the other pin (CAI-A2-45, image on the right) containing about 15 % ferrite, which indicates different heat treatment and a lower hardness. Fig. 43 shows images of the polished and unetched surface. In addition to the preparation relicts and the indentations from the hardness tests, it can only be seen that both specimens contain smaller grey dots, which are presumably carbides.

The conclusion is that although ordered and purchased as a lot of steel pins identical in hardness, CERCHAR pins may vary significantly in structure and hardness. Therefore, it is mandatory to check the structure and the hardness of purchased CERCHAR pins and also to take at least 5 single tests when examining the CERCHAR Abrasivity index.

4.4.3 LCPC impeller

The LCPC impellers also were purchased from the store Geotechnik Dunkel. The manufacturer of the impellers and with it the steel type and its tempering are unknown. According to Geotechnik Dunkel, the pins correspond to the specifications, as explained in chapter 5.2.2. The overview Tab. 13 provides information on the numbering, special characteristics of each sample, the material type and the conducted investigations.

Tab. 13: Compilation of the LCPC impellers used for investigations in this study.

LCPC impeller	Special characteristics	Material type	Conducted investigations
LCPC-A1-GF	processing form: milled	1.0580 (unalloyed mild steel)	OES, RLM, Knoop-, Vickers-hardness
LCPC-A2-GL	processing form: laser cut	1.0116 (unalloyed mild steel)	OES, RLM, Vickers-hardness

Structural analysis

For the investigations, two new and unused exemplary LCPC impellers were selected and designated as follows: LCPC-A1-GF and LCPC-A2-GL. The spark spectroscopy showed that both steels are unalloyed mild steel, but the milled impeller LCPC-A1-GF is made of the material 1.0580 and the laser cut impeller LCPC-A2-GL is made of the material 1.0116.

Both samples show an isotropic microstructure, whereby the grain size of LCPC-A1-GF is slightly coarser (Fig. 44, left image). Roughly estimated, the microstructure of both samples consists of about 30-40 % ferrite and about 60 to 70 % perlite. The smaller grain size of LCPC-A2-GL indicates that the hardness may be slightly higher. No images of the polished surface are given, as these did not provide any further information.

In order to investigate the influence of the production on the microstructure and the hardness, not only the central area of the LCPC impeller was examined, but also the edge area, which is basically the only contact with the rock to be tested. The milled impeller showed that the otherwise isotropic structure was altered, deformed and the grain size reduced by the milling process (Fig. 45). The deformation and reduction of the grain size probably leads to a slight increase in hardness in the marginal area during the testing procedure. In addition, it can be seen that smaller steel chips are also produced, which are easier to remove during the LCPC test and may simulate an increased loss of mass.

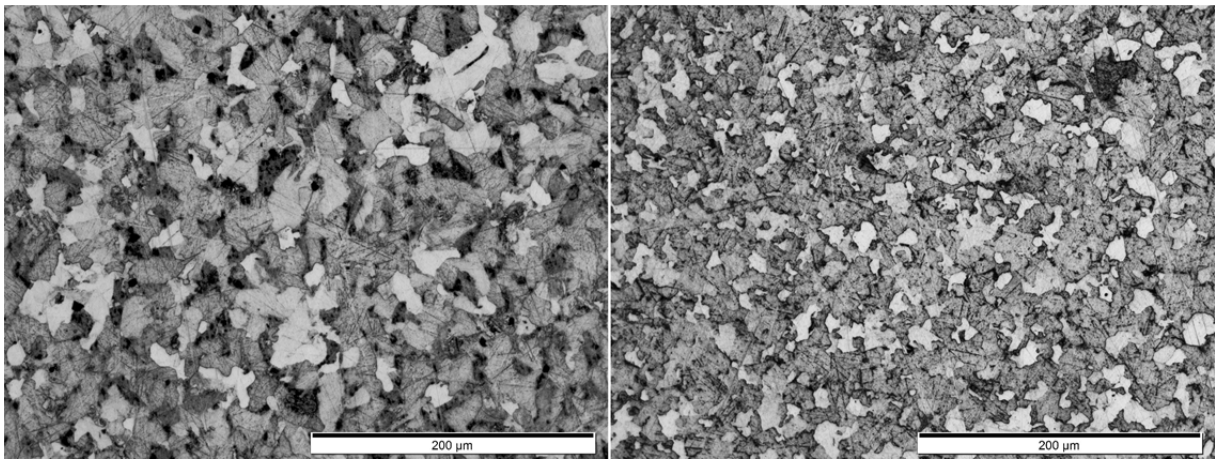

Fig. 44: Microscopic photos of polished and etched metallographic sections.
Left: LCPC-A1-GF, fine to middle-coarse grained and isotropic structure of estimated 30-40 % ferrite and 60-70 % perlite;
right: LCPC-A2-GL, fine grained and isotropic structure of estimated 30-40 % ferrite and 60-70 % perlite.

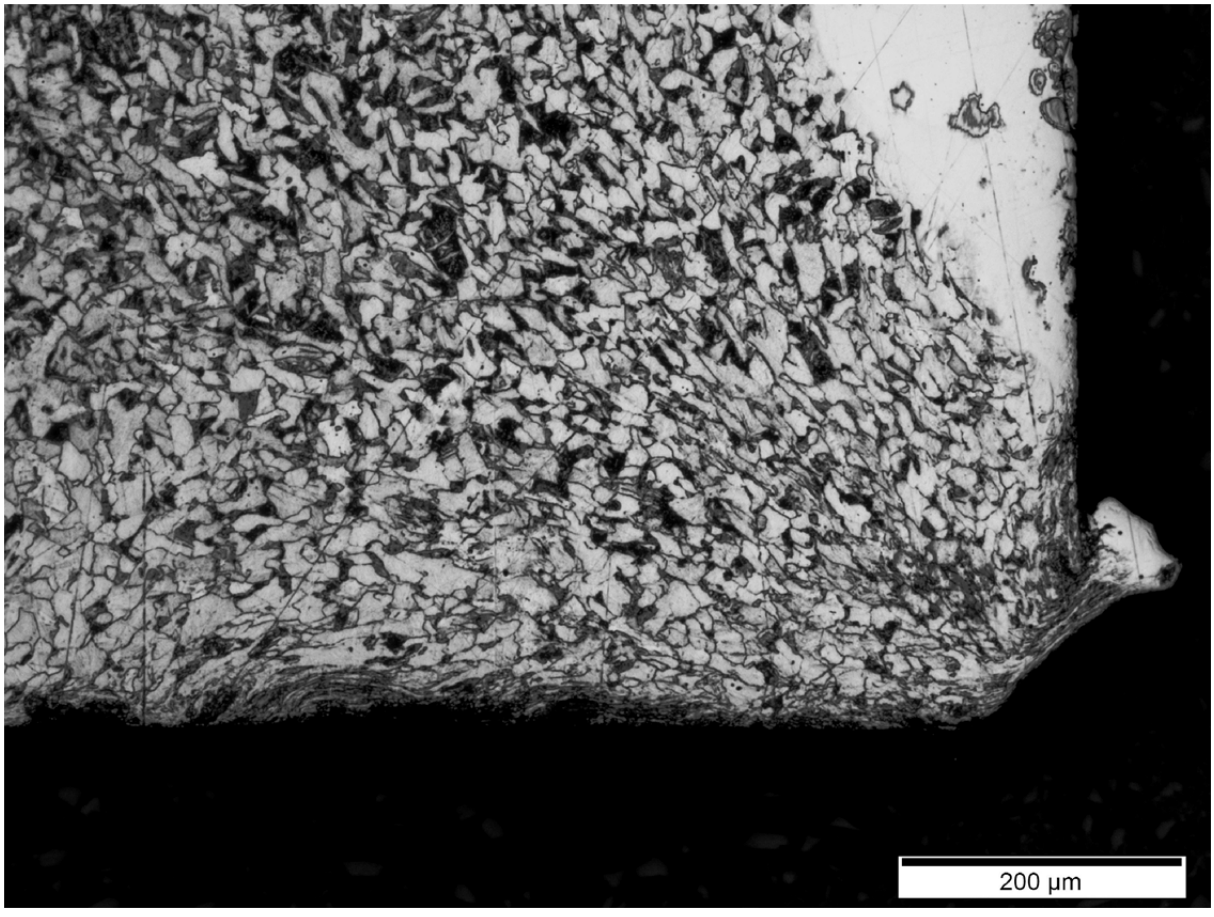

Fig. 45: Microscopic image of a polished and etched metallographic section of the milled LCPC impeller LCPC-A1-GF (the upper right corner is only polished). The photo shows a corner and the edge deformation of the crystallites by the milling process.

The LCPC-impeller, which was laser cut, shows a strong deformation and grain size reduction in the area of the starting and end point of the laser cut (Fig. 46, image a)), which leads to a presumably slightly higher hardness at this point. This probably has little effect on the test results as mainly the edges are in contact with the rock. The situation is different with the corners, which have the most contact with the rock to be tested. Here the right image of Fig. 46 shows that the laser cut leads to a change of the edge area with a width of about 40 to 80 µm due to the short but very intensive heat load. Here, a small white etching area has formed, which shows some thermal damage and a new hardening zone. This probably leads to a slightly lower hardness in the white etching area and to a higher hardness in the underlying layer with martensite formation. This may have an influence on the LCPC test results. A more detailed discussion of this phenomenon is given in chapters 6.3 and 7.

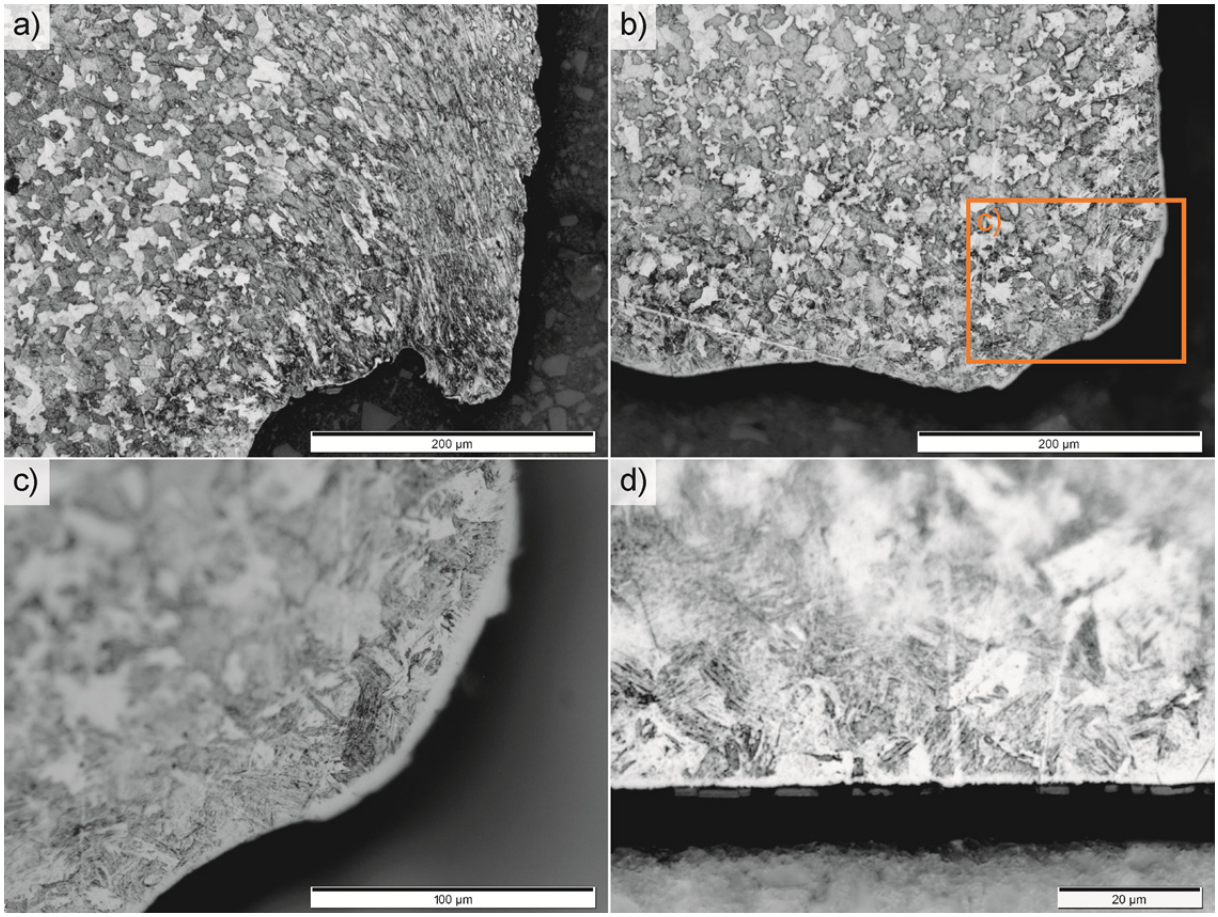

Fig. 46: Microscopic photos of polished and etched metallographic sections of LCPC-A2-GL which was laser cut.
a) This image shows the starting and the end point of the laser cut as well as the deformation of the crystallites towards the outside.
b), c), d) These images show a corner and the edge of the LCPC impeller and the formation of a white layer with a width of max. 10 µm and an underlying layer of about 40 to 80 µm in which martensite has formed.

5. Laboratory testing methodology

To analyze the hardness and other important parameters of minerals and rock types, an extensive laboratory program has been performed. This includes not only different hardness tests, but also rock mechanical properties, such as the uniaxial compressive strength and their dependency on rock hardness. The following sections explain the methods used in each laboratory test: the parameters of rock strength (chapter 5.1), their abrasivity (chapter 5.2) and different hardness tests on steel, minerals and rocks (chapter 5.2.3 and 5.4).

It should be noted that the laboratory tests were conducted between the years 2013 and 2017. For this reason, the standards were used and cited in this paper that were current at the time of testing.

5.1 Rock strength

The rock mechanics tests program was performed in the laboratories at the Chair of Engineering Geology at the Technical University of Munich. In total, 74 uniaxial compression tests, 89 Brazilian tensile tests and 201 point load tests (number of individual tests) were performed and analyzed. In combination with the petrographic analysis and the resulting abrasivity values, this data forms the basis of the characterization of the rock behavior. It illustrates how rocks react under different load situations.

5.1.1 Uniaxial Compression Test

For the determination of the rock strength, the uniaxial compression tests were performed according to Recommendation No. 1 for uniaxial compression testing with free lateral expansion (DGGT 2004), following the suggested methods of ISRM (1979). Specimen preparation and dimensions also meet the requirements given in ASTM D2938 (2002) and ASTM D7012 (2014).

Sample preparation

The test specimens are cylindrical drill cores with a length/diameter ratio of about 2:1. They are drilled with a diamond drill out of larger blocks and have a diameter of about 50 or 80 mm. With this size, they meet the recommendation that the diameter must be at least 10 times bigger than the size of the largest grain. If the length/diameter ratio is less than 2:1, the resulting uniaxial compressive strength (UCS) must be recalculated according to OBERT & DUVALL (1967) (see also Equation 4). It is well known, that anisotropy (foliation, schistosity or layering) has significant impact on rocks and their strength (THURO 1996: 57). For this reason, the foliated samples were prepared with a 90 degree angle to the loading direction whenever possible. Due to difficult sampling conditions, this was not the case. In these situations, it is mentioned in the test documentation and considered for further calculations.

To make both ends faces parallel and perpendicular to the core axis, they were ground by a lapping machine. The smoothness was controlled with a straightedge.

Testing device

For the test, the large loading frame (2,000 kN nominal load) of a servo-controlled hydraulic press (*ToniNorm*; Fig. 47) was used for loading and for measuring the failure load of the samples. The machine fits the accuracy requirements of class 1 in the German standard DIN 51220 (2003) and DIN EN ISO 7500-1 (2016). The samples were loaded with a constant deformation rate of 0.06 to 0.08 mm/min (depending on the length of the tested sample) until total failure of the rock occurred. The axial deformation of the sample was measured using three parallel connected digital inductive displacement transducers to record the stress-strain curve.

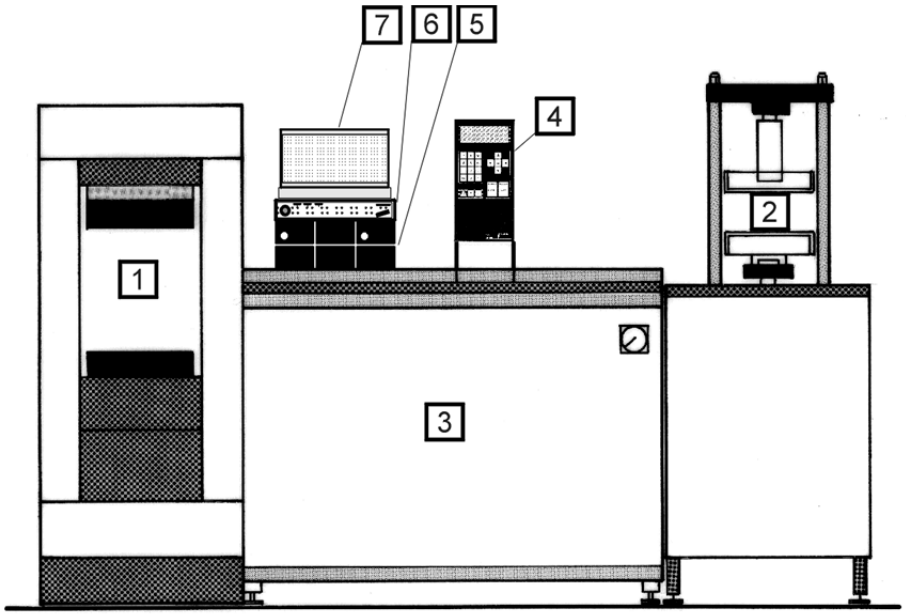

Fig. 47: Front view of “ToniNorm”-Compression-Testing-Machine (according to manufacturer information).

① Loading frame 1 (2,000 kN nominal load)
② Loading frame 2 (200 kN nominal load)
③ „Powerbox“ (hydraulic unit)
④ „ToniTrol“ control unit
⑤ Measurement amplifiers for deformation recording
⑥ HBM Spider 8 – buffer amplifier
⑦ Desktop PC with reporting software named „TestXpert“

Test analysis and calculations

The data of the test were recorded and analyzed by the software *TestXpert*. The compressive strength (q_u) is calculated as follows (Equation 3).

Equation 3: Calculation of the compressive strength σ_u.

$$\sigma_u = \frac{F_{max}}{A}$$

with:	σ_u	*Uniaxial compressive strength*	*[MPa]*
	F_{max}	*Failure load of the sample*	*[N]*
	A	*Cross-section area of the sample*	*[mm²]*

As mentioned before, the UCS has to be lowered after OBERT & DUVALL (1967) using Equation 4 if the length-to-diameter ratio is less than 2.

Equation 4: Calculation of adjusted compressive strength $\sigma_{u(2)}$.

$$\sigma_{u(2)} = \frac{8 \cdot \sigma_u}{7+2 \cdot \frac{D}{L}}$$

with:	$\sigma_{u(2)}$	*Revised compressive strength*	*[MPa]*
	σ_u	*Uniaxial compressive strength*	*[MPa]*
	D	*Diameter of sample*	*[mm]*
	L	*Length of sample*	*[mm]*

After considering the correction, if it is necessary, the UCS can be divided into different classes of strength. The ISRM (1978c: 348) provides the following classification (Fig. 48).

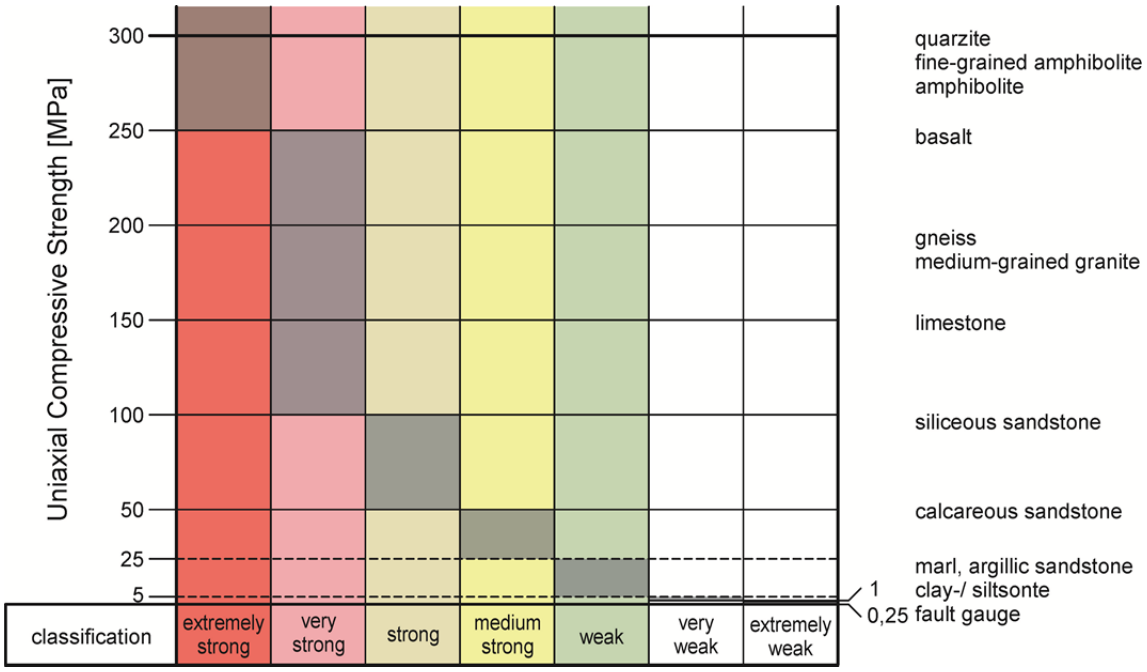

Fig. 48: Classification of the UCS of rocks with examples of widespread hard rock types (ISRM 1978c: 355, modified after THURO 1996: 57, Fig. 24).

Another important parameter is given by the deformation: The Young's modulus, which is calculated in the linear-elastic, pre-failure part of the stress-strain curve. In English, it is called E modulus and in German V modulus. According to the ISRM (1979), this modulus is called tangent Young's modulus E_t, which is generally measured at 50 % of uniaxial compressive strength (Fig. 49).

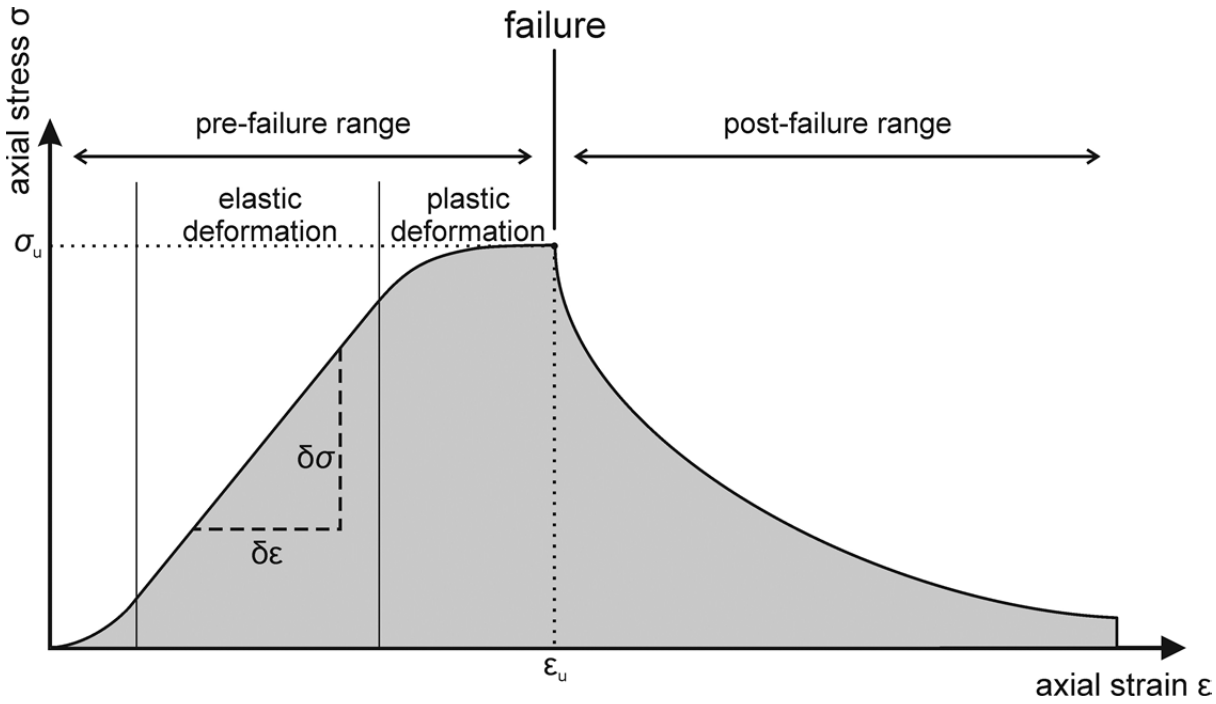

Fig. 49: Schematic stress-strain curve of the uniaxial compression test. With δσ and δε you can determine the Young's modulus E_t (first derivation of the linear curve segment) (inspired by ISRM 1979; MENSCHIK 2015: 23; WILFING 2016: 40).

5.1.2 Brazilian Tensile Test

The Brazilian Tensile Strength Test was carried out according to the German recommendation No. 10 of the DGGT (2008) following the suggested methods of ISRM (1978b). It was used as an indirect method to determine the Brazilian Tensile Strength (BTS) of rock samples. Fig. 50 illustrates the mechanic principle of the BTS: The applied compressive strength acts as a tensile stress over the longest distance of approx. 70 % (DGGT 2008).

Sample preparation

Cylindrical rock types were drilled (diameter of approx. 50 or 80 mm, depending on the grain size of the rock type) out of bigger blocks and cut with a water-cooled diamond saw to a length-to-diameter ratio of 0.5.

Testing device

For this test, the small loading frame (200 kN nominal load) of the servo-controlled hydraulic press (Fig. 47) was used for loading and the measurement of the failure load of the samples using the software *TestXpert*. Therefore, the loading frame was equipped with Brazilian tensile strength loading brace (Fig. 50).

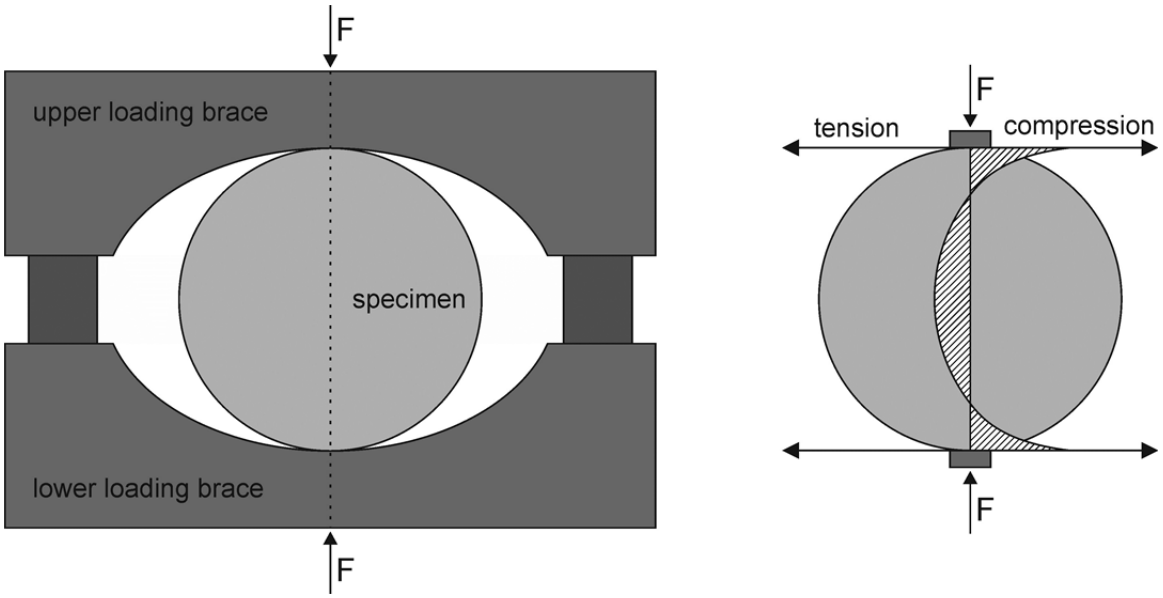

Fig. 50: Schematic illustration of the Brazilian Tensile Test. On the left side you can see the loading braces with the specimen; on the right side the stress distribution during the test (after ISRM 1978b; DGGT 2008).

Test analysis and calculations

The data of the test were recorded and analyzed by the software *TestXpert*. The Brazilian Tensile Strength (σ_t) is calculated as follows (Equation 5).

Equation 5: Calculation of the Brazilian Tensile Strength σ_t.

$$\sigma_t = \frac{2 \cdot F_{max}}{\pi \cdot D \cdot L}$$

with:	σ_t	*Brazilian Tensile Strength*	*[MPa]*
	F_{max}	*Failure Load*	*[kN]*
	D	*Diameter of sample*	*[mm]*
	L	*Length of sample*	*[mm]*

The factor z can be calculated from the ratio of the uniaxial compressive strength to the tensile strength (using Equation 6). Tab. 14 gives us a classification. This factor is regarded as the most important value for describing the toughness or brittleness, respectively the ductility of rocks (BECKER & LEMMES 1984). However, WILFING (2016) found that this value may not be suitable as a definition of toughness. For this reason, z is not used in this thesis.

Equation 6: Calculation of brittleness z.

$$z = \frac{\sigma_u}{\sigma_t}$$

with:	z	*Brittleness of sample*	*[-]*
	σ_u	*Uniaxial compressive strength*	*[kN]*
	σ_t	*Brazilian tensile strength*	*[mm]*

Tab. 14: Classification of brittleness (SCHIMAZEK & KNATZ 1976: 117; BECKER & LEMMES 1984: 74; THURO 1996: 74).

z [-]	Classification
> 20	very brittle
20 – 10	brittle
10 – 5	ductile
< 5	very ductile

5.1.3 Point Load Test

The Point Load Test (PLT) is an indirect method to determine the uniaxial compressive strength of rock samples and was performed according to the testing recommendation of the ISRM (1985) and DGGT (2010). Hereby the point load index (I_s) is calculated.

Sample preparation

The rock samples were cut into several cubic specimen ("block test"). Great effort was put into the sample preparation in order to get a cube near to the standardized size of 50 mm x 50 mm whenever possible.

Testing device

The tests were performed with a hydraulic hand pump from *Wille Geotechnik* (Fig. 51). It is equipped with a test frame, test tips and a digital manometer with a drag indicator to measure the force. The cubic samples were loaded by slowly pressing the hydraulic hand pump till the max. loading was reached and the failure occurred. This means, that the specimen was loaded with a non-constant loading rate. The maximum force can be directly read form the manometer. After the test, the geometry of the failure surface of the specimen was determined with a sliding caliper by two perpendicular measurements. Whenever possible, min. 5 rock cubes were tested for one sample number.

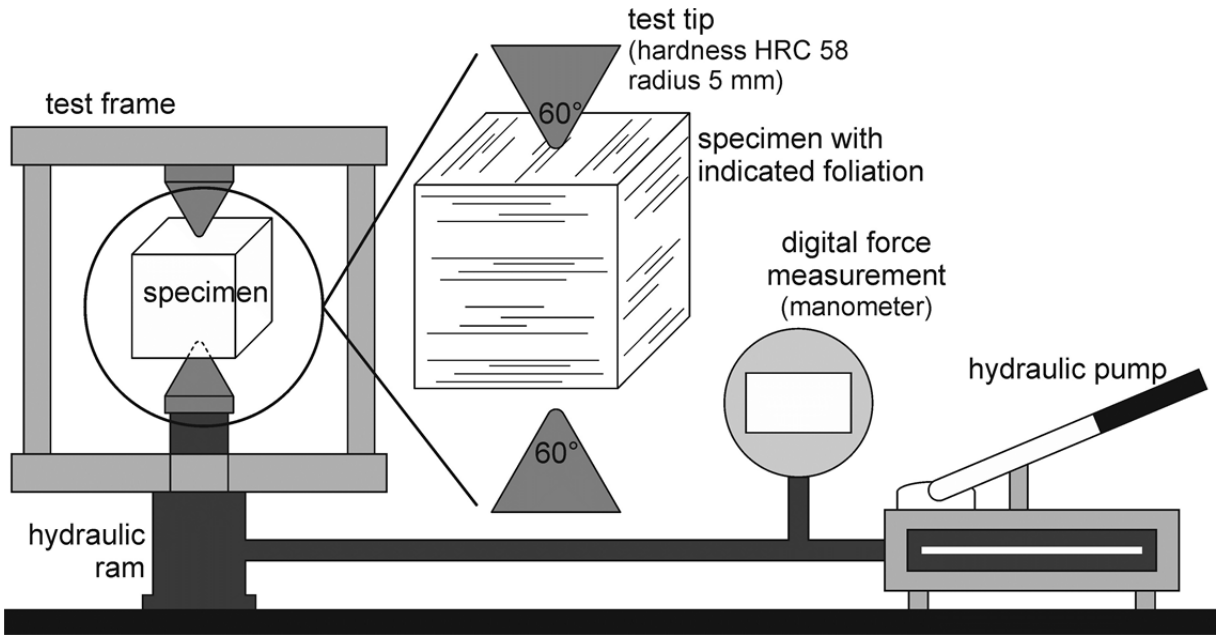

Fig. 51: Schematic diagram of the used point load testing apparatus by Wille Geotechnik with some important technical information (after DGGT 2010).

Test analysis and calculations

For the calculation of the point load index I_s (Equation 7), the failure load and the failure surface is needed.

Equation 7: Calculation of the point load index I_s.

$$I_s = \frac{F_{max}}{D_e^{\,2}} = \frac{F_{max}}{W \cdot L}$$

with:	I_s	*Point load index*	*[MPa]*
	F_{max}	*Failure Load*	*[kN]*
	$D_e^{\,2}$	*Area of failure surface*	*[mm]*
	W	*Width of failure surface*	*[mm]*
	L	*Length of failure surface*	*[mm]*

In order to compensate for the scaling effect, the point load index has to be correlated to a standard sample dimension of 50 x 50 x 50 mm. This is done using the method after BROOK (1993: 49) which is quoted in Equation 8.

Equation 8: Calculation of the point load index correlating to standard sample dimension of 50 x 50 x 50 mm*.*

$$I_{S(50)} = f \cdot I_s = \left(\frac{W \cdot L}{2500}\right)^{0.225} \cdot \frac{F_{max}}{W \cdot L}$$

with:	$I_{S(50)}$	point load index for 50 mm edge length	*[MPa]*
	f	*Correction factor*	*[kN]*
	F_{max}	*Failure Load*	*[kN]*
	W	*Width of failure surface*	*[mm]*
	L	*Length of failure surface*	*[mm]*

From the $I_{S(50)}$ the uniaxial compressive strength σ_m is derived using the correlation factor c (Equation 9). This factor is an empirically determined constant (c ~ 20) based on different studies. Since values for c can vary, the derived uniaxial compressive strength should only be considered as an approximation and is not used in this thesis.

Equation 9: *C*alculation of uniaxial compressive strength derived from $I_{S(50)}$.

$$\sigma_m = c \cdot I_{S(50)}$$

with:	σ_m	*Derived uniaxial compressive strength*	*[MPa]*
	c	*Correction factor ~ 20*	*[-]*
	$I_{S(50)}$	*Point load index for 50 mm edge length*	*[kN]*

5.2 Abrasivity

The abrasivity tests also have been performed in the laboratories at the Chair of Engineering Geology at the Technical University of Munich. In total, 40 CERCHAR abrasivity tests (200 individual tests) and 55 LCPC abrasivity tests were performed and analyzed. In combination with the previous strength parameters and the petrographic analysis, this data is the basis of the characterization of the rock behavior.

5.2.1 CERCHAR Abrasivity Test

The CERCHAR Abrasivity Test (also CERCHAR scratch test) was performed on the test specimen according to the recommendation No. 23 of the DGGT (KÄSLING & PLINNINGER 2016). It follows the recommendation of the Centre d'Etudes de Charbonnages de France (CERCHAR 1986) and ISRM ALBER et al. (2014) whereby the **C**ERCHAR **A**brasivity **I**ndex (CAI) was determined. This index is an indicator for the abrasiveness of rock causing wear on excavation tools.

Sample preparation

Rock samples with a rough surface, which is produced by fracturing the rock, are used for the CERCHAR Abrasivity Test. Typical used samples are specimen produced by the Brazilian tensile strength test or the point load test. Due to the testing condition for these tests, the failure surface was perpendicular to all potential occurring discontinuities.

Testing device

The testing device (Fig. 52) is in accordance with the modified CERCHAR-device presented in WEST (1989). The used steel pins have a standardized geometry and Rockwell hardness of 54-56 HRC. Each pin is loaded with a static load of 7 kg and scratched over 10 mm of the rough surface of the specimen. Each sample is scratched 5 times.

In some countries like Austria, the CERCHAR Abrasivity Test is performed on a saw cut surface. As some additional tests were performed under these conditions, it is stated in the laboratory form. ALBER et al. (2014) gives also a conversion (Equation 10) for rough and saw cut surfaces.

Equation 10: Conversion of the CAI on saw cut surfaces ($CAI_{saw\ cut}$) into rough surfaces (CAI_{rough}).

$$CAI_{rough} = CAI_{saw\ cut} \cdot 1.14$$

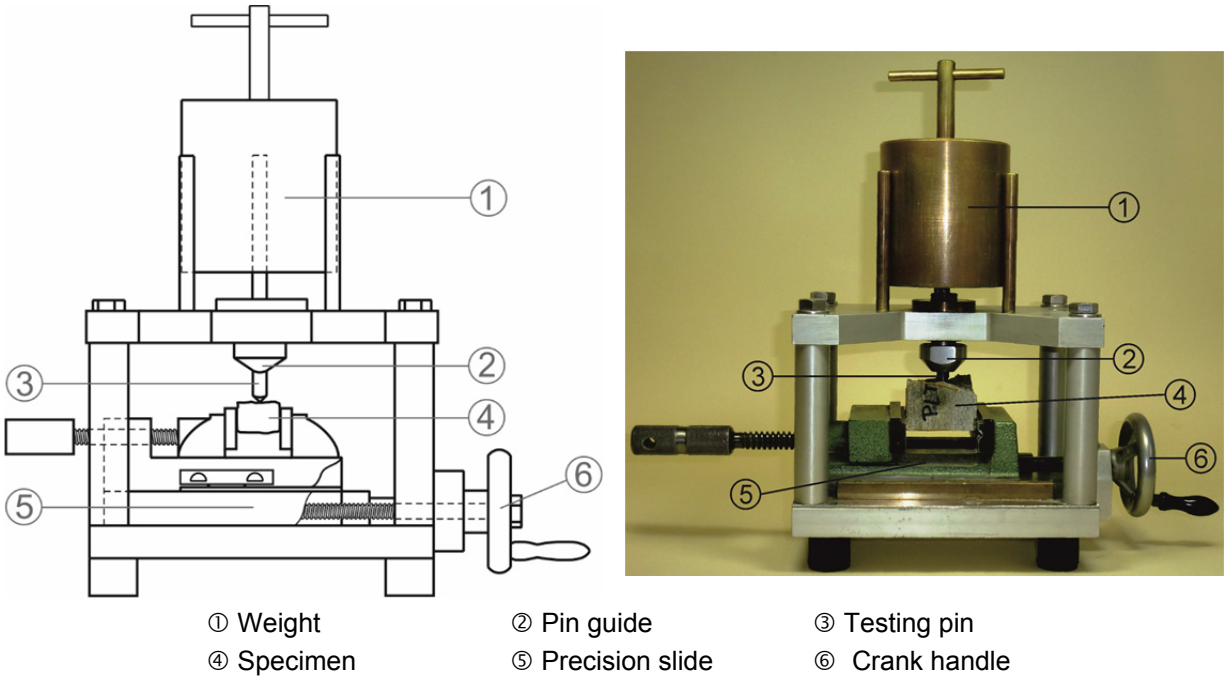

Fig. 52: CERCHAR-device for the determination of the CERCHAR-Abrasivity-Index (according to WEST 1989).

Test analysis and calculations

The resulting wear of the steel pin is determined with an accuracy of 0.02 mm using a reflected-light binocular with a measuring scale. According to KÄSLING et al. (2007), each steel pin is measured in 4 perpendicular directions and the results are averaged.

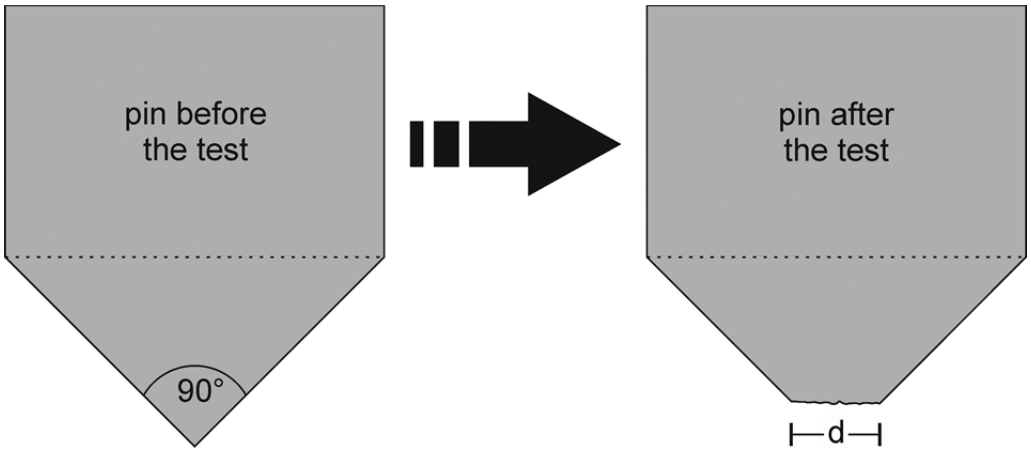

Fig. 53: Schematic sketch of the steel pin before (left) and after (b) testing (according to KÄSLING et al. 2007; ALBER et al. 2014).

The CERCHAR Abrasivity Index is calculated using Equation 11 from the wear of the steel pin (d, see also Fig. 53). An evaluation of the abrasiveness in this thesis is performed according to the classification table below (Tab. 15) after CERCHAR (1986). It should be noted that the current recommendations of the DGGT (KÄSLING et al. 2007) and ISRM (ALBER et al. 2014) specify different boundaries of the individual classes. However, these were not used in this thesis.

Equation 11: Calculation of the CERCHAR Abrasiveness Index (CAI).

$$CAI = d \cdot 10$$

with:	CAI	*CERCHAR Abrasiveness Index*	*[-]*
	d	*Averaged wear of the steel pin*	*[mm]*

Tab. 15: Abrasiveness classification using the CERCHAR Abrasivity Test (according to CERCHAR 1986).

CAI	Classification
0.3 – 0.5	not very abrasive
0.5 – 1.0	slightly abrasive
1.0 – 2.0	medium abrasiveness
2.0 – 4.0	very abrasive
4.0 – 6.0	extremely abrasive

5.2.2 LCPC Abrasivity Test

The LCPC abrasivity tests were performed on the rocks according to the French standard P 18-579 (AFNOR 2013). Further test conditions are described in THURO et al. (2006). The LCPC Abrasivity Test was developed for the determination of the abrasiveness and breakability of hard rock by the *Laboratoire Central des Ponts et des Chaussées* (LCPC). In the following test the **L**CPC **A**brasivity **C**oefficient (LAC) [g/t] and the **L**CPC **B**reakability **C**oefficient (LBC) [%] are determined.

Sample preparation

Due to the testing equipment dimensions only sample material with grain sizes smaller than 6.3 mm can be used in this test. Therefore, the sample is broken with a jaw breaker to a grain size of 4 to 6.3 mm until 500 g ± 2 g are prepared. Smaller particles are removed with dry sieving.

Testing device

The LCPC Abrasivity Test was performed at the Chair for Engineering Geology of the Technical University of Munich using an abrasivity testing device („abrasimeter“) Fig. 54 according to the French standard P 18-579 (AFNOR 2013). The motor of the abrasimeter has 700 W power, the rectangular metal impeller is at a standardized quality (Rockwell B: 60-75 HRB) and dimension (5 x 25 x 50 mm). The impeller rotates for five minutes with a speed of 4,500 rpm in the cylindrical container with the sample material.

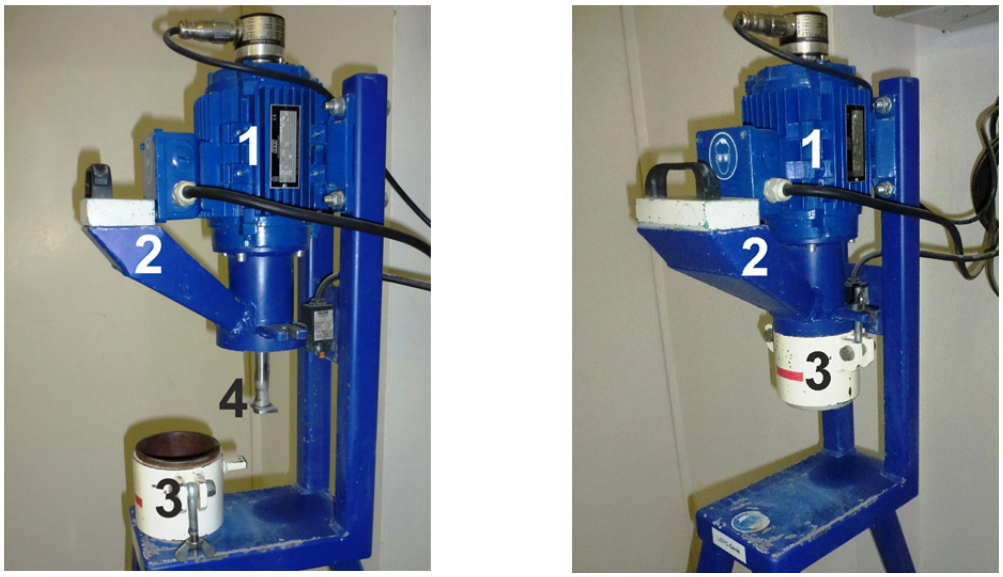

Fig. 54: Abrasimeter with a 700 W electric motor (1), funnel tube (2), sample container (3) and the impeller (4) which rotates with a speed of 4,500 rpm for 5 minutes through the sample. Left: device before filling. Right: unit in operating condition with closed sample container.

Test analysis and calculations

The impeller is weight two times with an accuracy of 0.01 g, before and after the test, to determine the weight loss and to calculate the sample abrasiveness (LAC) after Equation 12. The sample material is dry sieved to determine the mass with a grain size < 1.6 mm and to calculate the LBC (Equation 13), which allows a conclusion on the breakability or brittleness.

Equation 12: Calculation of the LCPC Abrasivity Coefficient (LAC).

$$LAC = \frac{m_{F0} - m_F}{M}$$

with:	LAC	*LCPC Abrasivity Coefficient*	*[g/t]*
	m_{F0}	*Mass of metal impeller prior test*	*[g]*
	m_F	*Mass of metal impeller after test*	*[g]*
	M	*Sample mass*	*[t]*

Equation 13: Calculation of the LCPC Breakability Coefficient (LBC).

$$LBC = \frac{100 - M_{1.6}}{M}$$

with:	LBC	*LCPC Breakability Coefficient*	*[g/t]*
	$M_{1.6}$	*Mass of sample material < 1.6 mm after test*	*[g]*
	M	*Sample mass*	*[t]*

For natural hard and soft rock samples the LAC normally is in the range of 0 to 2000 g/t. This range is characterized by 6 classes which are shown in Tab. 16. The abrasivity terminology has been chosen in accordance to the CERCHAR Abrasivity Index (CAI), which nearly shows a linear correlation to the LAC (THURO et al. 2006; THURO & KÄSLING 2009). The classification used by BÜCHI et al.(1995) does not support this correlation and therefore is not used.

Tab. 16: Classification of the LCPC Abrasivity Coefficient LAC in accordance to the CERCHAR Abrasivity Index CAI and the associated terminology (mod. from THURO et al. 2006: 286).

LAC [g/t]	CAI [-]	Classification according to CERCHAR 1986	Rock type examples
0 – 50	0 – 0.3	not abrasive	wood, turf
50 – 100	0.3 – 0.5	not very abrasive	clay-silt stone, marl
100 – 250	0.5 – 1.0	slightly abrasive	schist, sandstone (fine grained, argillaceous cement), limestone (pure), marble (pure)
250 – 500	1.0 – 2.0	medium abrasive	limestone (sandy), marble (containing quartz) sandstone (calcareous cement)
500 – 1,250	2.0 – 4.0	very abrasive	sandstone (siliceous cement), porphyry, andesite, basalt, phyllite, mica schist, some amphibolites
1,250 – 2,000	4.0 – 6.0	extremely abrasive	(vein-) quartz, flintstone, granite, quartzite, eclogite, gneiss, some amphibolites

5.2.3 XRD-Analysis and equivalent quartz content (EQC)

To calculate the equivalent quartz content (EQC), it is necessary to quantify the mineral content. This was done using the X-ray-diffraction (XRD) analysis. For this purpose, a representative sample was prepared from each rock and evaluated according to the Rietveld method.

As early as 1970, the method of the equivalent quartz content was introduced from SCHIMAZEK & KNATZ (1970) as a wear index for rock. Recent work with a detailed description of the method is given by THURO (1996, 2002) and PLINNINGER (2002).

Testing principle

In the X-ray diffractometry method, minerals are irritated with X-rays. Due to the crystal structure of a mineral, the rays are deflected or diffracted. The diffraction of the rays can be measured and has a specific pattern for each mineral. With the help of the Bragg equation, the lattice plane distance (d_{hkl}) can be calculated. The basis for the evaluation is a diffraction angle-dispersive RDA profile (diffractogram) with angles on the ordinate and intensities on the abscissa, which contains the mineral-type diffraction lines, so-called peaks (PETSCHICK 2002). If the analysis is carried out on a structureless powder preparation with several different minerals, the minerals can be determined using the characteristic diffraction lines and d values. The height of the peaks can also be used to calculate the share of the total sample. It should be noted that only crystalline phases can be analyzed with this method. Amorphous phases, such as glasses or poorly crystallized substances, give very broad wave crests in the diffractogram and allow almost no assignment.

As the abrasiveness of a rock is determined by the total mineral stock, its structure and texture, all minerals are important even though quartz is known as one of the most abrasive Mineral. Therefore, the EQC represents the totality of all minerals which are causing the wear as a sum of their percentages multiplied by their grinding strength, related to quartz. The determination of the grinding strength (in this context equated with grinding hardness) is still based on the work of ROSIWAL (1896, 1916).

Sample preparation

To get a representative sample of each rock, different amounts, depending on the grain size (typically 500 g), were first crushed and subsequently ground. For coarse grinding, an agate disk mill was used. The fine grinding was carried out with a McCrone mill with an agate cylinder grinder. The sample size/mass was reduced using a sample divider to keep it representative. Thus, 2 g of representative rock powder are produced.

Testing device and test analysis

The XRD-analysis was performed outside the TUM in the laboratory of “Röntgenlabor Dr. Ermrich”. According to the laboratory report (ERMRICH 2017), the analysis corresponds to DIN EN 13925-1 (2003), DIN EN 13925-2 (2003), DIN EN 13925-3 (2005) and

DIN EN 1330-1 (2015). The exact device data and their settings can also be taken from the laboratory report. The crystalline mineral phases are determined by their characteristic diffraction lines and the corresponding d-values with the Rietveld program "SiroQuant" (version V4.0).

Calculation of the EQC

The determination of the EQC was done according to THURO (1996: 51) on the basis of the grinding hardness of ROSIWAL (1896, 1916) with Equation 14:

Equation 14: Calculation of the equivalent quartz content (EQC).

$$EQC = \sum_{i=1}^{n} A_i \cdot R_i$$

with:	EQC	*Equivalent quartz content*	*[%]*
	A_i	*Proportion of the mineral i*	*[-]*
	R_i	*Grinding hardness of the mineral i*	*[% of quartz]*
	n	*Number of minerals*	*[-]*

The wear potential estimated from the equivalent quartz content is given in Tab. 17.

Tab. 17: Classification of the rock abrasiveness according to the equivalent quartz content (PLINNINGER 2002: 75, tab. 19).

EQC [%]	Abrasivity classification
< 10	not abrasive
10 - 25	slightly abrasive
25 - 50	abrasive
50 - 75	very abrasive
> 75	extreme abrasive

Tab. 18 shows the grinding hardness according to ROSIWAL (1896, 1916), the scratch hardness after MOHS (1822: 374ff., 506ff.) and the density. For the calculation of the EQC, the mean value of the grinding hardness is used, unless stated otherwise. The partly quite large differences between the minimum and maximum values are on the one hand due to formation of mixed crystals of some minerals and a different hardness along individual cleavage faces or the crystal anisotropy. On the other hand, there is a difference in weathering and decomposition resistance (THURO 2002: 61).

There are many error factors in the evaluation of the powder diffraction patterns. First, there is an error, caused by the used equipment which can't be further quantified. The second problem is that not all structure files fit completely with the contained minerals. If this is the case,

ERMRICH (2017) marks this. This second error is due to inclusions or deformation of the crystal lattice as well as mixed crystal formations. Therefore, the global error of the calculation of the EQC is usually between 5 and 10 percent. The exact error for every mineral can be taken from ERMRICH (2017).

However, a high quartz content does not automatically have to lead to high abrasion values and a high wear. The influence of the mineral content on abrasiveness is closely linked to the structural interlocking, the shape of the grains (HOWARTH & ROWLANDS 1987: 59) and their cohesion or the strength of a possibly existing cement (SCHIMAZEK & KNATZ 1970, 1976).

Tab. 18: Compilation of densities and mineral hardness of important rock forming minerals (summarized from ROSIWAL 1896, 1916; SALMINEN & VIITALA 1985; VERHOEF 1997: 123ff.; THURO 1996: 51, 2002: 62; PLINNINGER 2002: 75).

Mineral	Density [kg/m³]	Mohs hardness [-]	Grinding hardness (after ROSIWAL 1896, 1916) based on quartz = 100; [-]		
			Minimum	Mean	Maximum
Andalusite	3.2	7.5	-	177	-
Alkali feldspar (anorthoclase/microcline)	2.55 – 2.60	6	30	39	42
Alkali feldspar (orthoclase)	2.57	6	17	28	40
Amphibole (actinolite)	2.9 – 3.3	5.5 – 6	14	26	38
Amphibole (hornblende)	3.22	5 – 6	18	24	30
Anhydrite	2.9 – 3.2	3 – 3.5	2.3	3.0	3.7
Apatite	3.16	5	3.3	4.4	5.5
Aragonite	2.95	3.5	5.1	7.5	9.9
Biotite	3.01	2.5 – 3	1.8	3.65	5.6
Calcite	2.72	3	1.9	2.9	3.9
Cassiterite	6.84	6 – 7	-	136	-
Cordierite	2.64	7 – 7.5	-	45	-
Corundum - general	3.95	9	326	637.5	949
White corundum (sapphire)	3.95	9	-	1765	-
Chlorite	2.78	2 – 2.5	0.9	0.9	0.9
Cyanite	3.5 – 3.7	5 – 7	-	53	-
Diamond	3.5	10	-	11,700	-
Dolomite	2.85	3.5 – 4	3.5	4.65	5.8

Mineral	Density [kg/m³]	Mohs hardness [-]	Grinding hardness (after ROSIWAL 1896, 1916) based on quartz = 100; [-]		
			Minimum	Mean	Maximum
Epidote	3.39	6 – 7	54	61.5	69
Fluorite	3.18	4	2.8	3.6	4.4
Garnet (almandine/grossular)	3.8 – 4.2	6.5 – 7.5	203	206.5	210
Goethite	4.37	5 – 5.5	15	19	23
Gypsum	3.32	1.5 – 2	0.36	0.49	0.61
Graphite	2.26	1	-	0.5	-
Halite	2.16	2 – 2.5	1.2	1.3	1.4
Hematite	4.9	5.5 – 6.5	-	25	-
Ilmenite	4.7	5 – 6	15	26	37
Kaolinite	2.61 – 2.68	2 – 2.5	1	1.25	1.5
Leucite	2.47	5.5 – 6	-	40	-
Magnetite	5.15	5.5	-	34	-
Muscovite	2.85	2 – 3	1.5	3.8	6.1
Olivine group	3.41	6.5 – 7	-	80	-
Nepheline	2.55 – 2.66	5.5 – 6	18	29	40
Phlogopite	2.75 – 2.97	2 – 2.5	0.8	1.15	1.5
Plagioclase (albite/andesine)	2.61 – 2.76	6 – 6.5	37	47	57
Plagioclase (labradorite)	2.71	6	28	41	52
Plagioclase (oligoclase)	2.64	6	23	30.5	38
Plagioclase (disintegrated)	≈ 2.5	5	3	15	27
Pyrite	5.1	6 – 6.5	-	56	-
Pyroxene (Augite/Enstatite)	3.2 – 3.5	5 – 6	22	43.5	65
Quartz	2.65	7	74	100	127
Rutile	4.25	6 – 6.5	116	129.5	143
Scapolite	2.65	5.25	12	15.5	19
Serpentine	2.5	3 – 4	-	4	-
Spinel	3.5	8	-	389	-
Staurolite	3.74	7 – 7.5	-	83	-
Talk	2.74	1	0.47	0.53	0.59
Titanite	3.48	5 – 5.5	-	48	-
Topaz	3.56	8	87	117.5	148
Tourmaline	3.15	7 – 7.5	-	102	-
Zircon	4.45	7.5	367	367	367
Zoisite	3.3 – 3.4	6.5	58	61	64

5.3 Standardized hardness tests

After characterizing the rock strength and abrasivity of the samples, also the hardness has to be analyzed. A special focus is laid next to the rock types here on the minerals. The Knoop tests and some Vickers microhardness tests were performed in the laboratories at the DIATI (Dipartimento di Ingegneria dell'Ambiente, del Territorio e delle Infrastruttur) at the Politecnico di Torino. Some additional microhardness tests at the IWB (Institute for Machine Tools and Industrial Management) at the Technical University of Munich. The low-force Vickers hardness tests and the Vickers hardness tests were performed in the laboratories at the MPA BAU (material testing office for construction) at the Technical University of Munich.

All tests have in common that they are static penetration tests and not dynamic. As a result of this and the special test conditions, only the permanent indentations and thus only the plastic part of the deformation can be measured. An exception is the method after Rockwell, which also contains a certain amount of elastic deformation.

Such hardness tests are also important, because conclusions can be drawn about the material parameters of the steel, like the yield and tensile strength. The standard for this conversion is DIN EN ISO 18265 (2014). This data is based on empirical knowledge and depends on the respective material (HERRMANN 2007). It includes the conversion of the most common standardized hardness test values into another hardness values, for instance Rockwell hardness into Vickers hardness.

5.3.1 Sample preparation

For every hardness test, a clean, plane and good surface is needed. This applies both to minerals and rocks, as well as to the steel specimen. For steel, the respective standards of each testing method have to be respected. Typical guidelines say that the surface has to be smooth and even, free from oxide scale, foreign matter and, in particular, completely free from lubricants (DIN EN ISO 6507-1 2006). This applies equally to minerals and rocks and is also important for the hardness experiments themselves, but also for the evaluation under the microscope. The only test which doesn’t need such a high surface quality is the modified Vickers Hardness which is described in chapter 5.4.

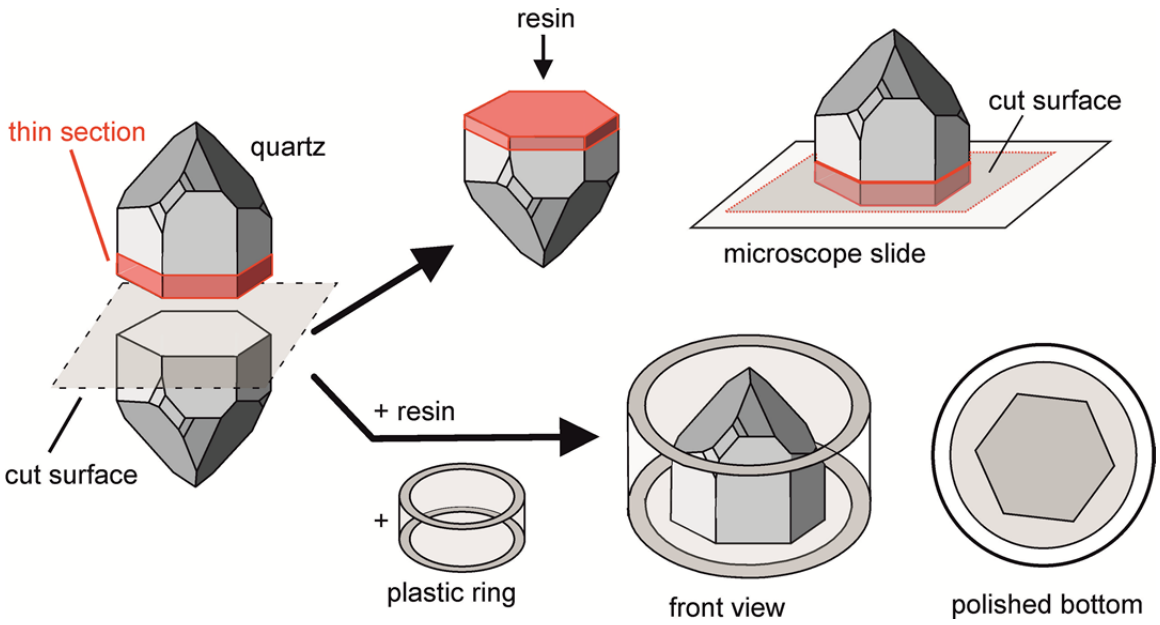

Fig. 55: Illustration of the specimen preparation with the mineral quartz as a sample (after FISCHER 2015).

The test specimens are parts of larger pieces which were cut out with different water-cooled diamond saws to give them the right shape and size. The rocks were formed to a cubic shape with an edge length of about 4 cm. Due to the further preparation in a lapping machine, two corners had to be beveled (Fig. 56). The minerals and the steel samples were cut into slices of about 1 to 2 cm thickness. In order to be able to analyze the rocks and minerals, one characteristic part was separated to prepare a thin section. For the hardness analysis, the slices were then embedded in a plastic ring with epoxy resin for better handling. For steel and some minerals, the resin was filled with hard aggregates like quartz grains and silicon carbide to improve the edge definition. Fig. 55 illustrates the complete preparation process.

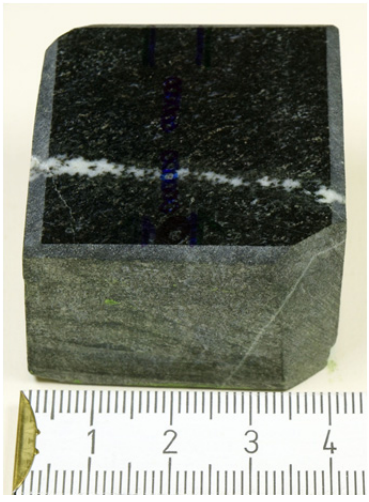

Fig. 56: Test specimen for hardness tests. The right front side and the rear left side shows the technically necessary bevel of the two corners. The used scale is in cm and illustrates the sample size.

After this step, the front and the back side were grinded by a lapping machine to get the required flatness and parallelism. This was followed by further grinding and finally polishing steps, in which the abrasive got finer step by step. In the first part, a rotating grinding wheel and the abrasive silicon carbide (SiC) with a grain size of 220 and 400 mesh was used to refine the surface. In the second part, 800, 1000 and 1200 mesh of SiC was used in combination with a glass plate. The third step consisted of polishing with various rotating plates coated with diamonds with a grain size of 1200, 2000 and 4000 mesh. In the fourth and last part, a 1 µm diamond suspension (the average size is around 1 µm) was used on a rotating felt plate to get a largely scratch-free surface.

5.3.2 Rockwell hardness test

The Rockwell hardness tests were carried out according to the standard DIN EN ISO 6508-1 (2016). It is actually the Rockwell C (HRC) method, which was used. This technique is typically applied to tempered steel, which is normally the case for TBM disc cutters. Due to the nature of test, the elastoplastic part of the material is being tested. The advantage of this method is that it is fast because only the depth of the indentation is measured during the test. Due to this, the test procedure can be completely automated. But this is at the same time the disadvantage, since the indentations cannot be measured again.

The requirements for the distances between the indentations, the minimum test thickness and the test times can be found in DIN EN ISO 6508-1 (2016) and they have been maintained.

Testing principle

This test is a static method to determine the hardness. A schematic sketch of the test principle is given in Fig. 57. In the experiment, an initial load (F_0) must be applied to an indenter with a diamond tip which has a conical shape (type Rockwell Cone). The resulting measuring base serves as a reference plan for the further test. The depth dial gauge is reset to zero (section a). Subsequently, an additional load (F_1) is applied, which causes a deeper penetration of the indenter into the specimen (section b). As a last step, the total test load F is reduced to F_0, so that an elastic rebound occurs (section c). With the resulting penetration depth h, the Rockwell hardness can be determined.

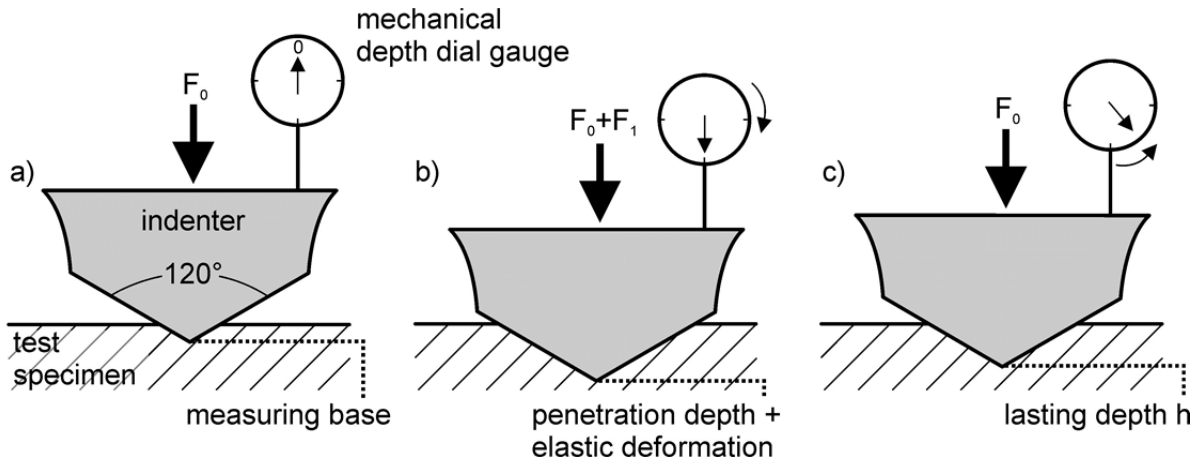

Fig. 57: Schematic sketch of the test principle after Rockwell. With this method, the lasting depth h is measured by a mechanical depth gauge during the test (modified after DIN EN ISO 6508-1 2016; FISCHER 2015: 9; WEIßBACH et al. 2015: 538).

Testing device

For the Rockwell C tests, a universal hardness tester from the company Wolpert (DIA TESTOR, model 2 Rc) from the year 1958 was used (Fig. 58). With this machine, not only Rockwell hardness tests, also Vickers und Brinell hardness tests are possible. Thus, this machine was also used for the Vickers low-force and hardness tests.

Fig. 58: The universal hardness tester DIA TESTOR, model 2 Rc manufactured from Wolpert in 1958 was used for the Rockwell hardness tests, the Vickers hardness tests and the modified Vickers hardness tests.

The hardness value for this model can be read directly on a mechanical depth dial gauge with an accuracy of around 0.5 HRC. This machine fits the accuracy and requirements given in DIN EN ISO 6508-2 (2015). The calibration of the machine is controlled and carried out annually by the MPA Stuttgart. Nevertheless, according to DIN EN ISO 6508-1 (2016), the hardness tester must be checked daily for accuracy by means of a hardness reference block. This test block has to be calibrated after DIN EN ISO 6508-3 (2015) and must not exceed the specified age.

Test analysis and calculations

For the calculation of the Rockwell hardness (HRC), the remaining penetration depth h under the initial load F_0 is needed (Equation 15).

Equation 15: Calculation of the Rockwell hardness Cone (HRC).

$$\mathrm{HRC} = 100 - \frac{\mathrm{h}}{0.002}$$

with:	HRC	*Hardness Rockwell Cone*	*[-]*
	h	*Lasting depth*	*[mm]*

The standard DIN EN ISO 6508-1 (2016) gives the following abbreviation and nomenclature of the Rockwell C hardness:

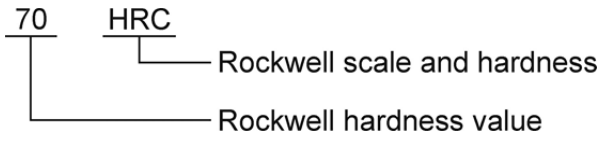

This also forms the basis for the calculation of the bias, the repeatability range and the error, which is performed according to DIN EN ISO 6508-1 (2016).

5.3.3 Vickers hardness test

The Vickers hardness tests were carried out according to the standard DIN EN ISO 6507-1 (2006). This static test method is also a standardized hardness test. It can be divided by the used test force into Vickers microhardness tests, Vickers low-force hardness tests and Vickers hardness tests. Tab. 19 gives an overview of this.

Tab. 19: Subdivision of the Vickers hardness tests by the used test forces (after DIN EN ISO 6507-1 2006, 2018).

Ranges of test force, F [N]	Hardness symbol	Designation
F ≥ 49.03	≥ HV 5	Vickers hardness test
1.961 ≤ F < 49.03	HV 0.2 to < HV 5	Low-force Vickers hardness test
0.009807 ≤ F < 1.961	HV 0.001 to < HV 0.2	Vickers microhardness test

The advantages of the Vickers tests in general are that they are standardized tests which can be used to test both hard and soft materials. As only the permanent indentation is measured, only the plastic part of the deformation is determined. The disadvantages here are the required high surface quality, the time-consuming analysis and the limited automation.

The requirements for the distances between the indentations, the minimum test thickness and the test times can be found in DIN EN ISO 6507-1 (2006) and DIN EN 843-4 (2005) and they have been maintained.

In addition to the standards mentioned so far, there are some other standards that address specific aspects of the Vickers hardness test. This includes DIN EN ISO 4516 (2002), which specifically highlights the aspects of the Vickers microhardness tests. The creation and execution of a hardness profile is inspired by DIN EN ISO 2639 (2003). DIN EN 843-4 (2005) treats hard and brittle ceramics. The basics of this are also valid for minerals and rocks and are therefore taken into consideration. For porous minerals and rocks, the principles of DIN EN ISO 4498 (2010) can be applied. In addition, DIN ISO 3878 (1991) is also considered.

Testing principle

This test belongs also to the static hardness tests. A schematic sketch of the test principle is given in Fig. 59. In the experiment, a diamond indenter, in the shape of a right pyramid with a square base and an angle of 136° is forced into to surface of the test specimen with a certain load (F). After removing the test force and the indenter, the size of the remaining indentation in the surface can be determined by measuring the two diagonals d_1 and d_2. The Vickers hardness is proportional to the quotient obtained by dividing the test force by the area of the sloped surface of indentation, which is assumed to be a right pyramid with a square base, and having at the vertex the same angle as the indenter.

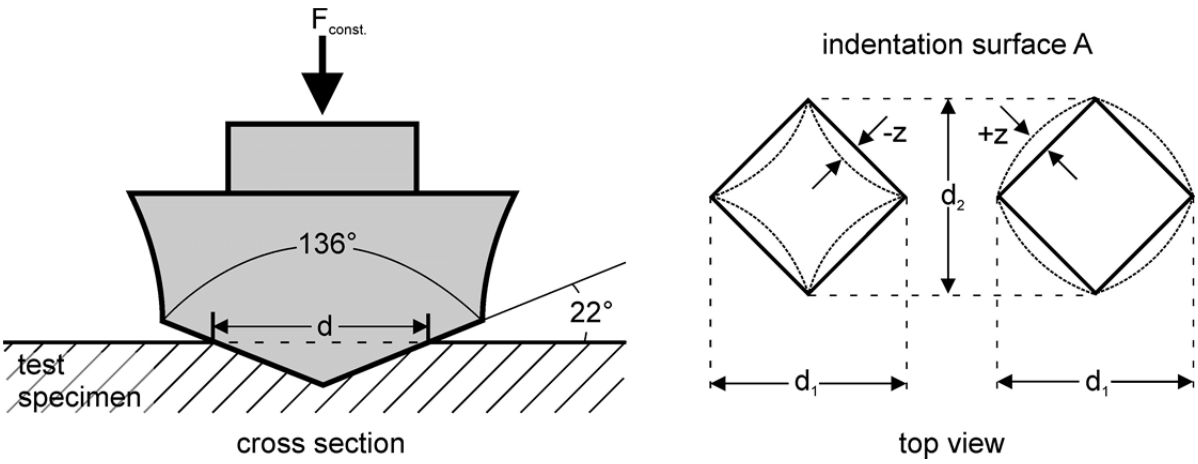

Fig. 59: Schematic sketch of the test principle of the Vickers hardness test. With this method, the permanent indentation (d) is measured. The right-hand image takes into account non-rectilinear indentations marked with "z" (modified after DIN EN ISO 6507-1 2006; MACHERAUCH & ZOCH 2011: 59; FISCHER 2015: 4).

Testing device

As even mentioned 5.2.3, three different devices were used for the for the Vickers hardness tests, each with an own Vickers indenter:

- Vickers Microhardness I: Leitz, model Durimet 2 (Fig. 60 left)
- Vickers Microhardness II: Zwick, model Z323 (Fig. 60 right)
- Vickers Low-force and Vickers hardness: Wolpert, model DIA TESTOR 2 Rc (Fig. 58)

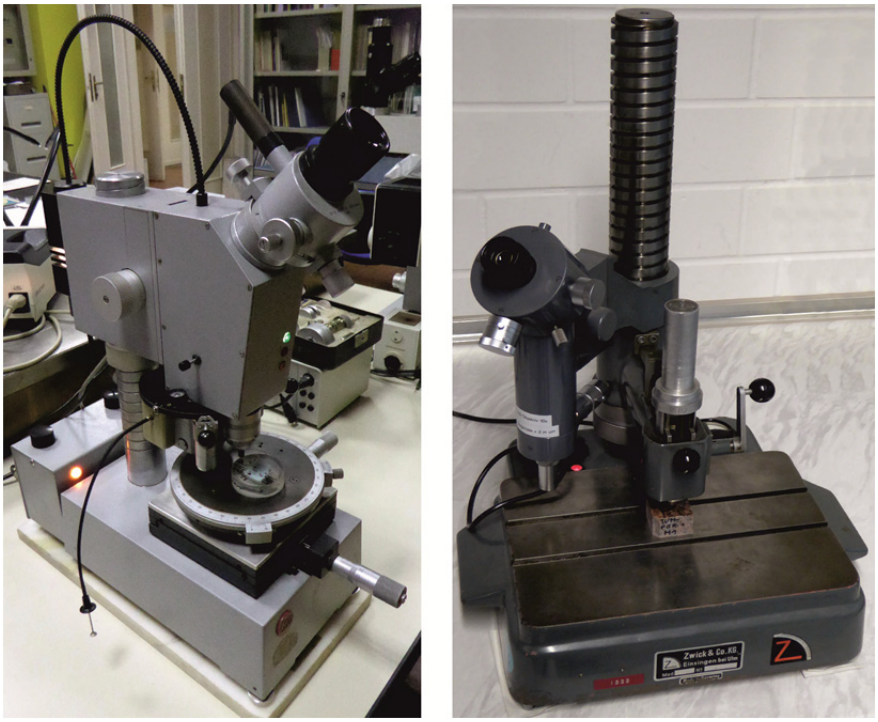

Fig. 60: Left: Vickers microhardness tester Leitz Durimet 2;
Right: Vickers microhardness tester Zwick, model Z323.

All the used devices meet the requirements given in the standards DIN EN ISO 6507-1 (2006), DIN EN ISO 4516 (2002) and DIN EN ISO 6507-2 (2013). As three different hardness testers were used for this thesis, three different indenters have also been used.

The calibration of the Wolpert hardness tester is controlled and carried out annually by the MPA Stuttgart (as mentioned in the previous chapter), the Leitz microhardness tester is controlled and carried out by Leica. Only the Zwick microhardness tester has no current certificate and thus deviates from the standard. Nevertheless, according to DIN EN ISO 6507-1 (2006), the hardness tester must be checked daily for accuracy by means of a hardness reference block. This test block has to be calibrated after DIN EN ISO 6507-3 (2006) and must not exceed the specified age.

To get the hardness values, the indentations have to be measured after the test. For both microhardness devices, the diagonals can be measured directly using the optical measurement unit. This system allows a measurement with an accuracy of approximately ± 0.5 µm. The indentations, produced with the Wolpert hardness tester (low-force Vickers hardness and the Vickers hardness tests), couldn't be measured directly with the device. They were measured afterwards with an optical microscope (Leica, model DMLM), equipped with an incident-light illuminator which allows an accuracy of around ± 1 µm.

Test analysis and calculations

For the calculation of the Vickers hardness (HV), the size of the indentations has to be measured. Since proper indentations have a square shape with two diagonals (the right side of Fig. 59), they are measured and the hardness is calculated according to Equation 16.

Equation 16: Calculation of the Vickers hardness (HV).

$$\mathrm{HV} = \text{constant} \cdot \frac{\text{test force}}{\text{surface area under indentation}}$$

$$HV = 0.102 \cdot \frac{2 \cdot \mathrm{F} \cdot \sin\left(\frac{136^\circ}{2}\right)}{\left(\frac{d_1+d_2}{2}\right)^2}$$

with:	*HV*	*Hardness after Vickers*	*[N/mm²]*
	0.102	*conversion factor of kgf in newton*	*[-]*
	F	*test force*	*[N]*
	d_1	*horizontal diagonal of the indentation*	*[mm]*
	d_2	*vertical diagonal of the indentation*	*[mm]*

The standard DIN EN ISO 6507-1 (2006) gives the following abbreviation and nomenclature of the Vickers hardness:

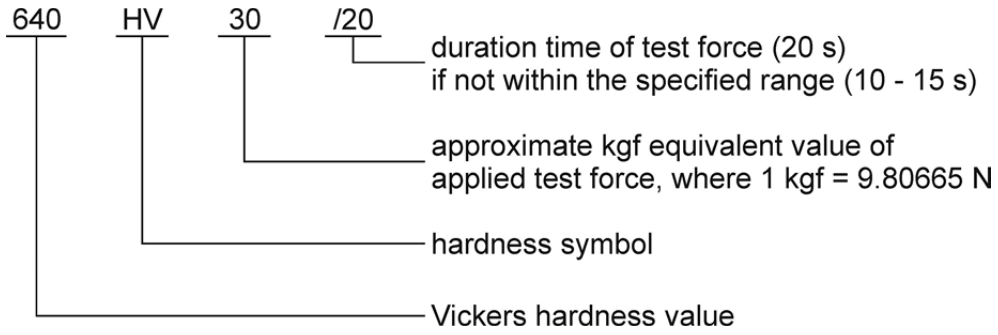

This also forms the basis for the calculation of the bias, the repeatability range and the error, which is performed according to DIN EN ISO 6507-1 (2006).

5.3.4 Knoop hardness test

The Knoop hardness tests were carried out according to the standard DIN EN ISO 4545-1 (2006). This static test method is also a standardized hardness test and related to the Vickers test. This makes the Knoop hardness test also suitable for metals as well as minerals, rocks, glass, and ceramics (brittle materials) CARDU & GIRAUDI (2012). As only the permanent indentation is measured, only the plastic part of the deformation is determined. The disadvantages here are the required high surface quality, the time-consuming analysis and the limited automation, like the Vickers hardness test.

The difference to the Vickers hardness test is in the shape of the diamond indenter and the evaluation of the results. Due to the different shape of the diamond, it does not penetrate so deep. Thus, the test produces fewer cracks and is more suitable for hard and brittle materials according to POLZIN (2007). Another difference is that the Knoop hardness tests are predominantly used for microhardness (test force < 1.961 N) and low-force hardness tests (1.961 – 49.03 N test force).

The requirements for the distances between the indentations, the minimum test thickness and the test times can be found in DIN EN ISO 4545-1 (2006) and DIN EN 843-4 (2005) and they have been maintained.

In addition to the standards mentioned so far, there are some other standards that address specific aspects of the Knoop hardness test. This includes DIN EN ISO 4516 (2002), which specifically highlights the aspects of the Knoop microhardness tests. The creation and execution of a hardness profile is inspired by DIN EN ISO 2639 (2003). DIN EN 843-4 (2005) treats hard and brittle ceramics. The basics of this are also valid for minerals and rocks and are therefore taken into consideration. For porous minerals and rocks, the principles of DIN EN ISO 4498 (2010) can be applied.

Testing principle

This test also belongs to the static hardness tests. A schematic sketch of the test principle is given in Fig. 61. In the experiment, a diamond indenter, in the shape of a rhombic pyramid with two different angles (172.5° and 130°) is forced into to surface of the test specimen with a certain load (F). After removing the test force and the indenter, the size of the remaining indentation in the surface can be determined by measuring the long diagonal d. The Knoop hardness is proportional to the quotient obtained by dividing the test force by the projected area of the indentation, which is assumed to be a rhombic-based pyramid, and having at the vertex the same angles as the indenter.

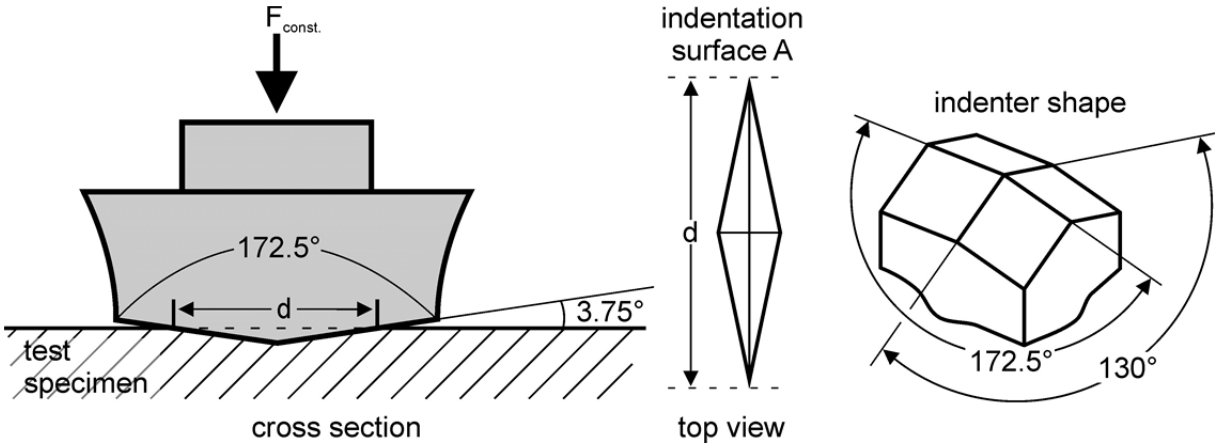

Fig. 61: Schematic sketch of the test principle of the Knoop hardness test. With this method, the permanent indentation (d) is measured. The right-hand image illustrates the rhombic-pyramidal shape of the diamond indenter (modified after DIN EN ISO 4545-1, 2006; MACHERAUCH & ZOCH 2011: 59).

Testing device

The Knoop tests were performed with the Leitz Durimet 2 (Fig. 60). This is the microhardness tester which also has been used for some Vickers hardness tests. Thus, it meets the requirements given in the standards DIN EN ISO 4545-1 (2006), DIN EN ISO 4516 (2002) and DIN EN ISO 4545-2 (2006).

The calibration is controlled and carried out annually by Leica. Nevertheless, according to DIN EN ISO 4545-1 (2006), the hardness tester must be checked daily for accuracy by means of a hardness reference block. This test block has to be calibrated after DIN EN ISO 4545-3 (2006) and must not exceed the specified age.

To get the hardness values, the indentations have to be measured after the test. For this purpose, the log diagonal d can be measured directly using the optical measurement unit. This system allows a measurement with an accuracy of approximately ± 0.5 µm.

Test analysis and calculations

For the calculation of the Knoop hardness (HK), the size of the indentations has to be measured. Since proper indentations have a rhombic-pyramidal shape with a shorter and a longer diagonal (the middle part of Fig. 61), only the longer one is measured and the hardness calculated according to Equation 17.

Equation 17: Calculation of the Knoop hardness (HK).

$$\mathrm{HK} = \text{constant} \cdot \frac{\text{test force}}{\text{projection surface of the indentation}}$$

$$\mathrm{HK} = 0.102 \cdot \frac{\mathrm{F}}{\left(\frac{\tan\frac{130^\circ}{2}}{2 \cdot \tan\frac{172.5^\circ}{2}}\right) \cdot (\mathrm{d})^2} \approx 1.451 \cdot \frac{\mathrm{F}}{\mathrm{d}^2}$$

with:	*HK*	*Hardness after Knoop*	*[N/mm²]*
	0.102	*conversion factor of kgf in newton*	*[-]*
	F	*test force*	*[N]*
	d	*longer diagonal of the indentation*	*[mm]*

The standard DIN EN ISO 4545-1 (2006) gives the following abbreviation and nomenclature of the Knoop hardness:

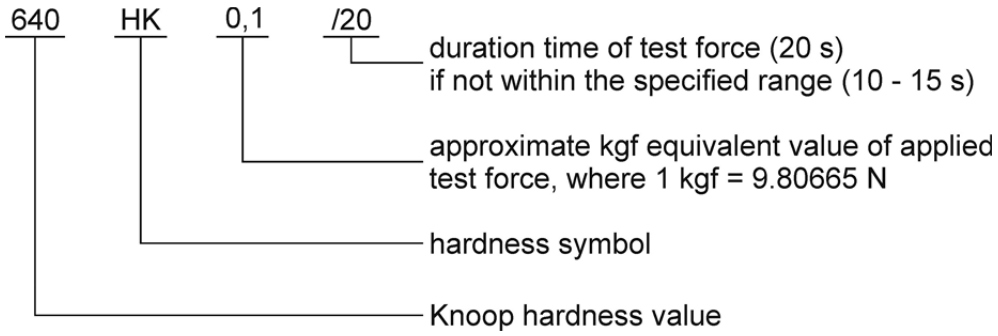

This also forms the basis for the calculation of the bias, the repeatability range and the error, which is performed according to DIN EN ISO 4545-1 (2006).

5.4 Modified Vickers hardness

This test method is developed by me and consists of a combination of the Vickers and the Rockwell test. Thus, this is also a static hardness test. By the use of the Vickers indenter in combination with the Rockwell testing principle, the advantages of each method could be combined: the steady shape of the Vickers diamond and the measurement of the penetration depth with a certain preload. Thus, the values can be read directly on the machine at the end of the test and due to the preload, the surface quality has a lower influence on the results. This increases the evaluability, objectivity and thus the reproducibility of the measurements compared to the Vickers hardness with high loads.

The disadvantages are, that there is no direct correlation with other standardized hardness tests and that the evaluation of the indentations is impossible after removing the initial load. Also, there are sometimes large scatterings with low penetration depth, caused by the geometry of the indenter and the accuracy of the used device.

The requirements for the distances between the indentations and the minimum test thickness are inspired by the Rockwell test principle (DIN EN ISO 6508-1, 2016), but they must also comply with the requirements of the Vickers standard (DIN EN ISO 6507-1, 2006). The test times are inspired by the Vickers method (DIN EN ISO 6507-1, 2006).

Sample preparation

The samples were prepared according to the same principle as explained in chapter 5.3.1. The only difference is that theoretically no polished surface is required. However, for reasons of comparability, each sample was polished.

Testing principle

This test is a static method to determine the hardness and similar to the Rockwell test method. A schematic sketch of the test principle is given in Fig. 57 on page 113. In the experiment, an initial load (F_0) with 10 kgf is applied to a Vickers indenter. The resulting measuring base serves as a reference plan for the further test, like in the Rockwell test. The depth dial gauge is reset to zero (section a). Subsequently, an additional load (F_1) is applied, which causes a deeper penetration of the indenter into the specimen (section b). As a last step, the total test load F is reduced to F_0, so that an elastic rebound occurs (section c). With the resulting penetration depth h, the Rockwell hardness can be determined.

Since this a new test method, it was first necessary to find out which load is to be applied to F_1. The following loads were tested: 5 kgf, 10 kgf, 20 kgf, 30 kgf, 40 kgf, 50 kgf and 62,5 kgf. It turned out that a load of 50 kgf is best suited for F_1. This was subsequently used for further experiments.

Testing device

The testing device is the same which was used for the Rockwell C and the Vickers hardness tests Fig. 58 (Wolpert DIA TESTOR, model 2 Rc). For this special test, the Vickers indenter was used. As even explained under 5.3.2, the hardness values can be read directly on the mechanical depth dial gauge with an accuracy of 0.5 scale units. One scale unit on the gauge corresponds to a depth of 2 µm. This results in an accuracy of approx. 1 µm.

Test analysis and calculations

For the calculation of the modified Vickers hardness (MVH), the remaining penetration depth h under the initial load F_0 is needed (Equation 18).

Equation 18: Calculation of the modified Vickers hardness (MVH).

$$\mathrm{MVH} = 100 - \frac{\mathrm{h}}{0.002}$$

with:	MVH	*Modified Vickers hardness*	*[-]*
	h	*Lasting depth*	*[mm]*

The abbreviations and nomenclature is inspired by the Rockwell hardness (DIN EN ISO 6508-1, 2016):

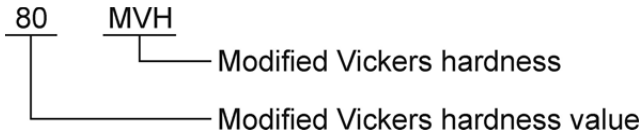

This also forms the basis for the calculation of the bias, the repeatability range and the error, which is inspired by and performed according to DIN EN ISO 6508-1 (2016).

Due to the pyramidal shaped geometry of the Vickers indenter, the penetration depth is approx. 1/7 of the diagonal length (POLZIN 2007).

6. Results and Interpretation

This chapter gives an overview of the results of this thesis. The first part includes the results of the geotechnical experiments for the general characterization of the rock investigated. In order to give a broad overview and to cover a large part of the rocks occurring in the upper earth crust, a large number of rock types were examined. The rocks consist of magmatic, metamorphic and sedimentary rocks and are also divided into these subgroups. In order to characterize the rock samples as comprehensively as possible, an extensive laboratory program was set up. The methodology of the laboratory tests has been described in chapter 4.4.

The second part consists of the studies of the TBM disc cutter, which originate from the Koralm Tunnel project. For this purpose, the disc cutters were classified according to their macroscopic wear type and the surface was examined more closely. In addition, metallographic cross sections were made of a large number of cutters and the microstructure and changes in the area of the cutting edge were also studied.

The third part presents the results of hardness tests on selected disc cutters, CERCHAR pins and LCPC impellers as well as on minerals and rocks. It is important to note that the hardness testing of minerals and rocks is not standardized and often very challenging.

Part of the laboratory testing has been performed in collaboration with L. Wilfing (WILFING 2016) and C. Wieser (WIESER 2016) within the scope of their doctoral theses at the Technical University of Munich. Furthermore, several Bachelor's and Master's theses contributed to the results of the testing program under my supervision (NGUYEN 2014; CHMIEL 2014; BRENNER 2015; HEUFT 2015; HIEBER 2016; PAHNKE 2016; SCHNEIDER 2014; DENINA 2014; FISCHER 2015; RAUCH 2016).

6.1 Rock strength and abrasivity

This chapter summarizes the basic laboratory results from equivalent quartz content, Uniaxial Compression Tests, Brazilian Tensile Tests, Point Load Tests, CERCHAR Abrasivity Tests and LCPC Abrasivity Tests. Tab. 20 lists the mean value of resulting laboratory parameters in brackets. The number of tests carried out, including minimum and maximum values are also given. The variation range is usually in the first line and the number of experiments is marked with an asterisk. Sample acquisition was mostly done by collecting cobbles of rock at quarries. As rock is a natural product and never really homogenous, this implies that rock samples deriving from the same rock material may obviously vary in their geotechnical parameters. The abovementioned classification into magmatic, metamorphic and sedimentary rock types is continued in this chapter and presents all about 19 different rock types.

Tab. 20: Summary of basic laboratory results: equivalent quartz content (EQC), uniaxial compressive strength (UCS), Brazilian tensile strength (BTS), point load index (Is), CERCHAR abrasivity index (CAI), LCPC abrasivity coefficient (LAC) and LCPC breakability coefficient (LBC).

	EQC [%]	UCS [MPa]	BTS [MPa]	$I_{s(50)}$ [MPa]	CAI [-]	LAC [g/t]	LBC [%]
Igneous rocks: Magmatites							
Larvikite (TUM-LAR)	41,6	170,6 – 209,2 (184,5) 5 *	8,3 – 10,2 (9,4) 3 *	8,8 – 13,8 (10,7) 12 *	3,5 – 4,8 (4,1) 3 *	1,380 – 1,440 (1,410) 2 *	45 – 47 (46) 2 *
Swedish Black/Ebony Black (TUM-SSW)	42,7	292,0 – 313,2 (301,8) 3 *	17,5 – 19,1 (18,3) 2 *	11,7 – 16,2 (13,7) 12 *	3,4 – 3,8 (3,6) 3 *	1,520 – 1,660 (1,590) 4 *	29 – 32 (30) 4 *
Diorite (TUM-GRF)	58,4	151,0 – 214,3 (190,6) 7 *	8,7 – 16,0 (13,7) 7 *	3,5 – 13,0 (8,3) 11 *	4,2 1 *	1,120 – 1,260 (1,190) 2 *	33 -34 (34) 2 *
Granite (TUM-GRZ)	-	159,9 – 213,3 (189,1) 3 *	9,2 – 14,1 (11,4) 7 *	6,8 – 11,6 (10,1) 9 *	4,9 1 *	1,200 – 1,220 (1,210) 2 *	50 2 *
Granite (TUM-MET)	-	70,3 – 88,1 (78,6) 6 *	5,9 – 8,4 (7,2) 9 *	5,4 – 6,9 (5,9) 10*	3,4 – 4,2 (3,7) 3 *	880 – 1,140 (1,860) 4 *	77 – 92 (83) 4 *
Quartzite (TUM-GQZ)	100	-	15,1 – 16,8 (23,5) 2 *	5,3 – 7,2 (6,4) 4 *	4,4 – 5,6 (5,2) 3 *	1,880 – 2,360 (2,120) 2 *	43 2*
Igneous rocks: Vulcanites							
Basalt (TUM-PB)	47,2	330,1 – 447,4 (397,4) 4 *	13,7 – 25,5 (19,1) 4 *	10,1 – 14,9 (12,4) 11 *	2,7 1 *	1,040 – 1,400 (1,173) 3 *	20 – 21 (21) 3 *
Metamorphic rocks							
Marble (TUM-LAM)	4,3	83,9 – 88,1 (86,3) 6 *	4,4 – 8,1 (6,2) 6 *	3,6 – 5,1 (4,1) 10 *	0,8 – 1,5 (1,1) 3 *	0 – 20 (10) 4 *	87 – 89 (88) 4 *
Marble (TUM-CAR)	-	*133*	-	-	-	-	-
Brixen Quartzphyllite (TUM-BQP)	-	-	8,6 – 10,4 (9,8) 6 *	4,8 – 9,1 (7,1) 14 *	0,3 1 *	100 – 120 (110) 2 *	46 – 47 (47) 2 *
Gneiss (TUM-FGG)	61,7	69,9 – 124,9 (105,4) 3 *	6,1 – 11,8 (9,4) 4 *	4,0 – 11,6 (8,6) 12 *	3,9 – 4,0 (3,9) 3 *	1,200 – 1,320 (1,267) 3 *	37 3 *
Amphibolite (TUM-OBM)	30,3	232,9 – 280,7 (253,9) 4 *	19,3 – 25,4 (21,4) 3 *	11,5 – 16,0 (13,2) 11 *	2,9 – 3,6 (3,3) 3 *	900 – 1,040 (986) 3 *	23 2 *
Sediments							
Flintstone (TUM-FLI)	100	589,2 – 658,3 (623,8) 2 *	18,3 – 61,2 (44) 4 *	11,4 – 17,7 (13,7) 13 *	2,7 – 3,3 (3,0) 3 *	2,720 – 2,800 (2,760) 2 *	38 2 *
Sandstone (TUM-DST)	94,3	175,5 – 195,4 (188,2) 3 *	8,4 – 11,0 (9,3) 3 *	6,5 – 10,2 (8,4) 12 *	3,8 1 *	1,280 – 1,320 (1,293) 3 *	54 – 63 (60) 3 *
Sandstone (TUM-KUC)	-	113,7 – 114,2 (114,0) 3 *	6,3 – 8,0 (7,3) 3*	5,9 – 8,2 (7,0) 17 *	2,5 1 *	160 – 180 (170) 4 *	32 – 34 (33) 4 *

	EQC [%]	UCS [MPa]	BTS [MPa]	$I_{s(50)}$ [MPa]	CAI [-]	LAC [g/t]	LBC [%]
Sandstone (TUM-ABO)	73,4	41,6 – 44,0 (42,5) 6 *	1,8 – 2,5 (2,3) 6 *	1,3 – 2,9 (1,8) 12 *	0,4 – 0,8 (0,6) 3 *	140 – 240 (176) 5 *	98 – 99 (99) 5 *
Sandstone (TUM-ABC)	73,7	25,3 – 28,3 (26,9) 6 *	1,8 – 2,6 (2,1) 6 *	0,4 – 1,7 (1,3) 14 *	0,4 1 *	120 – 200 (155) 4 *	99 4 *
Sandstone (TUM-POS)	99,4	53,6 – 63,9 (59,9) 8 *	3,4 – 4,5 (4,1) 10 *	3,2 – 3,7 (3,4) 10 *	2,0 – 2,5 (2,3) 3 *	120 – 180 (153) 3 *	99 3 *
Limestone (TUM-WIE)	-	123,3 – 156,7 (185,7) 5 *	7,2 – 14,6 (10,4) 4 *	4,0 – 4,9 (4,6) 7 *	0,4 – 0,7 (0,6) 3 *	20 3*	33 – 36 (35) 3 *
Marlstone (TUM-WME)	-	-	-	-	-	-	-

(mean values), * number of tests, *in italics -> data according to MÜLLER & KÖGLER (n.d.b)*

6.2 Macroscopic wear effects

This chapter provides an overview of the macroscopic wear phenomena that have occurred on the TBM disc cutters investigated for the Koralm Tunnel project. At first, the phenomena already known and mentioned in chapter 2.1.3 and Tab. 4 are dealt with and the geological conditions under which they occurred are described. It must be mentioned here that a large number of disc cutters have been investigated and only the best examples are shown here.

The images in Tab. 21 show different types of wear as they occur in reality. When selecting the images, care was taken to ensure that they correspond as far as possible to only one type of wear. During operation, however, it was found that there is often an overlap of different types of wear. In the course of the chapter several more images follow, showing special wear forms as well as the superposition of several types.

Tab. 21: Overview of the basic wear types during the Koralm Tunnel project, showing images of worn out cutter rings.

Wear type	Name	Sample images	Symbolic image
Abrasive wear	Abrasive wear / normal wear	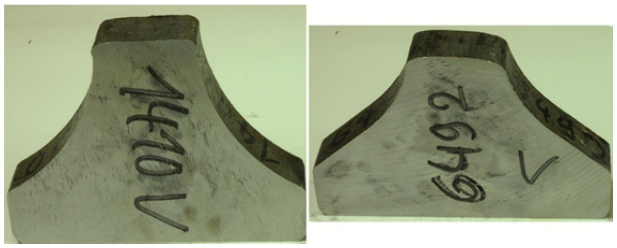	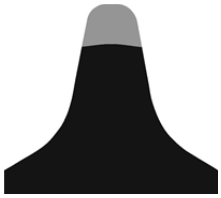
	Mushrooming		
	Chipping		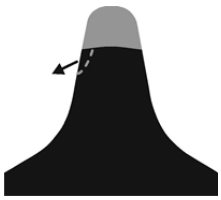
	Tapering		
	Asymmetric wear		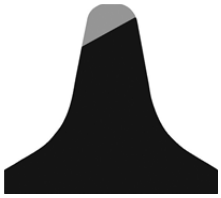

Wear type	Name	Sample images	Symbolic image
Special types	Brittle fracture	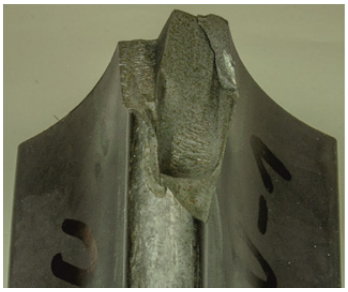	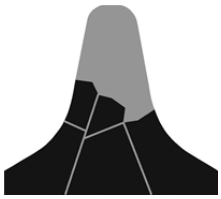
	Blockage	 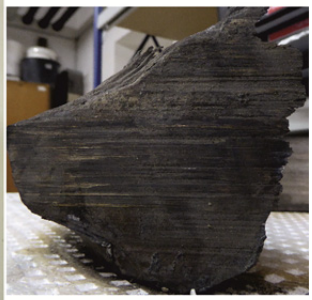	

6.2.1 Abrasive wear/Normal wear & Asymmetric wear

Abrasive wear or also called normal wear occurred typically in compact rock masses, which consists of strong rock (50 to 100 MPa, classification according to ISRM (1978c) and on face cutters. This type is considered optimal because of its high utilization rate (high mileage by low material removal). Anisotropies in the rock and the rock mass were usually rather small. If the wear is asymmetrical, we called it simply asymmetric wear. This type mainly appeared on center or gauge cutters, i.e. in the inner area or caliber region of the cutter head. This correlation has already been noted by THURO & PLINNINGER (2002) and KÄSLING (2009). (ELLECOSTA et al. 2018)

Fig. 62 illustrates types of normal and asymmetric wear. The two upper images show cutters mounted on the cutter head. At image b) you can clearly see that the edge of the cutter ring is worn much more towards the outside than towards the center of rotation. This was shown with all cutter rings showing asymmetrical wear.

Figure d) points at a cutter ring with asymmetrical wear. In addition, it can be seen that the upper side shows slight mushrooming with chipping in places. This type occurs mainly with cutter rings in the center or near the center due to the small radius of rotation. The mushrooming indicates strong contact forces and a high rock hardness. Due to strong deformation in the steel, chipping is accompanied by mushrooming.

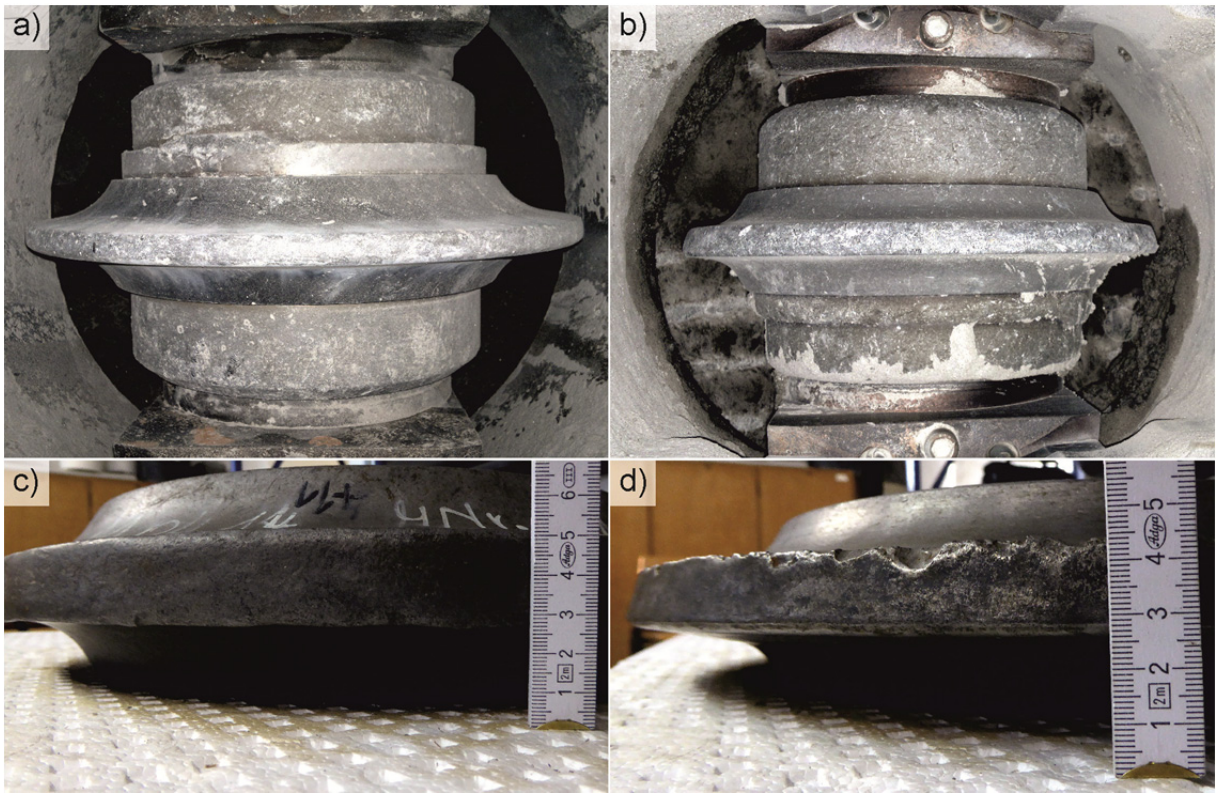

Fig. 62: TBM disc cutters showing types of abrasive wear and asymmetrical wear.
a) Abrasive wear during operation b) Asymmetric wear during operation c) Typical abrasive wear d) Asymmetric wear with mushrooming and partly chipping on one side.

6.2.2 Mushrooming & Chipping

The formation of an impact head on the cutter tip is known as mushrooming and occurs when the rock has a strong to extremely strong uniaxial compressive strength (UCS) (100 to > 250 MPa, classification according to ISRM (1978c)) and rather few joints. To cut such strong rock types by effective chipping, high contact pressures on the cutters (high cutter thrust) are necessary. The high cutter thrust forms an impact head which can be compared with a secondary and cold forging of the cutter ring. When this happens, the steel is stressed and deformed beyond its yield point or elasticity limit and irreversible, plastic deformation occurs. (ELLECOSTA et al. 2018)

If the deformation is very severe, large steel chips may break off laterally from mm to cm due to materials fatigue. This is called ring chipping or simply chipping and occurs mainly in fractured to highly fractured rock mass. In other projects, MACIAS et al. (2017a) also found out that ring chipping is preferred in fractured rock mass because the cutters will be exposed to large instantaneous loads which enhance the fatigue.

Fig. 63: TBM disc cutters showing types of mushrooming and chipping.
a) Mushrooming during operation b) Mushrooming and chipping during operation
c) Slight asymmetric mushrooming with partly chipping d) Chipping e) Chipping
f) Mushrooming with a crack that leads to chipping g) Massive chipping
h) Chipping on different scales i) Abrasive wear with chipping j) Tapering with chipping.

In addition, the Koralm Tunnel project showed a tendency for the effect of chipping to increase from the center cutters to the cutters in the caliber region. Other researchers (e.g. GENG et al. 2017) confirm this and report that the effect of extreme mushrooming with chipping primarily occurs on cutters in the outer region of the cutter head. Reasons for this may be a higher rock strength due to the stress distribution on the rock face (RAUCH 2016; LAGGER et al. 2015) and due to the higher rolling velocity and thus a more dynamic load (LINDHOLM et al. 1974; SANO et al. 1981; ZHANG et al. 2000). Furthermore, the cutters in the outer regions undergo usually more cycles during operation. GENG et al. (2017) also reports that the high rolling velocity causes higher impact loads on the cutters and thus results in more intense ring chipping, cutter blockage and bearing damage due to fatigue. (ELLECOSTA et al. 2018)

Fig. 63 shows some types of mushrooming and chipping and some superimposed phenomena. The two upper images show cutters mounted in the cutter head. Both show mushrooming, image b) points at mushrooming with chipping. Most of the other images show mushrooming, which can lead to chipping if it is very pronounced.

Figure f) points to a cutter ring with very strong mushrooming. Such extreme deformations cannot be tolerated by the disc cutter steel and this leads in a first step to cracks and later on, when the cutter ring is used furthermore, to the breakage of chips.

However, there are also other forms of wear than mushrooming, where chipping can occur. Images i) and j) show chipping on cutters that show normal wear and tapering. However, this is much less common and is believed to occur in connection with rolling over metallic objects (broken cutters or broken wear protection material) or due to material defects of the cutter ring.

Image h) shows very strong chipping, which is caused by strong mushrooming. The circled area marks a region, where smaller chips broke off first and this led to a break-off of a larger chip from the flank of the cutter ring. The breakage of such large pieces is caused by a brittle failure of the cutter ring. If the failure areas become even larger and the cutter ring is so limited in its functionality that it has to be replaced, we can already speak of brittle fracture. In some cases there is a transition from chipping to brittle fracture.

6.2.3 Tapering and grooving

Tapering or a self-sharpening of disc cutters is characteristic for loose rocks or extremely weak to medium weak rocks (0.25 to 50 MPa, classification according to ISRM (1978c) with a very poor interlocking or cementation. Grooving or more precisely a combination of tapering and grooving is possible, if the wear of the cutter is already advanced and the tip width has therefore increased. Both types can be asymmetric.

Fig. 64: TBM disc cutters showing types of tapering and sometimes grooving.
a) Tapering during operation b) Tapering with grooving during operation c) Tapering
d) Asymmetric tapering with grooving e) Tapering with grooving f) Close-up tapering with grooving g) Tapering with grooving and little mushrooming and chipping
h) Tapering with grooving, mushrooming and chipping.

Fig. 64 shows some types of tapering and grooving. The two upper images show cutters mounted in the cutter head. Both show tapering, image a) shows chipping and grooving, b) grooving. Image c) points at a typical tapering of a cutter ring, image d) a typical asymmetric tapering with grooving towards the flanks.

Images e) and f) show tapering with grooving. The detailed image on the right side shows that only the narrow, uppermost area transmits the contact pressure to the rock and contributes to rock cutting. The two grooves show mainly scratches in the direction of the flanks. This means that the grooves are created by the mining process, mainly by grinding of the crushed rock.

Image g) and h) show cutter rings with tapering and grooving as well as mushrooming and chipping. This combination is particularly well developed in image h). This effect was especially noticeable with typically rather moderate rock strengths such as mica slates, which, however, were pervaded with sometimes very thick quartz lenses of up to several meters in the tunnel face.

6.2.4 Brittle fracture

In addition to the normal wear types, special shapes or wear types can also occur, which are not or only minimally caused by geological conditions. The first one is called brittle fracture and means that bigger parts or the complete cutter ring crack suddenly and unpredictably due to brittle fracturing. Even if only a few parts of the cutter ring break off, functionality is usually reduced to such an extent that the entire disc cutter needs to be replaced (also necessary in order to avoid major damage, for example, at the bearing or the cutter head). (ELLECOSTA et al. 2018)

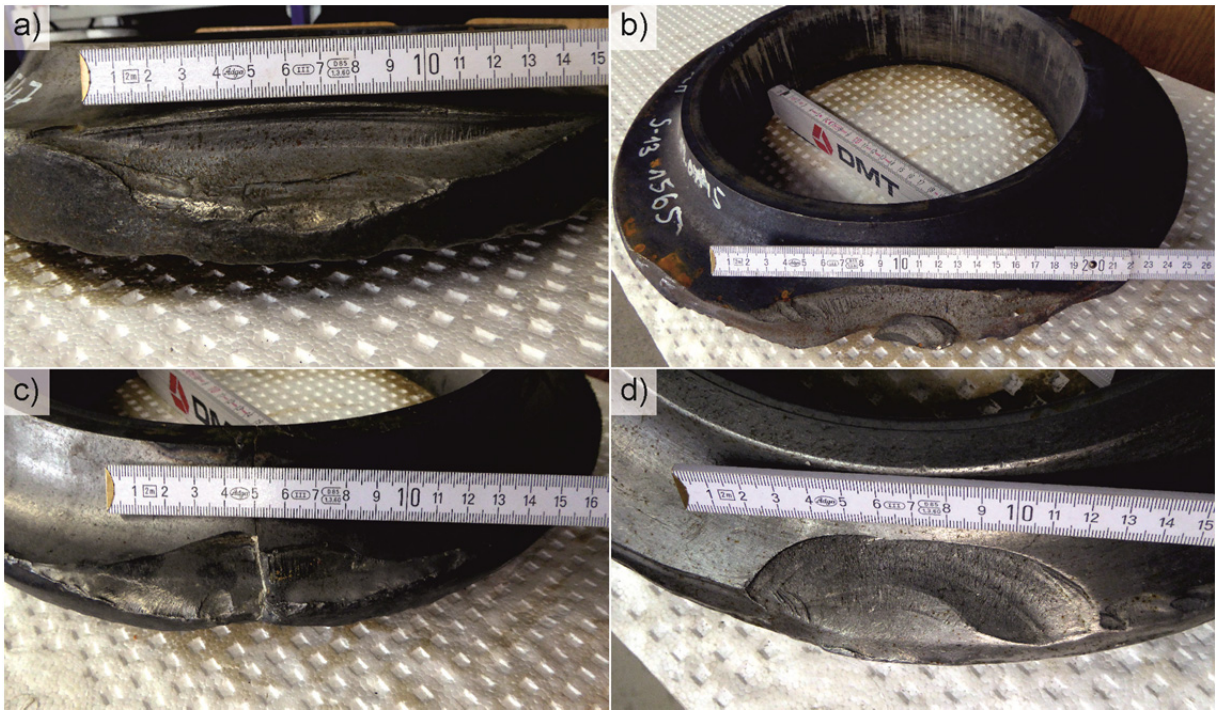

Fig. 65: TBM disc cutters showing brittle failure.
a) Massive Chipping / brittle fracture b) Massive Chipping / brittle fracture
c) Fracture of a cutter ring d) Massive Chipping / brittle fracture.

A rupture of the steel in general may be due to faulty or insufficient heat treatment of the cutter ring during the manufacturing process. Another possibility is that the heat treatment, i.e. the adjustment of the hardness, strength and toughness, is not adapted to the lithological conditions. It is also possible that tools may have run over metal parts that have fallen off, e.g. built-up welds, wear-protective material or disc fragments. This is an extreme dynamic overload (RÖTTGER et al. 2015) that can lead to total failure of the cutter ring, especially if this happens several times (fatigue). (ELLECOSTA et al. 2018)

Fig. 65 illustrates four examples of brittle fracture. Images a) and d) each show the loss of a massive steel chip, some of which is over 10 cm in size. In image b) the broken steel chip reaches a size of more than 15 cm. Figure c) shows a broken cutter ring. The images show that there is a transition from chipping to brittle fracture. If the broken steel chips reach such a size that the cutter ring is too limited in its functionality and must be replaced, this should already be considered as brittle fracture.

However, a certain correlation with geological conditions in highly fractured rock mass involving very hard and solid rocks have been found. In this combination, the tunnel face is blocky. An explanation for this effect can be high primary stresses. In order to be able to excavate these type of rock mass at all, very high contact pressures and forces must be applied to the cutter ring. However, since only part of the cutters come into contact with the tunnel face due to its blockyness, the permitted force per cutter is exceeded, and thus the likelihood of brittle and spontaneous failure increases, also as a result of fatigue.

In addition, it was found that this effect was more common on cutters the further out they were positioned on the cutter head. This is attributed to the higher rolling speed of the outer cutters. Due to the higher rolling speed, dynamic loads increase and lead to premature failure.

6.2.5 Blockage

Another special wear type appears when the roller bearing might be blocked, so that the cutter ring cannot rotate anymore and is abraded on one side. This generally can happen when stone dust and stone flour penetrate the seal and get into the bearing, or lubricating oil leaks out. If a bearing becomes too hot and the oil cannot sufficiently lubricate, it also blocks the cutter ring. Blockage wear type is therefore a blockage of the bearing and is caused by a problem in the base body. (ELLECOSTA et al. 2018)

Fig. 66 illustrates four examples of blocked base bodies and the resulting abrasion of cutter rings. Image a) and b) show an example of what happens when a blockage is detected relatively late. This is where complete abrasion of the cutter ring occurs. In extreme cases the base body is also abraded, like on the left image. If such a blockage is not detected, damage to the cutter head is also possible.

Figure c) shows a detailed view of a blocked cutter ring. The linear abrasion of the rock on the metal is clearly visible here. A strong heating of the steel until annealing is to be assumed.

Image d) points at a blockage, which also shows chipping. Due to the continued strong contact pressure on the tunnel face and possibly slight slipping of the bearing, strong impacts can act on the cutter ring, which leads to chipping.

Even if a blockage of the roller bearing does not seem to depend primarily on the geological conditions, the Koralm Tunnel project showed a slight increase of this wear type in fractured rock mass involving hard and solid rock.

Fig. 66: TBM disc cutters showing blockage damage.
a) Abrasion down to the base body b) Abrading nearly the whole cutter ring
c) Close-up on a blocked cutter ring d) Blockage caused chipping.

6.3 Microscopic wear effects

This chapter covers the microscopic wear phenomena that go beyond the classic macroscopic classification scheme. Most of the images show polished and etched metallographic cross sections of the cutter rings. The photos for the structural analysis are taken with a reflected light microscope (RLM, Leica DM LM) or a scanning election microscope (SEM, Zeiss LEO 1525 Gemini). During the SEM imaging, energy dispersive X-ray spectroscopy (EDX-analysis) was used to examine the steel and the buildup on the surface.

A first interpretation of how these phenomena occur is given in this chapter. It should be noted that nearly only effects resulting from rock excavation are shown. The original, unaltered steel-structure of tempered martensite is described and illustrated in chapter 4.4.1.

It must be mentioned that a large number of disc cutters have been investigated and only the best examples are shown here.

6.3.1 Alignment of crystallites

Typically, the structure of the cutter rings is isotropic. As soon as there are alignments of crystallites, it should be checked what this is due to.

Fig. 67 illustrates an alignment of crystallites parallel to the surface of the cutter tip. The cutter rings with the wear type mushrooming show usually a very deep reaching alignment of more than 100 µm. Sometimes several hundred µm are also achieved. Such deep and extreme structural changes are caused by cold forging when an impact head is formed, as material is forged outwards. This mostly plastic material flow towards the flanks is macroscopically visible.

Accordingly, the deformations become more pronounced towards the outside. In contrast, image b) with the abrasive wear shape shows only a rather small zone of up to about 40 µm depth. Below and next to it is the isotropic, original structure of the steel. When there is such a strong anisotropy in the otherwise typically isotropic structure, a shelled detachment of small steel particles parallel to the surface is promoted. Such a situation is shown in image a).

The difference between the two types of wear is probably the contact pressure with which the cutter rings are pressed on the tunnel face. While the maximum cutter thrust is often exhausted on mushrooming-cutters, it is often significantly lower on abrasive-cutters. As a result, cold forging is only possible on small and rather thin areas

The alignment of the crystallites on Fig. 68 has a different background. This concerns cutter rings with the wear shape mushrooming and/or chipping. The structural change occurs here mainly in the area just below the impact head on the flank. The massive deformation leads to hardening and enhanced brittleness, such that embrittlement and cracks can form more easily.

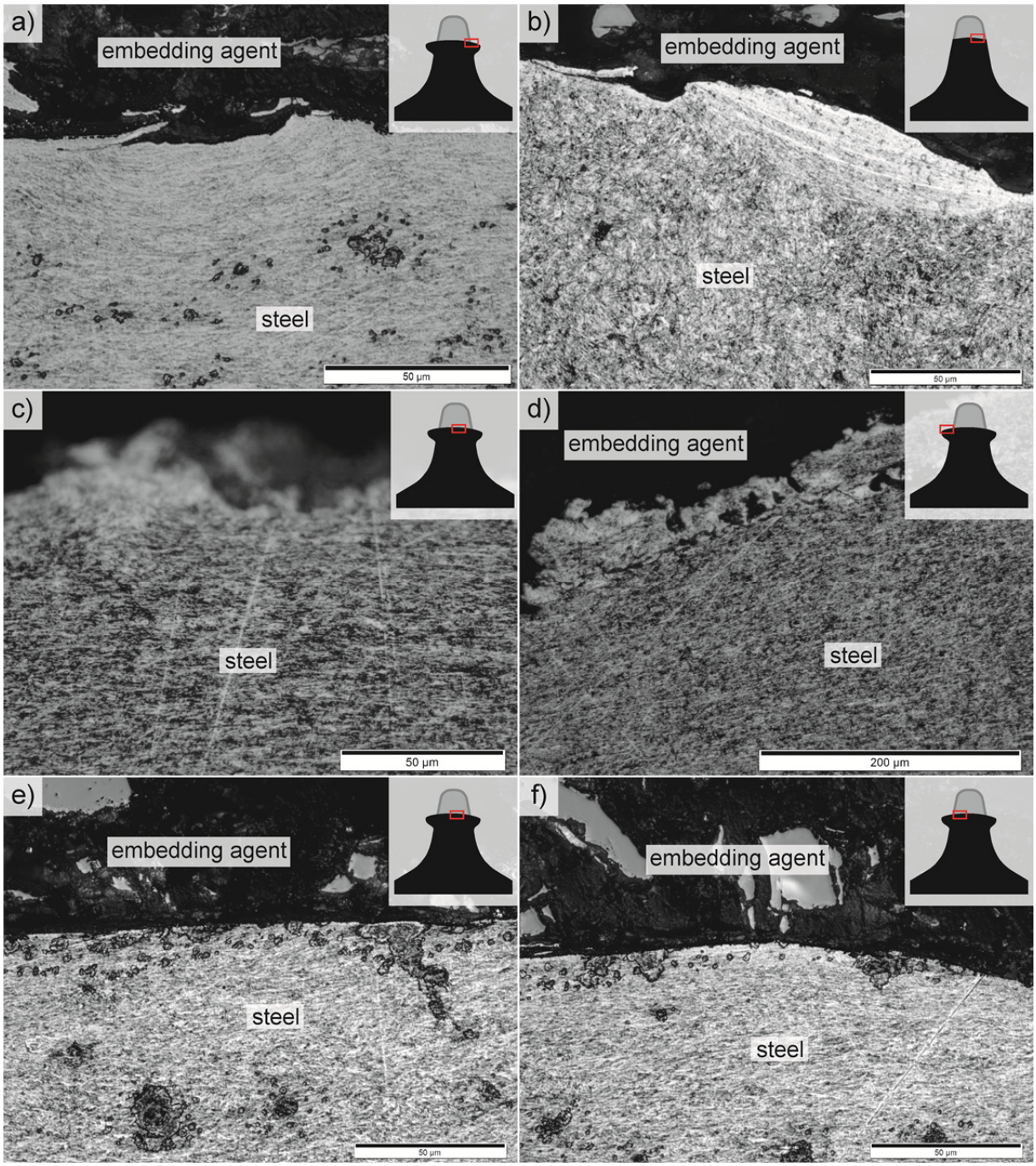

Fig. 67: TBM disc cutters showing an alignment of crystallites approximately parallel to the surface on the cutter tip. a) 901 b) 2408 c), d) 5669 e), f) 5840.

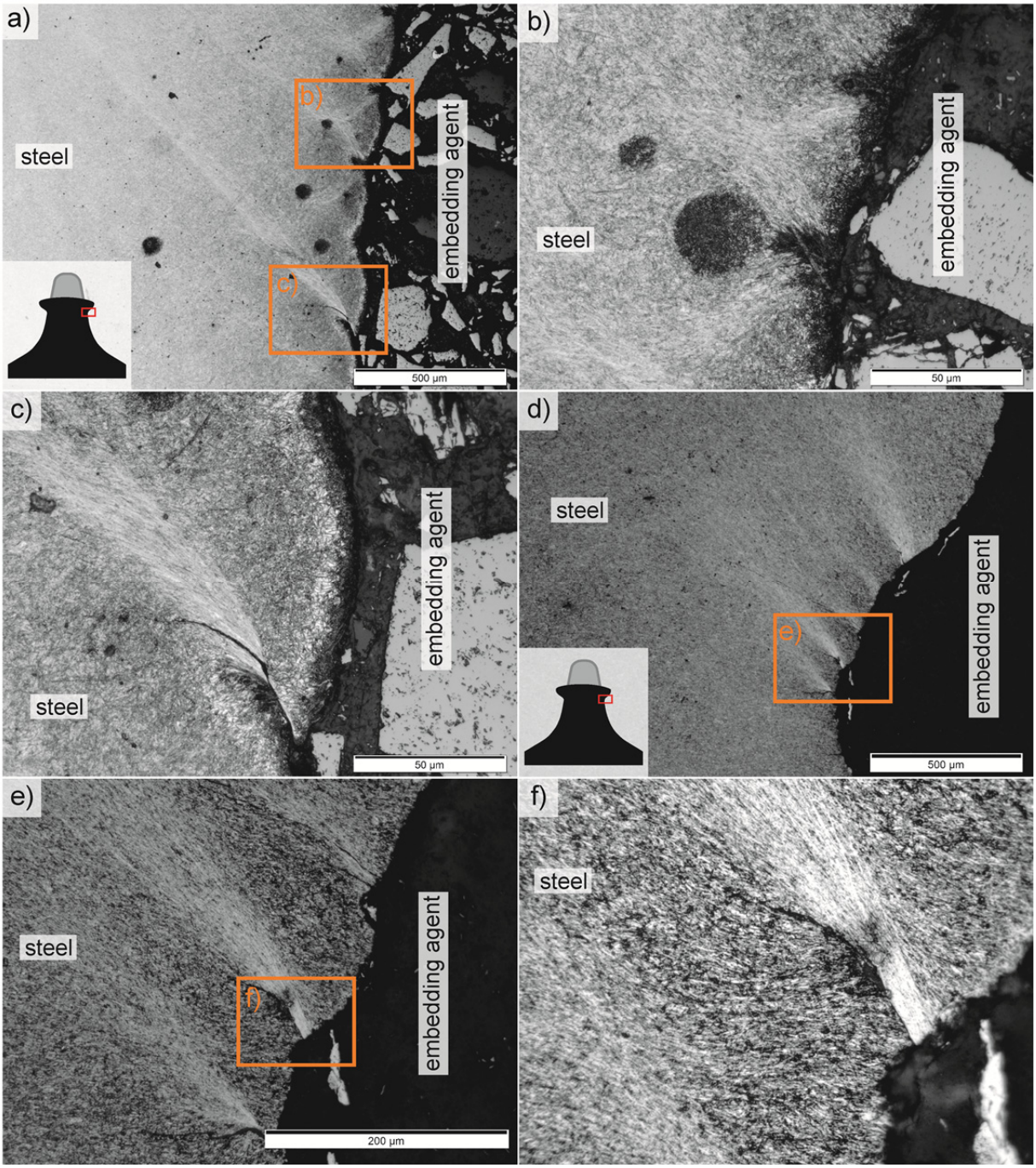

Fig. 68: TBM disc cutters showing an alignment of crystallites, which start from lateral cracks or imperfections and indicate shear planes or movement paths. a), b), c) 1472 d), e), f) 5669.

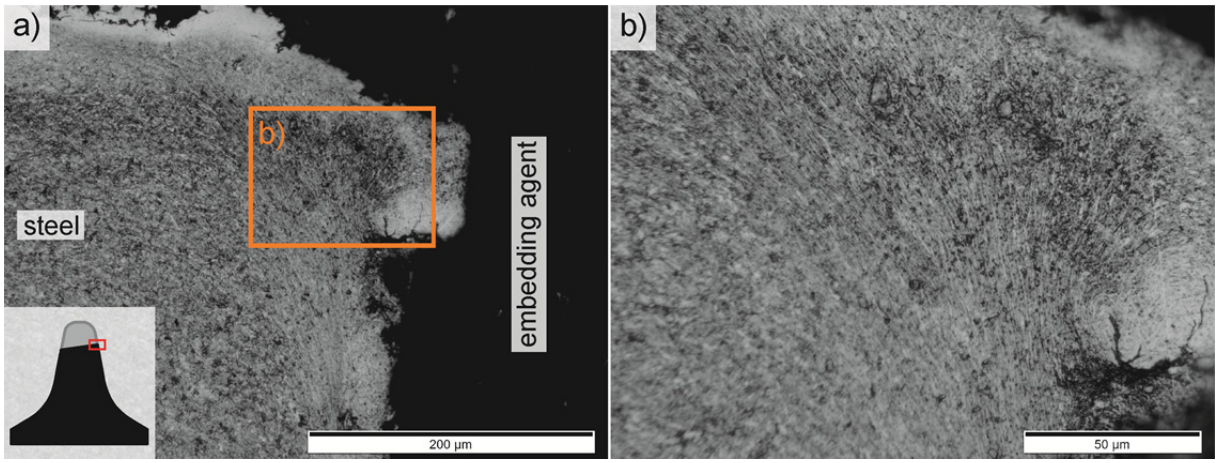

Fig. 69: TBM disc cutter 5837, showing the edge of a blocked cutter ring.

It could be observed that the cracks usually form directly below the impact head. In the vicinity of the cracks there is a change in the microstructure and the minerals are aligned. The cracks must therefore be preceded by a deformation in the steel, which is indicated by the structural change. It can also be clearly seen that even where the visible cracks end, the structure is already strongly deformed. Thus, further loading of the cutter ring during use increases the deformation, which promotes crack formation and allows the cracks to progress until a steel chip usually breaks off.

A third example in which crystallites are aligned is shown in Fig. 69. The wear type is blockage. For a better understanding, it should be mentioned that the sliding on the tunnel face caused by blocking resulted in material flow to the outside of the cutter ring. Thus, macroscopic deformation occurs that can be seen even without using a microscope. Such a situation is presented on Fig. 69. A massive deformation can also be seen under the microscope.

In contrast to cold forming in mushrooming, the grinding process on the tunnel face can be assumed to result in significantly higher temperatures of the cutter ring, possibly even up to annealing. As a result, hot deformation is more likely to occur with significantly less crack formation. The white etching areas (WEA) on Fig. 69 a) at the upper edge and the dark rim below are evidence of the extreme heating of the surface. A more detailed description of this effect is given in chapter 6.3.3.

6.3.2 Micro Penetration

This chapter illustrates different types of micro penetration. Micro-penetration is the penetration of rock and mineral particles into the steel. The basic idea here is that only minerals can indent the steel if they are harder than the crystallites of the steel.

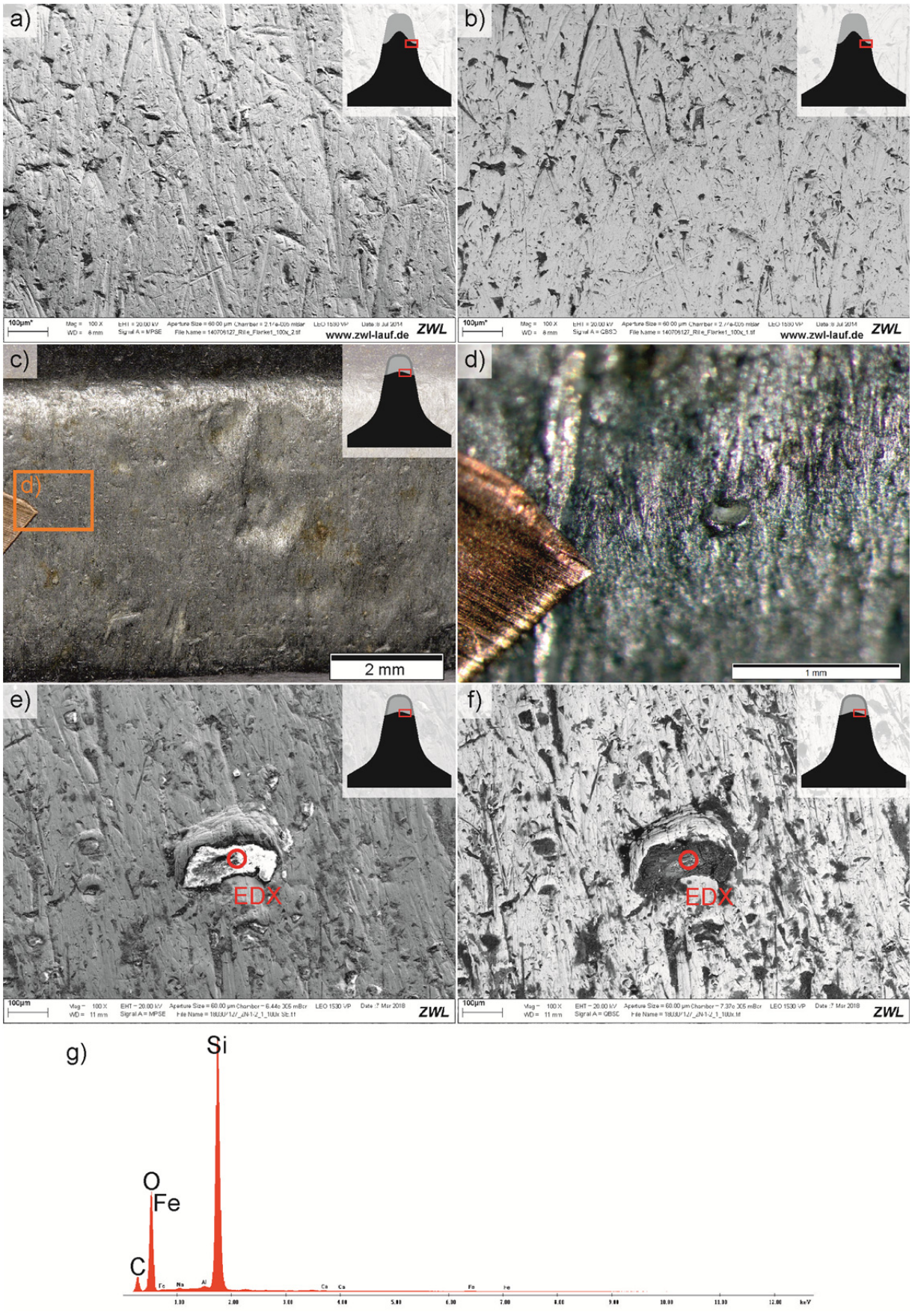

Fig. 70: Scratches and indentations into the cutter steel including an EDX analysis.
a), b) QS25-N8 c), d), e), f), g) ZN1.2.

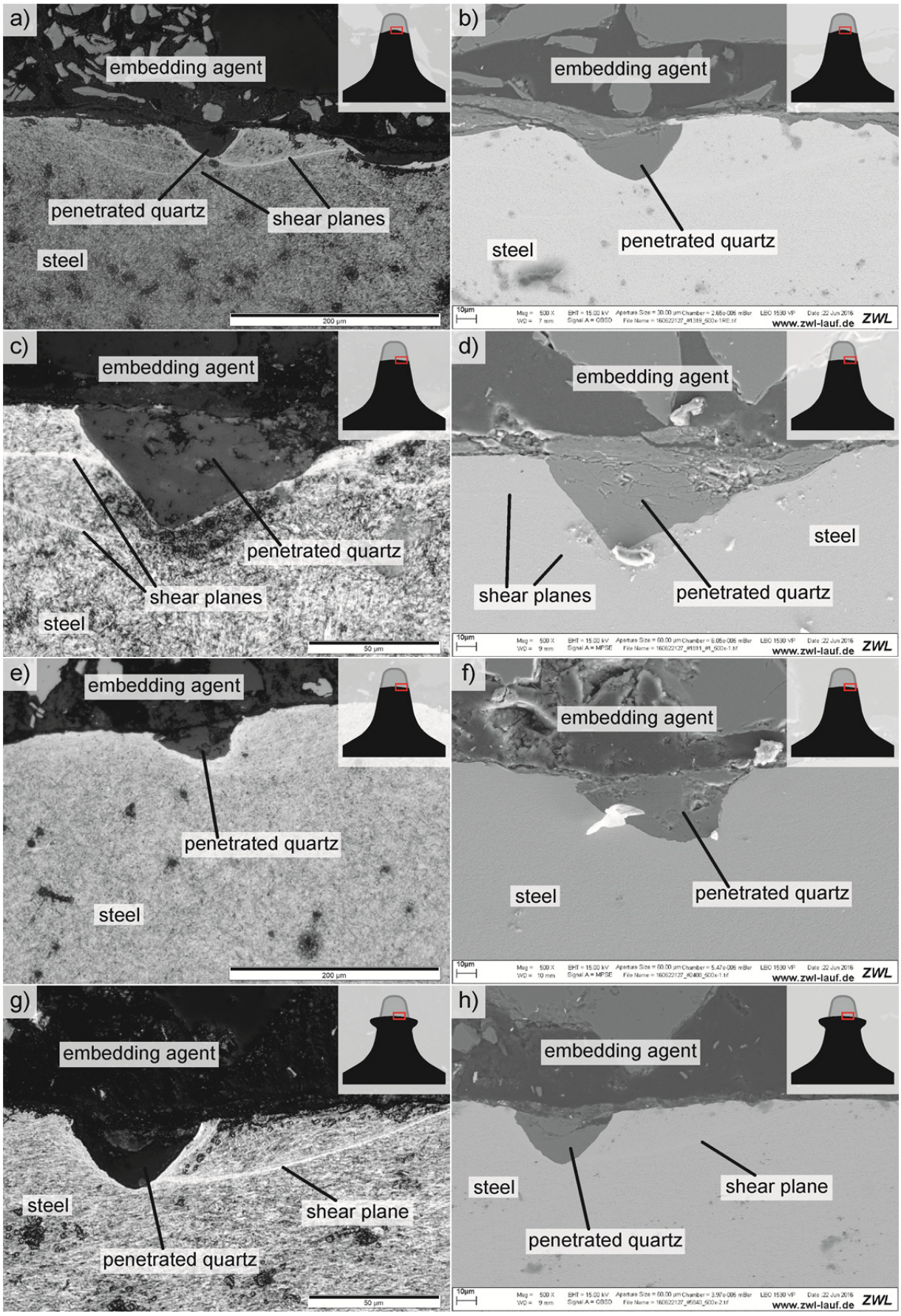

Fig. 71: Quartz grains penetrating the running surface of the cutter rings.
a), b) 1319 c), d) 1811 e), f) 2408 g) h) 5840.

Fig. 70 shows examples of typical micro penetration on cutter rings with tapering & grooving and abrasive wear with little tapering. The first two images (a) and b)) are SEM images of the running surface and show the same detail. While the left image uses secondary electron contrast (SE) to show the topography as accurately as possible, the right image uses the backscattered electron contrast (BSE) to show chemical and material differences.

With this backscattered electron contrast (BSE) method, heavy elements (like Fe) provide a strong backscatter, so that corresponding areas appear bright, such as steel. Areas with lighter elements (like C, O, Na, Mg, Al, Si), such as many minerals (quartz, feldspar, etc.) appear darker. So the dark areas are all rock particles that have indented into the steel. On both images, you can see many small and a few larger scratches due to micro-ploughing (PETRICA et al. 2013). In addition to the scratches, rock particles are also visible. These hard abrasive particles are located on the steel surface and even penetrated the softer steel surface.

Figures c) to f) show the same location of the running surface of a center cutter with normal/abrasive wear with little tapering. The two SEM-images (image e) and f)) show that there are many rock or mineral particles in the steel surface. One sliding direction dominates, namely from bottom to top. In the central area of both images there is a quartz grain, according to EDX analyses (image g)). This grain indented the steel with such force that massive deformations of the steel have occurred.

Fig. 71 shows microscopic cross sections of the running surface of cutter rings which show abrasive wear, sometimes with slight tapering, or mushrooming. All images show a quartz grain that has penetrated the steel up to max. 30 µm. The images on the left were taken by reflected light microscopy (RLM), the right images by scanning electron microscope (SEM).

The images on the left side show that the penetrated quartz has led to structural changes in the steel. Due to the low reflectivity of quartz (and also other rock forming minerals), the grain appears almost black on the left image (RLM). The steel was deformed by the emplacement of the quartz, which can be seen by the alignment of crystallites. In addition, the strong deformation leads to the formation of base-failure-like shear planes. The last excavated rock of the first three cutter rings was a mica-rich and strong gneiss (classification according to ISRM, 1978c).

The images on the right side show approximately the same section. EDX analyses could prove that it is always quartz that has penetrated the steel. The shear planes can also be seen on some SEM images. In addition, the SEM images show that on top of the penetrated quartz there is also a layer of rock material on the steel surface, i.e. the running surface of the cutter rings. This phenomenon is particularly evident in images b) and d).

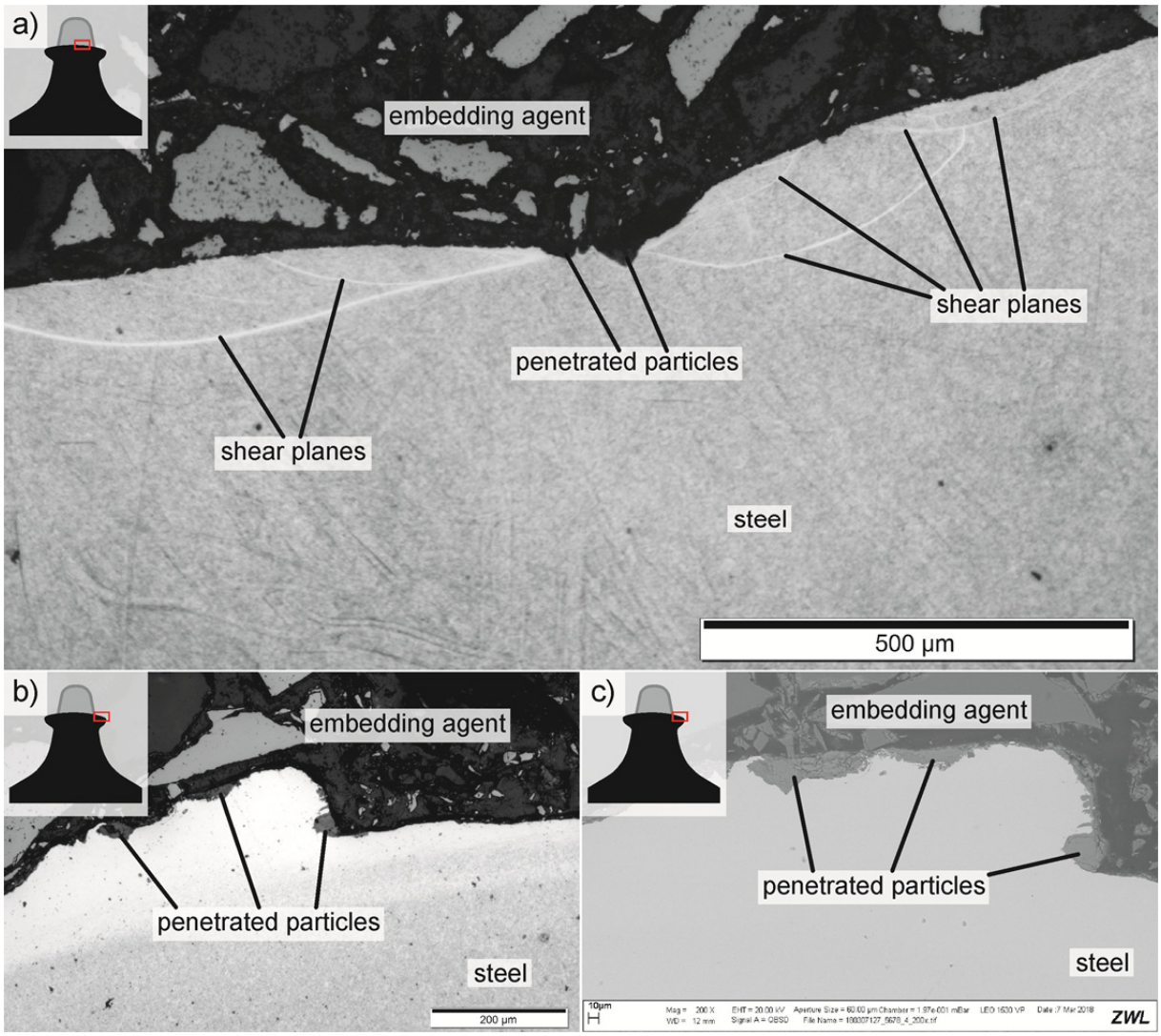

Fig. 72: Mineral particles penetrating the running surface of the cutter rings. a) 1688 b), c) 5678.

Fig. 72 points to image a) one mineral penetrating the running surface of a cutter ring with the wear type mushrooming. In contrast to the previous images, the shear planes in steel are much larger. They reach a length of over 1 mm and a depth of over 100 µm. Possible reasons for this can be the higher contact pressure forces, which lead to mushrooming.

Image b) and c) show nearly the same section. The macroscopic wear type is again mushrooming. Both images (a) RLM, b) SEM) show the formation of a steel spur into which rock particles have penetrated. The spur was probably formed by cold forging. Due to the high contact forces, minerals were able to penetrate. At the right end of the spur, the minerals were probably actively pressed in and additionally, due to the deformation of the steel, they were literally rolled in.

In addition, image b) shows that the area of the spur could be etched much worse and is therefore much brighter than the lower rest of the steel. This indicates a strong deformation in combination with strong heat development. It can clearly be seen that the outer right part of

the spur, which was presumably most deformed, appears brightest. Such white etching (WEA) areas are discussed in the next chapter.

The last three figures show that penetrating rock particles cause the most time a severe deformation in the steel. A precondition for penetrating minerals is a hardness contrast between the minerals of the rock and the steel. BESTE et al. (2008) coined the term “contact mixed layer” or “intermixed layer” for these types of indented rock particles. Since these particles also stuck in the surface of the cutter tool, there were reports of a “partial rock cover” (PETRICA et al. 2013). In addition to the hardness contrast of minerals and steel, MIRKOWSKA et al. (2016) reports about an additional reason for the formation of an “intermixed layer”. Referring thereto, the combination of frictional (lateral shear and frictional forces) and non-frictional contact (only normal force) between rock and cutter ring has a decisive influence. ELLECOSTA et al. (2018)

It was also found out that this phenomenon of mineral particles penetrating the steel is not a rarity: In the Koralm Tunnel project, this effect occurred in combination with quartz- and feldspar bearing rocks in the case of normal wear, mushrooming and tapering. However, very few authors report such effects. Besides BESTE et al. (2008), who has worked on tungsten carbide RÖTTGER et al. (2015) reports the possibility of penetrating particles, and PETRICA et al. (2013) also finds similar effects on cutter steel in laboratory experiments. ELLECOSTA et al. (2018)

6.3.3 White etching and side effects

Already in the previous chapters some images show white etching effects. These are areas in the microscopic cross sections of the steel that remain white without special treatment and are virtually not etched.

Images of cutter rings with a large-scale white etching effect are shown in Fig. 73. The two uppers (a) and b)) show such an effect with a thickness of over 0.6 mm. The corresponding cutter ring shows the wear type blockage. Image a) points at a metal chip formed by sliding over the tunnel face. The chip itself is even macroscopically visible. The massive deformation can also be seen under the microscope. The sliding on the tunnel face causes very high temperatures of the cutter ring, possibly even up to annealing. As a result, hot deformation occurs with typically very little crack formation. The white etching areas (WEA) on image a) and b) at the upper edge and the dark rim below are evidence of the extreme heating of the surface. The white area represents a new hardness zone, which can be described as white grinding burn.

The black edge below the white etching area shows that a mineral reaction or a structural change has occurred. Image c) provides a detailed view of the microstructure. The isotropic structure with needle-like, martensite crystals up to 50 µm in size is clearly visible. This means that the crystallites now have about 5 to 10 times the size of the original structure. The

microstructure has therefore changed to the extent that there has been a real tempering of the steel with crystal growth in this area.

Image d) points out another image of a blocked disc cutter and its edge. Here too, a steel chip has formed as a result of the hot forming and sliding process. The image illustrates particularly well that the entire outer area of the cutter ring has a white etching area, i.e. a re-hardening zone.

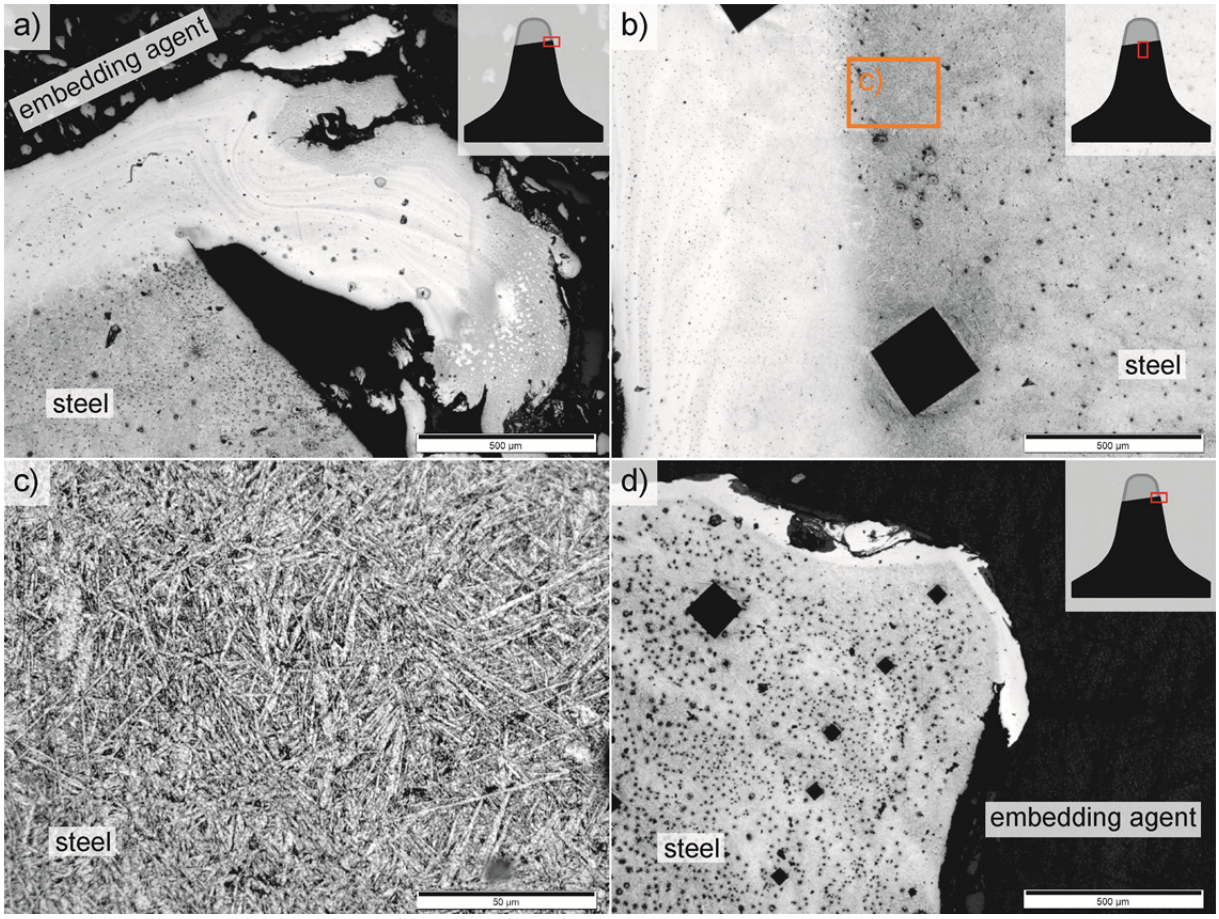

Fig. 73: TBM disc cutters showing the wear type blockage with new hardening zones and mineral growth. a), b), c) 586 d) QS25-N7.

Fig. 74 points at a set of images with a white layer on the cutter tip. The types of wear are abrasive wear with light tapering and tapering with grooving. The white etching area on the images reaches a thickness of a few µm up to about 10 to 15 µm. In contrast to the previous images, the white layer usually has a very sharp border to the underlying, almost unchanged structure.

In the images b), e) and f) the uneven surface of the steel is noticeable. In some cases, cracks parallel to the surface are also visible, which can apparently lead to the detachment of thin layers of steel by rolling over them again during operation. The detachment of thin steel layers is probably related to the fact that the white areas have undergone re-hardening, which

leads to high tensile stresses within this layer. Under dynamic loading, such as the mining process by rolling over the tunnel face, these tensile stresses lead to microcracks which continue to grow and result in increased material loss in the form of detachment of small steel layers.

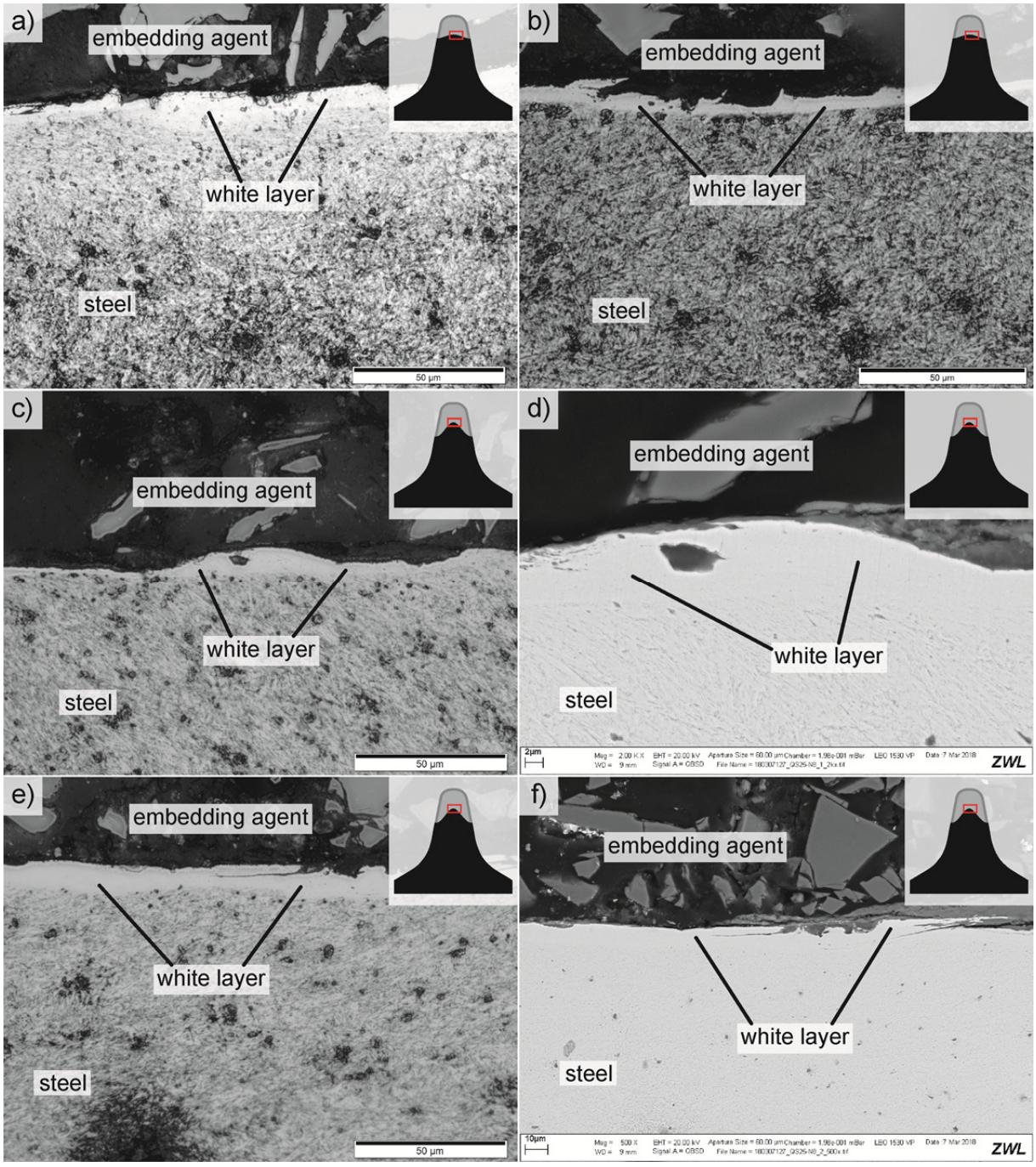

Fig. 74: TBM disc cutters showing a white etching effect. a), b) 1319 c), d), e), f) QS25-N8.

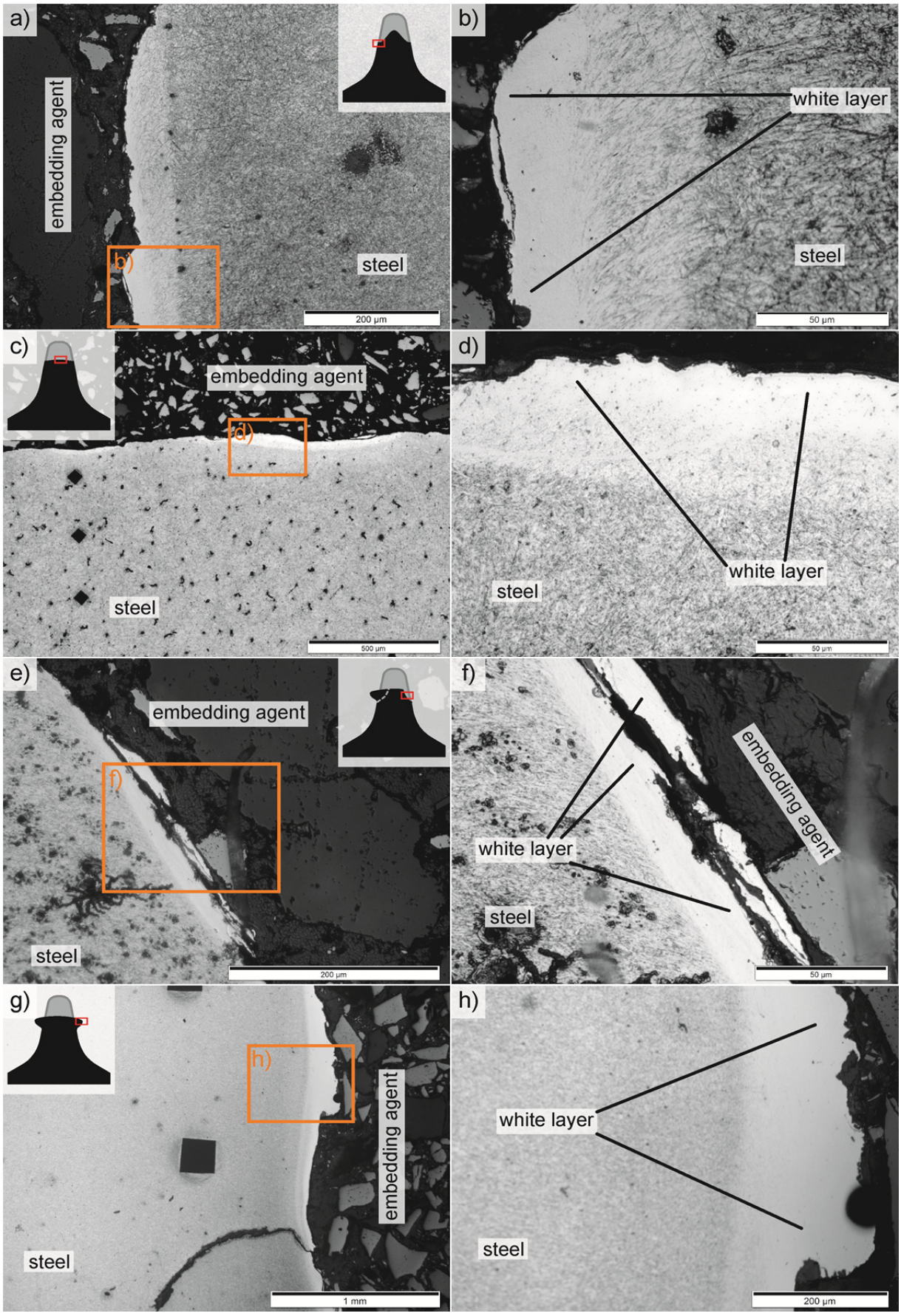

Fig. 75: TBM disc cutters showing a white etching effect. a), b) 573 c), d) 2408 e), f) 901 g) h) 5678.

Fig. 75 points at 4 further examples with a white layer. The right image represents an enlargement in each case. The first example shows a cutter ring with mainly tapering and grooving. On its lateral flank a white layer with a thickness of about 50 to 70 µm also appeared. The magnification on the right side clearly points at an alignment of the microstructure in the direction of the base body as well as a steel chip that has already been detached. This means that even below the running surface of the cutter ring, at least in places, there is a strong heating of the surface, which can also lead to increased material removal.

Image c) and d) show a cutter ring with abrasive wear. A white etching area can only be seen in some places and has a thickness of about 50 µm. Image e) and f) show a cutter ring with mushrooming and chipping. A steel chip has already broken off at the point where the image was taken. As the steel chip was probably broken off, several new rollover processes of the cutter occurred and the resulting channel was used by the rock material from the crushed zone for transport, this led to a visible structural change and heating. The crystallites show an alignment to the outside. In addition, it can be seen that a layer of steel of about 10 µm thickness has already detached itself.

The last two images show a cutter ring with mushrooming and chipping. The photos are taken from the far end of the impact head. A white layer with a thickness of about 200 µm is visible. The surface of the steel towards the outside is very uneven and frayed, which indicates that steel particles have been detached. In the lower part of image g) it can also be seen that a larger crack has formed from there.

With the presented images it could be shown that every macroscopic wear type can show white etching areas. This bright and structureless deformation layer is located the most time on the former contact area between the cutter ring and the rock mass. This layer was extremely deformed and heated up during use. This process is comparable to overheating that occurs during grinding (grinding burn), respectively the formation of a white etching area. ELLECOSTA et al. (2018)

A grinding burn is therefore a thermal damage caused by excessive heat input, usually by grinding processes. This process is similar to a hardening of the material. Due to the excessive heat input, grinding burn zones form in the edge structure which, as already mentioned, have high tensile stresses (SOMMER et al. 2014: 224). These can lead to cracks and failure or increased material removal.

The white areas normally consist of ultra fine, nano-recrystallized, carbide-free ferrite or ferrite with a very fine distribution of carbide particles and are around 10 to 50 % harder than the unaffected microstructure.

An accumulation of this effect was found with macroscopic normal wear and tapering. Excavated rock types in the analyzed project were mica-rich gneisses which typically had low to medium abrasive values, but are classified as strong (classification according to

ISRM, 1978c), with a medium uniaxial compressive strength of 60 to 80 MPa. ELLECOSTA et al. (2018)

However, it must be assumed that the accumulation occurs maybe because the white layer is removed relatively quickly after its formation due to the high abrasiveness and significantly higher steel wear in the case of mushrooming, for example.

In the case of very extensive white etching areas with a strong, sustained heat input under a normal atmosphere with oxygen, overlapping with the effect of decarburization may also occur. As a result, ferrite accumulates and the amount of carbides is reduced.

6.3.4 Special effects

This chapter addresses problems that are partly based on the effects already explained and/or are a combination of several of them. Fig. 76 points at exemplary images of cutter rings with mushrooming and a kind of steel flaking.

The upper two images (a) and b)) show the same location. Here it becomes clear that these are again white etching areas (WEA), which show a special delamination of the steel. The WEA has a thickness of about 200 µm. In it and just below it, the microstructure shows an adjustment of the crystallites towards the outside. The SEM-image on the right illustrates that rock particles have been pushed between the detached steel layers.

Figures c) to f) show a slightly different situation. Here, some steel layers have also been detached from the cutter ring, but only the spaces between them show a white etching effect. The individual steel layers show a horizontal alignment of the crystallites, as does the steel below. The typical isotropic structure begins much deeper in the steel. The two lower SEM images including EDX analyses show that the material between the steel layers also consists of the same steel and that no rock particles have been intruded here.

The formation of such structures can probably be explained by the rolling over of very hard and solid rock or metallic parts of the cutter head. The internal tensile stresses probably also play a major role in white etching effects. In the second example, the crack shown in figure c) probably contributes to this effect. Due to the constant rolling over, the steel layers, which have already been partially detached, repeatedly strike against each other, thus forming the intermediate and light steel areas.

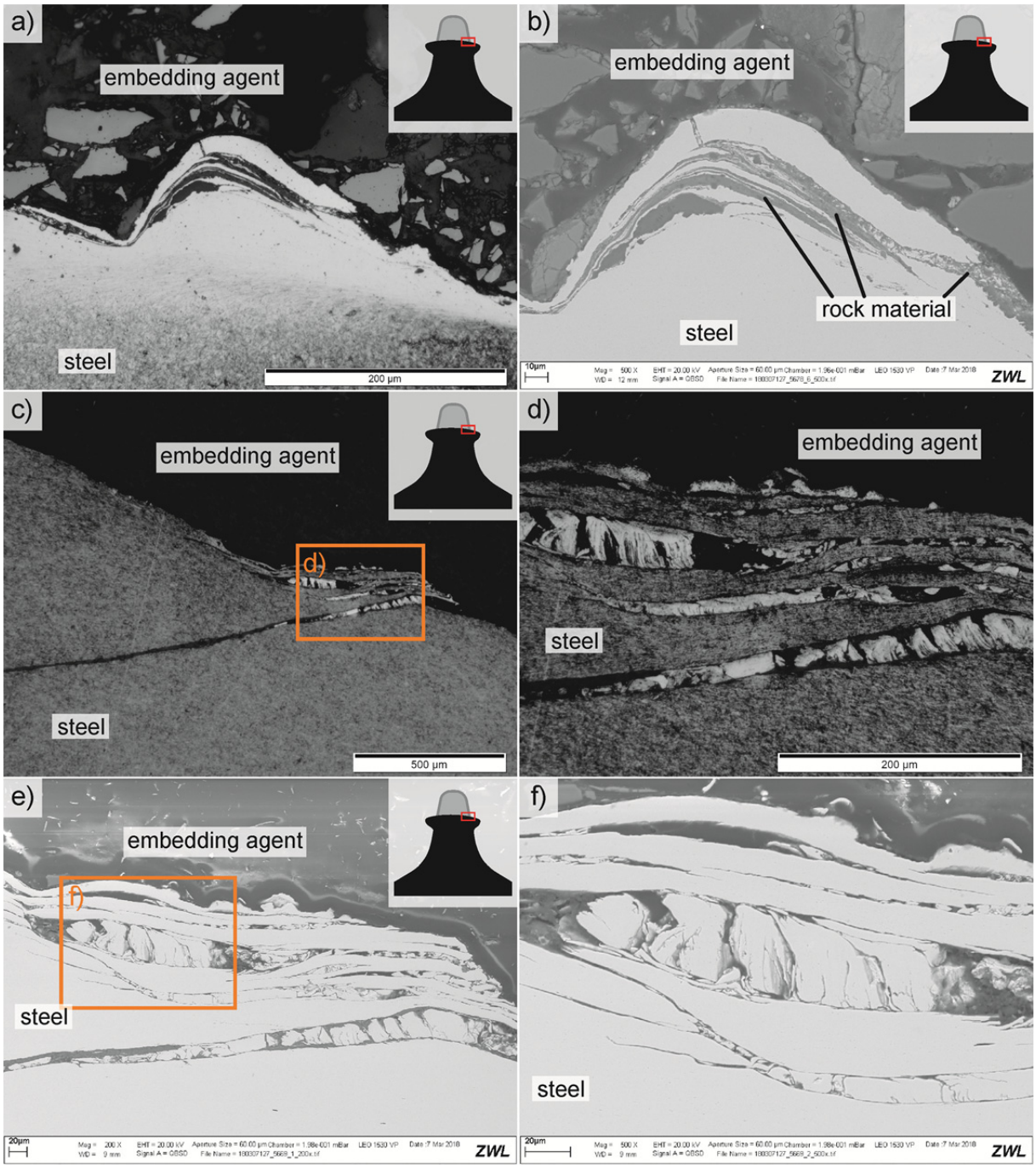

Fig. 76: TBM disc cutters showing the effect of flaking on the running surface and the penetration of rock particles into the resulting gaps. a), b) 5669 c), d), e), f) 5678.

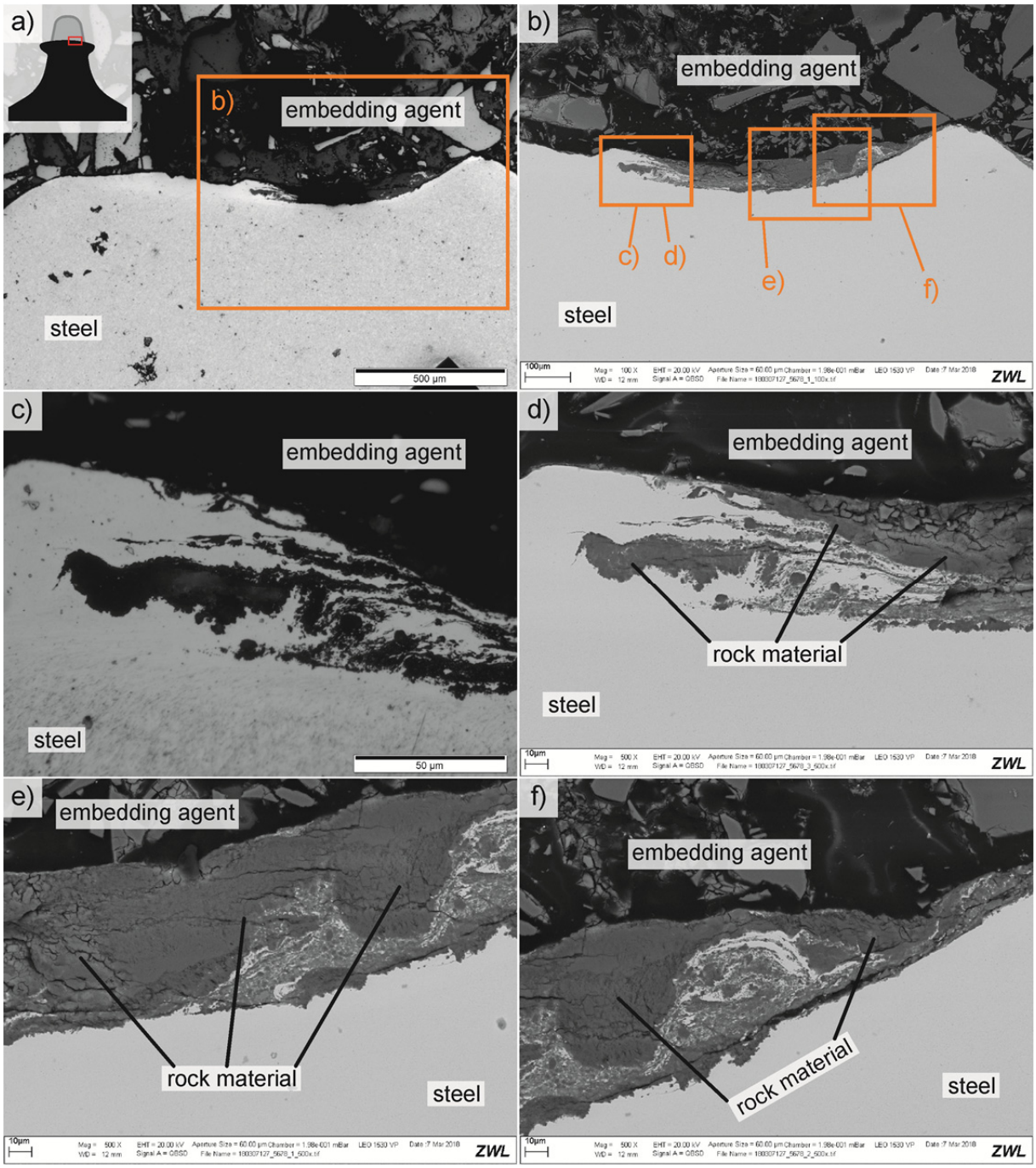

Fig. 77: Cutter ring 5678 showing the mixing of steel and rock particles on the surface of the cutter ring.

Fig. 77 points out a different situation. It is a cutter ring with mushrooming and chipping. The images show a point on the running surface. The images show a point on the running surface where a slight crescent-like groove and the formation of a steel chip and a white etching area has occurred. The white etching area mainly concerns the steel chip. The chip shows a deformation towards the right edge of the image and has probably rolled in rock particles due to its deformation. The SEM images also show that there are many rock particles in the back,

i.e. on the right side of the chip. In some cases, the steel has become very strongly mixed with the minerals, so that one can definitely speak of an "intermixed layer".

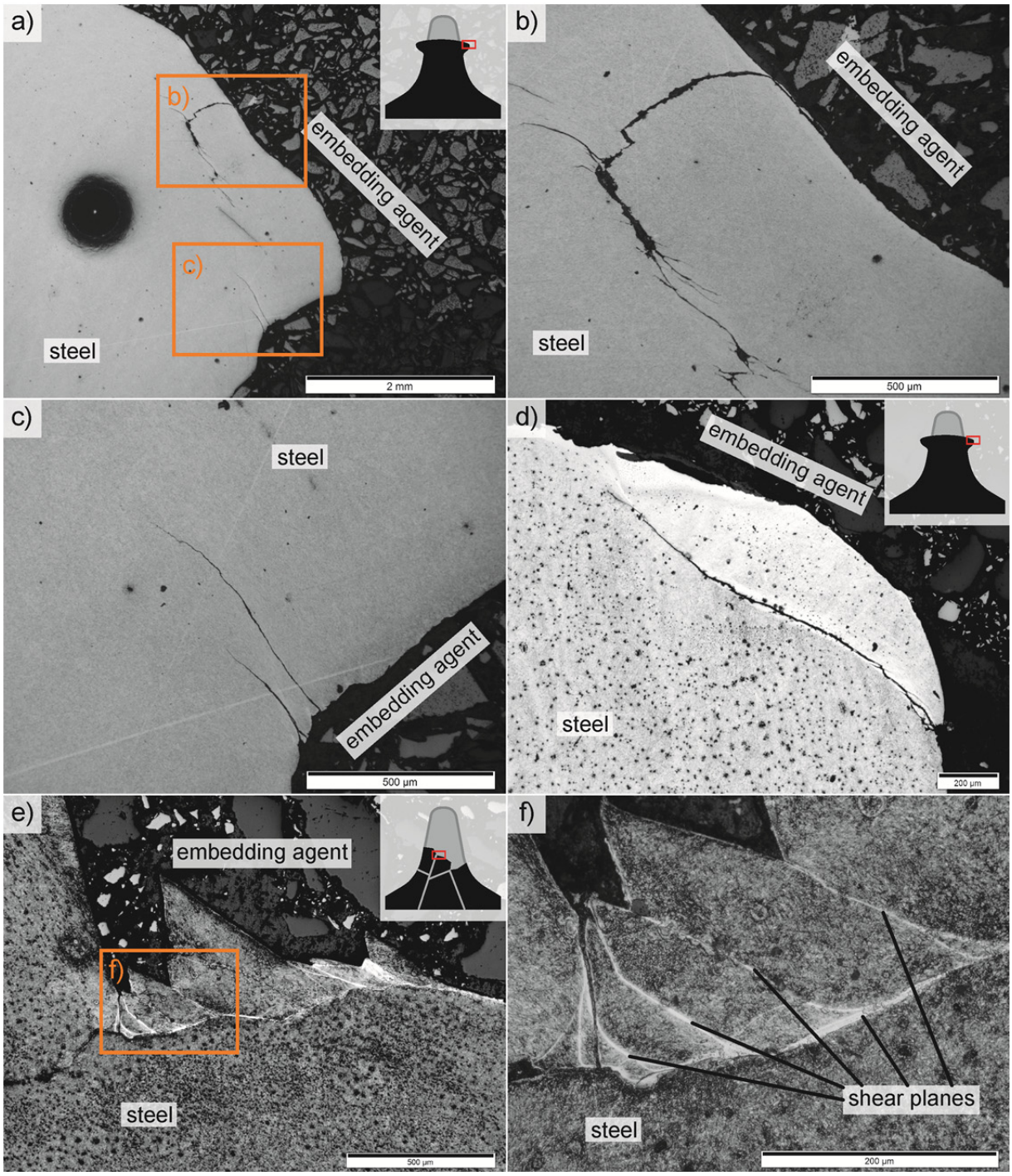

Fig. 78: Cutter rings showing cracks in the steel. a), b), c), 6483 d) QS25-N7 e), f) QS25-N9.

Fig. 78 is dedicated to the subject of cracks that occur both in cutter rings with macroscopic mushrooming, partly with chipping, and in brittle fracture. The first four images show the outermost edge of the impact head with corresponding crack formation. The massive deformation of the steel, caused by extreme contact pressures, leads to embrittlement in the

steel. The images show that the cracks developed slightly below and above the outer edge. Due to the continuous mining process with constant rotation and dynamic loading of the cutter, the cracks continue to grow until they join together and a piece several millimeters in size breaks off.

Figure d) points at a very similar situation, except that, in contrast to the first example, the cracks only start from a point below the outer edge. In addition, the image also shows a white etching area in the region of the chip and the direct contact area with the rock.

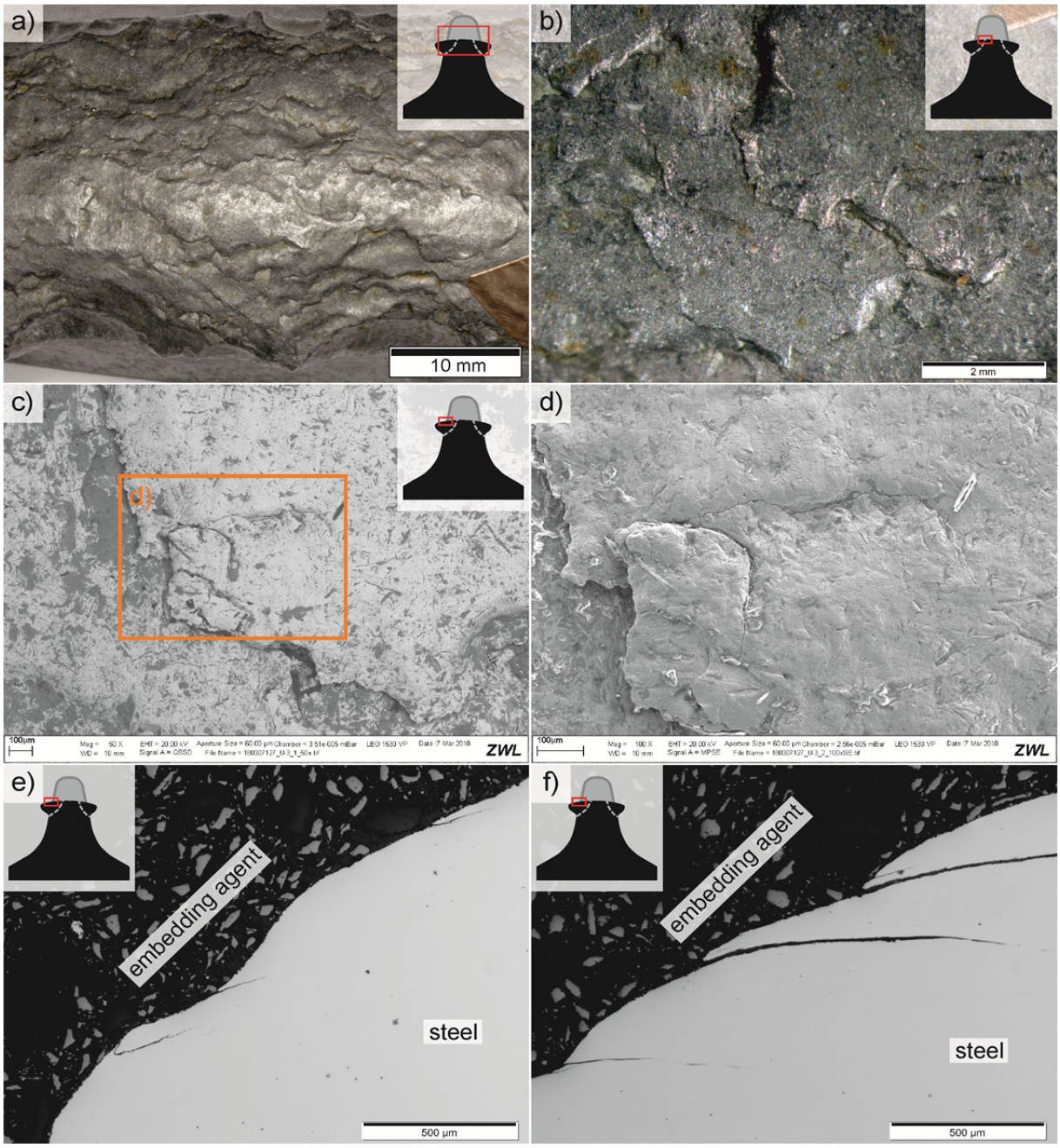

Fig. 79: Cutter ring that was recently exposed to an eclogite layer showing a flaky detachment of the surface. a), b), c), d) U3 e), f) U2.

The two images below (Fig. 78: e), f)) show a cutter ring which has fractured brittle. It can be seen that this did not result in a single fracture, but many small cracks occurred within the cutter ring. As already shown in previous images, deformations often do not occur homogeneously but along shear planes, which are visible by a structural change. The crystallites are aligned along the shear planes and the coloration is significantly lighter. The movement along these paths leads to hardening and embrittlement as well as to the effect of heating.

Fig. 79 points at images of two cutter rings with mushrooming and chipping, which last ran on an eclogite layer. The first two images show an optical image of the cutter tip. It can already be seen here that, in addition to chipping, there is a shell-like detachment of the steel on the running surface. The SEM images illustrate this once again. In addition, image c) shows that there are many minerals on or better in the surface of the steel (dark grey areas). They form a contact mixed layer again.

The two lower images show the same situation in metallographic cross sections. It is clear that the cracks are growing from the outside to the inside. Repeated rolling of the cutter due to the mining process causes the cracks to grow larger and larger until finally steel chips are broken off.

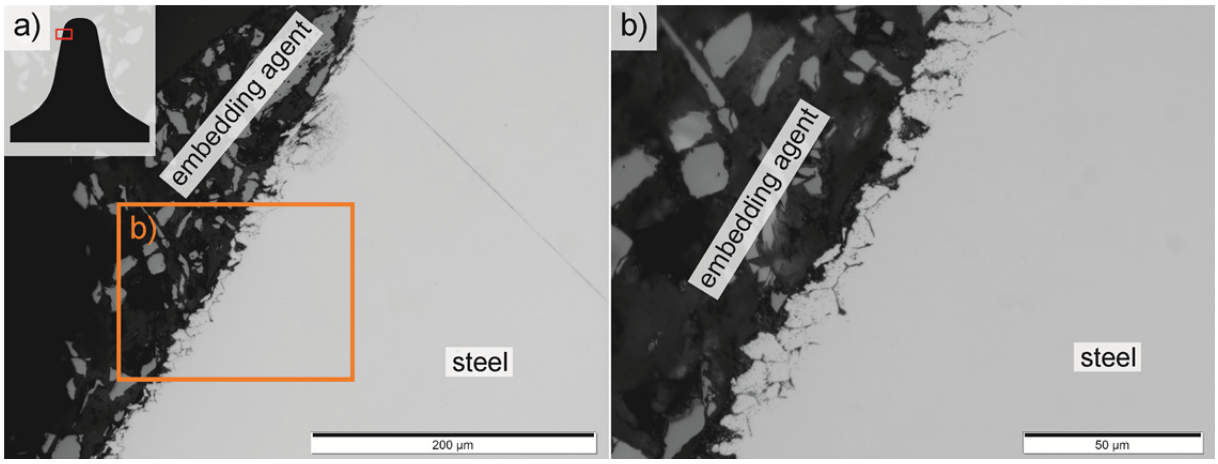

Fig. 80: A near mint and unused cutter ring 155 showing the effect of surface oxidation along grain boundaries in a polished and unetched metallographic cross-section.

Fig. 80 points at a merely polished metallographic cross section from an almost unused cutter ring. The images were taken in the upper part of the left flank and show a relatively rough or uneven surface. On the right image the grain boundaries can be seen at edge of the cutter ring. This indicates edge oxidation along the grain boundaries with a depth of around 20 µm, an effect that can occur during heat treatment.

Surface oxidation (grain boundary oxidation) is the enrichment of metal oxides of the alloying elements Cr, Mn, Si, Ti and V at the grain boundaries of the edge layer of a workpiece. This normally occurs as a result of heat treatment in an atmosphere with a high oxygen supply (or

oxygen partial pressure). The alloying elements set as oxides can no longer influence the transformation behavior during hardening in the surface layer, i.e. hardenability is reduced. As a result, the surface layer changes more easily and on cooling the austenite changes into pearlite and/or bainite instead of martensite. (WIRTSCHAFTSVEREINIGUNG STAHL 2008: 23)

The surface and edge hardness is therefore normally lower. So a kind of soft skin has formed. If this is not ground off, a lower wear resistance must first be expected. Due to the low thickness of about 20 µm, it can be assumed that this layer is ground down relatively quickly during operation and that increased wear occurs only initially. (WIRTSCHAFTSVEREINIGUNG STAHL 2008: 23)

6.4 Hardness testing

The fourth part of the results chapter is dedicated to the hardness tests, which presents the results of the Knoop, Vickers and Rockwell hardness tests. The individual chapters are divided into the results of the analysis of the cutter rings, the CERCHAR pins and the LCPC impellers. This is followed by a hardness analysis of rocks and minerals and a hardness comparison in the last chapter.

For reasons of practicability and comparability, the diagrams shown in the following use kilograms (kg) or grams (g) as the test load, since the test load is still set as the unit “kgf” today and is only converted to the unit “N” later. It should also be mentioned that most of the diagrams shown were created from a large number of individual hardness values and each data point in the diagram usually represents an average value.

The results of the modified Vickers hardness, described in chapter 5.4, are not part of this thesis. The reasons for this are that it is a completely independent test method, which is not standardized and can only be carried out on special equipment. Due to the high brittleness of minerals and rocks, there are many problems with conventional hardness testing and its evaluation. This method represents a further development, as the depth of the indentations is measured, thus providing more objective and reproducible results. All relevant data can be found in FISCHER (2015).

6.4.1 TBM disc cutter

Microhardness and low-force hardness

The term microhardness and low-force hardness refers to low and very low test loads of less than 0.2 and 5 kg respectively (compare chapter 5.3.3 and Tab. 19). Hardness tests with such low loads can be performed according to Knoop or Vickers. Fig. 81 points at two examined cutter rings with tapering and grooving (cutter 520) and abrasive wear with tapering (cutter 1786). The hardness tests took place approximately in the middle area of the cross section. At least 12 individual hardness tests were performed per data point.

A very evident effect can be seen when comparing hardness values and test loads (Fig. 81). The hardness increases with decreasing test load and with increasing load, the hardness seems to approach a value asymptotically. In literature, this effect is known as the indentation size effect. ONDRACEK (1995: 187) gives an explanation: With Knoop and Vickers hardness tests, only the plastic deformation of the material is measured. When using low testing loads, the elastic part of the deformation is high and you normally get small indentations or a high hardness. With an increasing load, the plastic part of the deformation grows while the elastic parts decreases. This occurs with the rising test load until a material-specific limit is reached, where the ratio stays constant (ELLECOSTA et al. 2015).

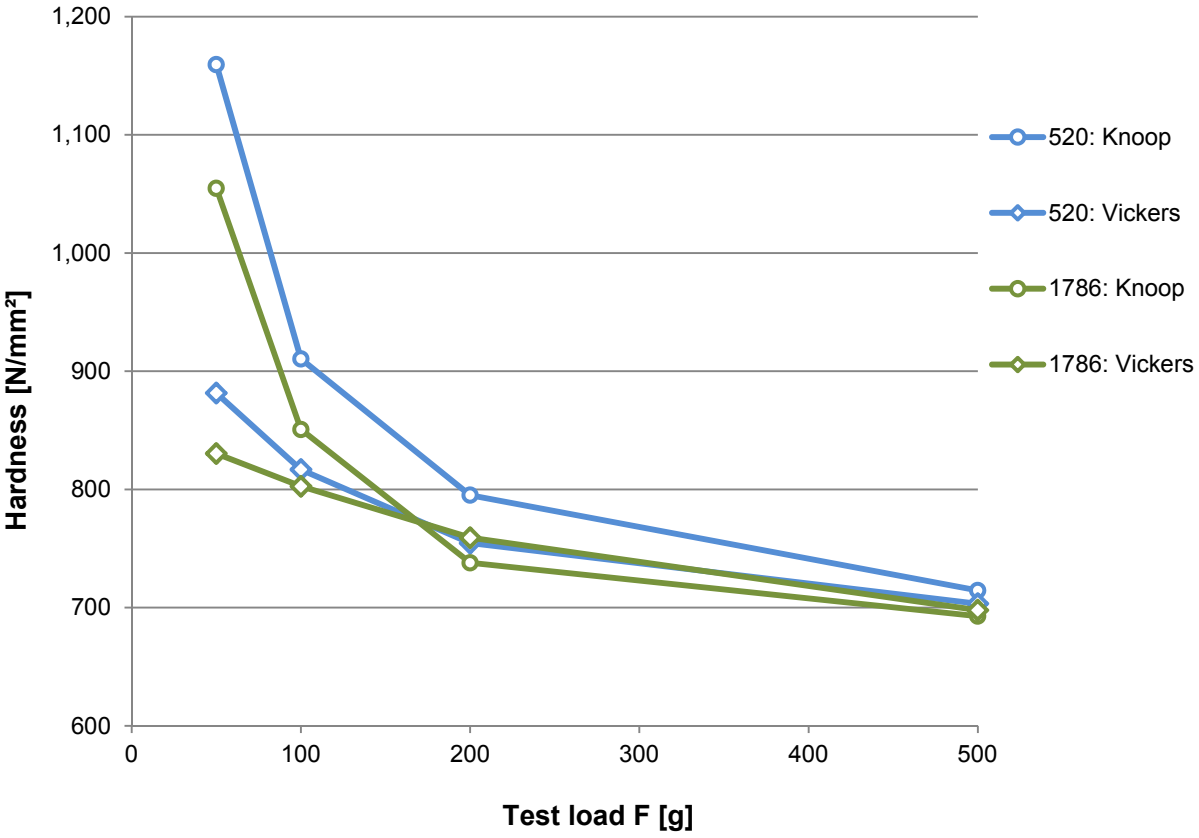

Fig. 81: Results of micro- and low-force hardness tests after Knoop and Vickers on two different TBM disc cutters. The data points represent the average value of several measurements.

When comparing the Knoop and Vickers hardness, it is noticeable that the indentation size effect is particularly strong when using the Knoop method. The difference between the two hardness values is maximum at the lowest load. The higher the test load, the closer the two hardness values are to each other. This is most likely due to the different shape of the indenter where the Vickers indenter gives more constant results.

Additionally, it can clearly be seen that the cutter ring 520 is somewhat harder than 1786 and that different cutter rings also have different degrees of hardness apart from their different microstructure (chapter 4.4.1).

Hardness mapping & hardness profiles

Fig. 81 already showed that the examined cutter rings have a high hardness. For further investigations of the cutter ring hardness, the Rockwell-C (HRC) method was often used. The Vickers hardness testing method, which is considerably more time-consuming, is still possible. To determine reliable Vickers values, the test load was set to ≥ HV30.

For a better optical illustration of the hardness distribution within the cutter ring, a kind of mapping was used and similarly hard areas were combined in one area. The data for this was developed in close cooperation with PAHNKE (2016).

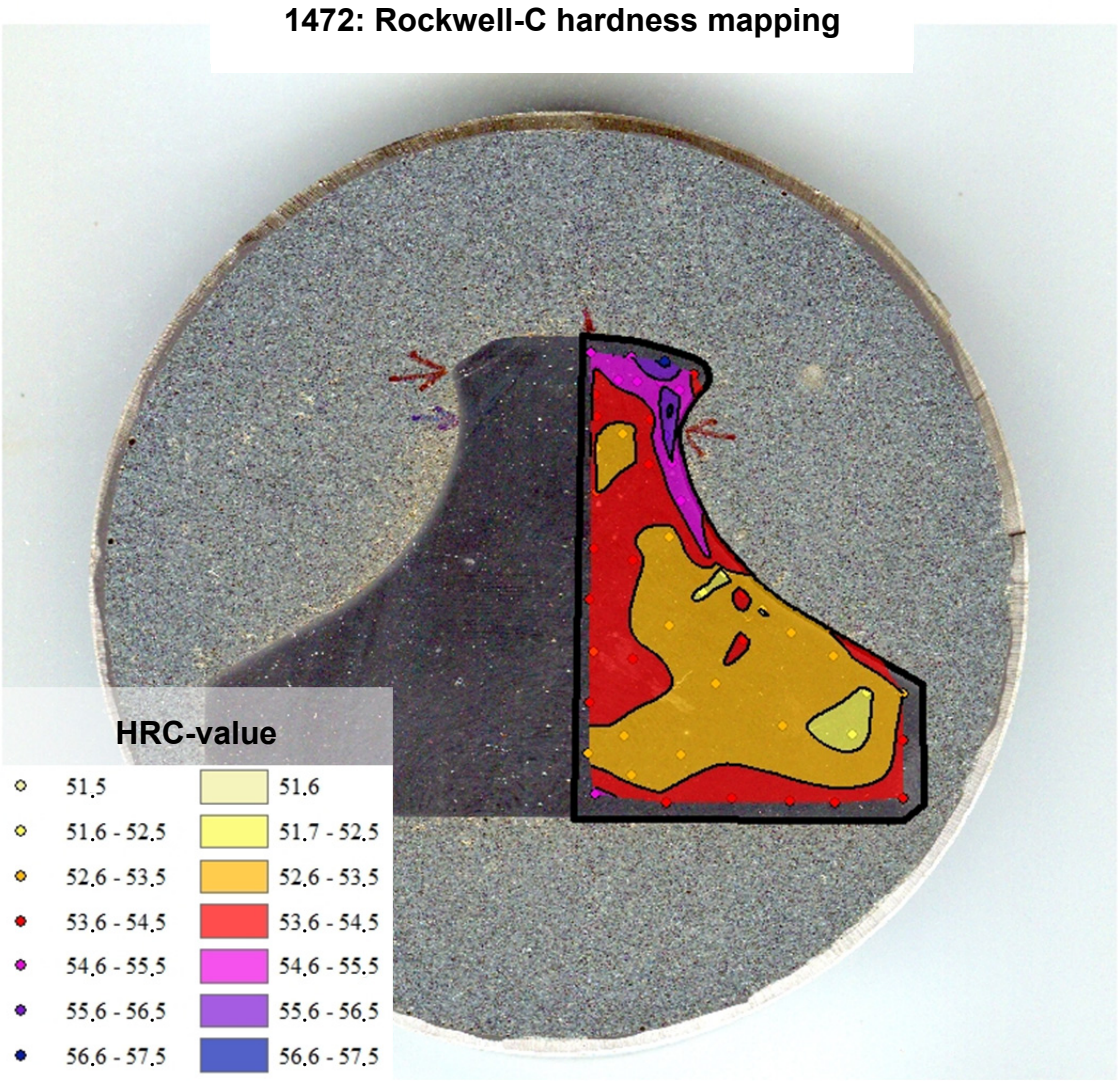

Fig. 82: HRC hardness mapping on the cutter ring 1472 with mushrooming. Measured points are highlighted. The width of the cutter ring is about 8 cm (modified after PAHNKE 2016).

Fig. 82 illustrates such a hardness mapping of the cutter ring 1472 with mushrooming. It can be clearly seen that the hardest areas are located in the zone of contact with the rock, i.e. the cutter tip and the zone of highest deformation (formation of the impact head). In these areas,

the HRC values reach up to 57 HRC and are sometimes about 9 % above the areas with the lowest hardness with 52 HRC. Based on the hardness distribution, it can be assumed that the areas with a hardness of more than 54.5 HRC were caused by rock excavation or wear.

Fig. 83 points at a related hardness profile diagram, starting from the cutter tip of cutter 1472 down towards the base body. This data is based on Vickers tests with test loads of 30 kg (HV30) and 125 kg (HV125). In addition to the hardness mapping on Fig. 82, both curves clearly show that the highest hardness is in the area of the cutter tip or the highest deformation and also the former contact area with the rock. In the area of the cutter tip, Vickers hardness values of up to about 680 N/mm² are achieved, while the inner area indicates an average Vickers hardness of 630 N/mm².

Thus, in addition to the structural change caused by the formation of the impact head (chapter 6.3), the already suspected hardening could also be proven. Hardening is always accompanied by embrittlement of the cutter ring, which leads to increased material removal as the mining process progresses. This can also be referred to as a kind of material fatigue.

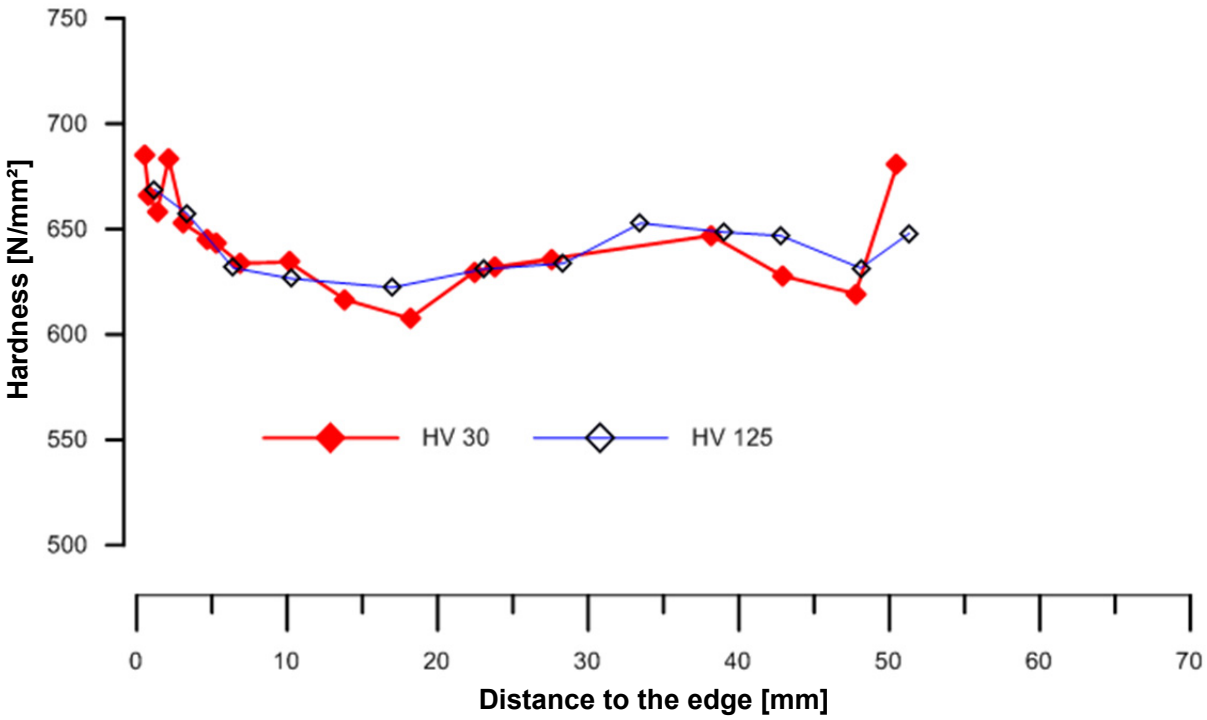

Fig. 83: Result of a hardness curve of cutter ring 1472 with mushrooming, starting from the cutter tip down towards the base body. Each data point represents a single measured value (modified after PAHNKE 2016).

Fig. 84 illustrates a hardness mapping of the cutter ring 1650 with brittle fracture. It is obvious that the wider and "lower" part of the cutter ring has a lower hardness than the thinner and "upper" part. The highest hardness values are located on the former contact area with the rock, i.e. the cutter tip with up to 58 HRC. The lower part has hardness values of around 55 HRC. The difference between the hardest area on the cutter tip and the mean

hardness in the lower part is about 3 HRC (approximately 5 %). According to the hardness distribution, it can be assumed that the different hardness was caused by the manufacturer's heat treatment.

The hardness curve diagram in Fig. 85 confirms this first impression. In the cutter tip area, Vickers hardness values of up to about 710 N/mm² are even measured. In the lower sections, the Vickers hardness averages around 630 N/mm² again. Thus the Vickers hardness tests of cutter 1650 show a much greater difference in hardness between the cutter tip and the lower, wide area of the cutter ring compared to cutter 1472.

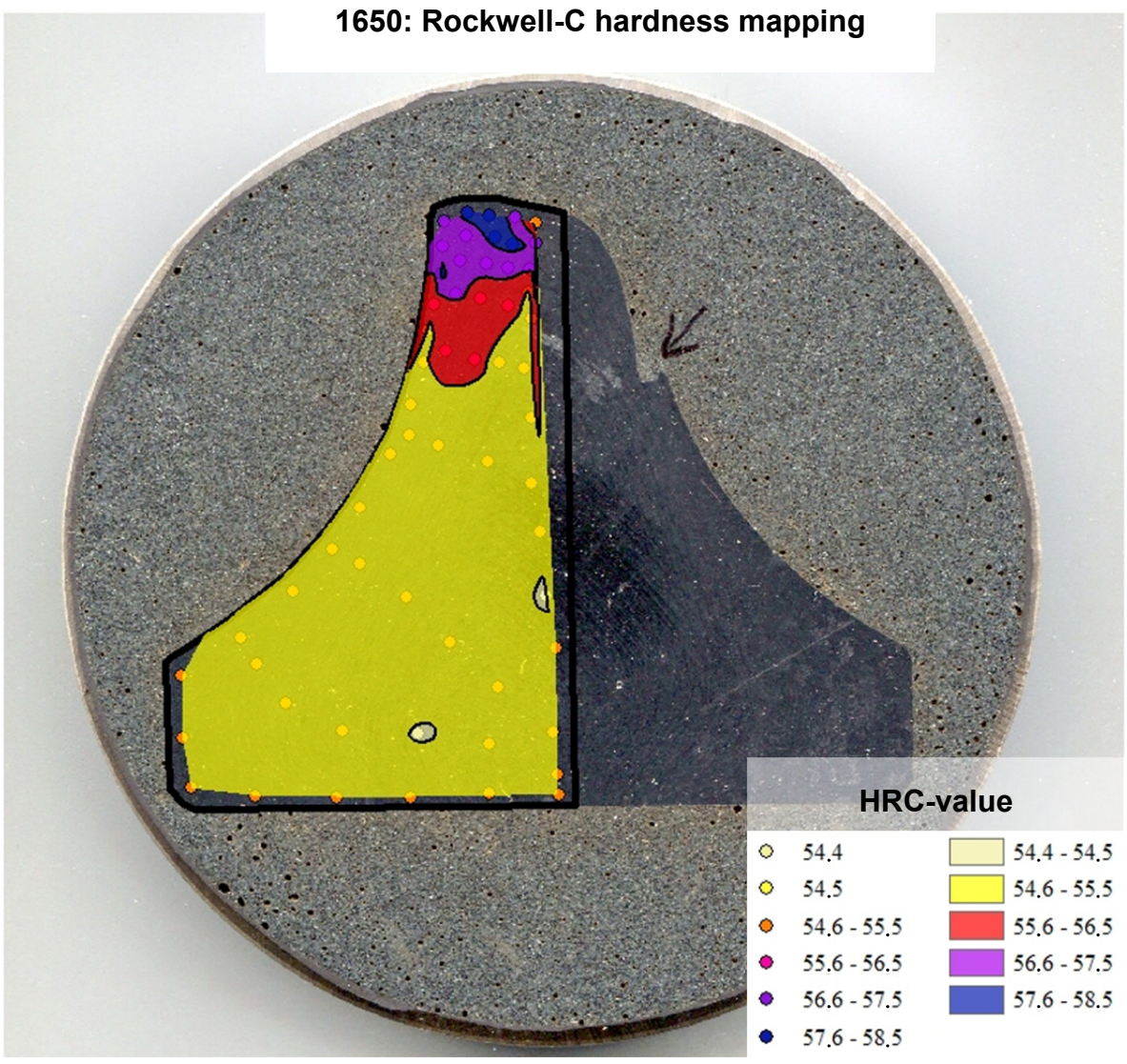

Fig. 84: HRC hardness mapping on the cutter ring 1650 with brittle fracture. Measured points are highlighted. The width of the cutter ring is about 8 cm (modified after PAHNKE 2016).

As the hardness correlates with the toughness of the material in this case as well, it must be assumed that the area of the cutter tip of cutter 1650 is significantly more brittle and more

susceptible to brittle fracture. The most recently excavated rock was a gneiss with a very strong uniaxial compressive strength (UCS) (approximately between 130 and 180 MPa) and distinct joints at intervals of 1 to 2 meters.

For effective rock cutting/excavation, high contact pressures on the cutters (high cutter thrust) are necessary. Joints in the rock lead to an uneven tunnel face which gives the cutters many individual hard shocks. If the toughness of the cutter ring is too low, brittle fractures can occur.

Thus the reason for the failure of the cutter ring 1650 can probably also be traced back to a heat treatment not adapted to the rock conditions.

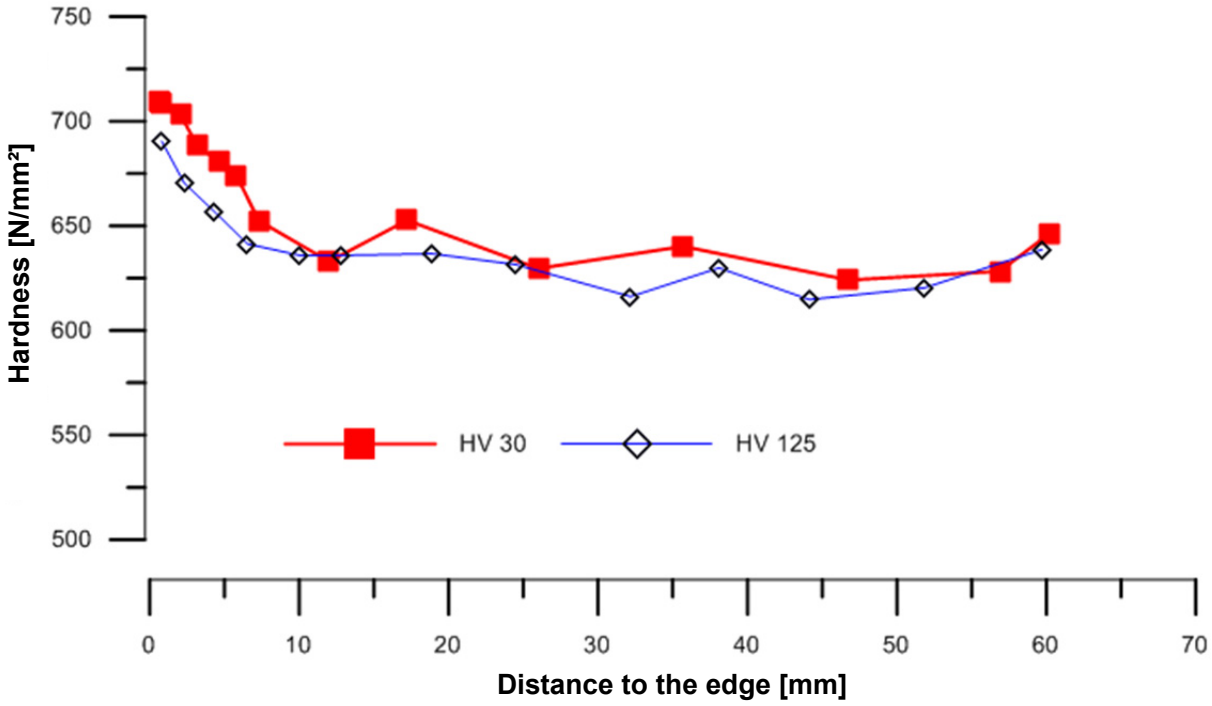

Fig. 85: Result of a hardness curve of cutter ring 1650 with brittle fracture, starting from the cutter tip down towards the base body. Each data point represents a single measured value (modified after PAHNKE 2016).

Fig. 86 illustrates a hardness mapping of the cutter ring 573. This cutter has a combined wear shape of abrasive wear, tapering and grooving. When looking at the hardness mapping, it is noticeable that the hardness is usually distributed quite uniformly, but that in the area of the cutter tip, i.e. the former contact area with the rock, a rather thin hardening zone has formed.

In the cutter tip area, Rockwell C hardness values of just over 58 are achieved. The largest area of the cutter ring has a hardness of mostly about 55 HRC with minimum values of about 53 HRC. This means that the hardest area of the cutter tip is about 3 HRC (approx. 5 %) above the average value and about 5 HRC (approx. 9 %) above the minimum value. A Vickers hardness curve diagram was not created.

The microstructural analysis could show that a white etching area has formed on this cutter ring in the contact area to the rock. The visible structural change has not exceeded a thickness of about 0.2 mm. Nevertheless, the hardness tests were able to show that the changes in the steel are significantly deeper, sometimes by several millimeters.

Whether the hardening of the steel close to the surface also provides wear protection cannot be answered, however. At first glance, a higher hardness offers increased wear resistance, but it also leads to embrittlement, which can increase micro-wear.

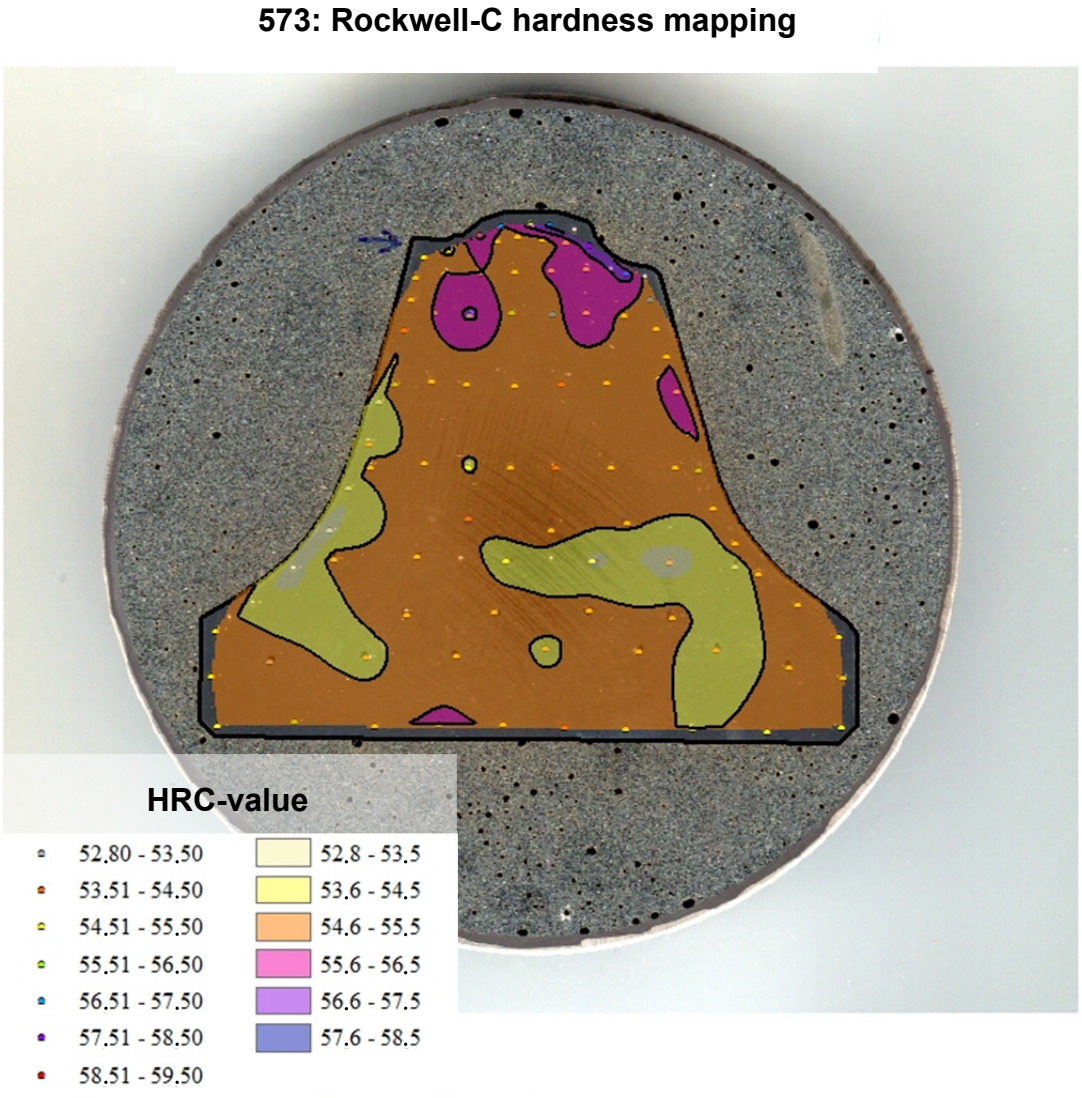

Fig. 86: HRC hardness mapping on the cutter ring 573 with abrasive wear + tapering + grooving. Measured points are highlighted. The width of the cutter ring is about 8 cm (modified after PAHNKE 2016).

6.4.2 CERCHAR pins and LCPC impeller

Microhardness and low-force hardness

To determine the micro- and low-force hardness, hardness tests according to Knoop and Vickers with 50 to 500 grams load were carried out on two CERCHAR (CAI) pins and one LCPC-impeller. It was observed that the two CAI pins have the highest hardness, but there are significant differences between the two CAI-steels tested. Fig. 87 illustrates that CAI-A2-45 is about 1.4 times harder than CAI-A1-62. The difference in hardness was already supposed during reflected light microscopy and could now be confirmed (chapter 4.4.2). The reason for this is most likely a different heat treatment during the curing process.

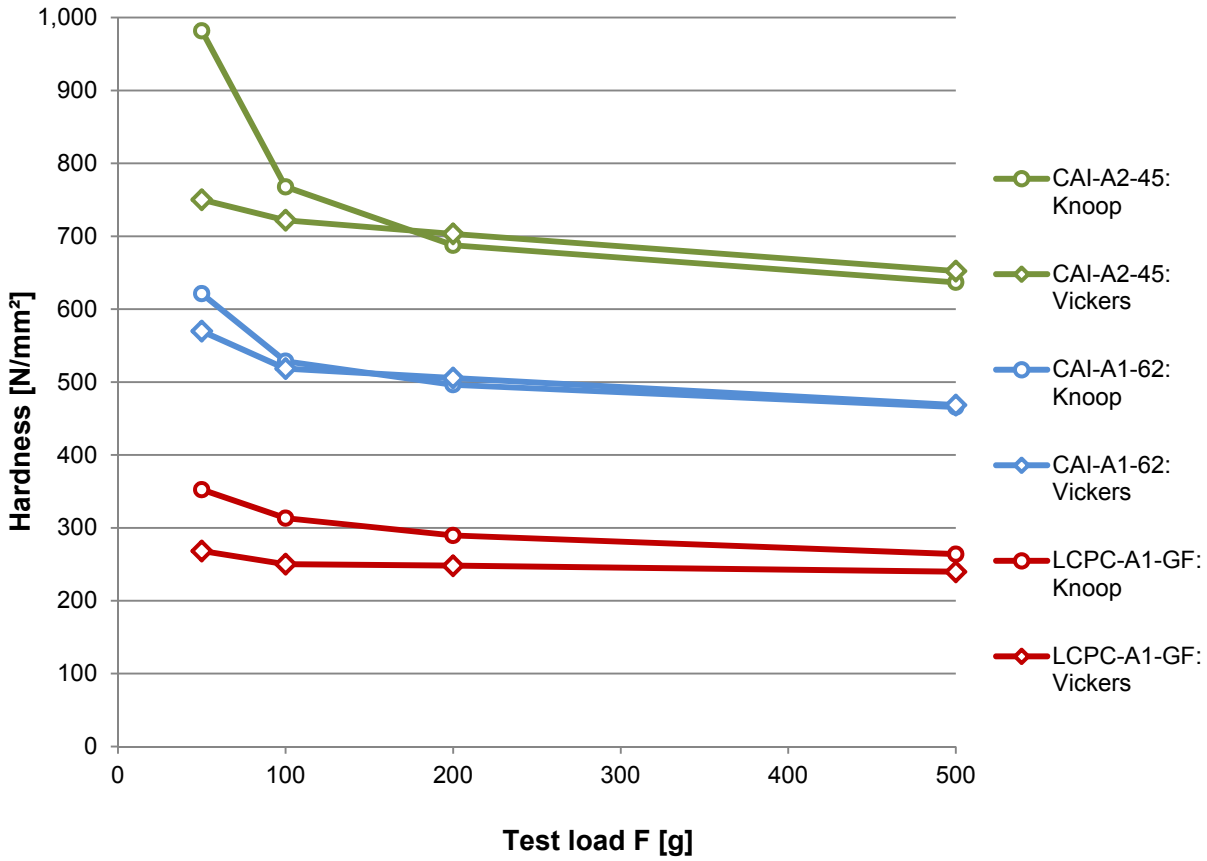

Fig. 87: Results of micro- and low-force hardness tests after Knoop and Vickers on CERCHAR pins and one LCPC-impeller. The data points represent the average value of several single measurements.

In addition, as already mentioned for the TBM disc cutter in the previous chapter, there may be a distinct difference between Knoop and Vickers hardness. Often the Knoop-hardness is higher than that of Vickers. The lower the test load, the more significant the difference. Furthermore, the indentation size effect is also obvious here, as both Knoop and Vickers hardness increase with decreasing test load.

Vickers hardness of LCPC-impellers

An examination of the hardness between a milled and a laser cut LCPC-impeller showed that the milled impeller had a significantly higher hardness (Tab. 22). In chapter 4.4.2 it was shown that the investigated impellers consist of different materials and have different grain sizes. The hypothesis that the sample LCPC-A1-GF with the coarser grain structure has a lower hardness could not be confirmed. Thus, the difference in hardness can probably be attributed to a slightly different material composition and different heat treatment during the curing process.

According to chapter 5.2.2 the impellers used for the LCPC test must have a hardness of about 60-75 HRB. The materials tested are too hard and not suitable for this purpose.

Tab. 22: Results of the Vickers hardness test of a milled and a laser cut LCPC-impeller.

LCPC impeller	Test load F [kg]	Number of tests	Hardness [N/mm²]	Min. / Max. [N/mm²]	Converted hardness into Rockwell-B (HRB) according to DIN EN ISO 18265 (2014)
LCPC-A1-GF (milled)	10	15	221,2 ± 10,9	204,2 / 240,7	95,2
	30	4	219,2 ± 6,2	209,6 / 226,9	-
LCPC-A2-GL (laser cut)	10	14	149,5 ± 3,0	146,0 / 155,7	78,5
	30	5	151,2 ± 1,9	149,4 / 154,5	-

6.4.3 Minerals

Similar to the previous investigations, the Knoop and Vickers hardness of selected minerals were investigated. The minerals studied are the minerals of the Mohs' hardness scale (except diamond) as well as garnet (almandine) and pyrite. Since the hardness tests with talc could not be evaluated, no own data are presented here.

Microhardness and low-force hardness

The results of the microhardness and low-force hardness tests of the minerals are shown in Fig. 88 and Fig. 89. The presentation takes place in two separate diagrams, as the readability would no longer be guaranteed due to the large variance of the minerals.

The first diagram (Fig. 88) with a hardness range from 0 to 250 N/mm² shows the minerals 2 (gypsum) to 4 (fluorite) of the Mohs' hardness scale. It becomes clear that the hardness according to Knoop is usually higher than that of Vickers. In most cases the Knoop and Vickers hardness values of a mineral match each other relatively well. Only the Knoop hardness of gypsum is often in the range of calcite and sometimes even higher. The exact reason for this is not known. Either it is due to an unrecognized systematic error in the evaluation or to the interaction of the mineral properties with the properties of the Knoop-indenter. The interim conclusion could be that Vickers hardness is better used for reproducible hardness tests.

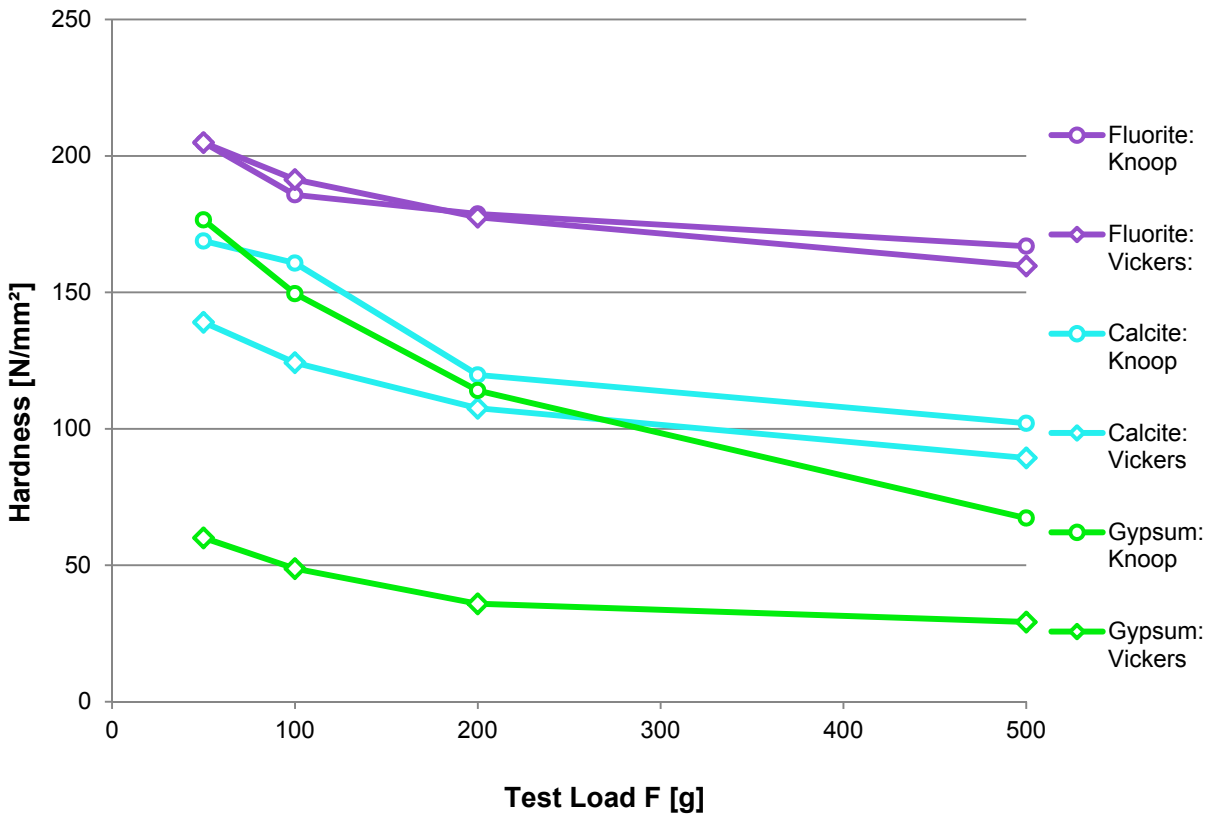

Fig. 88: Results of micro- and low-force hardness tests after Knoop and Vickers on gypsum, calcite and fluorite. The data points represent the average value of several single measurements.

The second diagram (Fig. 89) with a hardness range from 0 to 6,000 N/mm² shows the minerals 2 (gypsum) to 9 (corundum) of the Mohs' hardness scale and additionally garnet (almandine). The lower part of the diagram with the rather soft minerals gypsum, calcite and fluorite is very difficult to analyze. For this reason, Fig. 88 was prepared, which only shows the rather soft minerals.

In Fig. 89, the Knoop hardness is usually higher than that of Vickers again. In general, as already mentioned in the previous chapters, the indentation size effect is evident here again: the lower the test load, the higher the hardness. However, in contrast to steel, rocks and minerals usually behave brittle and form cracks, which have a strong influence on the hardness test results. As already mentioned, ONDRACEK (1995: 187) reports (in regard to the indentation size effect) that with an increasing load, the plastic part of the deformation grows while the elastic parts decreases. This occurs with the rising test load until a material-specific limit is reached, where the ratio stays constant. This statement applies to largely ductile materials such as steel.

With regard to more brittle materials such as ceramics, minerals and rocks, this statement cannot be applied. Upon reaching this limit, fracture processes normally occur which decrease the hardness. This effect is said to be particularly strong in the shape of the Vickers indenter,

which is confirmed by our own investigations. Another explanation for the indentation size effect gives WEISBARTH (2003: 84): With an increasing load on porous and disturbed materials like rocks and minerals (all have micro-pores and micro-cracks), the indentation depth and width enlarges. Out of this, a larger number of cracks and pores, which existed even before the test, will be closed. According to our own results, it looks like it would be a combination of these two effects. (ELLECOSTA et al. 2015)

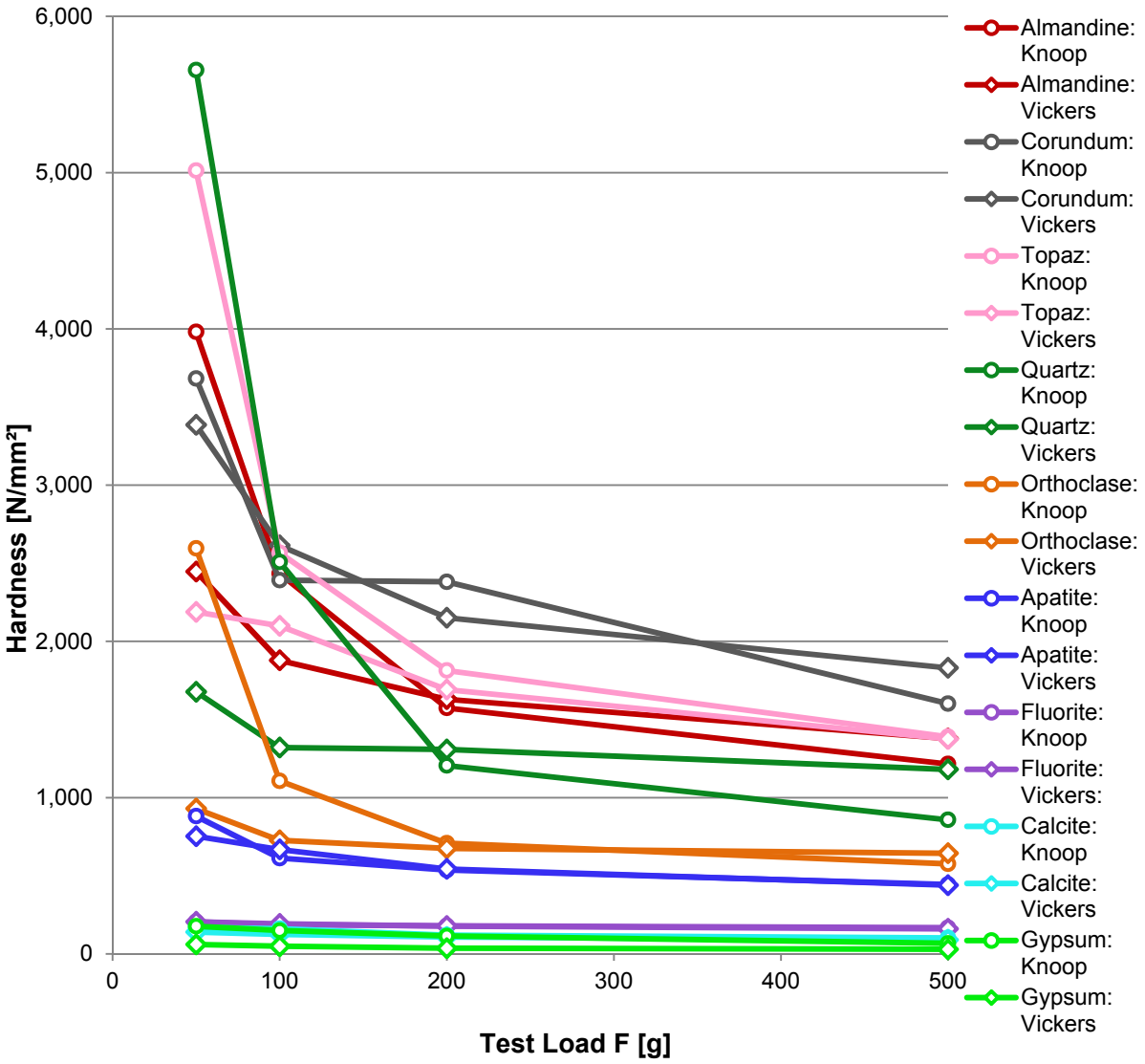

Fig. 89: Results of micro- and low-force hardness tests after Knoop and Vickers on a wide variety of minerals. The data points represent the average value of several single measurements. An enlarged view of the soft minerals gypsum, calcite and fluorite is shown in Fig. 88.

However, the Knoop hardness of quartz with the two lowest test loads of 50 and 100 g is particularly striking. Their hardness values are clearly above the tendency of the remaining minerals and even exceed the hardness value of corundum. A possible explanation for this could be that quartz, unlike the other minerals shown, is not fissile. Orthoclase and topaz possess perfect cleavage, corundum at least an indistinct cleavage or divisibility. Since the

shape of the Knoop indenter is significantly flatter and penetrates less deep into the test surface than the Vickers indenter, fewer cracks are caused by the Knoop hardness test, resulting in an apparently higher hardness.

The diagrams in Fig. 88 and Fig. 89 form, among other things, the basis for deciding which hardness test method and which load is best suited for the determination of the wear potential of minerals and rocks. It turned out that Vickers hardness with a load of 200 g (HV0.2) is the most appropriate. The detailed argumentation can be found in chapter 6.4.5.

Vickers hardness test

In addition to the micro- and low-force hardness results already described, Vickers hardness tests with up to 72.5 kg test load were also carried out. Since the area of influence of a single indentation has reached a size of 5 to 10 mm at such high loads, the number of individual tests had to be reduced for space reasons. Normally, at least three individual tests were carried out per load level.

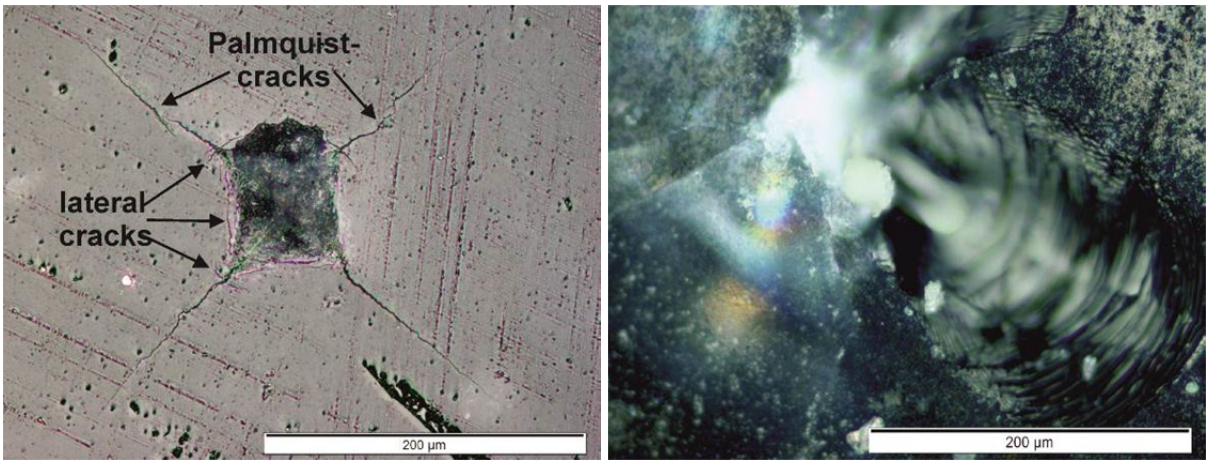

Fig. 90: Left: Indentation of a Vickers-diamond with a load of 5 kg (HV5) in a sample of pure quartz (flint). Even with this load the long Palmquist-cracks and the lateral cracks around the indentation can be seen. Right: Same setting in a sample of rock crystal. The overload is manifested by cracks and fractures and by stress birefringence around the lower left quadrant (ELLECOSTA et al. 2015).

The results of the Vickers hardness tests are shown in Fig. 91 in a half logarithmic chart: on the x-axis you can see the used test load and the logarithmically Vickers hardness plotted on the y-axis. The logarithmic scale was used because the hardness of the minerals from the Moh's scale increases nearly logarithmically. This diagram illustrates the results of the minerals of Mohs' hardness scale (gypsum to corundum) as well as garnet (almandine) and pyrite. Due to the limited mineral and indenter size, not all minerals could be tested with the maximum test load.

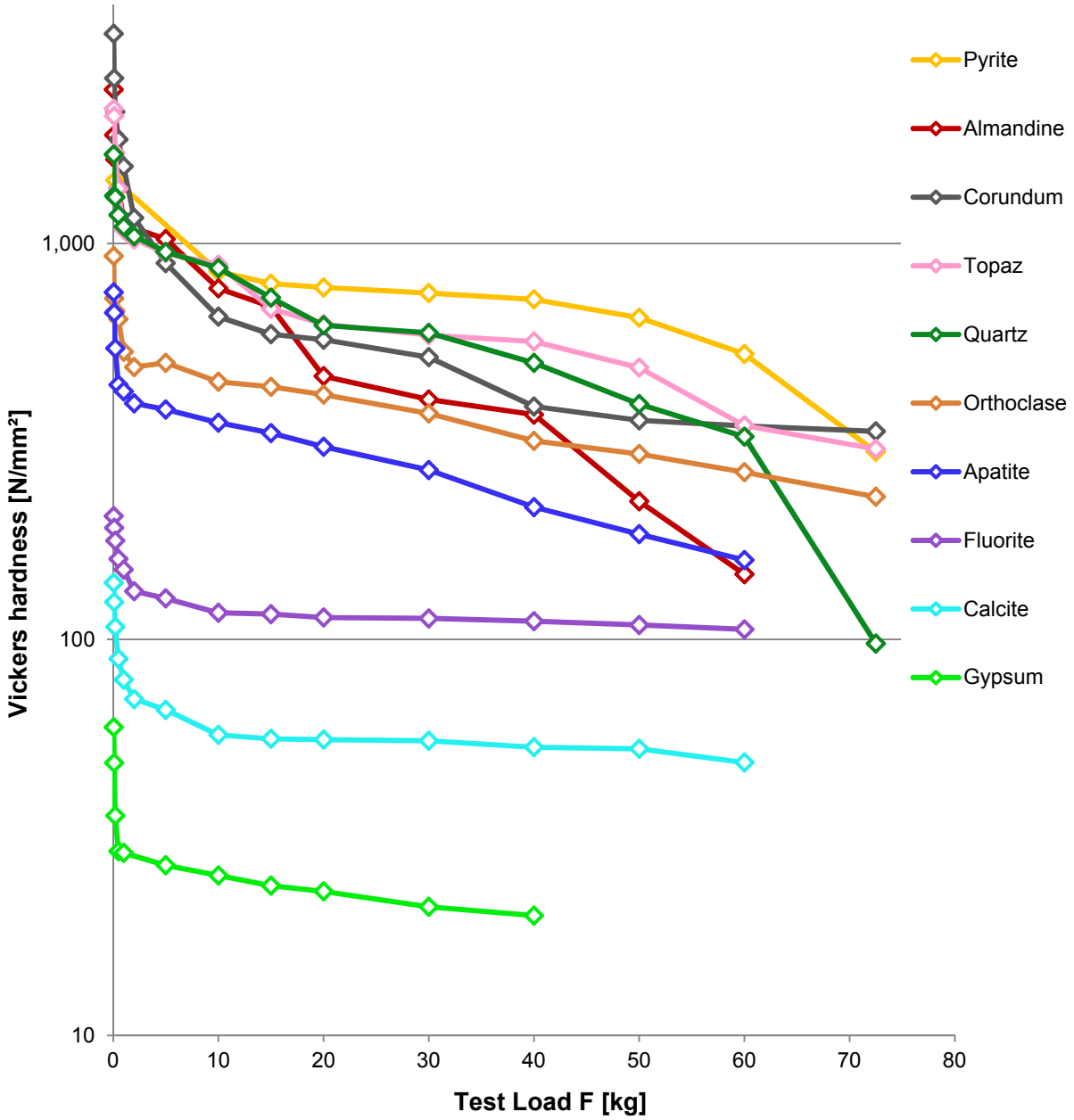

Fig. 91: Results of Vickers-hardness tests (microhardness to hardness) on a wide variety of minerals. The data points represent the average value of several single measurements.

It becomes clear that the hardness decreases with increasing load (indentation size effect). It is striking that every mineral has a distinct hardness for every load step. Since the Knoop and Vickers hardness of a mineral seems to be extremely load-dependent, a specific value can't be assigned for one mineral. Particularly in the area with a test load of over 5 to 10 kg, audible and visible cracks and fractures occurred in all minerals in the samples (Fig. 90). The cracks and fractures in the upper load ranges are the main reasons for the decreasing hardness. Especially the hardness of the relatively brittle reacting mineral quartz falls to the value of fluorite at a load of 72.5 kg.

It is also astonishing that the ore mineral pyrite with a Mohs' hardness of 6 to 6.5 usually achieves the highest hardness values in the range of about 10 kg test load and above. The reason for this is probably the relatively poor fissility.

Furthermore, it is noticeable that the hardness of minerals with a tendency to poor cleavage decreases more strongly at higher test loads than that of minerals with a very good cleavage. This is probably due to the fact that the hardness of minerals with good cleavage decreases considerably even at low and moderate test loads due to the activation of cleavage. If the test load is increased further, the hardness falls correspondingly less.

Influence of crystallographic characteristics

Depending on the molecular structure of the individual minerals, they have either a good or a bad or even no cleavage. The mineral calcite has a perfect cleavage in three spatial directions. Accordingly, it can be assumed that the orientation of the test surface to the cleavage has an influence on the hardness.

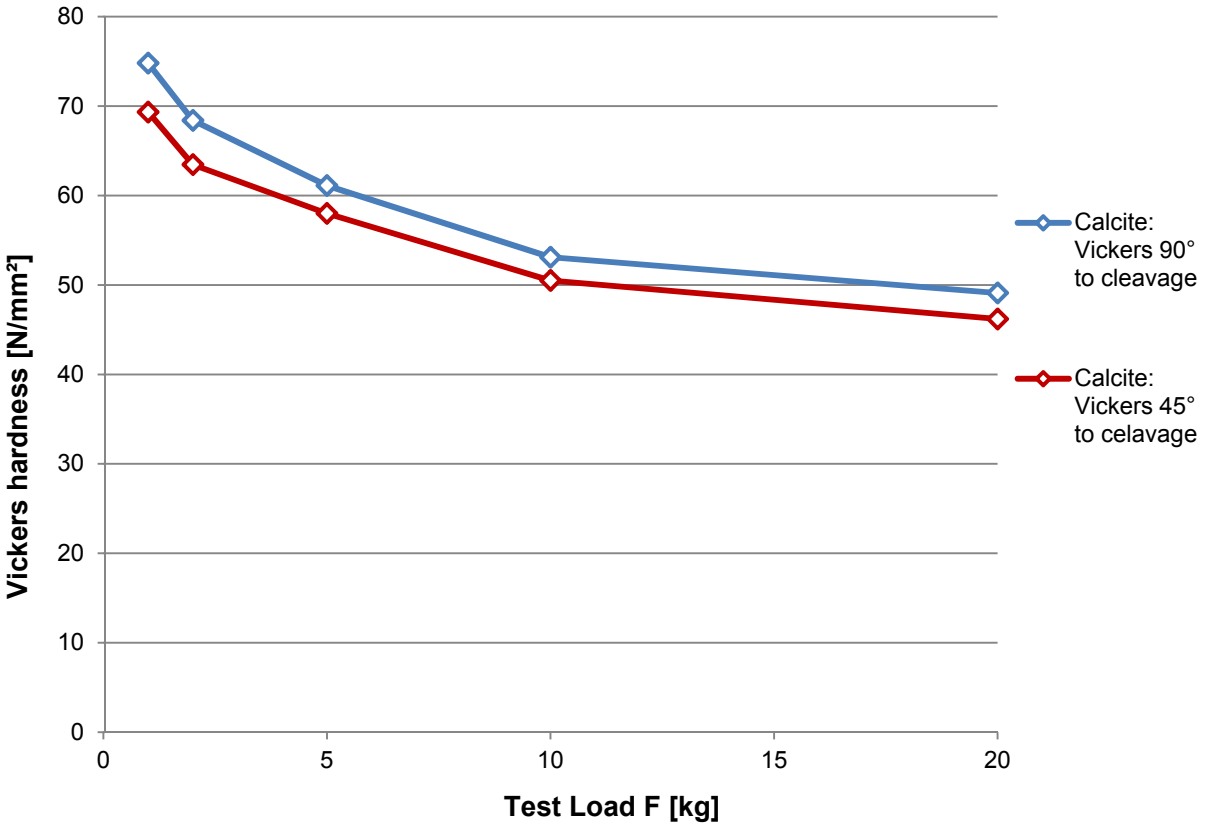

Fig. 92: Results of Vickers-hardness tests (low-force hardness to hardness) on calcite to show the influence of the crystallographic orientation. The data points represent the average value of several single measurements.

The influence of cleavage was examined exemplarily in Fig. 92 for calcite. Two polished sections of the same single crystal were prepared. Only the orientation of the test surface to

the cleavage was 90° for the first sample and 45° for the second sample. Hardness testing with test loads from 1 to 20 kg (HV1 to HV20) showed a very similar behavior of both samples.

The difference in hardness was about 3 to 6 N/mm² at all load levels. In addition, the indentation size effect was again apparent: the greater the test load, the lower the hardness. The higher hardness values were provided by the specimen in which the test surface was oriented perpendicular to the cleavage. The reason for this may be explained by the fact that at the 45° orientation, pieces of the mineral broke off during the test, allowing the diamond to penetrate deeper.

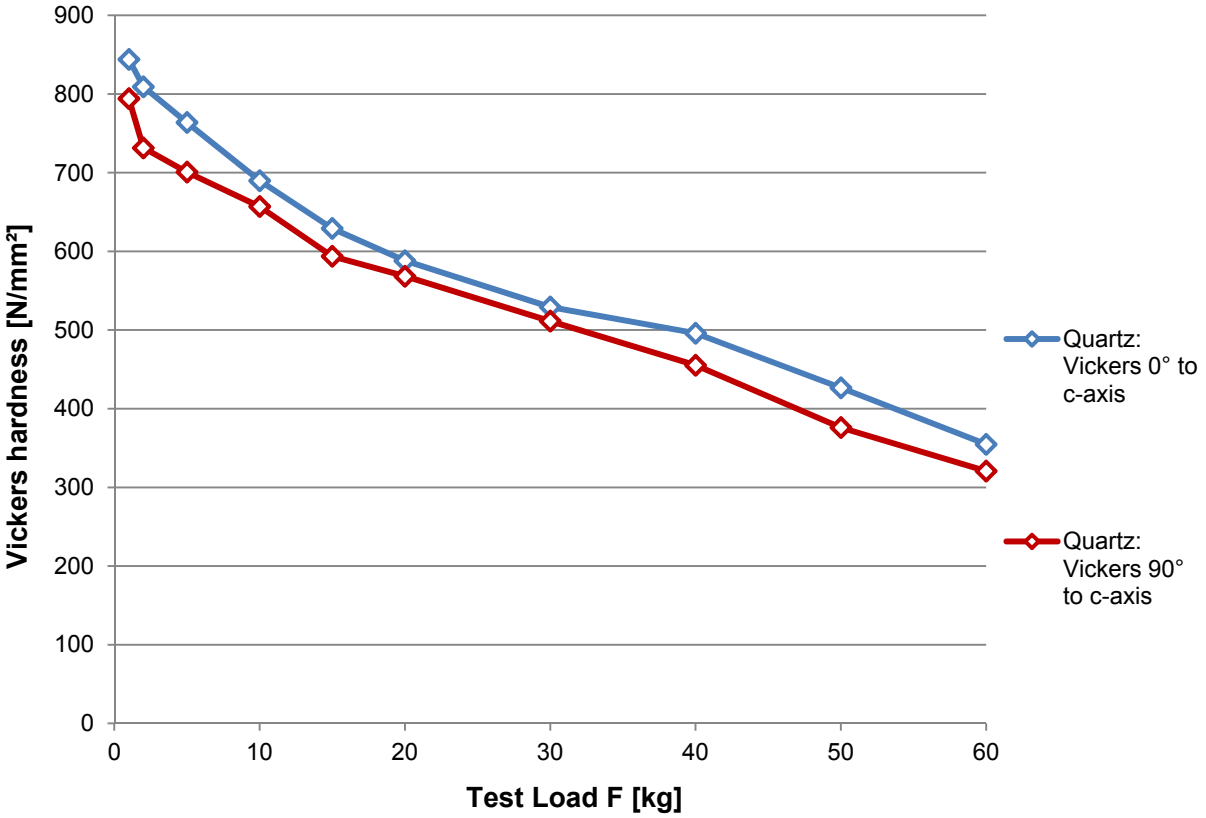

Fig. 93: Results of Vickers-hardness tests (low-force hardness to hardness) on quartz to show the influence of the crystallographic orientation. The data points represent the average value of several single measurements.

The anisotropy given by the crystallographic structure can normally also be transferred to hardness. Diamond, for example, is known to have different hardness values in different crystallographic directions and can therefore be cut and ground by other diamonds. The mineral quartz was examined as an example of this effect. The results are shown in Fig. 93. Two polished sections of the same single crystal were prepared. Only the orientation of the test surface to the c-axis was parallel (0°) for the first sample and vertical (90°) for the second sample. The hardness tests after Vickers were performed with 1 to 60 kg (HV1 to HV60).

As expected, the indentation size effect was again apparent: the greater the test load, the lower the hardness. The higher hardness values were achieved with the test specimen whose test surface is aligned parallel to the crystallographic c-axis. The difference in hardness between the two test specimens was approximately between 20 and 80 N/mm².

6.4.4 Rocks

Analogous to the previous studies, the Knoop and Vickers hardness of selected rock types was investigated. The selected rock types are calcareous, silicic and crystalline rocks, which were sampled in the field and tested at the Technical University of Munich. The material selected is based on typical rock types that are frequent in the upper earth's crust and therefore often are encountered during tunnel excavations.

Microhardness and low-force hardness

Fig. 94 illustrates the results of micro- and low-force-hardness for the Wiesenhofen limestone and Laas marble in comparison with calcite. Due to a technical defect, only the Vickers hardness of the Laas marble could be determined with 200 g test load. At first glance, the indentation size effect is apparent: the higher the test load, the lower the hardness. In contrast to the previous tendency in testing minerals, where the Knoop hardness is usually higher than that of Vickers, here the Vickers hardness of the rocks tends to have the higher values.

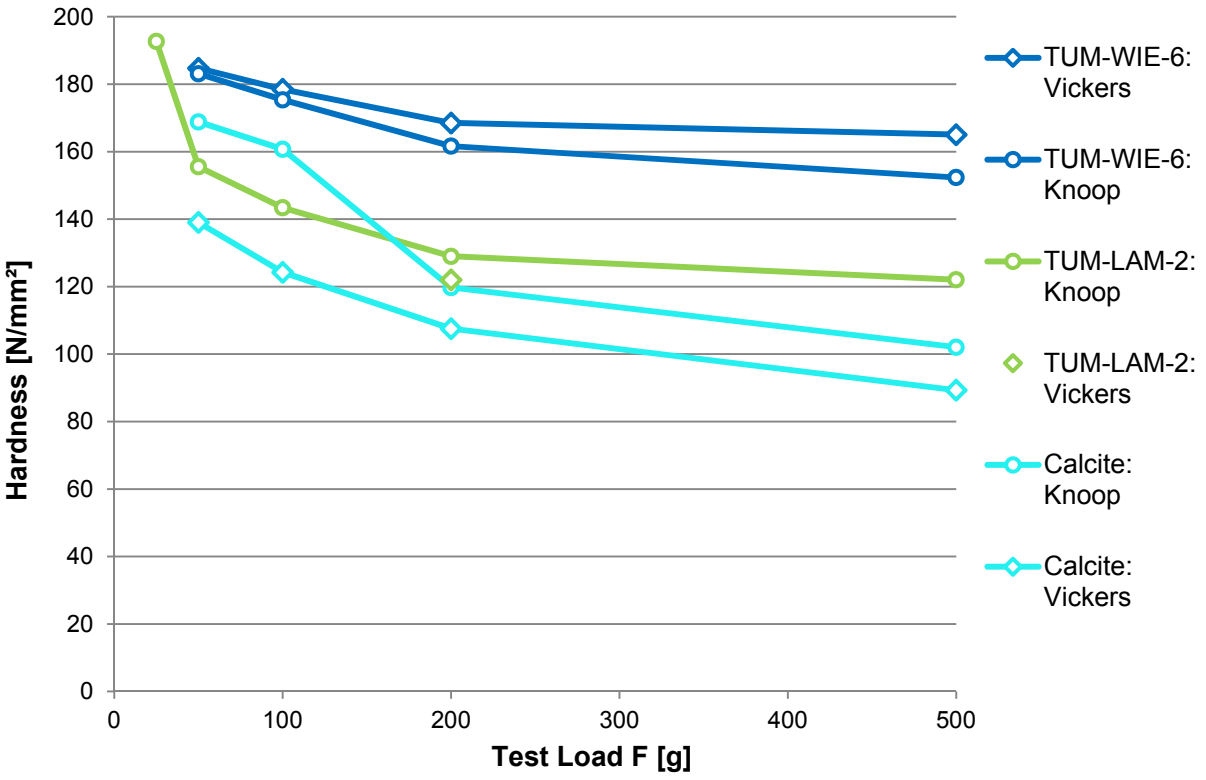

Fig. 94: Results of micro- and low-force hardness tests after Knoop and Vickers on the Wiesenhofen limestone WIE and the Laas marble LAM in comparison with calcite. The data points represent the average value of several single measurements.

Although both rock types consist almost entirely of the mineral calcite, a clear difference in hardness can be seen in Fig. 94. The grain size is primarily the difference between the two rock types. The limestone is very fine-grained (lutitic), the marble is much coarser. Accordingly, the difference in hardness is due to the grain size. On the one hand, it is known that fine-grained materials in most cases have a higher hardness. On the other hand, due to the grain size of up to 1.5 mm, the cleavage of calcite can be activated in marble, which leads to larger indentations and thus to lower hardness values.

The direct comparison of the marble with the hardness of the calcite single crystal shows that the two higher load levels (200 and 500 g) lead to lower hardness values and the two lower load levels (50 and 100 g) to higher hardness values. This circumstance can probably be explained by the fact that the lower load levels (50 and 100 g) do not or only minimally activate the cleavage of the calcite and single crystals usually show high hardness due to their high purity. Only at higher test loads (200 and 500 g) does the almost perfect cleavage have an effect in larger indentations and thus lower hardness values.

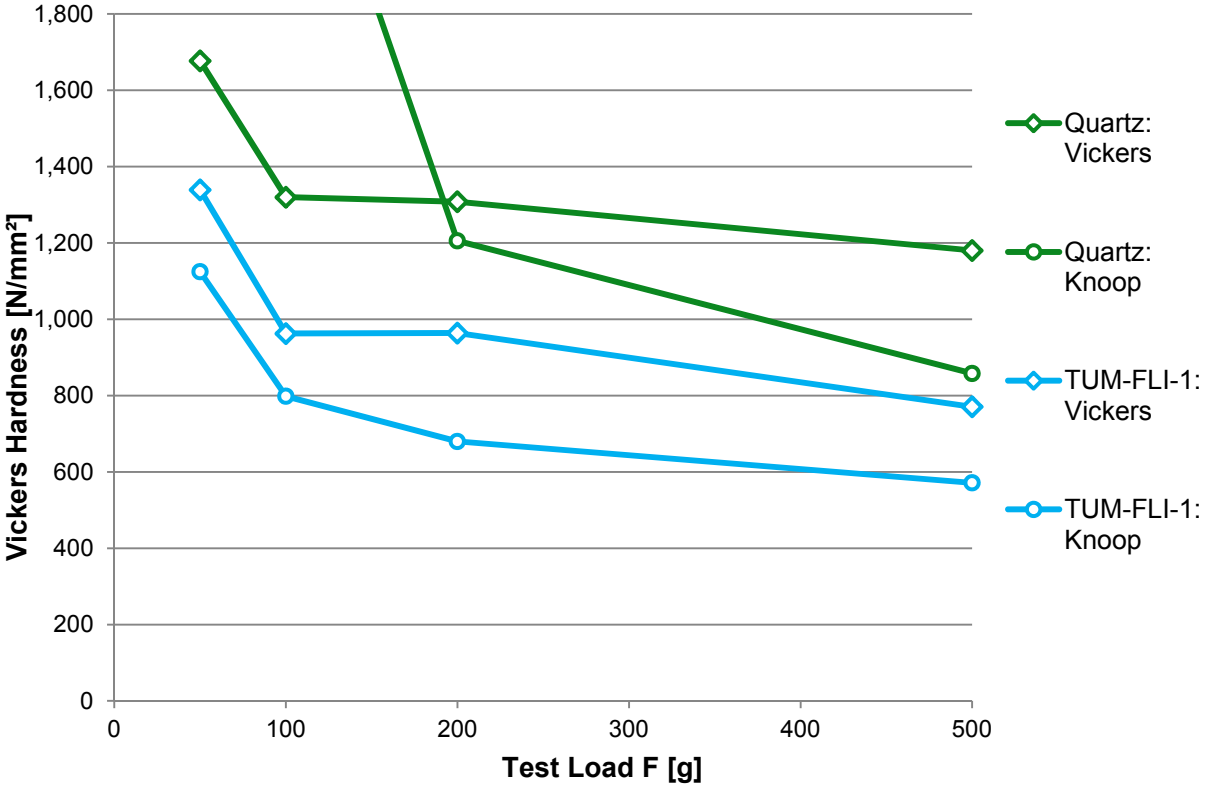

Fig. 95: Results of micro- and low-force hardness tests after Knoop and Vickers on a flintstone FLI in comparison with quartz. The data points represent the average value of several single measurements.

Fig. 95 illustrates the results of micro- and low-force-hardness for flintstone in comparison with quartz. For reasons of better representation, the diagram is cut off at a hardness of 1,800 N/mm². The missing Knoop hardness values can be taken from Fig. 89. At first glance,

the indentation size effect is apparent again: the higher the test load, the lower the hardness. In contrast to the previous tendency in testing minerals, where the Knoop hardness is usually higher than that of Vickers, here the Vickers hardness of the flintstone has the higher values.

It is also noticeable that the hardness of quartz is higher than that of the flintstone. Since the mineral quartz has no cleavage it is obvious that the mineral hardness is higher than the hardness of the rock.

The fact that the Vickers hardness of the investigated rock types (Wiesenhofen limestone and flintstone) is higher than the Knoop hardness is astonishing and was not expected. An explanation for this could be the grain size: The minerals examined were mainly monocrystals, while the grain size of the rocks was partly very fine-grained. In the monocrystals, individual cracks can spread much better because of the homogeneous atomic structure. In the rocks, there are many individual crystallites with different crystallographic orientations. Spreading of cracks beyond their grain boundaries requires additional energy and opposes crack propagation.

Vickers hardness tests

In addition to the micro- and low-force hardness results already described, Vickers hardness tests with up to 72.5 kg test load were also carried out. Since the area of influence of a single indentation has reached a size of 5 to 10 mm at such high loads, the number of individual tests had to be reduced for space reasons. Normally, at least three individual tests were carried out per load level. Therefore, not every rock could be tested with the full test load.

Fig. 96 illustrates the results of the calcareous rock types (mostly monomineral rocks) in comparison with calcite. First of all, it is noticeable that the hardness of each rock falls further and further with increasing test load and does not asymptotically approach a certain value. As already discussed in chapter 6.4.3, this is related to the formation of cracks and fractures (WEISBARTH 2003: 84).

As already discussed for the micro- and low-force hardness of rocks, the mineral hardness of calcite is usually below the rock hardness. This is related to the almost perfect cleavage of calcite again. The smaller the grain size of calcareous rock types, the higher is their hardness. Thus, the hardness of the coarser-grained Laas marble is below the hardness of the finer-grained Carrara marble. The mineralogical composition of both marbles is approximately the same.

Only the hardness of Wiesenhofen marl is lower than that of calcite, because with its high clay content it has a clearly different mineralogical composition.

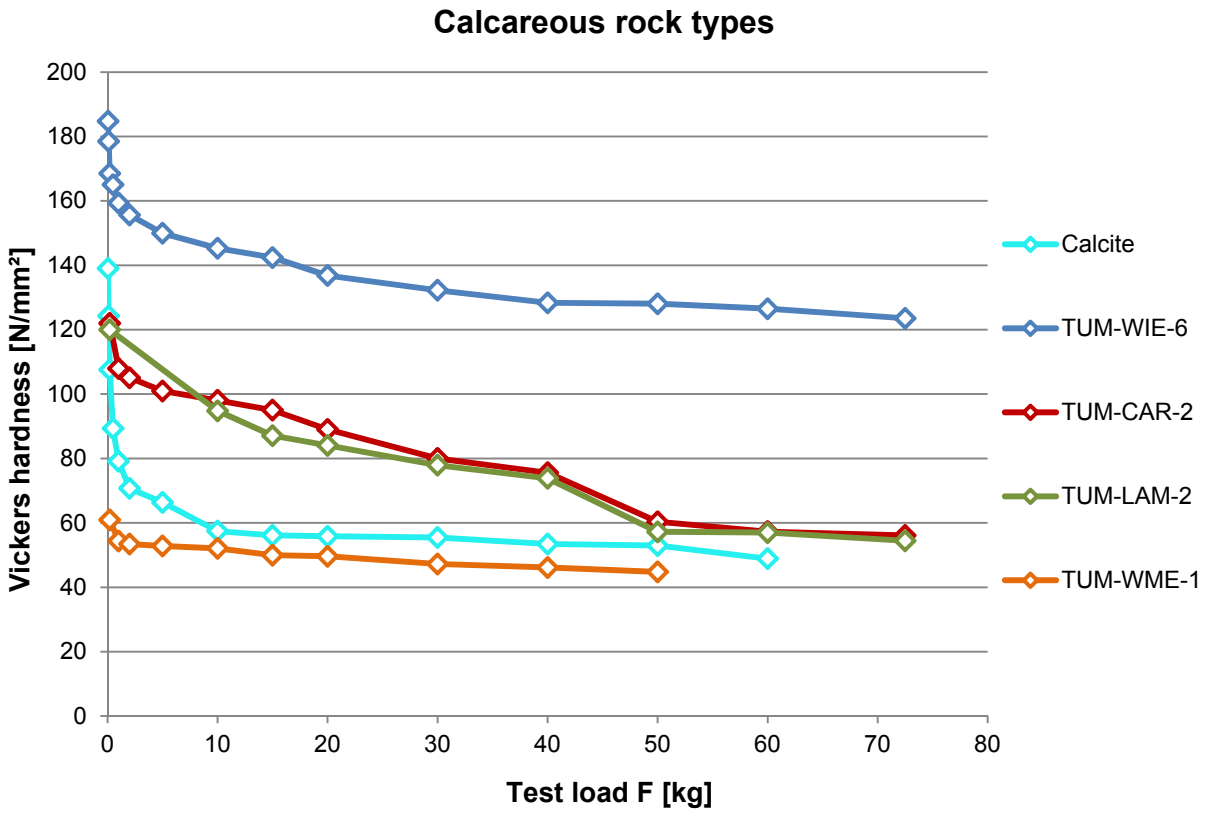

Fig. 96: Results of Vickers-hardness tests (microhardness to hardness) on calcareous rock types in comparison with calcite. The data points represent the average value of several single measurements. WIE – Wiesenhofen limestone, CAR – Carrara marble, LAM – Laas marble, WME – Wiesenhofen marl.

The results of the silicic rock types (mostly monomineral rocks) in comparison with quartz are shown in Fig. 97. Again, it can be seen that the hardness of each rock decreases further and further with increasing test load but does not asymptotically approach a certain value. As mentioned earlier, this is related to the formation of cracks and fractures (WEISBARTH 2003: 84).

In contrast to the calcareous rock types, the mineral hardness of quartz is usually higher than the rock hardness of silicic rock types. This is clearly related to the lack of fissility of quartz.

The hardness of the rock types among themselves is determined by mineralogy and grain bonding. The grains of the Abtswinder sandstones (TUM-ABC and TUM-ABO) consist of quartz to a high degree, but the binding is mostly clayey and therefore not very strong. Within these two sandstones the TUM-ABO is somewhat harder, which also correlates with a higher uniaxial compressive strength (chapter 6.1). The Küchen sandstone (TUM-KUC), on the other hand, is silicate-bonded and has a significantly higher hardness, which also correlates with the higher rock strength (chapter 6.1). The Dala sandstone has a much more pronounced silicate bond and better consolidation with a correspondingly lower proportion of pores. Accordingly, its hardness and also its rock strength is much higher (chapter 6.1).

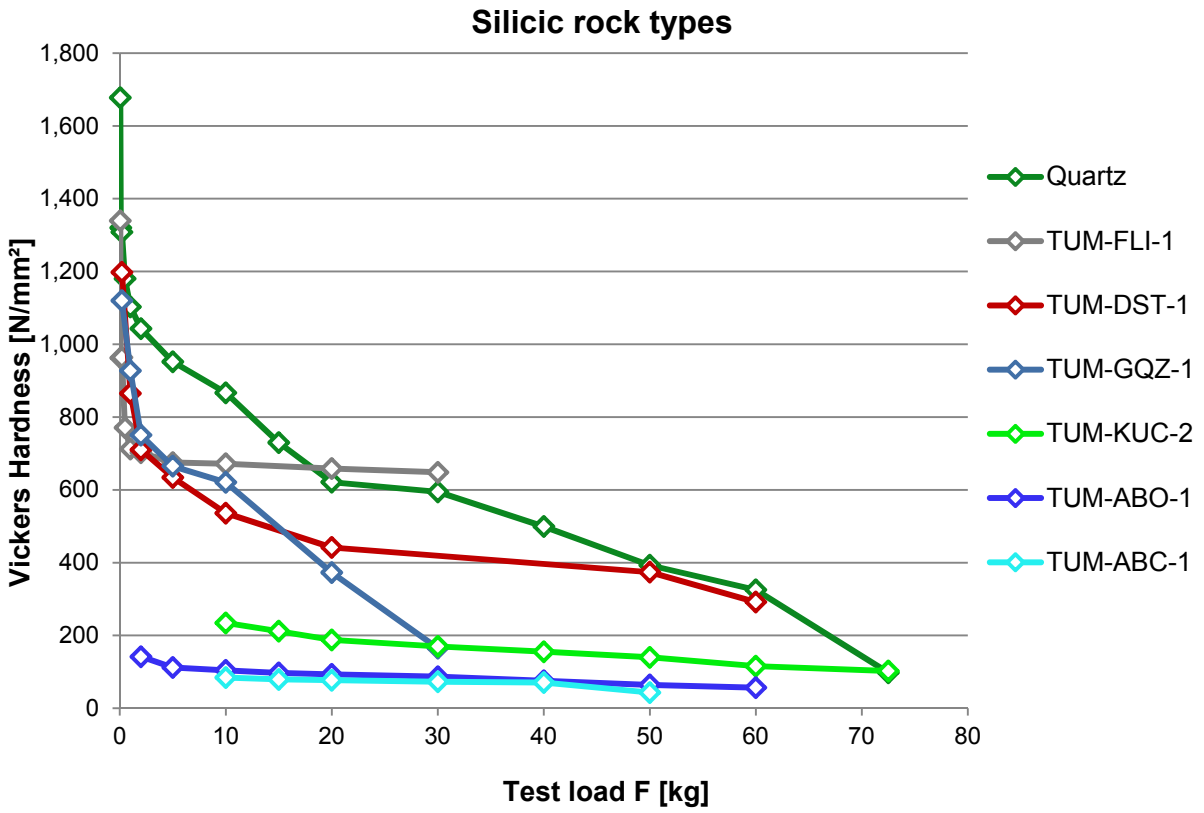

Fig. 97: Results of Vickers-hardness tests (microhardness to hardness) on silicic rock types in comparison with quartz. The data points represent the average value of several measurements. FLI – Flintstone, DST – Dala sandstone, GQZ – Vein quartz, KUC – Küchen sandstone, ABO – Abtswind sandstone “Ortels”, ABC – Abtswind sandstone “Castell”.

Besides the mineral quartz, only the pure quartz rocks possess a higher hardness: flintstone (TUM-FLI) and quartzite (TUM-GQZ). It is noticeable that the hardness of the quartzite drops extremely rapidly at test loads of 10 kg (HV10) and more due to its brittleness and many impurities.

Fig. 98 illustrates the hardness of the remaining investigated rock types, which are summarized under the term crystalline rocks. These show the indentation size effect again. The present rocks are polymineral rocks. In addition to hard minerals such as quartz, they also contain much softer minerals such as mica. This makes a hardness test challenging, as several minerals are within the influence area of indentation, especially at higher test loads.

In general, there is a strong tendency that rock types with a high rock strength also have a high hardness. These include larvikite (TUM-LAR), which consists almost exclusively of feldspar, and basalt (TUM-PB), which consists mainly of olivine, pyroxene and nepheline. Both rock types contain hardly any quartz.

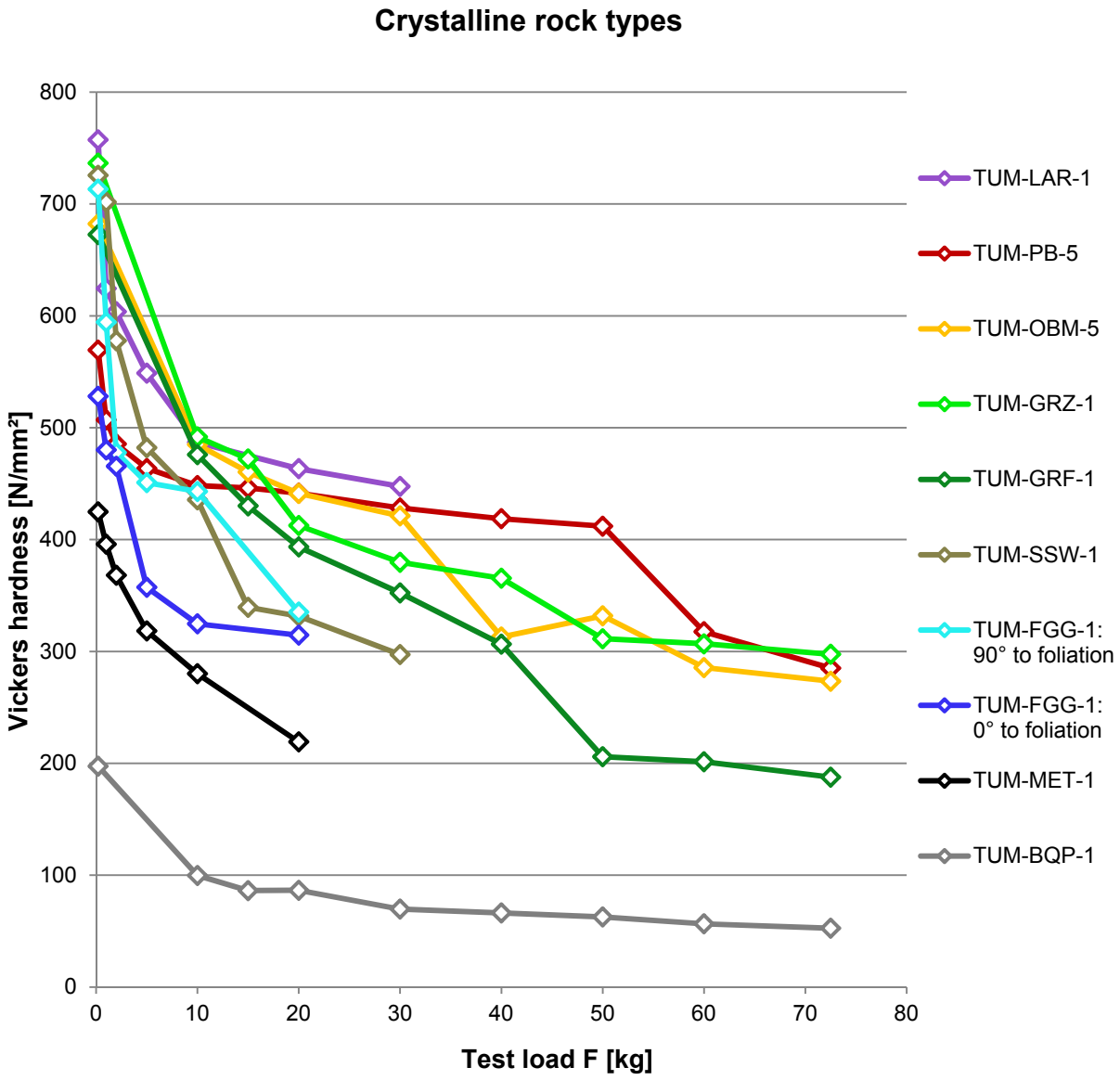

Fig. 98: Results of Vickers-hardness tests (microhardness to hardness) on crystalline rock types. The data points represent the average value of several measurements. LAR – Larvikite, PB – Pechbrunn basalt, OBM – Oberbaumühle amphibolite, GRZ – Gramlet granite, GRF – Gramlet Diorite, SSW - Swedish Black, FGG – Freiberg gneiss, MET – Metten granite, BQP – Brixen quartzphyllite.

Granitoid rocks like the twin mica granite (TUM-GRZ) and the spotted diorite (TUM-GRF) contain a significant amount of quartz. This is estimated to be 40 % in the sample TUM-GRZ and about 32 % in TUM-GRF. Despite a fairly similar rock strength of about 190 MPa (chapter 6.1), the hardness of the two-mica granite is significantly higher than that of the spotted diorite, which is due to the higher quartz content. Metten granite has a similar mineralogical composition and its hardness is nevertheless significantly lower. Again, the significantly lower rock strength plays an important role.

The influence of the orientation of anisotropic rocks is shown by the two gneiss samples TUM-FGG, which show a clear foliation. Both samples are from the same rock block. The surface of the first specimen is oriented perpendicular to foliation (90°), the surface of the second specimen is parallel to foliation (0°). A direct comparison of both curves clearly shows that the test piece with the test surface perpendicular to the foliation achieves the higher hardness values. This is probably due to the fact that the soft mica was increasingly tested more or less parallel to foliation. Only by testing a surface perpendicular to foliation is it possible to test all minerals according to their distribution around the rock.

In addition, testing of anisotropic rocks should always be carried out on surfaces perpendicular to the anisotropy in order to determine the maximum hardness values and obtain results that are as reproducible as possible.

6.4.5 Cutters and rock types – comparison of hardness

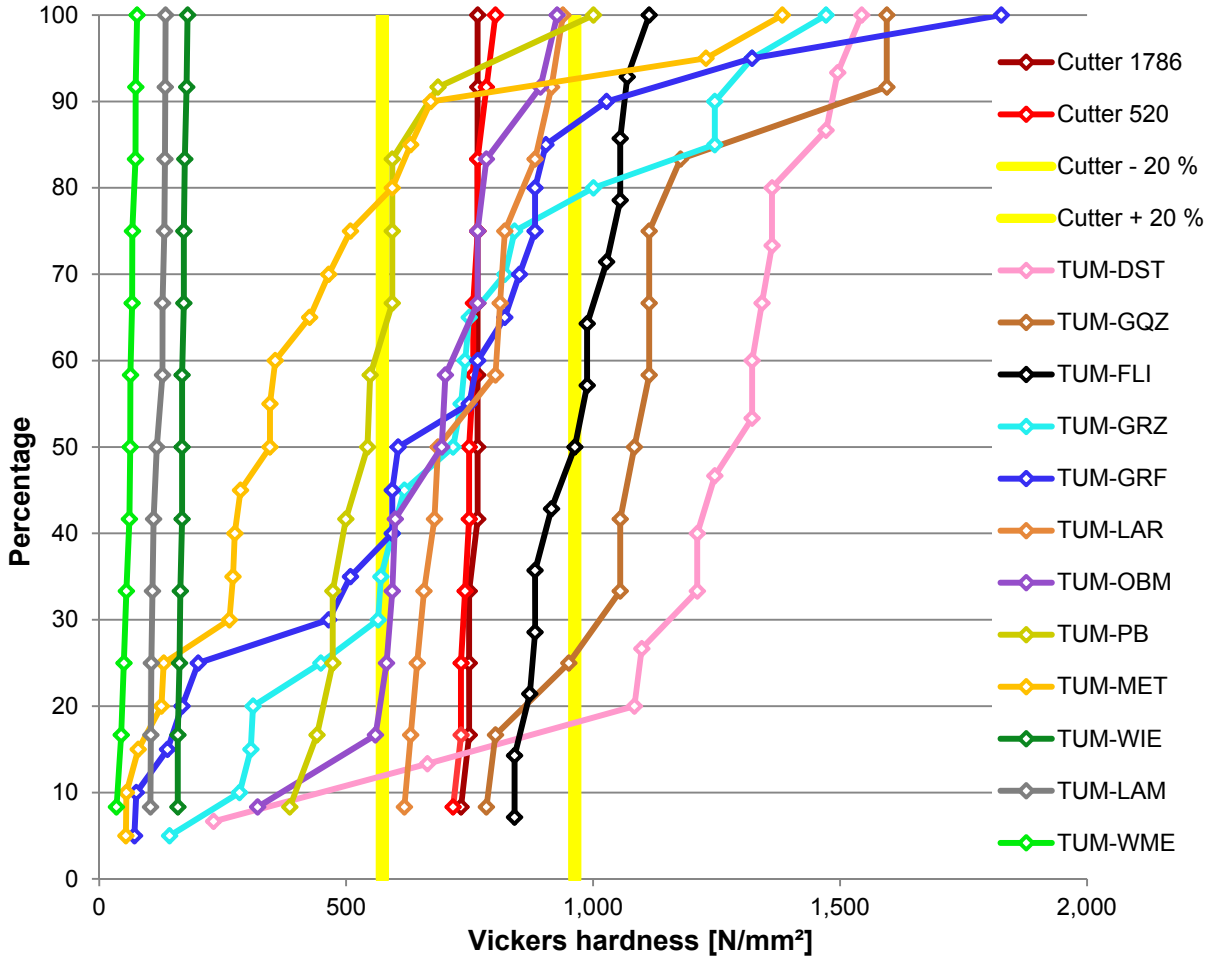

Fig. 99: Distribution of the hardness values of the tested rock types in comparison with the hardness of two TBM disc cutters. DST – Dala sandstone, GQZ – Vein quartz, FLI – Flintstone, GRZ – Gramlet granite, GRF – Gramlet Diorite, LAR – Larvikite, OBM – Oberbaumühle amphibolite, PB – Pechbrunn basalt, MET – Metten granite, WIE – Wiesenhofen limestone, LAM – Laas marble, WME – Wiesenhofen marl.

Particularly in the case of polymineral rocks, the sole representation of hardness mean values is not necessarily the method of choice, since both the soft and hard minerals cannot be represented. And according to general opinion, a large part of tool wear can be attributed to the content of the particularly hard minerals. Especially for polymineral rocks, it makes sense to use also another method, where the wide variability of the values can be better presented: the cumulative frequency distribution (CARDU & GIRAUDI 2012: 381).

Starting from the idea of CARDU & GIRAUDI (2012) the analysis was adapted to the own needs. Instead of the Knoop hardness, the Vickers hardness was selected. As the previous chapters have shown, the same load level should always be used when analyzing minerals, rocks and tool steel, as the hardness depends on the load applied. The reason for using the Vickers hardness is that it gave more consistent results and the indentation size effect was not as strong as for the Knoop hardness. Furthermore, the size of the indentation at Vickers is smaller than at Knoop applying the same load, which is due to the indenter geometry. Due to the smaller indentation, fewer minerals or crystallites are tested simultaneously. In addition, only the longer diagonal is measured for Knoop hardness, while both diagonals are measured for Vickers. This means that anisotropies can be measured much more precisely with the Vickers hardness. When testing the hardness of minerals, a load of 200 g (HV0.2) proved to be the most suitable for determining the Vickers hardness.

The results of this test method are presented in Fig. 99. For reasons of better representation some rock types had to be omitted. With this method, the individual measured values are arranged according to their hardness and then plotted versus each other according to their share.

It becomes clear that monomineral rock types like the Wiesenhofen limestone (TUM-WIE) or the Laas marble (TUM-LAM) show an almost vertical or only slightly inclined curve, which represents very similar hardness values with little deviation. The TBM disc cutters also produce an almost vertical curve. Polymineral rock types with soft minerals such as mica and hard minerals such as quartz, show an oblique curve, such as the twin mica granite (TUM-GRZ). With this illustration, the soft and hard structural constituents can be read off very well.

However, this diagram also offers the possibility to compare rock and mineral hardness very easy with the hardness of tool steel. In Fig. 99 the data of two analyzed TBM disc cutter are presented in red colors. TABOR 1954 postulated that a rock/mineral whose hardness is at least 20 % higher than that of the excavation tool can cause extreme wear. In contrast to this, experience has shown that wear is only minimal if the rock/mineral hardness is at least 20 % lower than the hardness of the excavation tool. The corresponding area is limited by a bold yellow line. In order to check whether a rock has the potential to cause heavy wear or whether only very little wear is to be expected, the proportion of the respective rock above and below the 20% line must be considered.

According to the data in Fig. 99, it can be seen that only the Wiesenhofen marl and limestone and the Laas marble would cause very little wear, as each hardness value is well below the 20% line. The situation is quite different for rock types that contain a very high proportion of quartz (e.g. flintstone (TUM-FLI), quartzite (TUM-GQZ) and Dala sandstone (TUM-DST)), as a very large proportion of the hardness is above the 20% line. These have the potential to cause extreme wear. The remaining rock types lie with their hardness values between the two mentioned extremes. Depending on the percentage by which these exceed the 20% line, a correspondingly high degree of wear is to be expected.

In their paper, CARDU & GIRAUDI (2012) present a considerably more elaborate evaluation option: For this, 40 individual Knoop hardness tests were carried out on a rock specimen. To calculate the wear potential, each value is set in relation to the other 39 values, which in total corresponds to 1,600 data points at the end. The relationship between the various hardness values can also be plotted in a diagram. An exact evaluation according to CARDU & GIRAUDI (2012) can be found in the master thesis of Marta Denina (DENINA 2014).

7. Discussion

This chapter discusses the results and compares them with the data of other researchers. Furthermore, a first rough summary is given.

7.1 Koralm Tunnel project

Our own investigations point out that the cutter rings used in the Koralm Tunnel project, despite different manufacturers, were all made of the same steel with the material number 1.2345. This is a hot work steel, also known as X50CrMoV5-1. According to KÜPFERLE et al. (2016a), this steel type is most commonly used for heavy duty cutter rings as they were applied in the Koralm Tunnel project. Only for TBM drives in rather slightly abrasive ground, somewhat cheaper cutter rings made of hot-work steel No. 1.2344 (X40CrMoV5-1) with a slightly lower chromium content are used. These are then no longer referred to as heavy duty. Both steel types are quenched and tempered to provide high material hardness and toughness (tempered in the region of secondary hardness, KÜPFERLE et al. (2016a)).

7.1.1 Macroscopic wear

As briefly outlined in the previous chapter, in practice there is usually a superposition of different basic wear types, which makes a systematic evaluation difficult, especially during real construction operations.

Abrasive wear / Normal wear & Asymmetric wear

In the best case, a large part of the cutter rings will feature the form of abrasive wear/normal wear, since an optimum degree of utilization is attributed to this. Asymmetrical wear often occurs in the center (center cutter) and outer areas (gauge cutter) of the cutter head. In addition to our own results, this relationship has already been reported by THURO & PLINNINGER (2002) and KÄSLING (2009).

The asymmetrical wear on the center cutters is due to the small turning radius, caused by the central position on the cutter head. Accordingly, the higher abrasion of the cutter tip takes place on the outer side of the cutter ring. The asymmetrical wear of gauge cutters is often caused by a machine-related inclined position of these cutters.

Mushrooming & Chipping

In the Koralm Tunnel project, mushrooming occurred mainly in sections with strong to extremely strong rocks with rather few joints, as the rock chipping required for cost-effective TBM tunnelling needs very strong contact forces (high cutter thrust). The high cutter thrust forms an impact head which can be compared with a secondary and cold forging of the cutter ring. When this happens, the steel is stressed and deformed beyond its yield point or elasticity

limit and irreversible, plastic deformation occurs (ELLECOSTA et al. 2018). See also Fig. 10 in chapter 2.1.3.

If the deformation of the cutter ring reaches a certain limit large steel chips break off laterally. This is called ring chipping or simply chipping and occurred mainly in tunnel sections with fractured to highly fractured rock mass. The highly fractured rock mass causes rock bursts so that the tunnel face no longer has a flat surface. As a consequence, the cutters will be exposed to large instantaneous loads. Under such conditions, a cutter ring exhibits a tendency to chip along its edge (MACIAS et al. 2017a). Extensive ring chipping and high cutter thrust may result in bevel edge wear, loosened rings and blocked bearings (MACIAS et al. 2017a).

The Koralm Tunnel project with its highly variable geology also offered the opportunity to test the influence of very hard and solid rocks on cutters. Eclogite proved to be an extreme case because this rock normally has a very high to extremely high strength. For operational reasons, no samples could be taken to determine rock parameters. According to information provided by the contractor, the average penetration recorded in the TBM was about 3 to 5 mm/rev although the maximum cutter thrust of 267 kN/cutter (thrust limit) was exploited. Such high rock strength results in a very low penetration rate and a grinding-dominated cutting process despite hitting the thrust limit for the cutters (VILLENEUVE 2017). FRENZEL (2010) was able to demonstrate in his Ph.D. thesis that the cutter wear is proportional to the rolling distance of each cutter. The lower the penetration, the more revolutions of the cutter head are required. According to this, the high cutter thrusts up to the thrust limit lead to an extreme mushrooming with massive ring chipping and thus to an extreme wear rate.

In addition, VILLENEUVE (2008) and VILLENEUVE et al. (2012) showed that mineralogy is an important parameter for tensile-dominated fracturing processes like the rock chipping process in hard rock TBM tunnelling. In particular, they found that rocks with low (< 10 %) and high (> 24 %) mica contents are not as sensitive to tensile-dominated fracturing and spalling as those with moderate mica content (VILLENEUVE 2017). This means that the almost mica-free eclogite is difficult to excavate, also because of its mineralogy, and therefore requires more revolutions of the cutter head and therefore tool wear is higher.

In Addition to the eclogite layers, mushrooming occurred mainly in the area of fine grain gneisses. According to information from the construction company, the maximum cutter thrust was usually used in these rock masses to achieve the fastest possible advance rate. The data of WILFING (2016: 128) points out that in these sections in most cases rock chipping occurs, but not very efficiently. In such rock masses, the high cutter thrust causes deep indentation in the tunnel face, but the mixed tensile-shear fracturing process in the kerf will lead to high rolling forces and high torque (YIN et al. 2014) without generating chips effectively (VILLENEUVE 2017). This leads to increased wear, also because more revolutions of the cutter head are necessary. Data from VILLENEUVE (2017) suggest that by achieving the critical thrust, wear is very high, but the advance rate is only slightly increased.

In the Koralm Tunnel project, a tendency was to be seen for the effect of ring chipping to increase from the center cutters to the gauge cutters. GENG et al. (2017) confirms this trend and reports that the effect of extreme mushrooming with chipping primarily occurs on cutters in the outer region of the cutter head. Under extreme rock conditions, however, inner face cutters also showed severe mushrooming with chipping. There are two main reasons for this: An increase in the rolling velocity towards the outside and thus a more dynamic load on the cutters (LINDHOLM et al. 1974; SANO et al. 1981; ZHANG et al. 2000; GENG et al. 2017) and a higher rock strength due to the stress distribution on the tunnel face (RAUCH 2016; LAGGER et al. 2015). In our opinion, a combination of both arguments is responsible for the strong mushrooming and ring chipping in the Koralm Tunnel project.

RAUCH (2016) has also shown in his thesis that the outer disc cutters can reach temperatures of over 100 °C. It should be noted that for operational reasons the temperature measurement could only be taken about 5 minutes after the end of the excavation process. Accordingly, a significantly higher temperature than 100 °C can be assumed. Such high temperatures can contribute to alterations in the cutter rings and promote mushrooming and chipping.

Tapering and grooving

Scientists agree that the cutter rings in rather soft rocks become sharper through a self-sharpening process. Due to the usually low strength, high penetration rates are often achieved. This goes so far that in such sections the advance force must be reduced so that the penetration permitted by the machine is not exceeded. Exceeding this limit would lead to problems with the removal of the excavated rock material. It is doubtful that the rock material cannot be removed in front of the cutter head, which means that the cutters and the cutter head itself are in contact with loose rock, which increases wear. This must be avoided.

The self-sharpening process depends on the interaction between the cutter and the rock (and its geotechnical properties). If the width of the cutter has already increased because of progressive wear, it can also lead to grooving (ELLECOSTA et al. 2018). Grinding marks on the grooves oriented transverse to the cutting direction illustrate that the area of the grooves does not or only slightly participate in the cutting process and the cutter steel is removed due to the material flow to the flanks.

Brittle fracture & Blockage

Besides the abrasive wear types there are also the special wear types “brittle fracture” and “blockage”. They are called special wear types because they are not or only minimally caused by geological conditions.

Brittle fracture of a cutter ring can happen if the heat treatment was faulty or insufficient or not adapted to the geotechnical properties of the rock mass. Other possibilities could be an extreme dynamic overload due to rollover over metal parts, especially if this happens several times (fatigue, RÖTTGER et al. 2015). They can consist of metal parts that have fallen off, e.g. built-up welds, wear-protective material or disc cutter fragments.

There is a certain transitional area between chipping and brittle fracture. If the broken-off steel chips reach a certain size so that the cutter ring can no longer work properly, one can speak of brittle fracture, since such large steel chips should not break off.

The special wear type blockage appears when the roller bearing might be blocked, so that the cutter ring cannot rotate anymore and is abraded on one side. Manufacturers like Herrenknecht indicate that this generally can happen when stone dust and stone flour penetrate the seal and get into the bearing, or lubricating oil leaks out. Another reason may be unsuitable oil or overheating of the oil.

The Koralm Tunnel project featured an increase of both special wear types in fractured rock mass involving hard and solid rocks. MACIAS et al. (2017a) have discovered the same correlation. According to them, one reason might be that in fractured rock masses or in situations where extremely effective rock chipping occurs, the cutters will be exposed to large instantaneous loads. Under such conditions, a cutter ring exhibits a tendency to chip along its edge. Extensive ring chipping and high cutter thrust may result in bevel edge wear, loosened rings and blocked bearings. So, this corresponds to bearing overload.

An explanation for blockiness of the tunnel face could be high primary stresses. In order to excavate these kinds of rocks at all, very high contact pressures and force must be applied to the cutter ring. However, since only parts of the cutters come into contact with the tunnel face due to its blockiness, the permitted force per cutter is exceeded, and thus the likelihood of brittle fracture and blockage increases, also as a result of fatigue.

Furthermore, a common occurrence of these two effects was with cutters, which are located more in the outer area of the cutter head where the rolling speed is at its highest and the cutters undergo usually more cycles during operation. GENG et al. (2017) report that the high rolling velocity causes higher impact loads on the cutters and thus results in more intense ring chipping, cutter blockage and bearing damage due to fatigue. The same statements were also made for the Koralm Tunnel project in this thesis.

Possible reasons for increased wear

In the Koralm Tunnel project an increase of wear on cutters in the outer area of the cutter head was observed. There can be a variety of reasons for this. The first reason is the general excavation technique of hard rock TBMs. The excavated rock chips usually first fall down before they are transported via the muck buckets in/behind the cutter head. This causes the outer cutters to be pulled through the rock debris, which leads to increased wear and also to an increase in temperature. That this influence can be quite pronounced is illustrated in Fig. 100.

It is known that the energy required for dynamic rock fracture is markedly greater than that for static rock fracture (ZHANG et al. 2000). In this context e.g. LINDHOLM et al. (1974) and SANO et al. (1981) found out that rock strength increases exponentially with load rate. Considering the rock-breaking mechanism of TBM disc cutters where the chips are formed due to the propagation of the lateral cracks driven by the contact of the cutter tip, high rolling

velocity may have adverse effect on the rock breaking since time is required for the energy accumulation and dissipation, as well as the crack initiation and propagation in the rock (MACIAS 2016; GENG et al. 2017). The faster a cutter rolls over the tunnel face, the more energy must be applied for rock cutting. This means that the rock in the outer parts of the tunnel face is more difficult to be fractured than the rock in the inner and middle parts for hard rock TBMs due to the higher rolling speed of the outer cutters. (GENG et al. 2017)

Fig. 100: Accumulation of rock debris in the area between the cutter head and the tunnel face.

Besides, the high rolling velocity causes higher impact loads on the cutters in the outer part of the cutterhead, which may result in additional cutter consumption due to ring chipping, cutter block and bearing damage (GENG et al. 2017).

Previous research of WILFING (2016) and RAUCH (2016) on the Koralm Tunnel project pointed out that there is an influence of primary stresses on wear and the penetration rate. In this context, LAGGER et al. (2015) was able to show with the help of numerical simulations that a stress arc is formed in the edge area of the tunnel face (approximately in the outer 20 % of the tunnel radius). The main stresses are about three times as high as the primary rock stresses in the edge area of the tunnel face. In the center of the tunnel face the principal stresses decrease by about 20 %.

7.1.2 Microscopic wear

The microscopic analysis of the cutter rings illustrated that there are definitely differences between the individual manufacturers (chapter 4.4.1, Fig. 41). However, as all the examined cutters were made of the same material, the differences are mainly due to different heat treatment. HASSANPOUR et al. (2014) had similar experiences with a TBM tunnel project: Due

to some limitations for providing standard high-quality disc cutters, the contractor was forced to use low quality cutters made by third party manufacturers. Sections, where these cutters were used, featured higher tool wear.

Alignment of crystallites

The microscopic analysis could illustrate that, as was to be expected, there was a deformation of the steel and an alignment of the crystallites, especially in disc cutters with mushrooming. This seems plausible, in so far as these cutter rings were probably exposed to the highest contact forces and macroscopic deformation already occurred. Nevertheless, other forms of wear also show a structural change, although this usually does not extend as deeply into the steel.

The deformations in steel are always accompanied by an alignment of the crystallites in the steel. The deformation results in brittleness, so that these areas are very often the starting point of cracks. Grooves or generally imperfections in the surface of the cutter rings enhance this effect, as such areas are weak points. This is comparable to screws, whose failure always starts from the bottom of a groove. It could be revealed that for the wear type mushrooming with chipping the cracks start slightly below the mushroom head at the shoulder of the cutter ring and progress towards the center, leading to the detachment of the steel chips.

Micro penetration & surface mixed layer

The microscopic analysis of the surface of the cutter rings could prove that the phenomenon of micro-penetration occurs with practically every macroscopic type of wear. However, a certain minimum contact pressure of the disc cutters against the tunnel face seems to be a prerequisite for this.

The EDX analyses verify that the particles or rock fragments that penetrated the steel were mostly quartz. However, it is generally conceivable that any mineral which is harder than steel can penetrate the steel. In the case of the rocks of the Koralm Tunnel, besides quartz it also may be feldspar. The accumulation of quartz that has penetrated the steel can be attributed not only to its hardness but also to its non-existent fissility and conchoidal fracture. This produces sharp-edged and hard fragments that can penetrate the steel.

The penetration of minerals into the cutter ring leads to a deformation of the steel. Microscopic images could demonstrate that base-failure-like shear planes are formed by the displacement of the steel.

In the investigated cutter rings of the Koralm Tunnel project a large part of the cutter tip was covered by rock particles / minerals. In the literature this phenomenon is known under the term "contact mixed layer" or “intermixed layer” (BESTE et al. 2008). However, BESTE et al. (2008) has discovered this effect in WC and CC drill buttons so that the transferability to disc cutter steel is limited.

According to BESTE et al. (2008), the intermixing of rock material and drilling material is facilitated by extreme local conditions of temperature and pressure associated to the intense intermittent contact between drill button and rock material. Each local rock impact results in a compressive shock wave and an associated high-temperature wave, induced by intense friction and plastic deformation despite active cooling (BESTE et al. 2008).

In addition, BESTE et al. (2008) found out that the intermixed layers grow with increasing drill depth and the resulting growth rate is determined by the competition between penetration rate and wear of the surface layer. Low wear rates result in deeper penetration of the rock particles (BESTE et al. 2008).

PETRICA et al. (2013) carried out laboratory tests to analyze wear mechanisms and their relation to rock properties. In a test with a 3-body abrasion contact with different abrasives, the authors observed that a heavily deformed wear surface was formed. They described the wear mechanisms as scratching and grooving combined with multiple indentations due to rolling/sliding particles of granite and they assume that indicated pronounced grooving is caused by hard quartz particles based on crushed granite.

Under 2-body conditions, PETRICA et al. (2013) reports that wear mechanisms such as ploughing and cutting dominate using granite. A mix of plastic deformation and particle embedment for meta-sandstone and abrasive embedment characterizes the interaction between sandstone and the tested specimens (PETRICA et al. 2013). Uniaxial compressive strength (UCS) can be seen as a mechanical rock property that describes the wear behavior under 2-body conditions. Thus, it can be concluded that rocks with high UCS values, as in the case of granite, produce mechanisms such as cutting or ploughing. A medium UCS value, as in the case of meta-sandstone, for example, produces plastic deformation and abrasion grooves. Rocks with low UCS values lead to a pronounced abrasive embedding within the metallic surface. (PETRICA et al. 2013)

Transferring the results to TBM excavation of the Koralm Tunnel, a combination of 3-body abrasion and 2-body abrasion may be assumed.

The formation of a contact mixed layer leads to a change in the steel surface and the material properties set during heat treatment. The formation of shear planes creates zones of weakness in the cutter tip. The continuous rolling of the cutter during operation can cause the shear planes to act as predetermined failure areas (fatigue). This leads to increased wear.

A reduction of the intermixed layer effect might be possible, if cutter head sprinkling is used. According to MIRKOWSKA et al. (2016), a change in humidity can modify the interaction of the surfaces due to a small water layer, which changes adhesion and friction. This could help to reduce wear.

White etching effects

Our own data point out that every macroscopic type of wear can exhibit white etching effects in some way (chapter 6.3.3, Fig. 73, Fig. 74 and Fig. 75). White areas normally consist of ultrafine, nano-recrystallized, carbide-free ferrite or ferrite with a very fine distribution of carbide particles and are around 10 to 50 % harder than the unaffected microstructure.

This effect was to be expected for cutters with a blockage. Grinding on the rock surface of the tunnel face was sometimes so pronounced that an increase in temperature until annealing must be assumed. Cutter rings with such a wear shape possessed white etching areas up to 0.6 mm wide, which represent a new hardening zone. Underneath there is usually a darker edge, which indicates mineral reactions and corresponds approximately to a tempering zone with a width of several millimeters.

Besides the wear shape blockage, abrasive wear and tapering featured white etching effects. The thickness of the uppermost bright and structureless area ranged from a few micrometers up to about 10 to 15 µm. In contrast to the blockage example, the white layer here usually has a very sharp border to the underlying, almost unchanged structure.

As known in literature (e.g. SOMMER et al. 2014: 224), such white etching areas have high tensile stresses. The rolling process of the cutters during operation produces high dynamic load on the cutter tip where the white etching areas are located. Due to the high tensile stresses, these areas are susceptible to the formation of micro cracks. These cracks grow and cause a detachment of thin steel layers which has been proven by some microscopic images (chapter 6.3.3, Fig. 74 and Fig. 75). Therefore, the internal stresses seem to play a major role in areas with white etching effects.

The formation of white etching areas again means a change in the steel and its original material properties. The superficial hardening is accompanied by embrittlement. In addition, strong tensile forces are formed which can lead to increased material removal which means increased material removal in return. A lowering of the tool temperature by sprinkling the cutter head with water during operation and a reduction of the cutter head RPMs could reduce this effect.

In the case of very extensive white etching areas with a strong, sustained heat input under a normal atmosphere with oxygen, overlapping with the effect of decarburization may also occur. As a result, ferrite accumulates, and the amount of carbides is reduced. This results normally in lower hardness values due to the lack of carbides.

Special effects

The phenomena summarized under the term special effects occurred only individually or under special conditions, which is why they can only be dealt with in part.

The first special effect is a kind of delamination of the steel (chapter 6.3.4, Fig. 76). The formation of such structures can probably be explained by cutting very hard and solid rock or

rolling over metallic parts. This effect is wear-relevant where this occurs, since such a delaminated area can take up virtually no load and increased material removal occurs.

The second special effect is the formation of a distinct intermixed layer which is illustrated in Fig. 77. Due to a very extreme deformation of a steel chip, a mixture of rock material and steel occurred, which is settled on the cutter tip. Where this effect occurs, it is also relevant to wear, as increased material removal can be assumed.

The third special effect shows cracks (Fig. 78). Here it could be demonstrated that the deformation of steel is always accompanied by an alignment of the microstructure, usually along individual paths. Along these paths, the movement causes hardening and embrittlement, which usually causes increased material removal.

An extreme example of cutter ring mushrooming with chipping occurred on cutters that have run on interlayered eclogite rock. These indicate a clear shell-like detachment of the surface, which is probably caused by the strong contact forces and the extreme dynamic load (Fig. 79). The images clearly illustrate that the cracks are forming on the outside and are going towards the cutter center.

The last special effect is independent of the wear processes itself, because it appears on fresh and unused disc cutters. This cutter ring features the effect of surface oxidation (grain boundary oxidation) with a thickness of around 20 µm (Fig. 80), which is an effect caused by the heat treatment and has an effect on the hardenability of the surface. The surface and edge hardness are normally lower than the hardness of the specimen. Due to the formation of such a soft skin, a lower wear resistance must be expected. Due to the low thickness of about 20 µm, it can be assumed that this layer is ground down relatively quickly during operation and that increased wear occurs only initially.

7.1.3 Optimization potential

This chapter provides an overview of the reasons for high wear and in particular presents ways in which a hard rock TBM drive could be optimized in terms of cutter wear.

Penetration rate & cutter thrust

As already partly discussed in previous chapters, stresses have an influence on the wear rate. Stresses in the rock mass can lead to both increased and decreased penetration. This is usually accompanied by increased or reduced wear.

In an investigation, VILLENEUVE (2017) found out that stress induced face instability can improve the penetration rate, in these two cases by 14 % and 19 %, respectively, making it easier to generate chips or creating larger blocks (GONG et al. 2012). But these measures do not capture the negative impacts of stress-induced face instability (VILLENEUVE 2008; GONG et al. 2012; YIN et al. 2014).

But there is also the possibility that stresses hinder fracture propagation so that the penetration is less (VILLENEUVE 2015; WILFING 2016). This is mainly the case when the stress is orientated parallel to the tunnel face and greater than 20 % of UCS (VILLENEUVE 2015). This was probably partly the case within the Koralm Tunnel project. The high primary stresses did not lead to a preconditioning of the tunnel face, so that the stresses decreased the penetration and increased the wear.

VILLENEUVE (2017) could also prove that geological characteristics play an important role in both the chipping process and stress-induced face stability. Both properties ultimately have a decisive influence on wear. According to VILLENEUVE (2017), rocks with well-defined fabric, oriented oblique to the tunnel face, were easier to be excavated and were more sensitive to stress-induced face instability than rocks without fabric or fabric oriented perpendicular to the face. In the Koralm Tunnel project, the rock fabric was mostly well developed and oriented oblique to the tunnel face over long distances. This means that the rock of the Koralm Tunnel had an increased susceptibility to stress-induced face stability.

In addition, VILLENEUVE (2017) noticed out that rocks with very high mica content were easier to be excavated but were less sensitive to stress-induced face instability than rocks with a moderate mica content. This explanation confirms the results in this study, where face instabilities hardly occurred in the mica-rich schistose gneisses but often in the area of fine grained gneisses and platy gneisses. In the area of schistose gneisses, the wear type tapering dominated. In sections of the fine-grained gneisses and platy gneisses mushrooming dominated, often with chipping, whereby the overburden was sometimes several hundred meters higher.

According to VILLENEUVE (2017), there are rocks which tend to be excavated via the grinding process. The critical thrust point which must be exceeded for effective rock cutting and the slope of the curve during chipping (as discussed in SAMUEL & SEOW 1984; ZHANG et al. 2003; GEHRING 2009), are related to rock strength, brittleness, mineralogy and fabric (VILLENEUVE et al. 2007, 2012; VILLENEUVE 2008), and the stress at the tunnel face (YIN et al. 2014). In the Koralm Tunnel project, some compact gneisses and other rock types like eclogite interstratifications belong to these rock types.

On such rocks, very little gain in penetration rate can be achieved by applying higher thrust, and wear and cutter damage could be minimized by lowering the thrust without substantially reducing the penetration rate. Chipping-dominated excavation may never be achieved in these rock types with very high strength, even if cutter thrust limits were increased, as the process will remain too energy intensive due to the high fracture initiation threshold and the poor fracture propagation in these rocks. (VILLENEUVE 2017)

TBM design

In addition to penetration and cutter thrust, the design of the TBM and the used cutters also have a decisive influence on wear. For example, the TBM design parameters limit the steady-state penetration rate, which defines performance limits (VILLENEUVE 2017).

The penetration limit is a function of muck conveyance, bucket design, cutter wear and the maximum head revolution speed (FRENZEL et al. 2012). The torque limit provides the transition from the penetration limit to the maximum thrust (FRENZEL et al. 2008), which is a function of the rotational speed and is controlled by the maximum torque capacity. The thrust limit is controlled by cutter type, maximum thrust capacity and TBM head design. The penetration limit for the TBM used in the Koralm Tunnel project KAT 2 is approximately 14 mm/rev. The torque limit for the TBMs in this study is approximately 30 % of the maximum torque capacity. The maximum net thrust on 432 mm cutters (17 inch) is typically around 267 kN (FRENZEL et al. 2008; MAIDL et al. 2008). (VILLENEUVE 2017)

However, in many cases it is necessary to reduce thrust and cutter head rotation on the TBM in order to optimize mucking out, prolong tool life, and avoid damage to the machine (MACIAS et al. 2014). According to STEINGRIMSSON et al. (2002), mixed face conditions influence machine design, tunnelling layout, actual penetration rate, machine utilization, and cutter life (MACIAS et al. 2014). Especially when the tunnel face is blocky and face instabilities occur, the time required to clear blocks as well as additional wear on TBM should be considered (VILLENEUVE 2015).

Due to the very small rotary radii of the cutters close to the center, mostly severe side sliding on the tunnel faces dominates. This can already be seen macroscopically by grooves in the cutter tip perpendicular to the cutting direction. This causes an increased material removal because the cutter only performs a very incomplete rolling movement. According to GENG et al. (2017), the side sliding wear of the inner cutters might be reduced by increasing the cutter spacing and decreasing the cutter distribution density.

Based on additional research, GENG et al. (2017) suppose that for hard rock TBMs the 2-spiral layout pattern (Fig. 2) is found to be the best one.

Aspects of materials science

From a materials science point of view, not only the proportion of hard structural components (carbides, borides or nitrides) is decisive, but also their size. According to KÜPFERLE et al. (2016a), small hard phases are insufficient for wear protection and will be worn out together with the metal matrix by the abrasives if coarse abrasives and a high normal load are present.

Typical hard phases form e.g. pearlite grains which contain the hard iron carbides of the Fe_3C type. Materials containing carbides, such as those used for cutter rings, have a high hard phase volume content (preferably chromium carbides of type M_7C_3 (BERNS & THEISEN 2008)). Depending on the morphology, size and distribution of the hard phases, these

can protect the softer metallic matrix (martensitic, bainitic, pearlitic/ferritic) against material removal. (KÜPFERLE et al. 2015)

KÜPFERLE et al. (2016a) made CERCHAR tests with pins with a different hardness and found out that very hard pins with a hardness of > 900 VH (Vickers Hardness) did not necessarily result in lower CAI values. In this special case, higher CAI values can be explained by small hard phases in the metal matrix, which increase the overall hardness of the material but possess insufficient wear resistance against coarse abrasives (KÜPFERLE et al. 2016a).

This means that the wear resistance of a fully metallic microstructure (ferritic, bainitic, martensitic steels) can be improved by the presence of hard phases like carbides, borides, or nitrides (BERNS & THEISEN 2008; KÜPFERLE et al. 2016a). KÜPFERLE et al. (2016a) mentions that hard phases only increase the wear resistance of the material if they are adapted to the respective tribological system. In this manner, the size of the hard phases should be as large as the groove width of the abrasives and the hard phase hardness should be equal or higher to those of the abrasives (KIEFFER & BENESOVSKY 1965; KÜPFERLE et al. 2016a). If coarse abrasives act with a simultaneously high load, smaller hard phases can be removed by the abrasives together with the metal matrix (BERNS 1998; KÜPFERLE et al. 2016a).

7.2 Hardness testing

7.2.1 TBM disc cutter

Microhardness and low-force hardness

Microhardness and low-force hardness tests proved that the analyzed cutter steel possesses the indentation size effect. According to ONDRACEK (1995: 187), only the plastic deformation of the material is measured with the performed Knoop and Vickers hardness tests. When using low test loads, the elastic part of the deformation is high and normally small indentations occur or a high hardness has been calculated. With an increasing load, the plastic part of the deformation grows while the elastic parts decreases. This occurs with rising test load until a material-specific limit is reached, where the ratio stays constant (ELLECOSTA et al. 2015).

Comparing Knoop and Vickers hardness, it was demonstrated that Knoop hardness increased almost exponentially at very low loads. Vickers hardness was more constant. The difference can be explained by the different indenter geometry. The Vickers indenter is a square pyramid with a relatively pronounced tip, so that it penetrates deeper into the material in relation to its size. The Knoop-indenter, on the other hand, consists of an elongated and much less pointed pyramid, which leads to significantly lower penetration depths in relation to size.

This difference leads to the fact that the Knoop-indenter is much more sensitive to lower loads, i.e. the indentation size effect, and the hardness increases much more at lower loads. This statement is initially limited to largely ductile materials such as the analyzed cutter rings.

Hardness mapping & hardness profiles

Hardness tests on cutter rings of the Koralm Tunnel project pointed out that the excavation process changes the steel and its properties, such as hardness. During the microscopic analysis a change in hardness was already claimed, which could now be proven. In most cases a hardening could be proven. This is also accompanied by embrittlement, which can lead to additional material removal.

As was to be expected, the macroscopic wear shape mushrooming featured the deepest hardening of several millimeters, as this is also where the strongest deformations took place (Fig. 82).

The cutters showing brittle fracture indicated a significantly higher hardness in the upper region where the contact with the rock takes place than in the lower part (Fig. 84). In our opinion this means that the upper and thinner part of the cutter ring has a higher hardness due to the heat treatment. Presumably, this should increase the wear resistance. However, since the greater hardness also means less toughness and greater brittleness, the probability of brittle failure has been increased. Due to the geotechnical properties of the rock, the occurring, partly dynamic loads were too strong, which led to a fracture of the complete cutter ring.

Amazingly, the macroscopic wear type abrasive wear and tapering also featured a noticeable hardening (Fig. 86). However, the thickness of this layer was only about 2 mm at most.

Due to the indentation size effect, the micro and low-force hardness of the cutters is significantly higher than the average hardness of 630 HV, which was determined with test loads of 30 kg (HV30) and 125 kg (HV125).

7.2.2 CERCHAR pins & LCPC impellers

Microhardness and low-force hardness

A comparison of the microhardness and the low-force hardness pointed out that, as in the case of the cutter rings, the indentation size effect occurs. Here again, the Knoop hardness is higher than the Vickers hardness and rises significantly more at low loads.

It was astonishing that two different CERCHAR pins had significantly different hardness values. According to KÄSLING & PLINNINGER (2016) this must not be the case. A conversion to the specification 55 HRC ± 1 according to DIN EN ISO 18265 (2014) was not possible because too low loads were applied.

The difference between the two CERCHAR pins can only be explained by a different heat treatment, as both pins are made of the same steel grade. This is clearly a case for a better quality monitoring of the steel tampering.

Vickers hardness of LCPC-impellers

Also, the evaluation of the hardness of two different LCPC-impellers indicated different values. A conversion according to DIN EN ISO 18265 (2014) was allowed due to the higher test loads and resulted in a hardness of 95.2 and 78.5 HRB.

According to AFNOR (2013) a hardness of about 60-75 HRB must be maintained. This means that both impellers are not officially allowed to be used for this test.

The difference can be explained both by a different steel grade and a different heat treatment. In this case too, better quality monitoring would be required in using the correct steel grade and tampering.

7.2.3 Testing of minerals and rocks

The reason why this work also deals with hardness tests on minerals and rocks is that other researchers like MACIAS et al. (2016) and HASSANPOUR et al. (2014) have found a strong influence of mineral and rock hardness on tool wear. In addition, own investigations showed that especially hard minerals penetrate the surface of disc cutters.

First of all, it should be mentioned that hardness testing on minerals and rocks is not standardized, as these are usually very brittle materials. This results in cracks, which have a significant influence on the indentation size and thus also on the calculated hardness value.

However, the present approach was to create cracks in the minerals and rocks and to accept their influence, since a TBM disc cutter also creates cracks during the excavation process permanently.

Microhardness and low-force hardness

The use of low loads of up to 500 g usually produced very well evaluable indentations in the tested minerals and rocks . Due to the low load, the resulting indentation is usually so small that a single crystal hardness is often determined. Depending on the brittleness, cracks already appeared here. The tendency for the Knoop-indenter to produce fewer cracks under the same load was confirmed. Accordingly, the Knoop hardness was mostly above that of Vickers.

Whether the Knoop or the Vickers hardness is better suited to determine mineral or rock hardness depends on the investigation target. In our opinion, the Knoop hardness is better suited if the influence of cracks is to play a minimum role. If a certain influence of cracks is to be accepted and considered, the Vickers hardness is the better choice.

It should also be noted that the indentation size effect is significantly stronger for Knoop hardness than for that of Vickers. This means that the hardness values of different loads cannot be compared with each other and that the Vickers hardness in relation is less influenced by the indentation size effect.

Since the Vickers hardness can also be performed with very large test loads, e.g. over 100 kg, it was decided to focus more on the Vickers hardness.

The comparison between the mineral calcite and the monomineral and extreme fine-grained Wiesenhofen limestone (TUM-WIE-6) pointed out that rock hardness is higher than mineral hardness. Monomineral and extreme fine grained flintstone (TUM-FLI-1) and mineral quartz behaved differently: in this case the mineral hardness was above the hardness of the rock. The difference can be explained by the fact that calcite has a perfect cleavage while quartz has no cleavage. If mineral cleavage can be activated due to indentation load, its hardness is also reduced. In the tested Wiesenhofen limestone, the cleavage of the calcite could not be activated due to its extremely fine grain size.

But the fact that the Vickers hardness of the investigated Wiesenhofen limestone and flintstone is higher than the Knoop hardness is astonishing and was not expected. An explanation for this could be again the grain size. The related minerals examined were mainly monocrystals, while the grain size of the rocks was very fine-grained. In monocrystals, individual cracks can spread much better because of the homogeneous atomic structure. In rocks, there are many individual crystallites with a different crystallographic orientation. Spreading of cracks beyond their grain boundaries requires additional energy and opposes crack propagation.

Influence of crystallographic characteristics and orientations

To demonstrate the influence of crystallographic orientation, two of the most common minerals in the upper earth's crust were selected: calcite and quartz. The difference between the two minerals is not only their significantly different hardness, but also the perfect cleavage of calcite while quartz has no cleavage.

Of both minerals, two specimens with different orientations were prepared from the same sample. For calcite, the orientation to the cleavage and for quartz the orientation to the crystallographic c-axis was decisive.

The analysis of the Vickers hardness with test loads of 1 to max. 60 kg illustrates that on average there was a difference in hardness of between about 5 and 10 %. This result clearly shows that the orientation of the mineral has an influence on its hardness. Accordingly, the crystallographic orientation of minerals should always be taken into account in hardness tests.

In the case of calcite, the surface of the specimen should be oriented perpendicular to the cleavage, whereas in the case of quartz, the surface of the specimen should be oriented parallel to the C-axis to determine the maximum hardness.

Vickers hardness test

The evaluation of the Vickers hardness tests on the selected minerals again features a clear indentation size effect (chapter 6.4.3, Fig. 88, Fig. 89 and chapter 6.4.4, Fig. 91). In the load range between about 10 and 50 kg, some minerals showed only a very slight decrease in hardness. Extreme hardness reductions occurred at the maximum load level of 72.5 kg (HV72.5), which is attributed to very large cracks and fractures in the indentation area.

Up to a test load of about 5 kg the occurring cracks were visible but did not represent a major obstacle for the evaluation. From a test load of about 5 to 10 kg, the formation of cracks could already be acoustically perceived during the hardness test. After the test had been carried out, the cracks could also be seen macroscopically. Sometimes strong outbreaks in the indentations area made an evaluation difficult and time-consuming. In addition, there was a certain subjective scope for interpretation when measuring the indentations.

It has been demonstrated that the actually high hardness of garnet (almandine, Moh's hardness of approx. 7-7.5), due to its high brittleness at high loads, sometimes even falls below the hardness of apatite. In contrast, pyrite with an actually lower hardness (Moh's hardness of approx. 6-6.5) usually featured the highest hardness values at test loads of 10 kg and higher. In our opinion, this is due to the higher toughness (lower brittleness) of pyrite.

The evaluation of the hardness of the calcareous rock types (chapter 6.4.4, Fig. 96) pointed out that the grain size has the greatest influence. The extremely fine-grained Wiesenhofen limestone possessed the highest hardness values. A direct comparison of the Carrara and the Laas marble demonstrated that the finer-grained Carrara marble had a slightly higher hardness. Thus, it could be revealed for monomineral rocks consisting of the mineral calcite that the smaller their grain size, the higher their hardness. It is quite similar with the strength and wear parameters of the tested rocks. The smaller the grain size, the higher the strength and the higher CAI and LCPC values are achieved on average. The higher CAI value of the Laas marble can be explained by the quartz content, which was detected by the thin section analysis.

The evaluation of the silicic rock types (Fig. 97) demonstrates the influence of the grain size as well as the influence of the grain bonding. Despite a very high quartz content, the Abtswind sandstone possesses only very low hardness, which is attributed to its clayey binding. Rocks like the vein quartz show very high hardness at low test loads. However, at loads of 10 kg and more, they drop very sharply, which is attributed to their brittleness. The hardness of these rocks can also usually be correlated relatively well with the strength and wear parameters of the rocks. The discrepancy in the CAI value of the flintstone can be explained by the fact that the conchoidal fracture surfaces are very smooth and the CERCHAR pin literally slides on the smooth surface so that the determined CAI-value is too low. This is also known as the ‘‘skating effect’’ and results in an underestimation of wear (ALBER et al. 2014; MACIAS et al. 2015).

In summary, it can be stated that the hardness of monomineral rocks is usually dependent on the strength and wear parameters, or is related and correlated to them, especially at test loads of 10 kg and higher. The reason for this is that the strength and wear parameters are only material parameters which, like hardness, depend on mineralogy and grain bonding.

The greater influence of rock hardness at higher test loads is related to the fact that larger indentations are produced, and their zone of influence no longer affects just a single mineral

grain, but usually several. Thus, not only a single crystal hardness, but also a structural hardness is determined (chapter 2.2.1, Fig. 11).

The investigation of the hardness of the crystalline rocks (polymineral rocks) revealed that there is a strong influence of the rock strength and the wear characteristics on their hardness. However, the prerequisite here is that similar rocks are compared with each other, e.g. granitoid rocks (granite and diorite).

In addition, the influence of the orientation of the foliation direction could be demonstrated on the Freiberg gneiss. The surface of the test specimen is oriented parallel and perpendicular to foliation. A direct comparison clearly points out that the test piece with the test surface perpendicular to foliation achieves higher hardness values. This is probably due to the fact that soft mica was increasingly tested during the test parallel to foliation. Only by testing the surface perpendicular to foliation is it possible to test all minerals according to their distribution in the rock.

In addition, testing of anisotropic rocks should always be carried out on surfaces perpendicular to foliation in order to determine the maximum hardness values and obtain results that are as reproducible as possible. Layered rocks should therefore not be tested on their layering surface, but perpendicular to it.

7.2.4 Cutters and rock types – comparison of hardness

The results of the Vickers hardness tests have proven that monomineral rocks can be characterized relatively well. The situation is different in the case of polymineral rocks, as these usually consist of a combination of soft and hard minerals. Although averaging may work, it cannot cover the range of minerals contained in the rock. Especially hard minerals, which are the main reason for high wear, are not adequately represented.

Based on an idea by CARDU & GIRAUDI (2012), the individual results of the hardness test of a load stage can be entered in a diagram according to their hardness value (cumulative frequency distribution). Since the main purpose is to determine a single crystal hardness, it was decided to use the relatively small and square Vickers indentation instead of the elongated Knoop indentation. A test load of 200 g (HV0.2) was determined based on CARDU & GIRAUDI (2012) and own results. By plotting the hardness values on a diagram (chapter 6.4.5, Fig. 99), a percentage distribution of the individual hardness values in the rock is obtained and it is relatively easy to see how many hard and soft minerals are contained.

Here, the question arises, why direct hardness tests are carried out at all, since the mineral content can also be determined by thin section microscopy or X-ray diffractometer analysis. On the basis of the mineral content, hardness distribution can also be established with the help of literature values, or the equivalent quartz content (EQC) or the Vickers Hardness Number Rock (VHNR) can be calculated.

In addition to the own findings, MACIAS et al. (2016) and HASSANPOUR et al. (2014) have found that the Vickers method is suitable for wear prediction and analysis. They also demonstrated in their own investigations that there is a strong relationship between cutter life and intact rock parameters like the VHNR and the uniaxial compressive strength (UCS). Consequently, the Abrasiveness index (ABI) was developed which is a multiplication of the VHNR and the UCS (HASSANPOUR et al. 2011, 2014). Instead of the VHNR, the Vickers hardness should be determined directly via the cumulative frequency distribution to get more accurate results.

Our own investigations could prove, however, that there is a strong variance in hardness, e.g. for calcite, depending on grain size. If only the hardness value from literature is used, this is a rather strong simplification which does not correspond to reality. Also, the influence of the crystallographic orientation is not considered. Accordingly, hardness tests on rock samples, as carried out in this work, are much more accurate. A combination of the presented method with already existing wear prediction models would be significant for further development.

A further advantage of the presented cumulative frequency distribution according to CARDU & GIRAUDI (2012) is that the hardness of excavation tools or CERCHAR pins or LCPC impellers can be shown and directly compared. Thus, it is immediately recognizable at first glance which rock is harder than the tool steel and thus has the potential to cause wear.

According to TABOR (1954) a mineral or rock with a hardness difference of about 20 % can cause extreme wear on the excavation tool when it is higher and only low wear when the hardness is 20 % lower. This 20 % range can be plotted very easily and quickly into the hardness diagram. In order to check whether a rock has the potential to cause heavy wear or whether only very little wear is to be expected, the proportion of the respective rock above and below the 20 % line must be considered. This can be checked easily and quickly.

With this procedure it is possible to compare each material directly with the given rock material and make an initial wear forecast. It should be noted here that usually only the abrasive wear can be determined. Stronger wear as a result of excessive hardness and a resulting brittle fracture cannot be predicted with this method.

8. Conclusion

The efficiency of rock excavation in TBM tunnelling is strongly dependent on the tribological processes that occur between the excavation tool and the rock. The more accurately the interaction of both partners is known, the better the wear prediction can be performed. But in practice, it is difficult to study the contact area of TBM disc cutters at the tunnel face during active tunnel excavation (ELLECOSTA et al. 2017). Due to the high contact stresses and the rotational movement of the cutter head and the cutter rings themselves, it is extremely difficult to install sensors or measuring devices in the contact area or to route sensor signals backwards to a data logger (ELLECOSTA et al. 2018). First attempts were made, e.g. by ENTACHER (2013) and SCHULLER et al. (2015).

Worn tools provide information about the tribological processes on the basis of the wear phenomena that occur. This requires a precise macroscopic and microscopic analysis. Microscopic analysis must not be based solely on observation of the surface of worn excavation tools. Rather, deeper changes in the structure must also be taken into account. For this purpose, it is necessary to prepare metallographic sections and to analyze the structure of the steel. Only in this way it is possible to visualize wear phenomena below the surface.

In order to be able to grasp wear induced changes of the cutter ring structure not only qualitatively but also quantitatively, the use of hardness tests is useful. These can also be used for the classification of steel grades. Depending on the selected load during hardness testing, a micro-hardness can be determined up to a "normal" hardness – with high loads. In order to ensure the greatest possible comparability, hardness testing according to Vickers is recommended. With this method it is possible to generate very small indentations and thus also to show possible wear induced changes of the excavation tools, especially in the area of cutter tip close to the edge.

In order to keep measurement errors during hardness testing to a minimum, higher test loads such as 30 kg (HV30) or 125 kg (HV125) are recommended. With these test loads it is also possible to convert the Vickers hardness into other hardness data according to DIN EN ISO 18265 (2014). In this way, the results of the Vickers hardness can be easily and quickly compared with the frequently used Rockwell hardness. A prerequisite for this is that the steel types of the cutter rings are known. If necessary, this can be determined in advance by spark spectroscopy.

A not entirely new approach is to determine the wear potential of a rock using hardness tests. The present study focuses on the indentation hardness according to Vickers and Knoop. Older studies such as TAYLOR (1949) and TOURENQ (1966) already have compared the minerals of the Mohs' hardness scale with Vickers hardness. Nevertheless, there is very little information about mineral and rock hardness in literature.

The same applies to recommendations on how to perform indentation hardness tests on minerals and rocks. One of the biggest problems of hardness testing on minerals and rocks is

that they react very brittle. Cracks have a decisive influence on the indentation size and thus the hardness value. With regard to the excavation process of a TBM, however, it should be noted that cracks are also produced in the rock and are therefore acceptable.

Despite all the limitations, the present study was able to show that the Vickers hardness test with loads up to 72.5 kg (HV72.5) is possible and can be evaluated. At high test loads there is usually a large influence of rock strength on the hardness value and a good correlation with wear parameters. At low test loads the influence is much less and the tendency is to determine a mineral hardness.

In addition, the indentation size effect could be proven on minerals and rocks as well as on cutter rings of the Koralm Tunnel project. This means that different test loads produce different hardness values on the same material. Accordingly, the same test load must always be used for a corresponding hardness analysis. In the course of the investigation, 200 g (HV0.2) turned out to be the ideal testing load.

In 1985 SALMINEN & VIITALA determined the Vickers Hardness Number Rock (VHNR) in order to draw conclusions about the wear potential of a rock material from the Vickers hardness. Today's approaches for a wear prediction consist of linking at least two relevant parameters. In the case of rock hardness this is the VHNR and the uniaxial compressive strength (UCS). From this the Abrasiveness index (ABI) can be calculated (HASSANPOUR et al. 2011, 2014).

However, the weak point is that the determination of the VHNR is based on a modal analysis of the mineral content and on literature values for the mineral hardness. This study could show that differences in hardness caused by grain size or crystallographic orientation cannot be taken into account. Accordingly, the VHNR should be determined directly on a rock specimen.

However, in this thesis a faster and easier way to determine the wear potential of a rock is presented. It is based on the idea of the cumulative frequency distribution of CARDU & GIRAUDI (2012). The major advantage of this method is that the hardness tests are performed directly on a rock specimen and a direct comparison with the hardness of excavation tools is also possible. Thus, changes due to wear can also be taken into account. In addition, the necessary parameters can easily be determined in the preliminary stages of tunnelling projects.

Besides to all advantages mentioned, rock mass influence is not included in the developed hardness methods. However, these have a considerable influence on the advance rate and wear, so they should be taken into account. One possibility is to develop a new cutter life prediction model that includes rock mass and hardness parameters. Another possibility is to revise an existing wear prediction model and include rock mass and hardness parameters.

9. Bibliography

AFNOR (1990): Normalisation Française P18-579 (12/1990): Granulats: Essai d'abrasivité et de broyabilité. – 9 p., Paris (afnor groupe).

AFNOR (2013): Granulats: Essai d'abrasivité et de broyabilité (NF P18-579). – 8 p. Paris (afnor groupe).

ALBER, M. (2008): An Integrated Approach to Penetration, Advance Rates and Disc Cutter Wear for Hard Rock TBM Drives - Ganzheitlicher Ansatz zur Abschätzung von Penetration, Vortriebsleistung und Diskenmeißelverschleiß von Vortrieben mit Hartgesteins-TBM. – Geomechanics and Tunnelling, 1 (1): pp. 29–37.

ALBER, M., YARALI, O., DAHL, F., BRULAND, A., KÄSLING, H., MICHALAKOPOULOS, T.N., CARDU, M., HAGAN, P., AYDIN, H. & ÖZARSLAN, A. (2014): ISRM Suggested Method for Determining the Abrasivity of Rock by the CERCHAR Abrasivity Test. – Rock Mech Rock Eng, 47 (1): pp. 261–266.

ANDERSEN, T., ERAMBERT, M., LARSEN, A.O. & SELBEKK, R.S. (2013): Petrology of nepheline syenite pegmatites in the Oslo Rift, Norway. – Mineralogia, 44 (3-4): pp. 61–92.

ANTONOV, M., HUSSAINOVA, I., VEINTHAL, R. & PIRSO, J. (2012): Effect of temperature and load on three-body abrasion of cermets and steel. – Tribology International, 46 (1): pp. 261–268.

ASTM D2938 (2002): Standard Test Method for Unconfined Compressive Strength of Intact Rock Core Specimens. – 3 p., West Conshohocken (ASTM International).

ASTM D3967 (2008): Test Method for Splitting Tensile Strength of Intact Rock Core Specimens. – 4 p., West Conshohocken (ASTM International).

ASTM D7012 (2014): Standard Test Methods for Compressive Strength and Elastic Moduli of Intact Rock Core Specimens under Varying States of Stress and Temperatures. – 9 p., West Conshohocken (ASTM International).

ASTM D7625 (2010): Test Method for Laboratory Determination of Abrasiveness of Rock Using the CERCHAR Method. – 6 p., West Conshohocken (ASTM International).

BADISCH, E., KATSICH, C., WINKELMANN, H., FRANEK, F. & ROY, M. (2010): Wear behaviour of hardfaced Fe-Cr-C alloy and austenitic steel under 2-body and 3-body conditions at elevated temperature. – Tribology International, 43 (7): pp. 1234–1244.

BALCI, C. (2009): Correlation of rock cutting tests with field performance of a TBM in a highly fractured rock formation. – Tunnelling and Underground Space Technology, 24 (4): pp. 423–435.

BARGEL, H.-J. & SCHULZE, G. (2005): Werkstoffkunde. – 9th edition, 441 p., Berlin (Springer).

BARTON, N. (2000): TBM tunnelling in jointed and faulted rock. – 1st edition, 173 p., Rotterdam (Balkema).

BARZEGARI, G., UROMEIHY, A. & ZHAO, J. (2015): Parametric study of soil abrasivity for predicting wear issue in TBM tunneling projects. – Tunnelling and Underground Space Technology, 48: pp. 43–57.

BAYER, M. (1997): Die Himmelfahrt Fundgrube: Ein Führer durch das Lehr- und Besucherbergwerk der TU Bergakademie Freiberg. – 144 p., Freiberg (Druckspecht).

BECKER, H. & LEMMES, F. (1984): Gesteinsphysikalische Untersuchungen im Streckenvortrieb. – Tunnelling, 2: pp. 71–76.

BECK-MANNAGETTA, P. (1952): Zur Geologie und Paläontologie des Teriärs des unteren Lavanttals. – Verhandlungen der Geologischen Bundesanstalt Wien, pp. 1–102.

BECK-MANNAGETTA, P., EISENHUT, M., ERTL, V. & HOMANN, O. (1991): Geologische Karte der Republik Österreich 1 : 50.000 - Blatt 189 Deutschlandsberg. – Vienna (Geological Survey of Austria).

BEJARI, H. & KHADEMI HAMIDI, J. (2013): Simultaneous Effects of Joint Spacing and Orientation on TBM Cutting Efficiency in Jointed Rock Masses. – Rock Mech Rock Eng, 46 (4): pp. 897–907.

BENJUMEA, R. & SIKARSKIE, D.L. (1969): A note on the penetration of a rigid wedge into a nonisotropic brittle material. – Int. J. Rock Mech. Min. Sci. Geomech. Abstr. , 6 (4): pp. 343–352.

BERNS, H. (1998): Hartlegierungen und Hartverbundwerkstoffe. – 329 p., Berlin (Springer).

BERNS, H. & THEISEN, W. (2008): Eisenwerkstoffe - Stahl und Gusseisen. – 4th edition, 417 p., Berlin (Springer).

BESTE, U., JACOBSON, S. & HOGMARK, S. (2008): Rock penetration into cemented carbide drill buttons during rock drilling. – Wear, 264 (11-12): pp. 1142–1151.

BHUSHAN, B. (2000): Modern tribology handbook. – 1st edition, 1760 p., Boca Raton (CRC Press).

BIENIAWSKI, Z.T., CELADA TAMAMES, B., GALERA FERNÁNDEZ, J.M. & ÁLVAREZ HERNÁNDEZ, M. (2006): Rock Mass Excavability (RME) indicator: new way to selecting the optimum tunnel construction method. – Tunnelling and Underground Space Technology, 21 (3-4): pp. 237–244.

BIENIAWSKI Z.T., CELADA C.B., GALERA J.M. & TARDAGUILA I.G. (2009): Prediction of cutter wear using RME. – In: International Tunnelling and Underground Space Association (ITA-AITES) (ed.): ITA-ITAES World Tunnel Congress, Budapest, Hungary, May 23–28 2009, pp. 1–7, Lausanne (ITA-ITAES).

BILGIN, N., COPUR, H. & BALCI, C. (2014): Mechanical excavation in mining and civil industries. – 366 p., Boca Raton (CRC Press).

BLINDHEIM, O.T. (1979): Boreability predictions for tunneling. –PhD-thesis, Department of geological engineering, Norwegian Institute of Technology (NTNU), 406 p., Trondheim (NTNU).

BLUMENAUER, H. & PUSCH, G. (1993): Technische Bruchmechanik. – 3rd edition, 28: 244 p., Leipzig (Deutscher Verlag für Grundstoffindustrie).

BOWDEN, F.P. & TABOR, D. (1951): The Friction and Lubrication of Solids. – Science, 113 (2938): pp. 443–444.

BRENNER, D. (2015): Untersuchungen zum Einfluss der Härte und Struktur von Rollmeißeln auf deren Verschleißform. – unpublished Bachelor's thesis, Chair for engineering geology, Technical University of Munich, 406 p., Munich (TUM).

BROOK, N. (1993): The measurement and estimation of basic rock strength. – In: HUDSON, J.A. (ed.): Rock testing and site characterization. – 1st edition, Comprehensive rock engineering, 3: pp. 41–81, Oxford (Pergamon Press).

BRULAND, A. (1998a): Hard rock tunnel boring - Vol. 3 - Advance rate and cutter wear. – PhD-thesis, Faculty of Engineering Science and Technology, Norwegian Institute of Technology (NTNU), 54 p., Trondheim (NTNU).

BRULAND, A. (1998b): Hard rock tunnel boring - Vol. 8 - Drillability test methods. – PhD-thesis, Faculty of Engineering Science and Technology, Norwegian Institute of Technology (NTNU), 22 p., Trondheim (NTNU).

BRULAND, A. (1999): Hard rock tunnel boring - Vol. 10 - Drillability test methods. – PhD-thesis, Faculty of Engineering Science and Technology, Norwegian Institute of Technology (NTNU), 110 p., Trondheim (NTNU).

BRULAND, A. (2000a): Hard rock tunnel boring - Vol. 1 - Background and discussion. – PhD-thesis, Faculty of Engineering Science and Technology, Norwegian Institute of Technology (NTNU), 49 p., Trondheim (NTNU).

BRULAND, A. (2000b): Hard rock tunnel boring - Vol. 7 - The boring process. – PhD-thesis, Faculty of Engineering Science and Technology, Norwegian Institute of Technology (NTNU), 86 p., Trondheim (NTNU).

BÜCHI, E. (1984): Einfluss geologischer Parameter auf die Vortriebsleistung einer Tunnelbohrmaschine. – 136 pp., PhD-thesis, Philosophisch-naturwissenschaftliche Fakultät, University of Bern,

BÜCHI, E., MATHIER, J.F. & WYSS, C. (1995): Gesteinsabrasivität – ein bedeutender Kostenfaktor beim mechanischen Abbau von Fest- und Lockergestein. – Tunnel, 95 (5): pp. 38–44.

CARDU, M. & GIRAUDI, A. (2012): Metal-rock pair characterization in excavation engineering. – The Journal of The South African Institute of Mining and Metallurgy, 112 (5): pp. 379–386.

CERCHAR – Centre d'E´tudes et des Recherches des Charbonnages de France (1986): The Cerchar Abrasiveness Index. – 8 p., Verneuil.

CHEN, Y., WEI, T. & GONG, T. (2018): Research on optimal layout of cutter-head system of rock tunnel-boring machine based on Archimedes spiral theory. – Advances in Mechanical Engineering, 10 (2): pp. 1–10.

CHMIEL, D. (2014): Verschleißformen von Rollenmeißeln - Entstehung und Interpretation. – unpublished Bachelor's thesis, Chair for engineering geology, Technical University of Munich, 36 p., Munich (TUM).

CIGLA, M., YAGIZ, S. & OZDEMIR, L. (2001): Application of tunnel boring machines in underground mine development. – In: IMCET (ed.): Proceedings of the 17th international mining congress and exhibition of Turkey, Ankara, 19-22 June 2001), pp. 155–164, Ankara (Chamber of Mining Engineers of Turkey).

COHEN, K.M., HARPER, D.A.T., GIBBARD, P.L. & FAN, J.-X. (2020): International Chronostratigraphic Chart. – International Commission on Stratigraphy, https://stratigraphy.org/ICSchart/ChronostratChart2020-03.pdf.

COPUR, H., AYDIN, H., BILGIN, N., BALCI, C., TUMAC, D. & DAYANC, C. (2014): Predicting performance of EPB TBMs by using a stochastic model implemented into a deterministic model. – Tunnelling and Underground Space Technology, 42: pp. 1–14.

CZICHOS, H. (1978): Tribology. – Tribology series, 1: 400 p., Amsterdam (Elsevier).

CZICHOS, H. & HABIG, K.-H. (1992): Tribologie-Handbuch. – 560 p., Braunschweig (Vieweg).

CZICHOS, H., KLAFFKE, D., SANTNER, E. & WOYDT, M. (1995): Advances in tribology. – Wear, 190 (2): pp. 155–161.

DAHL, F., BRULAND, A., JAKOBSEN, P.D., NILSEN, B. & GRØV, E. (2012): Classifications of properties influencing the drillability of rocks, based on the NTNU/SINTEF test method. – Tunnelling and Underground Space Technology, 28: pp. 150–158.

DENGEL, D. (1989): Auswirkung einer Spitzenverrundung des Prüfdiamanten auf die Mikrohärte unter Prüfkraft. – Materialprüfung, 31 (7-8): pp. 227–229.

DENINA, M. (2014): Comparison of Knoop-microhardness with rock strength and rock abrasivity parameters. – unpublished Master's thesis, Department of Environment, Land and Infrastructure Engineering, Politecnico di Torino, 82 p., Turin.

DESSAU, G. (1974): Die Lagerstätten Toskanas im Lichte der geologischen Entwicklung des Landes. – Archiv für Lagerstättenforschung in den Ostalpen, Montanuniversität Leoben, Sonderband 2 Festschrift O.M. Friedrich: pp. 51–77, Leoben.

DETERS, L., FISCHER, A., SANTNER, E. & STOLZ, U. (2002): GfT-Arbeitsblatt 7: Tribologie. Verschleiß, Reibung: Definitionen, Begriffe, Prüfung. – 52 p., https://neu.gft-ev.de/wp-content/uploads/2002_AB_7_Tribologie.pdf.

DGGT (2004): Neufassung der Empfehlung Nr.1 des Arbeitskreises "Versuchstechnik Fels" der Deutschen Gesellschaft für Geotechnik e.V.: Einaxiale Druckversuche an zylindrischen Gesteinsprüfkörpern. – Bautechnik, 81 (10): pp. 825–834.

DGGT (2008): Empfehlung Nr. 10 des Arbeitskreises 3.3 “Versuchstechnik Fels” der Deutschen Gesellschaft für Geotechnik e. V: Indirekter Zugversuch an Gesteinsproben - Spaltzugversuch. – Bautechnik, 85 (9): pp. 623–627.

DGGT (2010): Empfehlung Nr. 5 “Punktlastversuche an Gesteinsproben“ des Arbeitskreises 3.3 “Versuchstechnik Fels“ der Deutschen Gesellschaft für Geotechnik. – Bautechnik, 87 (6): pp. 322–330.

DIN 50320 (1979): Verschleiß; Begriffe, Systemanalyse von Verschleißvorgängen, Gliederung des Verschleißgebietes. – 6 p., Berlin (Beuth).

DIN 50323-1 (1988): Tribologie; Begriffe. – 2 p., Berlin (Beuth).

DIN 50323-2 (1995): Tribologie - Verschleiß - Teil 2: Begriffe. – 13 p., Berlin (Beuth).

DIN 50323-3 (1993): Tribologie; Reibung; Begriffe, Arten, Zustände, Kenngrößen. – 2 p., Berlin (Beuth).

DIN 51220 (2003): Werkstoffprüfmaschinen - Allgemeines zu Anforderungen an Werkstoffprüfmaschinen und zu deren Prüfung und Kalibrierung. – 9 p., Berlin (Beuth).

DIN EN 843-4 (2005): Hochleistungskeramik - Mechanische Eigenschaften monolithischer Keramik bei Raumtemperatur - Teil 4: Härteprüfung nach Vickers, Knoop und Rockwell. – 22 p., Berlin (Beuth).

DIN EN 1330-1 (2015): Zerstörungsfreie Prüfung - Terminologie - Teil 1: Allgemeine Begriffe. – 24 p., Berlin (Beuth).

DIN EN 12407 (2019): Prüfverfahren für Naturstein - Petrographische Prüfung. – 24 p., Berlin (Beuth).

DIN EN 12440 (2018): Naturstein - Kriterien für die Bezeichnung. – 113 p., Berlin (Beuth).

DIN EN 12670 (2019): Naturstein - Terminologie. – 110 p., Berlin (Beuth).

DIN EN 13925-1 (2003): Zerstörungsfreie Prüfung - Röntgendiffraktometrie von polykristallinen und amorphen Materialien - Teil 1: Allgemeine Grundlagen. – 14 p., Berlin (Beuth).

DIN EN 13925-2 (2003): Zerstörungsfreie Prüfung - Röntgendiffraktometrie von polykristallinen und amorphen Materialien - Teil 2: Verfahrensabläufe. – 25 p., Berlin (Beuth).

DIN EN 13925-3 (2005): Zerstörungsfreie Prüfung - Röntgendiffraktometrie von polykristallinen und amorphen Materialien - Teil 3: Geräte. – 41 p., Berlin (Beuth).

DIN EN ISO 2639 (2003): Stahl - Bestimmung und Prüfung der Einsatzhärtungstiefe. – 9 p., Berlin (Beuth).

DIN EN ISO 4498 (2010): Sintermetalle, ausgenommen Hartmetalle - Bestimmung der Sinterhärte und der Mikrohärte. – 16 p., Berlin (Beuth).

DIN EN ISO 4516 (2002): Metalllische und andere anorganische Überzüge - Mikrohärteprüfungen nach Vickers und Knoop. – 16 p., Berlin (Beuth).

DIN EN ISO 4545-1 (2006): Metallische Werkstoffe - Härteprüfung nach Knoop - Teil 1: Prüfverfahren. – 23 p., Berlin (Beuth).

DIN EN ISO 4545-2 (2006): Metallische Werkstoffe – Härteprüfung nach Knoop – Teil 2: Prüfung und Kalibrierung der Prüfmaschinen. – 23 p., Berlin (Beuth).

DIN EN ISO 4545-3 (2006): Metallische Werkstoffe – Härteprüfung nach Knoop – Teil 3: Kalibrierung von Härtevergleichsplatten. – 16 p., Berlin (Beuth).

DIN EN ISO 6507-1 (2006): Metallische Werkstoffe – Härteprüfung nach Vickers – Teil 1: Prüfverfahren. –29 p., Berlin (Beuth).

DIN EN ISO 6507-1 (2018): Metallische Werkstoffe - Härteprüfung nach Vickers - Teil 1: Prüfverfahren. – 45 p., Berlin (Beuth).

DIN EN ISO 6507-2 (2013): Metallische Werkstoffe – Härteprüfung nach Vickers – Teil 2: Prüfung und Kalibrierung der Prüfmaschinen. – 28 p., Berlin (Beuth).

DIN EN ISO 6507-3 (2006): Metallische Werkstoffe – Härteprüfung nach Vickers – Teil 3: Kalibrierung von Härtevergleichsplatten. –16 p., Berlin (Beuth).

DIN EN ISO 6508-1 (2016): Metallische Werkstoffe - Härteprüfung nach Rockwell - Teil 1: Prüfverfahren. –38 p. Berlin (Beuth).

DIN EN ISO 6508-2 (2015): Metallische Werkstoffe – Härteprüfung nach Rockwell – Teil 2: Überprüfung und Kalibrierung der Prüfmaschinen und Eindringkörper. –27 p., Berlin (Beuth).

DIN EN ISO 6508-3 (2015): Metallische Werkstoffe – Härteprüfung nach Rockwell – Teil 3: Kalibrierung von Härtevergleichsplatten. – 20 p., Berlin (Beuth).

DIN EN ISO 7500-1 (2016): Metallische Werkstoffe - Kalibrierung und Überprüfung von statischen einachsigen Prüfmaschinen - Teil 1: Zug- und Druckprüfmaschinen - Kalibrierung und Überprüfung der Kraftmesseinrichtung. – 23 p., Berlin (Beuth).

DIN EN ISO 18265 (2014): Metallische Werkstoffe - Umwertung von Härtewerten. – 86 p., Berlin (Beuth).

DIN ISO 3878 (1991): Hartmetalle; Vickers-Härteprüfung: 1983. – 3 p., Berlin (Beuth).

DOLLINGER, G.L., HANDEWITH, H.J. & BREEDS, C.D. (1998): Use of the punch test for estimating TBM performance. – Tunnelling and Underground Space Technology, 13 (4): pp. 403–408.

DRUCKER, P. (2011): Abrasivität von Lockergesteinen und der Werkzeugverschleiß im Tief- und Tunnelbau. – Österreichische Ingenieur und Architekten-Zeitschrift, 156 (1-12): pp. 219–225.

DULCE, G. (1989): Tektonik und Petrographie des Quarzphyllit-Komplexes in den Dolomiten (Südalpin, Norditalien). –PhD-thesis, Fachbereich Erdwissenschaften, University Hannover, 160 p., Hannover.

DUNHAM, R.J. (1962): Classification of carbonate rocks according to depositional texture. – In: HAM, W.E. (ed.): Classification of carbonate rocks, 1: pp. 108–121, Tulsa, (AAPG).

EICKHOFF BAUMANN, L.P. (2008): Mineralogische und mechanische Untersuchungen zur Mahlbarkeit von Zementklinkern. – Münchner Geologische Hefte - Reihe B, Heft 0: 130 p., Munich (TUM).

ELLECOSTA, P., KÄSLING, H. & THURO, K. (2017): Verschleißphänomene beim TBM Hartgesteinsvortrieb – Gründe und Auswirkungen. – In: Deutsche Gesellschaft für Geotechnik e.V. (DGGT) (ed.): Fachsektionstage Geotechnik, Interdisziplines Forum - Tagungsband, Würzburg, Germany, 6–8 September 2017, pp. 240–245, Essen (DGGT).

ELLECOSTA, P., KÄSLING, H. & THURO, K. (2018): Tool wear in TBM hard rock drilling - backgrounds and special phenomena. – Geomechanics and Tunnelling, 11 (2): pp. 142–148.

ELLECOSTA, P., KÄSLING, H. & THURO, K. (2018): Wear Phenomena in Tunnel Boring Machine (TBM) Hard Rock Drilling - Reasons and Consequences. – In: SHAKOOR, A. & CATO, K. (eds.): IAEG/AEG Annual Meeting Proceedings, San Francisco, 17–21 September 2018, 4: 57–64, Cham (Springer).

ELLECOSTA, P., SCHNEIDER, S., KÄSLING, H. & THURO, K. (2015): Hardness – A New Method for Characterising the Interaction of TBM Disc Cutters and Rocks? – In: HASSANI, F. (ed.): Proceedings of the 13th Congress on Rock Mechanics (ISRM Congress 2015), Montréal, Canada, 10–13 May 2015, pp. 1–11, Montreal (CIM).

EMMERT, U. (1965): Erläuterungen zur Geologischen Karte von Bayern 1:25 000 Blatt Nr. 6228 Wiesentheid. – 132 p., Munich (Geological Survey of Bavaria).

ENTACHER, M. (2013): Measurement and interpretation of disc cutting forces in mechanized tunneling. – 153 p., Leoben.

ERBEN, H. (2013): Punch penetration tests - Input parameter for TBM performance prediction. – unpublished Diploma thesis, Chair for Subsurface Engineering, Montanuniversität Leoben, 102 p., Leoben.

ERMRICH, M. (2017): Prüfbericht M78 - 01. – unpublished test report, Röntgenlabor Dr. Ermrich, 12 p., Reinheim.

ESPALLARGAS, N., JAKOBSEN, P.D., LANGMAACK, L. & MACIAS, F.J. (2015): Influence of Corrosion on the Abrasion of Cutter Steels Used in TBM Tunnelling. – Rock Mechanics and Rock Engineering, 48 (1): pp. 261–275.

EWENDT, G. (1989): Erfassung der Gesteinsabrasivität und Prognose des Werkzeugverschleißes beim maschinellen Tunnelvortrieb mit Diskenmeißeln. – PhD-thesis, Ruhr-Universität Bochum, Bochumer geol. u. geot. Arbeiten, 33: 88 p., Bochum (RUB).

FARROKH, E., ROSTAMI, J. & LAUGHTON, C. (2012): Study of various models for estimation of penetration rate of hard rock TBMs. – Tunnelling and Underground Space Technology, 30: pp. 110–123.

FISCHER, P. (2015): Entwicklung eines Verfahrens zur Härteprüfung von Gesteinen. – unpublished Master's thesis, Chair for engineering geology, Technical University of Munich, 236 p., Munich (TUM).

FLÜGEL, H.W. & NEUBAUER, F. (1984): Geologische Karte der Steiermark 1 : 200.000. – Vienna (Geological Survey of Austria).

FLÜGEL, H.W., NEUBAUER, F. & NEUBAUER, F. (1984): Steiermark. – Geologie der österreichischen Bundesländer in kurzgefaßten Einzeldarstellungen, 127 p., Vienna (Geological Survey of Austria).

FOLK, R.L. (1959): Practical petrographic classification of limestones. – American Association of Petroleum Geologists Bulletin, 43: pp. 1–38.

FRENZEL, C. (2010): Verschleißkostenprognose für Schneidrollen bei maschinellen Tunnelvortrieben in Festgesteinen. – Münchner Geowissenschaftliche Abhandlungen. Reihe B, Ingenieurgeologie, Hydrogeologie, Geothermie, 15: 64 p., Munich (Pfeil).

FRENZEL, C. (2011): Disc Cutter Wear Phenomenology and their implications on disc cutter consumption for TBM. – In: American Rock Mechanics Association (ed.): 45th U.S. Rock Mechanics / Geomechanics Symposium, San Francisco,26–29 June, pp. 1–7, Alexandria (ARMA).

FRENZEL, C., GALLER, R., KÄSLING, H. & VILLENEUVE, M. (2012): Penetration tests for TBMs and their practical application / Penetrationstests für Tunnelbohrmaschinen und deren Anwendung in der Praxis. – Geomechanics and Tunnelling 5 (5): pp. 557–566.

FRENZEL, C., KÄSLING, H. & THURO, K. (2008): Factors Influencing Disc Cutter Wear. – Geomechanics and Tunnelling, 1 (1): pp. 55–60.

FREUDENBERGER, W. (1996): Trias. – In: FREUDENBERGER, W. & SCHWERD, K. (eds.): Erläuterungen zur Geologischen Karte von Bayern 1:500 000. – 4th edition, pp. 65–89, Munich (Geological Survey of Bavaria).

FRÖHLICH, F., GRAU, P. & GRELLMANN, W. (1977): Performance and analysis of recording microhardness tests. – Phys Stat Sol (a), 42 (1): pp. 79–89.

FUCHS, K. (1997): Natursteine aus aller Welt, entdecken, bestimmen, anwenden. – 2nd edition, 257 p., Munich (Callwey).

GÅHLIN, R. & JACOBSON, S. (1999): The particle size effect in abrasion studied by controlled abrasive surfaces. – Wear, 224 (1): pp. 118–125.

GEHRING, K. (1995): Leistungs- und Verschleißprognose im maschinellen Tunnelbau. – Felsbau Magazin, 13 (6): pp. 448–493.

GEHRING, K. (1997): Classification of drillability, cuttability, borability and abrasivity in tunnelling. – Felsbau Magazin, 15 (3): pp. 183–189.

GEHRING, K. (2009): The influence of TBM design and machine features on performance and tool wear in rock. – Geomechanics and Tunnelling, 2 (2): pp. 140–155.

GENG, Q., BRULAND, A. & MACIAS, F.J. (2017): Analysis on the Relationship Between Layout and Consumption of Face Cutters on Hard Rock Tunnel Boring Machines (TBMs). – Rock Mechanics: pp. 1–19.

GENG, Q., WEI, Z., DU J. & TANG, Y. (2013): A Cutter Layout Optimization Method for Full-Face Rock Tunnel Boring Machine. – In: LEE, J., LEE, M.C., LIU, H. & RYU, J.-H. (eds.): Intelligent Robotics and Applications. – Lecture Notes in Computer Science / Lecture Notes in Artificial Intelligence, 8103: pp. 727–737, Berlin (Springer).

GERTSCH, R. (2000): Rock toughness and disc cutting. –PhD-thesis, University of Missouri-Rolla, 255 p., Missouri (Missouri S&T).

GERTSCH, R., GERTSCH, L. & ROSTAMI, J. (2007): Disc cutting tests in Colorado Red Granite. – Int. J. Rock Mech. Min. Sci., 44 (2): pp. 238–246.

GHARAHBAGH, E.A., ROSTAMI, J. & PALOMINO, A.M. (2011): New soil abrasion testing method for soft ground tunneling applications. – Tunnelling and Underground Space Technology, 26 (5): pp. 604–613.

GIRMSCHEID, G. (2013): Bauprozesse und Bauverfahren des Tunnelbaus. – 3rd edition, 760 p., Berlin (Wiley).

GONG, Q.M., JIAO, Y.Y. & ZHAO, J. (2006): Numerical modelling of the effects of joint spacing on rock fragmentation by TBM cutters. – Tunnelling and Underground Space Technology, 21 (1): pp. 46–55.

GONG, Q.M., YIN, L.J., WU, S.Y., ZHAO, J. & TING, Y. (2012): Rock burst and slabbing failure and its influence on TBM excavation at headrace tunnels in Jinping II hydropower station. – Engineering Geology, 124: pp. 98–108.

GONG, Q.M. & ZHAO, J. (2009): Development of a rock mass characteristics model for TBM penetration rate prediction. – Int. J. Rock Mech. Min. Sci., 46 (1): pp. 8–18.

GONG, Q.-M., ZHAO, J. & JIAO, Y.-Y. (2005): Numerical modeling of the effects of joint orientation on rock fragmentation by TBM cutters. – Tunnelling and Underground Space Technology, 20 (2): pp. 183–191.

GRAU, P., BERG, G. & DENGEL, D. (1996): Vickershärte richtig gemessen. – Materialprüfung, 35 (11-12): pp. 339–342.

GREENWOOD, J.A. & WILLIAMSON, J.B. (1966): Contact of Nominally Flat Surfaces. – Proceedings of the Royal Society A: Mathematical, Physical and Engineering Sciences, 295 (1442): pp. 300–319.

GRUNERT, S. (2007): Der Elbsandstein: Vorkommen, Verwendung, Eigenschaften. – Geologica Saxonica - Journal of Central European Geology, 52/53: pp. 3–22.

HANDEWITH, H.J. (1970): Predicting the economic success of continuous tunneling and hard rock. – In: 71st Annual General Meeting of the CIM, 63: pp. 595–599, Montréal (CIM).

HASSANPOUR, J., ROSTAMI, J., KHAMEHCHIYAN, M. & BRULAND, A. (2009): Developing new equations for TBM performance prediction in carbonate-argillaceous rocks. – Geomechanics and Geoengineering, 4 (4): pp. 287–297.

HASSANPOUR, J., ROSTAMI, J., KHAMEHCHIYAN, M., BRULAND, A. & TAVAKOLI, H.R. (2010): TBM Performance Analysis in Pyroclastic Rocks: A Case History of Karaj Water Conveyance Tunnel. – Rock Mech Rock Eng, 43 (4): pp. 427–445.

HASSANPOUR, J., ROSTAMI, J., TARIGH AZALI, S. & ZHAO, J. (2014): Introduction of an empirical TBM cutter wear prediction model for pyroclastic and mafic igneous rocks; a case history of Karaj water conveyance tunnel, Iran. – Tunnelling and Underground Space Technology, 43: pp. 222–231.

HASSANPOUR, J., ROSTAMI, J. & ZHAO, J. (2011): A new hard rock TBM performance prediction model for project planning. – Tunnelling and Underground Space Technology, 26 (5): pp. 595–603.

HECKEL, K. (1991): Einführung in die technische Anwendung der Bruchmechanik. – 3rd edition, Hanser-Studienbücher, 222 p., Munich (Hanser).

HEINIÖ, M. (ed.) (1999): Rock Excavation Handbook. – 363 p., (Sandvik Tamrock Corporation).

HERRMANN, K. (2007): Grundlagen der Härteprüfung. – In: HERRMANN, K., KOMPATSCHER, M., POLZIN, T., ULLNER, C. & WEHRSTEDT, A. (eds.): Härteprüfung an Metallen und Kunststoffen. – Reihe Technik, pp. 1–22, Renningen (Expert-Verlag).

HERRMANN, K., KOMPATSCHER, M., POLZIN, T., ULLNER, C. & WEHRSTEDT, A. (2007): Härteprüfung an Metallen und Kunststoffen. – Reihe Technik, 251 p., Renningen (Expert-Verlag).

HERTZ, H. (1881): Über die Berührung fester elastischer Körper. – Journal für die reine und angewandte Mathematik, 92: pp. 156–171.

HEUFT, C. (2015): Untersuchungen zum Einfluss der Härte und Struktur von Rollmeißeln auf deren Verschleißform. – unpublished Bachelor's thesis, Chair for engineering geology, Technical University of Munich, 110 p., Munich (TUM).

HIEBER, R. (2016): Härteprüfung nach Vickers von Mineralen und monomineralischen Gesteinen. – unpublished Bachelor's thesis, Chair for engineering geology, Technical University of Munich, 103 p., Munich (TUM).

HOWARTH, D.F. (1981): The effect of jointed and fissured rock on the performance of tunnel boring machines. – In: JORDEN, E.E. & HANNA, A.M. (eds.): Proceedings of the International Symposium on Weak Rock, International Society for Rock Mechanics and Rock Engineering, Tokyo, Japan , 21–24 September 1981, pp. 1069–1074, Lisbon (ISRM).

HOWARTH, D.F. & ROWLANDS, J.C. (1987): Quantitative assessment of rock texture and correlation with drillability and strength properties. – Rock Mechanics and Rock Engineering, 20 (1): pp. 57–85.

HUO, J., SUN, W., CHEN, J., SU, P. & DENG, L. (2010): Optimal disc cutters plane layout design of the full-face rock tunnel boring machine (tbm) based on a multi-objective genetic algorithm. – Journal of Mechanical Science and Technology, 24 (2): pp. 521–528.

HUO, J., SUN, W., CHEN, J. & ZHANG, X. (2011): Disc cutters plane layout design of the full-face rock tunnel boring machine (TBM) based on different layout patterns. – Computers & Industrial Engineering, 61 (4): pp. 1209–1225.

HUO, J., SUN, W., SU, P. & DENG, L. (2009): Optimal Disc Cutters Plane Layout Design of the Full-Face Rock Tunnel Boring Machine (TBM) Using an Ant Colony Optimization Algorithm. – In: XIE, M., XIONG, Y., XIONG, C., LIU, H. & HU, Z. (eds.): Intelligent robotics and applications. Lecture notes in computer science Lecture notes in artificial intelligence, 5928: pp. 443–452, Berlin (Springer).

IGUAL MUÑOZ, A. & ESPALLARGAS, N. (2011): Tribocorrosion mechanisms in sliding contacts. – In: LANDOLT, D. & MISCHLER, S. (eds.): Tribocorrosion of passive metals and coatings. Woodhead Publishing Series in Metals and Surface Engineering: pp. 118–152, Cambridge (Woodhead Publishing).

ILSCHNER, B. & SINGER, R.F. (2016): Werkstoffwissenschaften und Fertigungstechnik. – 6th edition, 511 p., Berlin (Springer Vieweg).

ISRM (1978a): Suggested method for petrographic description of rocks. – Int. J. Rock Mech. Min. Sci. Geomech. Abstr., 15 (2): pp. 43–45.

ISRM (1978b): Suggested methods for determining tensile strength of rock materials. – Int. J. Rock Mech. Min. Sci. Geomech. Abstr., 15 (2): pp. 99–103.

ISRM (1978c): Suggested methods for the quantitative description of discontinuities in rock masses. – Int. J. Rock Mech. Min. Sci. Geomech. Abstr., 15 (2): pp. 319–368.

ISRM (1979): Suggested methods for determining the uniaxial compressive strength and deformability of rock materials. – Int. J. Rock Mech. Min. Sci. Geomech. Abstr., 16 (2): pp. 138–140.

ISRM (1985): Suggested methods for determining point load strength. – Int. J. Rock Mech. Min. Sci. Geomech. Abstr., 22 (2): pp. 51–60.

ISRM (1998): Draft ISRM Suggested Method for Determining the Indentation Hardness Index of Rock Materials. – Int. J. Rock Mech. Min. Sci. Geomech. Abstr., 6 (35): pp. 831–835.

JÄGER BAU GMBH (n.d.): TUNNEL KORALM KAT2. – unpublished project report, 2 p., Schruns (Jäger Bau GmbH).

JAKOBSEN, P.D., LANGMAACK, L., DAHL, F. & BREIVIK, T. (2013): Development of the Soft Ground Abrasion Tester (SGAT) to predict TBM tool wear, torque and thrust. – Tunnelling and Underground Space Technology, 38: pp. 398–408.

JOHNSON, K.L. (1995): Contact Mechanics. – Cambridge (Cambridge University Press).

JOST, H.P. (1966): Lubrication (tribology): education and research; a report on the present position and industry's needs. – 79 p., London (H.M.S.O).

KAHRAMAN, S., FENER, M. & KOZMAN, E. (2012): Predicting the compressive and tensile strength of rocks from indentation hardness index. – The Journal of the South African Institute of Mining and Metallurgy, 112 (5): pp. 331–339.

KAIM, M. (1990): Geologie und Petrographie der Basalte Hirschentanz/ Grasfurt und vergleichende Untersuchungen an den Basalten des Teichelberges und Zinster Berges in der Oberpfalz. – unpublished Diploma thesis, Chair for engineering geology, Technical University of Munich, 117 p., Garching (TUM).

KÄSLING, H. (2009): Bestimmung der Gesteinsabrasivität. – PhD-thesis, Chair for engineering geology, Technical University of Munich, 123 p., Munich (TUM).

KÄSLING, H. & PLINNINGER, R.J. (2016): Bestimmung der Abrasivität von Gesteinen mit dem CERCHAR-Versuch. – Bautechnik, 93 (6): pp. 409–415.

KÄSLING, H., THIELE, I. & THURO, K. (2007): Abrasivitätsuntersuchungen mit dem Cerchar-Test – eine Evaluierung der Versuchsbedingungen. – In: OTTO, F. (ed.): Veröffentlichungen von der 16. Tagung für Ingenieurgeologie und vom Forum Junge Ingenieurgeologen, Technische Fachhochschule Georg Agricola Bochum, 7–10 March 2007, pp. 229–235, Bochum (DGGT).

KÄSLING, H. & THURO, K. (2010): Determining rock abrasivity in the laboratory. – In: ZHAO, J., LABIOUSE, V., DUDT, F., MATHIER, J.F. (eds.): ISRM European Rock Mechanics Symposium (EUROCK 2010), Lausanne, Switzerland, 15–18 June 2010, pp. 425–428, London (Taylor & Francis Group).

KATSICH, C. & BADISCH, E. (2011): Effect of carbide degradation in a Ni-based hardfacing under abrasive and combined impact/abrasive conditions. – Surface and Coatings Technology, 206 (6): pp. 1062–1068.

KIEFFER, R. & BENESOVSKY, F. (1965): Hartmetalle. – 546 p., Vienna (Springer).

KNORR, N. (2011): Squeezing out hydrated protons: low-frictional-energy triboelectric insulator charching on a microscopic scale. – AIP Advances, 1 (2): pp. 1–22.

KÜPFERLE, J., RÖTTGER, A., ALBER, M. & THEISEN, W. (2015): Assessment of the LCPC abrasiveness test from the view of material science / Bewertung des LCPC-Abrasivitätstests aus werkstofftechnischer Sicht. – Geomechanics and Tunnelling, 8 (3): pp. 211–220.

KÜPFERLE, J., RÖTTGER, A., THEISEN, W. & ALBER, M. (2016a): Microscopic and Experimental Analysis of the Tribological System of TBM Tools. – In: UCA of SME (eds.): ITA-AITES World Tunnel Congress 2016 (WTC 2016), San Francisco, California, 22–28 April 2016, pp. 2494– 2503, Red Hook, NY (Curran Associates Inc).

KÜPFERLE, J., RÖTTGER, A., THEISEN, W. & ALBER, M. (2016b): The RUB Tunneling Device – A newly developed test method to analyze and determine the wear of excavation tools in soils. – Tunnelling and Underground Space Technology, 59: pp. 1–6.

KÜPFERLE, J., RÖTTGER, A., THEISEN, W. & ALBER, M. (2017): Wear prediction for soft-ground tunneling tools – a new approach regarding the dominant influencing factors in the tribological system of tunneling tools. – In: International Tunnelling and Underground Space Association (ITA) (ed.): World Tunnel Congress 2017 - Surface challenges - Underground solutions, Bergen, Norway, 9–15 June 2017, pp. 1–10, Lausanne (ITA-AITES).

LABADZ, A.F. & LOWELL, J. (1991): Contact charge density and penetration depth. – Journal of Electrostatics, 26 (3): pp. 251–260.

LAGGER, M., HENZINGER, M.R., RADONCIC, N. & SCHUBERT, W. (2015): Influence of the primary stress state on the disc cutter penetration. – In: SCHUBERT, W. & KLUCKNER, W. (eds.): ISRM European Regional Symposium (EUROCK 2015) & 64th Geomechanics Colloquy, Salzburg, Austria, pp. 1139–1144, Salzburg (Taylor & Francis Group).

LE BAS, M.J. & STRECKEISEN, A.L. (1991): The IUGS systematics of igneous rocks. – Journal of the Geological Society, 148 (5): pp. 825–833.

LE MAITRE, R.W. (2005): Igneous Rocks: A Classification and Glossary of Terms, Recommendations of the International Union of Geological Sciences Subcommission on the Systematics of Igneous Rocks. – 2nd edition, 256 p., Cambridge (Cambridge University Press).

LEHRBERGER, G. (2007): Granit - das Höchste und das Tiefste. – In: HELM, W. (ed.): Granit: pp. 19–49, Hauzenberg (Granitzentrum Bayerischer Wald).

LINDHOLM, U.S., YEAKLEY, L.M. & NAGY, A. (1974): The dynamic strength and fracture properties of dresser basalt. – Int. J. Rock Mech. Min. Sci. Geomech. Abstr., 11 (5): pp. 181–191.

LINDQVIST, P.-A. & HAI-HUI, L. (1983): Behaviour of the crushed zone in rock indentation. – Rock Mechanics and Rock Engineering, 16 (3): pp. 199–207.

LISLERUD, A. (1997): Principles of mechanical excavation. – Posiva-raportti Posiva report, 97-12: 186 p., Helsinki (Posiva Oy).

LUDEMA, K.C. (1991): Cultural Impediments to Practical Modeling of Wear Rates. – In: LUDEMA, K.C. & BAYER, R.G. (eds.): Tribological modeling for mechanical designers. – ASTM STP, 1105: 180 p., Philadelphia (ASTM).

MACHERAUCH, E. & ZOCH, H.-W. (2011): Praktikum in Werkstoffkunde. – 11th edition, Wiesbaden (Vieweg+Teubner Verlag / Springer Fachmedien Wiesbaden GmbH).

MACIAS, F.J. (2016): Hard Rock Tunnel Boring: Performance Predictions and Cutter Life Assessments. – PhD-thesis, Faculty of Engineering Science and Technology, Norwegian Institute of Technology (NTNU), 390 p., Trondheim (NTNU).

MACIAS, F.J., DAHL, F. & BRULAND, A. (2016): New Rock Abrasivity Test Method for Tool Life Assessments on Hard Rock Tunnel Boring: The Rolling Indentation Abrasion Test (RIAT). – Rock Mech. Rock Eng., 49 (5): 1679–1693.

MACIAS, F.J., DAHL, F. & BRULAND, A. (2017a): Applicability of the new rock abrasivity test method (RIAT) to cutter life assessments in hard rock tunnel boring. – In: International Tunnelling and Underground Space Association (ITA) (ed.): World Tunnel Congress 2017 - Surface challenges - Underground solutions, Bergen, Norway, 9–15 June 2017, pp. 34–39, Lausanne (ITA-AITES).

MACIAS, F.J., DAHL, F., BRULAND, A., KÄSLING, H. & THURO, K. (2017b): Drillability Asessment in Hard Rock. – In: JOHANSSON,E. & RAASAKKA,V. (eds.): 3rd Nordic Rock Mechanics Symposium (NRMS 2017), 11–12 October 2017, Helsinki, Finland, pp. 105–115, Helsinki (RIL).

MACIAS, F.J., DAHL, F. & BRULAND, A. (2015): New rock abrasivity test method by rolling disc. – In: HASSANI, F. (ed.): Proceedings of the 13th Congress on Rock Mechanics (ISRM Congress 2015), Montréal, Canada, 10–13 May 2015, pp. 1–11, Montreal (CIM).

MACIAS, F.J., JAKOBSEN, P.D., SEO, Y. & BRULAND, A. (2014): Influence of rock mass fracturing on the net penetration rates of hard rock TBMs. – Tunnelling and Underground Space Technology, 44: pp. 108–120.

MAIDL, B., HERRENKNECHT, M., MAIDL, U. & WEHRMEYER, G (2012): Mechanised shield tunnelling. – 2nd edition, 470 p., Berlin (Ernst & Sohn).

MAIDL, B., SCHMID, L., RITZ, W. & HERRENKNECHT, M. (2008): Hardrock tunnel boring machines. – 343 p., Berlin (Ernst & Sohn).

MARTENS, A. (1912): Handbuch der Materialienkunde für den Maschinenbau. – 234 p., Berlin (Springer).

MASEN, M.A., DE ROOIJ, M.B. & SCHIPPER, D.J. (2005): Micro-contact based modelling of abrasive wear. – Wear, 258 (1-4): pp. 339–348.

MCGUIGGAN, P.M. (2008): Stick slip contact mechanics between dissimilar materials. – Langmuir: the ACS journal of surfaces and colloids, 24 (8): pp. 3970–3976.

MENSCHIK, F.M. (2015): Analysis of Performace and Wear of Electrical Rock Hammer Drills. – PhD-thesis, Chair for engineering geology, Technical University of Munich, 139 p., Munich (TUM).

MEYER, R. & SCHMIDT-KALER, H. (1996): Jura. – In: FREUDENBERGER, W. & SCHWERD, K. (eds.): Erläuterungen zur Geologischen Karte von Bayern 1 : 500 000. – 4th edition, pp. 90–111, Munich (Geological Survey of Bavaria).

MIRKOWSKA, M., KRATZER, M., TEICHERT, C. & FLACHBERGER, H. (2016): Principal Factors of Contact Charging of Minerals for a Successful Triboelectrostatic Separation Process – a Review. – Berg Huettenmaenn Monatsh, 161 (8): pp. 359–382.

MOHS, F. (1822): Grundriss der Mineralogie. – 604 p., Dresden (Arnoldische Buchhandlung).

MORITZ, B., WAGNER, H., MUSSGER, K., HANDKE, D. & HARER, G. (2011): Criteria for the selection of tunnelling method through the example of the Koralm Tunnel. – Geomechanics and Tunnelling, 4 (4): pp. 305–316.

MÜLLER, F. & KÖGLER, R. (n.d.a): INSK kompakt: die internationale Naturwerksteinkartei für den aktuellen Markt. Granit. – 2, Ulm (Ebner Verlag).

MÜLLER, F. & KÖGLER, R. (n.d.b): INSK kompakt: die internationale Naturwerksteinkartei für den aktuellen Markt. Marmor Sandstein Sedimentgesteine fest und weich. – 6, Ulm (Ebner Verlag).

MÜLLER, F. & KÖGLER, R. (n.d.c): INSK kompakt: die internationale Naturwerksteinkartei für den aktuellen Markt. Plutonite ohne Quarz Vulkanite. – 3, Ulm (Ebner Verlag).

NÄHER, U. (1989): Geologische Kartierung der näheren Umgebung Kulmain (Oberpfalz) im Maßstab 1 : 10 000 und einer Korrelation von Chemismus und Petrographie nordostbayerischer Basalte mit ihrem gesteinstechnischen Verhalten, am Beispiel der Basalte des Zinster Berges, des Großen Teichelberges, des Hirschentanzes und des Grasfurter Vorkommens. – unpublished Diploma thesis, Chair for engineering geology, Technical University of Munich, 88 p, Garching (TUM).

NAKAYAMA, K. & MARTIN, J.-M. (2006): Tribochemical reactions at and in the vicinity of a sliding contact. – Wear, 261 (3-4): pp. 235–240.

NELSON, P.P., ABD AL-JALIL, Y. & LAUGHTON, C. (1994): Tunnel Boring Project Data Bases and Construction Simulation. – Geotechnical Engineering Center Report GR, 94-4, Austin, Texas (The University of Texas at Austin).

NELSON, P.P., ABD AL-JALIL, Y. & LAUGHTON, C. (1999): Improved strategies for TBM performance prediction and project management. – In: American Institute of Mining, Metallurgical, and Petroleum Engineers (ed.): Proceedings of the Rapid Excavation Tunnelling Conference (RETC 1999), Orlando, Florida, 21–23 June 1999, pp. 963–979, Littleton, Colorado (Society for Mining, Metallurgy, and Exploration).

NGUYEN, H.D.-A. (2014): Untersuchung zur Härte von Rollmeißeln. – unpublished Bachelor's thesis, Chair for engineering geology, Technical University of Munich, 57 p., Munich (TUM).

ÖBB-INFRASTRUKTUR AG (2009): Koralmbahn Graz–Klagenfurt Baulos KAT2. – unpublished project document, 171 p.

ÖBB-INFRASTRUKTUR AG (2012): Breakthrough into the Future. – unpublished project report, 168 p., Graz.

OBERT, L. & DUVALL, W.I. (1967): Rock mechanics and the design of structures in rock. – 650 p., New York (Wiley).

OETTEL, H. & SCHUMANN, H. (2011): Metallografie. – 15th edition, 934 p., Weinheim (Wiley-VCH).

OLSEN, V. (2009): Rock Quarrying. – PhD-thesis, Faculty of Engineering Science and Technology, Norwegian Institute of Technology (NTNU), 183 p., Trondheim (NTNU).

OLSSON, M., YVELL, K., HEINRICHS, J., BENGTSSON, M. & JACOBSON, S. (2017): Surface degradation mechanisms of cemented carbide drill buttons in iron ore rock drilling. – Wear, 388-389: pp. 81–92.

ONDRACEK, G. (1995): Werkstoffkunde. Leitfaden für Studium und Praxis. – 305 p., Renningen-Malmsheim (Expert).

OTTO, M. (2005): Härteumwertung nach E DIN EN ISO 18265 - Richtig angewendet. – In: DIN e.V (ed.): Messunsicherheit und neue Verfahren der Härteprüfung: pp. 57–69, Berlin (Beuth).

OZDEMIR, L., MILLER, R. & WANG, F. (1977): Mechanical tunnel boring prediction and machine design: Annual Report. – 313 p., Washington, D.C. (National Science Foundation).

PAHNKE, F. (2016): Meißelverschleiß beim TBM Hartgesteinsvortrieb. – unpublished Bachelor's thesis, Chair for engineering geology, Technical University of Munich, 82 p., Munich (TUM).

PASSCHIER, C.W. & TROUW, R.A. (2005): Microtectonics. – 2nd edition, 366 p., Berlin, (Springer).

PATERSON, M.S. & WONG, T.-F. (2005): Experimental Rock Deformation - The brittle field. – 2nd edition, 347 p., Berlin (Springer).

PETRICA, M., BADISCH, E. & PEINSITT, T. (2013): Abrasive wear mechanisms and their relation to rock properties. – Wear, 308 (1-2): pp. 86–94.

PETRICA, M., PAINSI, M., BADISCH, E. & PEINSITT, T. (2014): Wear Mechanisms on Martensitic Steels Generated by Different Rock Types in Two-Body Conditions. – Tribology Letters, 53 (3): pp. 607–616.

PLINNINGER, R.J. (2002): Klassifizierung und Prognose von Werkzeugverschleiß bei konventionellen Gebirgslösungsverfahren im Festgestein. – Münchner geologische Hefte Reihe B, 17: 117 p., Munich (Pfeil).

PLINNINGER, R.J. (2010): Hardrock abrasivity investigation using the Rock Abrasivity Index (RAI). – In: WILLIAMS, A.L. (ed.): Geologically active, pp. 3445–3452, Boca Raton (CRC Press).

PLINNINGER, R.J. & RESTNER, U. (2008): Abrasiveness Testing, Quo Vadis? – A Commented Overview of Abrasiveness Testing Methods. – Geomechanics and Tunnelling, 1 (1): pp. 61–70.

PLINNINGER, R.J., SPAUN, G. & THURO, K. (2002): Prediction and Classification of tool wear in drill and blast tunnelling. – In: VAN ROOY, J.L. & JERMY, C.A. (eds.): Engineering Geology for Developing Countries, Proceedings of the 9th IAEG Congress, 16-20 September 2002, Durban, South Africa, pp. 2226–2236.

POLZIN, T. (2007): Härteprüfung von Metallen. – In: HERRMANN, K., KOMPATSCHER, M., POLZIN, T., ULLNER, C. & WEHRSTEDT, A. (eds.): Härteprüfung an Metallen und Kunststoffen. – Reihe Technik: pp. 33–72, Renningen (Expert).

POPOV, V.L. (2015): Kontaktmechanik und Reibung. – 3rd edition, 397 p. (Springer Vieweg).

PRINZ, H. & TIEDEMANN, J. (1983): Geologisch-ingenieurgeologische Erkundung tektonischer Strukturen für den Tunnelbau im Buntsandstein. – In: Deutsche Gesellschaft für Erd- und Grundbau e.V. (DGEG) (ed.): 4. Nationale Tagung für Ingenieurgeologie, pp. 139–150, Essen (DGEG).

RABINOWICZ, E. (1965): Friction and wear of materials. – 2nd edition, 315 p., New York, NY (Wiley).

RAMALHO, A. & MIRANDA, J.C. (2006): The relationship between wear and dissipated energy in sliding systems. – Wear, 260 (4-5): pp. 361–367.

RAMEZANZADEH, A. (2005): Performance analysis and development of new models for performance prediction of hard rock TBMs in rock mass. – PhD-thesis, Institut National des Sciences Appliquées de Lyon (INSA), 333 p., Lyon, France.

RANZINGER, F. (2013): Gesteinstechnische Untersuchungen an veränderlich festen Mergelsteinen im Oberen Jura (Steinbruch Wiesenhofen) im Hinblick auf Optimierung des Abbau- und Aufbereitungsprozess für Betonzuschlag. – unpublished Master's thesis, Chair for engineering geology, Technical University of Munich, 81 p., Munich (TUM).

RATIA, V., HEINO, V., VALTONEN, K., VIPPOLA, M., KEMPPAINEN, A., SIITONEN, P. & KUOKKALA, V.T. (2014): Effect of abrasive properties on the highstress three-body abrasion of steels and hard metals. – Tribologia, 1 (32): pp. 3–18.

RAUCH, R. (2016): Einfluss des Gebirges auf die Vortriebsleistung und den Diskenverschleiß beim tiefliegenden TBM-Vortrieb am Koralmtunnel (Österreich). – unpublished Master's thesis, Chair for engineering geology, Technical University of Munich, 73 p., Munich (TUM).

REINERT, U. & SCHUBERT, R. (n.d.): Einfluß von Legierungselementen auf die Eigenschaften von Eisenwerkstoffen. – 12 p., https://www.hs-bremen.de/internet/hsb/struktur/mitarbeiter/schubert/lehrveranstaltungen/werk/materialien/118_zusatzinfos_einflu___legierungselemente.pdf.

REINISCH, R. (1920): Erläuterungen zur Geologischen Karte von Sachsen im Maßstab 1 : 25 000 Nr. 100 Blatt Dippoldiswalde-Frauenstein. – 32 p., Leipzig.

RIBACCHI, R. & FAZIO, A.L. (2005): Influence of Rock Mass Parameters on the Performance of a TBM in a Gneissic Formation (Varzo Tunnel). – Rock Mech. Rock Eng., 38 (2): pp. 105–127.

RICHTER-BERNBURG, G. (1974): Stratigraphische Synopsis des deutschen Buntsandsteins. – Geologisches Jahrbuch Reihe A: Sammelheft - Karawanken-Tektonik, Kreide-Ammoniten, Pollen-Präparation und Buntsandstein-Stratigraphie, 25: pp. 127–132.

RISPOLI, A., FERRERO, A.M., CARDU, M., BRINO, L. & FARINETTI, A. (2016): Hard Rock TBM performance: Preliminary study based on an exploratory tunnel in the Alps. – In: Taylor & Francis Group (ed.): Proceedings of the ISRM International Symposium - EUROCK 2016, 29–31 August 2016, Cappadocia, Turkey, pp. 469–474, London (Taylor & Francis Group).

ROBBINS, R.J. (1970): Economic factors in tunnel boring. – In: VAN RENSBURG, P.W.J. (ed.): Proceedings of the South African tunnelling conference: the technology and potential of tunnelling, Johannesburg, South Africa, S2: pp. 217–221, Johannesburg (The Southern African Institute of Mining and Metallurgy).

ROHRMÜLLER, J., MIELKE, H. & GEBAUER, D. (1996): Gesteinsfolge des Grundgebirges nördlich der Donau und im Molasseuntergrund. – In: FREUDENBERGER, W. & SCHWERD, K. (eds.): Erläuterungen zur Geologischen Karte von Bayern 1 : 500 000. – 4th edition, pp. 16–54, Munich (Geological Survey of Bavaria).

PETSCHICK, R. (2002): Röntgendiffraktometrie in der Sedimentoligie (K5). – In: HÜSSNER, H., HINDERER, M., GÖTZ, A. & PETSCHICK, R. (eds.): Sediment, Darmstadt, Germany, 29–31 May 2002, 18: pp. 99–118, Frankfurt am Main.

ROSIWAL, A. (1896): Neue Untersuchungsergebnisse über die Härte von Mineralien und Gesteinen. – Verhandlungen der k. k. geologischen Reichsanstalt, 17+18: pp. 475–491.

ROSIWAL, A. (1916): Neuere Ergebnisse der Härtebestimmung von Mineralien und Gesteinen. - Ein absolutes Maß für die Härte spröder Körper. – Verhandlungen der k. k. geologischen Reichsanstalt, 5+6: pp. 117–147.

ROSSMANITH, H.-P. (1982): Grundlagen der Bruchmechanik. – 266 p., Vienna (Springer).

ROSTAMI, J. (1997): Development of a force estimation model for rock fragmentation with disc cutters trough theoretical modeling and physical measurement of crushed zone pressure. – PhD-thesis, Colorado School of Mines, 384 p., Golden, Colorado (CSM).

ROSTAMI, J. (2013): Study of pressure distribution within the crushed zone in the contact area between rock and disc cutters. – Int. J. Rock Mech. Min. Sci., 57: pp. 172–186.

ROSTAMI, J., GERTSCH, R. & GERTSCH, L. (2002): Rock fragmentation by disc cutter: a critical review and an update. – In: HAMMAH, R., BAWDEN, W., CURRAN, J. & TELESNICKI, M. (eds.): Mining and tunnelling innovation and opportunity: Proceedings of the 5th North American Rock Mechanics Symposium and 17th Tunnelling Association of Canada Conference (NARMS-TAC 2002), Toronto, Canada, 7–10 July, 2002, 1: pp. 977–986, Toronto (University of Toronto Press).

ROSTAMI, J., GHARAHBAGH, E.A., PALOMINO, A.M. & MOSLEH, M. (2012): Development of soil abrasivity testing for soft ground tunneling using shield machines. – Tunnelling and Underground Space Technology, 28: pp. 245–256.

ROSTAMI, J., GHASEMI, A., ALAVI GHARAHBAGH, E., DOGRUOZ, C. & DAHL, F. (2014): Study of Dominant Factors Affecting Cerchar Abrasivity Index. – Rock Mech. Rock Eng., 47 (5): pp. 1905–1919.

ROSTAMI, J. & OZDEMIR, L. (1993): A new model for performance prediction of hard rock TBMs. – In: American Institute of Mining, Metallurgical, and Petroleum Engineers (ed.): Proceedings of the Rapid Excavation Tunnelling Conference (RETC 1993), Boston, Massachusetts, 13–17 June 1993, pp. 793–809, Littleton, Colorado (Society for Mining, Metallurgy, and Exploration).

RÖTTGER, A., KÜPFERLE, J., BRUST, S., MOHR, A. & THEISEN, W. (2015): Abrasion in Tunneling and Mining. – In: THEISEN, W., DENKENA, B. & TILLMANN, W. (eds.): Abrasivity of rock and soil: Proceedings of the 3rd International Conference on Stone and Concrete Machining (ICSCM), Ruhr-Universität Bochum, Lehrstuhl für Werkstofftechnik, Bochum, 2–3 November 2015, pp. 246–261, Bochum (Ruhr-Universität Bochum, Lehrstuhl für Werkstofftechnik).

ROXBOROUGH, F.F. & PHILLIPS, H.R. (1975): Rock excavation by disc cutter. – Int. J. Rock Mech. Min. Sci. Geomech. Abstr., 12 (12): pp. 361–366.

ROXBOROUGH, F.F. & RISPIN, A. (1973): The mechanical cutting characteristics of the lower chalk. – Tunnels & Tunnelling International, 5 (1): pp. 45–67.

RUDOLPH, F. (2016): Strandsteine. – 12th edition, 159 p., Neumünster (Wachholtz).

SALMINEN, P. & VIITALA, R. (1985): Rock drillability study. – unpublished technical report, Helsinki University of Technology. Department of Minig and Metallurgy. Mining Engineering, 6 p., Otaniemi (Helsinki University of Technology).

SALOP, L.J. (1983): Geological Evolution of the Earth during the Precambrian. – 459 p., Berlin (Springer).

SAMUEL, A.E. & SEOW, L.P. (1984): Disc force measurements on a full-face tunnelling machine. – Int. J. Rock Mech. Min. Sci. Geomech. Abstr., 21 (2): pp. 83–96.

SANIO, H.P. (1983): Nettovortriebsprognose für Einsätze von Vollschnittmaschinen in anisotropen Gesteinen. – PhD-thesis, Ruhr-Universität Bochum, 147 p., Bochum (RUB).

SANIO, H.P. (1985): Prediction of the performance of disc cutters in anisotropic rock. – Int. J. Rock Mech. Min. Sci. Geomech. Abstr., 22 (3): pp. 153–161.

SANO, O., ITO, I. & TERADA, M. (1981): Influence of strain rate on dilatancy and strength of Oshima granite under uniaxial compression. – J. Geophys. Res., 86 (B10): pp. 9299–9311.

SAPIGNI, M., BERTI, M., BETHAZ, E., BUSILLO, A. & CARDONE, G. (2002): TBM performance estimation using rock mass classifications. – Int. J. Rock Mech. Min. Sci., 39 (6): pp. 771–788.

SCHALLHAMMER, K. (2014): Felsmechanische und petrographische Untersuchungen der Schäden an Gesteinsproben durch einaxiale Druckbelastung. – unpublished Master's thesis, Chair for engineering geology, Technical University of Munich, 96 p., Munich (TUM).

SCHIMAZEK, G. & KNATZ, H. (1970): Der Einfluss des Gesteinsaufbaus auf die Schnittgeschwindigkeit und den Meißelverschleiß von Streckenvortriebsmaschinen. – Glückauf, 106 (6): pp. 274–278.

SCHIMAZEK, J. & KNATZ, H. (1976): Die Beurteilung von Gesteinen durch Schneid- und Rollenbohrwerkzeuge. – Erzmetall, 29: pp. 113–119.

SCHMID, S.M., FÜGENSCHUH, B., KISSLING, E. & SCHUSTER, R. (2004): Tectonic map and overall architecture of the Alpine orogen. – Eclogae geol. Helv., 97 (1): pp. 93–117.

SCHMIDT, W. (1990): Vorsicht bei der Bewertung des Werkstoffverhaltens mit Hilfe nichtgenormter Härteprüfverfahren. – In: VDI/ VDE- Gesellschaft Mess- und Automatisierungstechnik (eds.): Härteprüfung in Theorie und Praxis. Hardness Testing in Theory and Practice, VDI-Berichte, 804: pp. 29–41, Düsseldorf (VDI Verlag).

SCHMIDT, W. (1995): Betrachtungen zur Umwertung von Härtewerten. – In: VDI/ VDE-Gesellschaft Mess- und Automatisierungstechnik (eds.): Härteprüfung in Theorie und Praxis. Hardness Testing in Theory and Practice. – VDI-Berichte, 1194: pp. 211–221, Düsseldorf (VDI Verlag).

SCHNEIDER, E., THURO, K. & GALLER, R. (2012): Forecasting penetration and wear for TBM drives in hard rock - Results from the ABROCK research project / Prognose von Penetration und Verschleiß für TBM-Vortriebe im Festgestein - Erkenntnisse aus dem Forschungsprojekt ABROCK. – Geomechanics and Tunnelling, 5 (5): pp. 537–546.

SCHNEIDER, S. (2014): Untersuchungen zum Einfluss unterschiedlicher Mineralhärten auf Gesteinslöseprozesse. – unpublished Master's thesis, Chair for engineering geology, Technical University of Munich, 181 p., Munich (TUM).

SCHULLER, E., GALLER, R., BARWART, S. & WENIGHOFER, R. (2015): The transparent face - development work to solve problems in mechanized hard rock tunnelling / Die gläserne Ortsbrust - Entwicklungsarbeiten zur Lösung von Fragestellungen rund um maschinelle Vortriebe im Festgestein. – Geomechanics and Tunnelling, 8 (3): pp. 200–210.

SCHUMANN, H. (1991): Metallographie. – 13th edition, 764 p., Leipzig (Deutscher Verlag für Grundstoffindustrie).

SCHUSTER, R. (2003): Das eo-Alpidische Ereignis in den Ostalpen: Plattentektonische Situation und interne Struktur des Ostalpinen Kristallins. – Arbeitstagung Geologische Bundesanstalt Blatt 148 Brenner: pp. 141–159.

SEBASTIAN, U. (2013): Die Geologie des Erzgebirges. – 268 p., Berlin (Springer Spektrum).

SHEREMETI-KABASHI, F. (2002): Untersuchungen der Gefügeanisotropie von Carrara Marmor und deren Einfluss auf Verwitterung. – PhD-thesis, Faculty of Geosciences, Ludwig Maximilians-Universität München, 141 p., Munich (LMU).

SKOČEK, V. & VALEČKA, J. (1983): Paleogeography of the Late Cretaceous Quadersandstein of Central Europe. – Palaeogeography, Palaeoclimatology, Palaeoecology, 44 (1-2): pp. 71–92.

SNOWDON, R.A., RYLEY, M.D. & TEMPORAL, J. (1982): A study of disc cutting in selected British rocks. – Int. J. Rock Mech. Min. Sci. Geomech. Abstr., 19 (3): pp. 107–121.

SOMMER, K., HEINZ, R. & SCHÖFER, J. (2014): Verschleiß metallischer Werkstoffe. – 2nd edition, 604 p., Wiesbaden (Springer Vieweg).

STACHOWIAK, G.B. & STACHOWIAK, G.W. (2001): The effects of particle characteristics on three-body abrasive wear. – Wear, 249 (3-4): pp. 201–207.

STACHOWIAK, G.W. & BATCHELOR, A.W. (2005): Engineering tribology. – 3rd edition, 801 p., Amsterdam (Elsevier Butterworth-Heinemann).

STEINGRIMSSON, J.H., GRØV, E. & NILSEN, B. (2002): The significance of mixed-face conditions for TBM performance. – World Tunnelling, 15 (9): pp. 435–441.

STINGL, V. & MAIR, V. (2005): Einführung in die Geologie Südtirols. – 80 p., Brixen/Vahrn (Kraler Druck).

STOLARSKI, T.A. (2000): Tribology in machine design. – 298 p., Oxford (Butterworth-Heinemann).

STRECKEISEN, A. (1980): Classification and nomenclature of plutonic rocks. – Geologische Rundschau, 63: pp. 773–788.

STRUNZ, H., PAULITSCH, P., SEELIGER, E. & TENNYSON, C. (1966): Die Mineralien im Basalt von Groschlattengrün in der Oberpfalz. – Acta Albertina Ratisbonesia, 26: pp. 9–34.

SUN, W., HUO, J., CHEN, J., LI, Z., ZHANG, X., GUO, L., ZHAO, H. & ZHAO, Y. (2011): Disc cutters' layout design of the full-face rock tunnel boring machine (TBM) using a cooperative coevolutionary algorithm. – Journal of Mechanical Science and Technology, 25 (2): pp. 415–427.

TABOR, D. (1954): Mohs's Hardness Scale - A Physical Interpretation. – Proceedings of the Physical Society. Section B, 67 (3): pp. 249–257.

TARKOY, P.J. & MARCONI, M. (1991): Difficult rock comminution and associated geological conditions. – In: Institute of Mining and Metallurgy (ed.): Tunneling '91, Sixth International Symposium, London, England, 14–18 April 1991, pp. 195–207, London (Elsevier Applied Science).

TAYLOR, W.E. (1949): Correlation of the Mohs's scale of hardness with the Vickers's hardness numbers. – Mineralogical Magazine and Journal of the Mineralogical Society, 28 (206): pp. 718–721.

TEALE, R. (1964): The mechanical excavation of rock-Experiments with roller cutters. – Int. J. Rock Mech. Min. Sci. Geomech. Abstr., 1 (1): pp. 63–78.

THOME, K.N. (1998): Einführung in das Quartär. Das Zeitalter der Gletscher. – 287 p., Berlin (Springer).

THURO, K. (1996): Bohrbarkeit beim konventionellen Sprengvortrieb. – Münchner geologische Hefte Reihe B: Angewandte Geologie, 1: 146 p., Munich (Pfeil).

THURO, K. (1997): Drillability prediction. – Geologische Rundschau, 86 (2): pp. 426–438.

THURO, K. (2002): Geologisch-felsmechanische Grundlagen der Gebirgslösung im Tunnelbau. – Münchner Geologische Hefte, Reihe B: Angewandte Geologie, 18: 160 p., Munich (Pfeil).

THURO, K. & KÄSLING, H. (2009): Classification of the abrasiveness of soil and rock. – Geomechanics and Tunnelling, 2 (2): pp. 179–188.

THURO, K. & PLINNINGER, R.J. (2002): Klassifizierung und Prognose von Leistungs- und Verschleißparametern im Tunnelbau. – In: Deutsche Gesellschaft für Geotechnik (ed.): Tunnelbau 2003: pp. 62–126, Essen (Glückauf).

THURO, K., SINGER, J. & BAUER, M. (2006): Abrasivitätsuntersuchungen an Lockergesteinen im Hinblick auf die Gebirgslösung. – In: DGGT (ed.): 29. Baugrundtagung 2006 mit Fachausstellung Geotechnik in Bremen, Bautechnik 83 (8): pp. 283–290, Bremen.

THURO, K., SINGER, J., KÄSLING, H. & BAUER, M. (2007): Determining abrasivity with the LCPC Test. – In: American Rock Mechanics Association (eds.): 1st Canada - U.S. Rock Mechanics Symposium, Vancouver, Canada, 27–31 May 2007, Alexandria (ARMA).

TOLLMANN, A. (1977): Die Zentralalpen. – Geologie von Österreich, 1: 766 p., Vienna (Franz Deuticke).

TORRANCE, A.A. (2005): Modelling abrasive wear. – Wear, 258 (1-4): pp. 281–293.

TOURENQ, C. (1966): La dureté vickers des minéraux et des roches. – Bulletin Liasion Laboratoires des Ponts et Chaussèes, 19, rèf 332:1–12.

TREZONA, R.I., ALLSOPP, D.N. & HUTCHINGS, I.M. (1999): Transitions between two-body and three-body abrasive wear. – Wear, 225-229: pp. 205–214.

TROLL, G. (1964): Das Intrusivgebiet von Fürstenstein (Bayerischer Wald). – Geologica Bavarica, 52: 140 p., Munich (Geological Survey of Bavaria).

TUNCDEMIR, H., BILGIN, N., COPUR, H. & BALCI, C. (2008): Control of rock cutting efficiency by muck size. – Int. J. Rock Mech. Min. Sci., 45 (2): pp. 278–288.

ULLNER, C. (2007): Instrumentierte Eindringprüfung. – In: HERRMANN, K., KOMPATSCHER, M., POLZIN, T., ULLNER, C. & WEHRSTEDT, A. (eds.): Härteprüfung an Metallen und Kunststoffen. – Reihe Technik: pp. 167–236, Renningen (Expert).

UNTERWURZACHER, M. & OBOJES, U. (2012): White marble from Laas (Lasa), South Tyrol - its occuoccurence, use and petrographic-isotopical characterisation. – Austrian Journal of Earth Science, 105 (3): pp. 26–37.

URBAKH, M., KLAFTER, J., GOURDON, D. & ISRAELACHVILI, J. (2004): The nonlinear nature of friction. – Nature, 430 (6999): pp. 525–528.

USTINOVSHCHIKOV, Y.I. (2013): Secondary hardening mechanism of alloy steels. – Metal Science, 18 (7): pp. 337–344.

VALANTIN, A. (1974): Description des tests CERCHAR, “Durete et abrasivite des roches”. – Travaux Publics 167, N 322: pp. 88–92.

VERHOEF, P.N. (1997): Wear of rock cutting tools. – 327 p., Rotterdam (A.A. Balkema).

VILLENEUVE, M.C. (2008): Examination of geological influence on machine excavation of highly stressed tunnels in massive hard rock. – PhD-thesis, Queen’s University, Kingston, 788 p., Canada.

VILLENEUVE, M.C. (2015): Geomechanical Characterisation of Hard Rocks for Disc Cutting in Deep Tunnels. – In: LOLLINO, G., GIORDAN, D., THURO, K., CARRANZA-TORRES, C., WU, F., MARINOS, P. & DELGADO, C. (eds.): Engineering Geology for Society and Territory, 6: pp. 439–442, Cham (Springer International Publishing).

VILLENEUVE, M.C. (2017): Hard rock tunnel boring machine penetration test as an indicator of chipping process efficiency. – Journal of Rock Mechanics and Geotechnical Engineering, 9 (4): pp. 611–622.

VILLENEUVE, M.C., DIEDERICHS, M.S. & KAISER, P.K. (2012): Effects of Grain Scale Heterogeneity on Rock Strength and the Chipping Process. – Int. J. Geomech., 12 (6): pp. 632–647.

VILLENEUVE, M.C., DIEDERICHS, M.S., KAISER, P.K. & FRENZEL, C. (2007): Geomechanical characterisation of massive rock for deep TBM tunnelling. – In: EBERHARDT, E., STEAD, D. & MORRISON, T. (eds.): Rock mechanics. – Balkema - Proceedings and Monographs in Engineering, Water and Earth Sciences, pp. 1131–1139, London, England (CRC Press).

WAN, Z., SHA, M. & ZHOU, Y. (2002): Study on disk cutters for hard rock (1)-application of TB880E TBM in Qinling Tunnel. – Mod. Tunn. Technol., 39: pp. 1–11.

WAN, Z., SHA, M. & ZHOU, Y. (2003): Study on disk cutters for hard rock (3)-application of TB880E TBM in Qinling Tunnel. – Mod. Tunn. Technol., 40: pp. 1–6.

WANG, L., KANG, Y., CAI, Z., ZHANG, Q., ZHAO, Y., ZHAO, H. & SU, P. (2012): The energy method to predict disc cutter wear extent for hard rock TBMs. – Tunnelling and Underground Space Technology, 28: pp. 183–191.

WANG, L., KANG, Y., ZHAO, X. & ZHANG, Q. (2015): Disc cutter wear prediction for a hard rock TBM cutterhead based on energy analysis. – Tunnelling and Underground Space Technology, 50: pp. 324–333.

WANNER, H. & AEBERLI, U. (1979): Tunnelling machine performance in jointed rock. – In: International Society for Rock Mechanics (eds.): 4th Congress of the International Society for Rock Mechanics, Montreux, Switzerland, 2–8 September 1979, pp. 573–580, Rotterdam (A.A. Balkema).

WARREN, P.D., HILLS, D.A. & DAI, D.N. (1995): Mechanics of Hertzian cracking. – Tribology International, 28 (6): pp. 357–362.

WEILER, W. & BEHNCKE, H.-H. (1990): Anforderungen an Eindringkörper für die Universalhärteprüfung. – Materialprüfung, 32 (10): pp. 301–303.

WEISBARTH, R. (2003): Formkörper, mechanische Eigenschaften und Verbundswerkstoffe amorpher Si/B/N/C-Keramiken. – PhD-thesis, Rheinische Friedrich-Wilhelms-Universität Bonn, 180 p., Bonn (Rheinische Friedrich-Wilhelms-Universität Bonn).

WEIßBACH, W., DAHMS, M. & JAROSCHEK, C. (2015): Werkstoffkunde. – 19th edition, 597 p., Wiesbaden (Springer Vieweg).

WEST, G. (1989): Rock abrasiveness testing for tunnelling. – Int. J. Rock Mech. Min. Sci. Geomech. Abstr., 26 (2): pp. 151–160.

WHITTAKER, L.V. & MATTHEWS, A. (2004): Comparison of a simulated ‘in-service’ rig test with a standardised laboratory abrasion test. – Surface and Coatings Technology, 177-178: pp. 603–610.

WIESER, C. (2016): Quantifying the Effect of Stress Changes on the Deformation and Cracking Behavior of Solid Rock using Acoustic Emission. – PhD-thesis, Chair for engineering geology, Technical University of Munich, 166 p., Munich (TUM).

WIJK, G. (1992): A model of tunnel boring machine performance. – Geotechnical & Geological Engineering, 10 (1): pp. 19–40.

WILFING, L.S. (2016): The influence of geotechnical parameters on penetration prediction in TBM tunneling in hard rock. – PhD-thesis, Chair for engineering geology, Technical University of Munich, 168 p., Munich (TUM).

WILFING, L.S. & THURO, K. (2017): Die TBM Leistungsprognose auf dem Prüfstand. – In: Deutsche Gesellschaft für Geotechnik e.V. (DGGT) (ed.): Fachsektionstage Geotechnik, Würzburg, Germany, 6–8 September 2017, pp. 246–251, Essen (DGGT).

WIRTSCHAFTSVEREINIGUNG STAHL (2008): Merkblatt 452, Einsatzhärten. – Merkblatt 452: 41 p., Düsseldorf (Wirtschaftsvereinigung Stahl).

WOLDMAN, M., VAN DER HEIDE, E., SCHIPPER, D.J., TINGA, T. & MASEN, M.A. (2012): Investigating the influence of sand particle properties on abrasive wear behaviour. – Wear, 294-295: pp. 419–426.

WRIGHT, V.P. (1992): A revised classification of limestones. – Sedimentary, 76: pp. 177–186.

XIE, Y. & BHUSHAN, B. (1996): Effects of particle size, polishing pad and contact pressure in free abrasive polishing. – Wear, 200 (1-2): pp. 281–295.

XIE, Y. & WILLIAMS, J.A. (1996): The prediction of friction and wear when a soft surface slides against a harder rough surface. – Wear, 196 (1-2): pp. 21–34.

YAGIZ, S. (2002): Development of rock fracture and brittleness indices to quantify the effects of rock mass features and toughness in the CSM model basic penetration for hard rock tunneling machines. – PhD-thesis, Colorado School of Mines, Arthur Lakes Library, 128 p., Golden, Colorado (CSM).

YAGIZ, S. (2008): Utilizing rock mass properties for predicting TBM performance in hard rock condition. – Tunnelling and Underground Space Technology, 23 (3): pp. 326–339.

YAGIZ, S. (2009a): Assessment of brittleness using rock strength and density with punch penetration test. – Tunnelling and Underground Space Technology, 24 (1): pp. 66–74.

YAGIZ, S. (2009b): Geotechnical considerations on TBM tunnelling in rock mass. – In: Turkish National Committee of Soil Mechanics and Geotechnical Engineering (ed.): Proceedings of the 2nd International Conference on New Developments in Soil Mechanics and Geotechnical Engineering, Lefkosa, North Cyprus, 28–30 May 2009, pp. 504–511, Nicosia (Near East University Press).

YAGIZ, S., ROSTAMI, J., KIM, T., OZDEMIR, L. & MERGUERIAN, C. (2009): Factors Influencing Performance of Hard Rock Tunnel Boring Machines. – In: VRKLJAN,I. (ed.): Rock Engineering in Difficult Ground Conditions – Soft Rocks and Karst: pp. 671–700, London (Taylor & Francis Group).

YIN, L.J., GONG, Q.M. & ZHAO, J. (2014): Study on rock mass boreability by TBM penetration test under different in situ stress conditions. – Tunnelling and Underground Space Technology, 43: pp. 413–425.

ZARE, S. (2007): Drill and Blast Tunnelling – Advance Rate. – PhD-thesis, Faculty of Engineering Science and Technology, Norwegian Institute of Technology (NTNU), 138 p., Trondheim (NTNU).

ZHANG, Y. & SHAO, T. (2013): Effect of contact deformation on contact electrification. – J. Phys. D: Appl. Phys., 46 (23).

ZHANG, Z. (2001): Laboratory studies of dynamic rock fracture and in-situ measurements of cutter forces for a boring machine. – PhD-thesis, Luleå University of Technology, 51 p., Luleå, Sweden (LTU).

ZHANG, Z. & QIAO, Y. (2011): Research on the layout of TBM disc cutter. – Eng Mech, 28: pp. 172–177.

ZHANG, Z.X., KOU, S.Q., JIANG, L.G. & LINDQVIST, P.-A. (2000): Effects of loading rate on rock fracture. – International Journal of Rock Mechanics and Mining Sciences, 37 (5): pp. 745–762.

ZHANG, Z.X., KOU, S.Q., TAN, X.C. & LINDQUIST, P.A. (2003): In-situ Measurements of Cutter Forces on Boring Machine at Äspö Hard Rock Laboratory Part I. Laboratory Calibration and In-situ Measurements. – Rock Mech. Rock Eng., 36 (1): pp. 39–61.

ZHAO, Z., GONG, Q., ZHANG, Y. & ZHAO, J. (2007): Prediction model of tunnel boring machine performance by ensemble neural networks. – Geomechanics and Geoengineering, 2 (2): pp. 123–128.

ZUM GAHR, K.H. (1985): Tribologie: Reibung-Verschleiß-Schmierung. – Naturwissenschaften, 72: pp. 260–267.

ZUM GAHR, K.H. (1987): Microstructure and Wear of Materials. – Tribology, 559 p., Burlington (Elsevier).

ZUM GAHR, K.H. (1988): Modelling of two-body abrasive wear. – Wear, 124 (1): pp. 87–103.

10. URL Resources

www-01: http://www.hsm-stahl.de/fileadmin/user_upload/datenblatt/HSM_Datenblatt_1.2344.pdf, last access on July 23, 2020

www-02: http://www.dorrenberg.es/download/aceros/DOE/1.2345_deu.pdf, last access on July 23, 2020

www-03: https://www.asminternational.org/web/hts/news/newswire/-/journal_content/56/10192/26120368/NEWS, last access on July 23, 2020

www-04: http://www.dorrenberg.es/download/aceros/DOE/1.2344_deu.pdf, last access on July 23, 2020

www-05: http://kwf.at/wibis/elemente/druck/Karten/Oesterreich/Oesterreich.png, last access on March 23, 2017

www-06: https://www.google.de/maps, last access on March 23, 2017

www-07: http://www.jaegerbau.com/uploads/tx_jaegergallery/Hauptbaulose-Koralmtunnel-k_01.jpg; last access on March 09, 2017

www-08: https://www.bauforum24.biz/forums/topic/57002-aker-wirth-zweite-tunnelbohrmaschine-steht-fur-projekt-kat2-bereit/; last access on March 09, 2017

www-09: http://www.nationalpark-jasmund.de/index.php?article_id=92; last access on October 12, 2017

www-10: http://www.stein-mueller.de/; last access on October 09, 2017

www-11: http://www.graniteland.de/naturstein/abtswinder-sandstein-grun; last access on October 09, 2017

www-12: http://www.graniteland.de/naturstein/abtswinder-schilfsandstein; last access on October 09, 2017

Appendix

H-O-T GmbH
Kleinreuther Weg 118
90425 Nürnberg
Tel.: 0911/36014-40
Fax: 0911/36014-37

H-O-T®
LET'S OPTIMIZE EXCELLENCE

Analysen - Protokoll

H-O-T Auftrag:	201811-025367-01	Soll - Härte:	
Kunde:	Lehrstuhl für Ingenieurgeologie TU München	Ist - Härte:	
Bemerkung1:	Probenbezeichnung: CAI-A1-62		
Bemerkung2:			
Programm:	FE_T_100	Prüfer:	Herr Ziske

Messwerte:

	Fe	C	Si	Mn	P	S	Cr	Mo	Ni	Al	Co	Cu	Nb
1	97.4	1.17	0.205	0.241	< 0.0040	0.0049	0.710	0.0046	0.0257	0.0238	0.0042	0.0390	< 0.0020
2	97.5	1.15	0.201	0.238	< 0.0040	0.0042	0.700	0.0044	0.0274	0.0239	0.0044	0.0404	< 0.0020
3	97.5	1.15	0.203	0.242	< 0.0040	0.0049	0.695	< 0.0040	0.0261	0.0249	0.0034	0.0423	< 0.0020
Mw	97.5	1.16	0.203	0.240	< 0.0040	0.0047	0.702	< 0.0040	0.0264	0.0242	0.0040	0.0406	< 0.0020

	Ti	V	W	Pb	Sn	B	Zr	As	Bi
1	0.0021	0.0983	< 0.0250	< 0.0150	0.0035	< 0.0010	< 0.0020	0.0105	< 0.0150
2	0.0018	0.0963	< 0.0250	0.0177	0.0020	< 0.0010	< 0.0020	< 0.0050	< 0.0150
3	0.0014	0.0907	< 0.0250	< 0.0150	0.0027	< 0.0010	< 0.0020	< 0.0050	< 0.0150
Mw	0.0018	0.0951	< 0.0250	< 0.0150	0.0027	< 0.0010	< 0.0020	< 0.0050	< 0.0150

Soll-Material:

Ist-Material: 1.2210

Datum: 06.04.2018 Unterschrift: 

H-O-T GmbH
Kleinreuther Weg 118
90425 Nürnberg
Tel.: 0911/36014-40
Fax: 0911/36014-37

H-O-T®
LET'S OPTIMIZE EXCELLENCE

Analysen - Protokoll

H-O-T Auftrag: 201811-025367-01 Soll - Härte:

Kunde: Lehrstuhl für Ingenieurgeologie TU München Ist - Härte:

Bemerkung1: Probenbezeichnung: CAI-A2-45

Bemerkung2:

Programm: FE_T_100 Prüfer: Herr Ziske

Messwerte:

	Fe	C	Si	Mn	P	S	Cr	Mo	Ni	Al	Co	Cu	Nb
1	97.4	1.21	L 0.114	0.347	< 0.0040	0.0030	0.671	0.0153	0.0889	< 0.0020	0.0059	0.0541	< 0.0020
2	97.4	1.16	L 0.115	0.353	< 0.0040	0.0054	0.673	0.0124	0.0871	< 0.0020	0.0056	0.0541	< 0.0020
3	97.4	1.17	L 0.112	0.350	< 0.0040	0.0037	0.674	0.0162	0.0868	< 0.0020	0.0050	0.0518	< 0.0020
Mw	97.4	1.18	L 0.114	0.350	< 0.0040	0.0040	0.673	0.0146	0.0876	< 0.0020	0.0055	0.0533	< 0.0020

	Ti	V	W	Pb	Sn	B	Zr	As	Bi
1	0.0017	0.0816	< 0.0250	< 0.0150	0.0041	< 0.0010	< 0.0020	< 0.0050	< 0.0150
2	0.0013	0.0816	< 0.0250	< 0.0150	< 0.0020	< 0.0010	< 0.0020	< 0.0050	< 0.0150
3	0.0018	0.0803	< 0.0250	< 0.0150	< 0.0020	< 0.0010	< 0.0020	< 0.0050	< 0.0150
Mw	0.0016	0.0812	< 0.0250	< 0.0150	0.0023	< 0.0010	< 0.0020	< 0.0050	< 0.0150

Soll-Material:

Ist-Material: 1.2210

Datum: 06.04.2018 Unterschrift:

H-O-T GmbH
Kleinreuther Weg 118
90425 Nürnberg
Tel.: 0911/36014-40
Fax: 0911/36014-37

H-O-T®
LET'S OPTIMIZE EXCELLENCE

Analysen - Protokoll

H-O-T Auftrag: 201811-025367-01 Soll - Härte:

Kunde: Lehrstuhl für Ingenieurgeologie TU München Ist - Härte:

Bemerkung1: Probenbezeichnung: LC PC A1-GF

Bemerkung2:

Programm: FE_T_400 Prüfer: Herr Ziske

Messwerte:

	Fe	C	Si	Mn	P	S	Cr	Mo	Ni	Al	Co	Cu	Nb
1	97.4	0.171	0.175	1.27	< 0.0050	0.0111	0.284	0.0196	0.174	0.0114	0.0026	0.407	< 0.0030
2	97.4	0.168	0.181	1.25	< 0.0050	0.0100	0.279	0.0186	0.171	0.0116	< 0.0010	0.422	< 0.0030
3	97.4	0.166	0.178	1.29	< 0.0050	0.0096	0.284	0.0183	0.172	0.0114	0.0021	0.415	< 0.0030
Mw	97.4	0.168	0.178	1.27	< 0.0050	0.0102	0.283	0.0189	0.172	0.0115	0.0015	0.415	< 0.0030

	Ti	V	W	Sn
1	0.0143	0.0056	< 0.0250	0.0216
2	0.0143	0.0091	< 0.0250	0.0219
3	0.0147	0.0054	< 0.0250	0.0236
Mw	0.0145	0.0067	< 0.0250	0.0224

Soll-Material:

Ist-Material: 1.0580

Datum: 06.04.2018 Unterschrift:

H-O-T GmbH
Kleinreuther Weg 118
90425 Nürnberg
Tel.: 0911/36014-40
Fax: 0911/36014-37

H-O-T
LET'S OPTIMIZE EXCELLENCE

Analysen - Protokoll

H-O-T Auftrag:	201811-025367-01	Soll - Härte:	
Kunde:	Lehrstuhl für Ingenieurgeologie TU München	Ist - Härte:	
Bemerkung1:	Probenbezeichnung: LC PC A2-GL		
Bemerkung2:			
Programm:	FE_T_100	Prüfer:	Herr Ziske

Messwerte:

	Fe	C	Si	Mn	P	S	Cr	Mo	Ni	Al	Co	Cu	Nb
1	99.2	0.0746	0.0096	0.500	< 0.0040	< 0.0030	0.0257	< 0.0040	0.0114	0.0248	0.0057	0.0215	0.0051
2	99.3	0.0681	0.0108	0.467	< 0.0040	< 0.0030	0.0253	< 0.0040	0.0140	0.0243	0.0055	0.0201	0.0035
3	99.3	0.0641	0.0084	0.471	< 0.0040	< 0.0030	0.0254	0.0058	0.0128	0.0234	0.0060	0.0199	0.0032
Mw	99.2	0.0689	0.0096	0.479	< 0.0040	< 0.0030	0.0254	< 0.0040	0.0127	0.0242	0.0057	0.0205	0.0039

	Ti	V	W	Pb	Sn	B	Zr	As	Bi
1	0.0015	0.0035	< 0.0250	< 0.0150	0.0031	< 0.0010	< 0.0020	0.0528	< 0.0150
2	0.0017	0.0030	< 0.0250	< 0.0150	< 0.0020	< 0.0010	< 0.0020	0.0241	< 0.0150
3	< 0.0010	0.0030	< 0.0250	< 0.0150	< 0.0020	< 0.0010	< 0.0020	0.0277	< 0.0150
Mw	0.0013	0.0032	< 0.0250	< 0.0150	< 0.0020	< 0.0010	< 0.0020	0.0349	< 0.0150

Soll-Material:

Ist-Material: 1.0116

Datum: 06.04.2018 Unterschrift: 

H-O-T GmbH
Kleinreuther Weg 118
90425 Nürnberg
Tel.: 0911/36014-40
Fax: 0911/36014-37

H-O-T
LET'S OPTIMIZE EXCELLENCE

Analysen - Protokoll

H-O-T Auftrag: 201811-025367-01 Soll - Härte:

Kunde: Lehrstuhl für Ingenieurgeologie TU München Ist - Härte:

Bemerkung1: Probenbezeichnung: 520-N

Bemerkung2:

Programm: FE_T_300 Prüfer: Herr Ziske

Messwerte:

	Fe	C	Si	Mn	P	S	Cr	Mo	Ni	Al	Co	Cu	Nb
1	90.9	0.518	0.863	0.312	< 0.0050	< 0.0030	4.96	1.39	0.0836	0.0102	0.0086	0.0544	< 0.0020
2	90.9	0.501	0.853	0.314	< 0.0050	< 0.0030	5.00	1.37	0.0864	0.0109	0.0081	0.0533	< 0.0020
3	90.9	0.499	0.861	0.315	< 0.0050	< 0.0030	4.98	1.37	0.0825	0.0110	0.0081	0.0542	< 0.0020
Mw	90.9	0.506	0.859	0.314	< 0.0050	< 0.0030	4.98	1.37	0.0842	0.0107	0.0083	0.0540	< 0.0020

	Ti	V	W	Pb	Se
1	0.0039	0.859	< 0.0400	< 0.0150	< 0.0100
2	0.0044	0.862	< 0.0400	< 0.0150	< 0.0100
3	0.0046	0.867	< 0.0400	< 0.0150	< 0.0100
Mw	0.0043	0.863	< 0.0400	< 0.0150	< 0.0100

Soll-Material:

Ist-Material: 1.2345

Datum: 06.04.2018 Unterschrift:

H-O-T GmbH
Kleinreuther Weg 118
90425 Nürnberg
Tel.: 0911/36014-40
Fax: 0911/36014-37

H-O-T®
LET'S OPTIMIZE EXCELLENCE

Analysen - Protokoll

H-O-T Auftrag:	201811-025367-01	Soll - Härte:	
Kunde:	Lehrstuhl für Ingenieurgeologie TU München	Ist - Härte:	
Bemerkung1:	Probenbezeichnung: QS25-N4		
Bemerkung2:			
Programm:	FE_T_400	Prüfer:	Herr Ziske

Messwerte:

	Fe	C	Si	Mn	P	S	Cr	Mo	Ni	Al	Co	Cu	Nb
1	90.7	L 0.469	0.907	0.349	< 0.0050	< 0.0030	5.00	1.31	0.0802	0.0156	0.0037	0.117	0.0265
2	90.7	L 0.469	0.917	0.353	< 0.0050	0.0048	4.97	1.34	0.0843	0.0167	0.0039	0.118	0.0275
3	90.7	L 0.471	0.916	0.351	< 0.0050	0.0039	5.03	1.27	0.0800	0.0154	0.0040	0.118	0.0259
Mw	90.7	L 0.470	0.914	0.351	< 0.0050	0.0038	5.00	1.31	0.0815	0.0159	0.0039	0.118	0.0266

	Ti	V	W	Sn
1	< 0.0010	0.963	< 0.0250	0.0074
2	< 0.0010	0.961	< 0.0250	0.0068
3	< 0.0010	0.965	< 0.0250	0.0061
Mw	< 0.0010	0.963	< 0.0250	0.0067

Soll-Material:

Ist-Material: 1.2345

Datum: 06.04.2018 Unterschrift:

H-O-T GmbH
Kleinreuther Weg 118
90425 Nürnberg
Tel.: 0911/36014-40
Fax: 0911/36014-37

H-O-T®
LET'S OPTIMIZE EXCELLENCE

Analysen - Protokoll

H-O-T Auftrag: 201811-025367-01 Soll - Härte:

Kunde: Lehrstuhl für Ingenieurgeologie TU München Ist - Härte:

Bemerkung1: Probenbezeichnung: 1510

Bemerkung2:

Programm: FE_T_300 Prüfer: Herr Ziske

Messwerte:

	Fe	C	Si	Mn	P	S	Cr	Mo	Ni	Al	Co	Cu	Nb
1	90.2	H 0.539	1.01	H 0.742	< 0.0050	0.0131	5.00	H 1.54	0.0870	0.0661	0.0123	0.0691	< 0.0020
2	90.1	H 0.532	1.03	H 0.753	< 0.0050	0.0090	5.11	H 1.51	0.0922	0.0661	0.0125	0.0707	< 0.0020
3	90.0	H 0.536	1.02	H 0.759	< 0.0050	0.0073	5.13	H 1.50	0.0866	0.0671	0.0118	0.0717	< 0.0020
Mw	90.1	H 0.536	1.02	H 0.751	< 0.0050	0.0098	5.08	H 1.52	0.0886	0.0664	0.0122	0.0705	< 0.0020

	Ti	V	W	Pb	Se
1	0.0032	L 0.724	< 0.0400	< 0.0150	< 0.0100
2	0.0032	L 0.720	< 0.0400	0.0168	< 0.0100
3	0.0033	L 0.740	< 0.0400	0.0151	< 0.0100
Mw	0.0032	L 0.728	< 0.0400	0.0156	< 0.0100

Soll-Material:

Ist-Material: 1.2345

Datum: 06.04.2018 Unterschrift:

H-O-T GmbH
Kleinreuther Weg 118
90425 Nürnberg
Tel.: 0911/36014-40
Fax: 0911/36014-37

H-O-T®
LET'S OPTIMIZE EXCELLENCE

Analysen - Protokoll

H-O-T Auftrag:	201811-025367-01	Soll - Härte:	
Kunde:	Lehrstuhl für Ingenieurgeologie TU München	Ist - Härte:	
Bemerkung1:	Probenbezeichnung: 1650		
Bemerkung2:			
Programm:	FE_T_400	Prüfer:	Herr Ziske

Messwerte:

	Fe	C	Si	Mn	P	S	Cr	Mo	Ni	Al	Co	Cu	Nb
1	90.8	L 0.462	0.929	0.354	< 0.0050	0.0067	4.85	1.31	0.0889	0.0175	0.0042	0.148	0.0271
2	90.9	L 0.457	0.933	0.351	< 0.0050	0.0059	L 4.77	1.32	0.0938	0.0172	0.0055	0.138	0.0271
3	90.8	L 0.455	0.919	0.352	< 0.0050	0.0046	4.90	1.29	0.0950	0.0165	0.0031	0.135	0.0275
Mw	90.9	L 0.458	0.927	0.352	< 0.0050	0.0057	4.84	1.31	0.0926	0.0171	0.0043	0.140	0.0272

	Ti	V	W	Sn
1	< 0.0010	0.971	< 0.0250	0.0094
2	< 0.0010	0.954	< 0.0250	0.0122
3	< 0.0010	0.960	< 0.0250	0.0114
Mw	< 0.0010	0.961	< 0.0250	0.0110

Soll-Material:

Ist-Material: 1.2345

Datum: 06.04.2018 Unterschrift: 

H-O-T GmbH
Kleinreuther Weg 118
90425 Nürnberg
Tel.: 0911/36014-40
Fax: 0911/36014-37

H-O-T®
LET'S OPTIMIZE EXCELLENCE

Analysen - Protokoll

H-O-T Auftrag:	201811-025367-01	Soll - Härte:	
Kunde:	Lehrstuhl für Ingenieurgeologie TU München	Ist - Härte:	
Bemerkung1:	Probenbezeichnung: H573		
Bemerkung2:			
Programm:	FE_T_300	Prüfer:	Herr Ziske

Messwerte:

	Fe	C	Si	Mn	P	S	Cr	Mo	Ni	Al	Co	Cu	Nb
1	90.9	0.512	0.899	0.230	< 0.0050	< 0.0030	5.01	1.39	0.0905	0.0056	0.0084	0.0841	< 0.0020
2	90.9	0.511	0.880	0.227	< 0.0050	< 0.0030	5.03	1.37	0.0915	0.0054	0.0072	0.0839	< 0.0020
3	90.9	0.508	0.888	0.229	< 0.0050	< 0.0030	5.02	1.37	0.0912	0.0047	0.0083	0.0835	< 0.0020
Mw	90.9	0.510	0.889	0.229	< 0.0050	< 0.0030	5.02	1.38	0.0911	0.0052	0.0080	0.0838	< 0.0020

	Ti	V	W	Pb	Se
1	0.0030	0.889	< 0.0400	< 0.0150	< 0.0100
2	0.0035	0.878	< 0.0400	< 0.0150	< 0.0100
3	0.0034	0.877	< 0.0400	< 0.0150	< 0.0100
Mw	0.0033	0.881	< 0.0400	< 0.0150	< 0.0100

Soll-Material:

Ist-Material: 1.2345

Datum: 06.04.2018 Unterschrift: 

H-O-T GmbH
Kleinreuther Weg 118
90425 Nürnberg
Tel.: 0911/36014-40
Fax: 0911/36014-37

H-O-T LET'S OPTIMIZE EXCELLENCE

Analysen - Protokoll

H-O-T Auftrag: 201811-025367-01 Soll - Härte:

Kunde: Lehrstuhl für Ingenieurgeologie TU München Ist - Härte:

Bemerkung1: Probenbezeichnung: ZN-1.2

Bemerkung2:

Programm: FE_T_300 Prüfer: Herr Ziske

Messwerte:

	Fe	C	Si	Mn	P	S	Cr	Mo	Ni	Al	Co	Cu	Nb
1	91.0	0.485	0.881	0.269	< 0.0050	< 0.0030	4.92	1.32	0.136	0.0092	0.0076	0.143	< 0.0020
2	91.0	0.488	0.878	0.270	< 0.0050	< 0.0030	4.90	1.31	0.134	0.0087	0.0090	0.137	< 0.0020
3	91.0	0.488	0.878	0.270	< 0.0050	< 0.0030	4.92	1.31	0.124	0.0086	0.0072	0.131	< 0.0020
Mw	91.0	0.487	0.879	0.270	< 0.0050	< 0.0030	4.91	1.31	0.131	0.0088	0.0079	0.137	< 0.0020

	Ti	V	W	Pb	Se
1	0.0060	0.851	< 0.0400	< 0.0150	< 0.0100
2	0.0062	0.848	< 0.0400	< 0.0150	< 0.0100
3	0.0060	0.848	< 0.0400	< 0.0150	< 0.0100
Mw	0.0061	0.849	< 0.0400	< 0.0150	< 0.0100

Soll-Material:

Ist-Material: 1.2345

Datum: 06.04.2018 Unterschrift:

H-O-T GmbH
Kleinreuther Weg 118
90425 Nürnberg
Tel.: 0911/36014-40
Fax: 0911/36014-37

H-O-T
LET'S OPTIMIZE EXCELLENCE

Analysen - Protokoll

H-O-T Auftrag: 201811-025367-01 Soll - Härte:

Kunde: Lehrstuhl für Ingenieurgeologie TU München Ist - Härte:

Bemerkung1: Probenbezeichnung: U2-H2

Bemerkung2:

Programm: FE_T_400 Prüfer: Herr Ziske

Messwerte:

	Fe	C	Si	Mn	P	S	Cr	Mo	Ni	Al	Co	Cu	Nb
1	90.9	H 0.535	0.862	0.272	< 0.0050	< 0.0030	L 4.78	1.38	0.176	0.0178	0.0032	0.154	0.0269
2	90.9	H 0.535	0.858	0.274	< 0.0050	< 0.0030	L 4.78	1.36	0.176	0.0168	0.0035	0.131	0.0262
3	90.9	H 0.533	0.854	0.278	< 0.0050	< 0.0030	L 4.78	1.36	0.168	0.0170	0.0038	0.117	0.0262
Mw	90.9	H 0.534	0.858	0.275	< 0.0050	< 0.0030	L 4.78	1.36	0.173	0.0172	0.0035	0.134	0.0264

	Ti	V	W	Sn
1	< 0.0010	0.918	< 0.0250	0.0123
2	0.0011	0.915	< 0.0250	0.0107
3	< 0.0010	0.920	< 0.0250	0.0083
Mw	< 0.0010	0.918	< 0.0250	0.0105

Soll-Material:

Ist-Material: 1.2345

Datum: 06.04.2018 Unterschrift:

H-O-T GmbH
Kleinreuther Weg 118
90425 Nürnberg
Tel.: 0911/36014-40
Fax: 0911/36014-37

H-O-T
LET'S OPTIMIZE EXCELLENCE

Analysen - Protokoll

H-O-T Auftrag: 201811-025367-01 Soll - Härte:

Kunde: Lehrstuhl für Ingenieurgeologie TU München Ist - Härte:

Bemerkung1: Probenbezeichnung: 1555

Bemerkung2:

Programm: FE_T_300 Prüfer: Herr Ziske

Messwerte:

	Fe	C	Si	Mn	P	S	Cr	Mo	Ni	Al	Co	Cu	Nb
1	90.8	0.486	0.894	0.316	< 0.0050	< 0.0030	4.94	1.34	0.163	0.0114	0.0105	0.159	< 0.0020
2	90.7	0.495	0.900	0.322	< 0.0050	< 0.0030	4.99	1.35	0.174	0.0111	0.0096	0.157	< 0.0020
3	90.8	0.487	0.888	0.313	< 0.0050	< 0.0030	4.96	1.34	0.164	0.0121	0.0094	0.152	< 0.0020
Mw	90.8	0.489	0.894	0.317	< 0.0050	< 0.0030	4.96	1.34	0.167	0.0115	0.0098	0.156	< 0.0020

	Ti	V	W	Pb	Se
1	0.0049	0.863	< 0.0400	< 0.0150	< 0.0100
2	0.0052	0.860	< 0.0400	0.0173	< 0.0100
3	0.0059	0.858	< 0.0400	0.0152	< 0.0100
Mw	0.0053	0.860	< 0.0400	0.0153	< 0.0100

Soll-Material:

Ist-Material: 1.2345

Datum: 06.04.2018 Unterschrift: